Institut für Nutzpflanzenwissenschaften und Ressourcenschutz

– Pflanzenernährung –

Molecular mechanisms of *Pseudomonas*-enhanced plant performance in Brachypodium under limited nitrogen

Dissertation

zur Erlangung des Grades

Doctor of Philosophy (Ph. D.)

der Agrar-, Ernährungs- und Ingenieurwissenschaftlichen Fakultät
der Rheinischen Friedrich-Wilhelms-Universität Bonn

und

Faculty of Science, School of BioSciences
The University of Melbourne

von

Stefan Sanow

aus

Brilon, Deutschland

Bonn, Melbourne, 2025

Doctoral Research and Thesis Supervisors

Angefertigt mit Genehmigung der Agrar-, Ernährungs- und Ingenieurwissenschaftlichen Fakultät der Universität Bonn und der Faculty of Science, School of BioSciences der University of Melbourne.

The University of Bonn

Referent / Principal Supervisor: Prof. Dr. Gabriel Schaaf

Korreferentin / Second Supervisor: Prof. Dr. Michelle Watt

The University of Melbourne

Referentin / Principal Supervisor: Prof. Dr. Ute Roessner

Korreferentin / Second Supervisor: Prof. Dr. Michelle Watt

Prüfungsdatum / Exam date: July 04, 2024

Abstract

While the world population is increasing, the use of nitrogenous fertilizers has become obligatory to increase yields to meet the global food demand. Overuse of synthesized N fertilizers does not only negatively impact the environment during its energy intensive Haber-Bosch process, but also affects ground water bodies due to nitrate leaching losses and elevated N_2O emissions. Improved use of N by crops may be achieved with N-fixing plant-growth promoting bacteria (PGPB).

In this thesis, I investigated the temporally resolved morphological and biochemical responses of *Brachypodium distachyon* to inoculation with *Pseudomonas koreensis* a bacterial species previously shown to harbor plant growth-promoting properties. This investigation was conducted under different N levels. *P. koreensis* was tested for its ability to fix N via a ^{15}N natural abundance approach. Under zero and limited N, inoculated plants have shown trends to a decreased $\delta^{15}N$ signature, indicating an additional ^{14}N source. A whole-plant increase in N content was observed in plants grown in limited N conditions when inoculated with *P. koreensis*, whereas the root C-content was significantly decreased. Limited N supplied plants inoculated with *P. koreensis* have shown several improvements in morphological parameters, such as (projected) leaf area, fresh weight, dry weight, and lateral root length at 21 days after sowing (DAS). The molecular mechanisms were investigated utilizing proteomics and lipidomics measurements. Inoculated limited N supplied plants have shown a comparable protein profile to sufficient N control plants. The lipid profile primarily responded to the two N levels. Additionally, *P. koreensis* inoculation altered the abundance of membrane and storage lipids prior to the growth promotion at 19 DAS.

The generated descriptive data have the potential to shape future research to increase our understanding of plant-microbe interactions, leading to a decrease in synthetic N fertilizer production and application.

Zusammenfassung

Aufgrund einer wachsenden Weltbevölkerung, ist der Einsatz von Stickstoffdüngern zur Steigerung der Erträge zwingend erforderlich geworden, um den weltweiten Nahrungsmittelbedarf zu decken. Der übermäßige Einsatz von synthetischen Stickstoffdüngern wirkt sich nicht nur durch den energieintensiven Haber-Bosch-Prozess negativ auf die Umwelt aus, sondern beeinträchtigt auch die Grundwasserkörper durch Nitratauswaschung und erhöhte N_2O-Emissionen. Mit N-fixierenden, pflanzenwachstumsfördernden Bakterien (PGPB) kann eine bessere Nutzung von N durch Nutzpflanzen erreicht werden.

In dieser Arbeit untersuchte ich die zeitlich aufgelösten morphologischen und biochemischen Reaktionen von *Brachypodium distachyon* auf die Inokulation mit *Pseudomonas koreensis*, einer Bakterienart, die nachweislich pflanzenwachstumsfördernde Eigenschaften besitzt. Diese Untersuchung wurde unter verschiedenen N-Konzentrationen durchgeführt. *P. koreensis* wurde auf seine Fähigkeit zur N-Fixierung mittels eines ^{15}N-Ansatzes (natürliche Häufigkeit) getestet. Bei Null und begrenztem Stickstoffgehalt zeigten inokulierte Pflanzen Tendenzen zu einer verringerten $\delta^{15}N$-Signatur, was auf eine zusätzliche ^{14}N-Quelle hinweist. Bei mit P. koreensis beimpften Pflanzen, die unter begrenzten N-Bedingungen wuchsen, wurde ein Anstieg des N-Gehalts in der gesamten Pflanze beobachtet, während der C-Gehalt in der Wurzel deutlich abnahm. Mit *P. koreensis* inokulierte Pflanzen mit begrenzter Stickstoffzufuhr zeigten mehrere Verbesserungen bei morphologischen Parametern wie (projizierte) Blattfläche, Frischgewicht, Trockengewicht und Seitenwurzellänge 21 Tage nach der Aussaat (DAS). Die molekularen Mechanismen wurden mit Hilfe von Proteomics- und Lipidomics-Messungen untersucht. Inokulierte Pflanzen mit begrenzter N-Versorgung wiesen ein vergleichbares Proteinprofil auf wie Kontrollpflanzen mit ausreichender N-Versorgung. Das Lipidprofil reagierte in erster Linie auf die beiden N-Gaben. Zusätzlich veränderte die Inokulation mit *P. koreensis* die Häufigkeit von Membran- und Speicherlipiden vor der Wachstumsförderung bei 19 DAS.

Die gewonnenen beschreibenden Daten haben das Potenzial, die künftige Forschung zu beeinflussen, um unser Verständnis der Wechselwirkungen zwischen Pflanzen und Mikroben zu verbessern, was zu einer Verringerung der Produktion und des Einsatzes synthetischer Stickstoffdünger führt.

Declaration

I, Stefan Sanow, declare that this thesis titled, 'Molecular mechanisms of *Pseudomonas*-enhanced plant performance in Brachypodium under limited nitrogen' and the work presented in it are my own.

This is to certify that

i. the thesis comprises only my original work towards the PhD;

ii. due acknowledgement has been made in the text to all other material used; and

iii. the thesis is fewer than 100,000 words in length, exclusive of tables, maps, bibliographies and appendices.

Date: January 02, 2025 **Signature:**

Preface

This document has been written to the best of my knowledge as a synergy of the structures for doctoral dissertations at The University of Melbourne and the University of Bonn.

The candidate has contributed more than 51% of the content of this thesis and is the primary author of all publications derived from this thesis.

The plant and bacteria cultivation, experimental optimisations, periodic plant phenotyping, time-course harvest, sample preparation, morphological and biochemical measurements and analyses, results interpretation and statistical analyses were carried out by the candidate. Project supervisors, Prof. Ute Roessner, Prof. Gabriel Schaaf Prof. Michelle Watt, Prof. Pitter Huesgen, Dr. Robert Walker and Dr. Borjana Arsova were involved in the design of the experiments and supervision of the candidate.

Chapter 3 – Dr. Andreas Lücke was involved in the experimental design of the ^{15}N natural abundance experiments. Holger Wissel performed ^{15}N measurements. Dr. Sabine Willbold and her lab performed the elemental analyses. Helena Bochmann performed WinRhizo scans during the time-course harvest. Elena Sturm performed the bacterial N-fixation plate assay.

Chapter 4 – Melissa Mantz performed the LC-MS/MS untargeted protein data acquisition from the Forschungszentrum Jülich. Dr. Atul Bhatnagar performed the LC-MS untargeted lipid data acquisition from the Sydney Mass Spectrometry facility. Dr. Thusita Rupasinghe, Dr. Allene Macabuhay and Alina Ebert provided training for the MS-DIAL lipid analysis.

All authors discussed the results and their implications and provided feedback on the manuscript at all stages.

Publications

Published Articles

Sanow, S., Kuang, W., Schaaf, G., Huesgen, P., Schurr, U., Roessner, U., Watt, M. & Arsova, B. (2023). Molecular mechanisms of Pseudomonas assisted plant nitrogen uptake-opportunities for modern agriculture. *Molecular Plant-Microbe Interactions*, (https://doi.org/10.1094/MPMI-10-22-0223-CR).

Presented in Chapter 2

Publication-in-progress

Sanow, S., Mantz, M., Wissel, H., Bhatnagar, A., E. Sturm, J. Kelm, Walker, R., Lücke, A., Schaaf, G., Huesgen, P., Roessner, U., Watt, M. and Arsova, B. *Molecular mechanisms of Pseudomonas-enhanced plant performance in Brachypodium under limited nitrogen.*

From Chapter 3 & 4

Co-Author Articles

Kuang, W., **Sanow, S.**, Kelm, J. M., Müller Linow, M., Andeer, P., Kohlheyer, D., ... & Arsova, B. (2022). N-dependent dynamics of root growth and nitrate and ammonium uptake are altered by the bacterium Herbaspirillum seropedicae in the cereal model Brachypodium distachyon. *Journal of experimental botany*, *73*(15), 5306-5321, (https://doi.org/10.1093/jxb/erac184).

Personal contribution: Primer design and testing of the performed qPCR, partial execution of the experiment (together with Jana Kelm), analyses of the qPCR data, writing of the respective materials and methods sections and initial figure design.

Acknowledgements

First, I would like to thank my whole supervisor team, consisting of Dr. Borjana Arsova, Dr. Robert Walker, Prof. Dr. Pitter Huesgen, Prof. Dr. Michelle Watt, Prof. Dr. Gabriel Schaaf and Prof. Dr. Ute Roessner. Having such a great, interdisciplinary team with experts from various disciplines, allowed me to learn from multiple scientists at the same time.

Special thanks to Dr. Borjana Arsova, Prof. Michelle Watt and Prof. Ute Roessner for giving me the opportunity to do my PhD in the JUMPA program. Thank you, Borjana, for being my everyday supervisor over the past five years (including M.Sc.) and being patient with me. Thank you, Ute, Michelle, and Gabriel, for being my principal supervisors at the University of Bonn and the University of Melbourne. Although Gabriel joined the team a little bit later and (I think) we have never met in person, I am very grateful for having you as my principal supervisor at the University of Bonn! Together with Ute, I am very proud to have had you both as my 'doctor parents'!

However, there have been many more important people during the past five years. First, I want to start with the group, which I have spent the most time with: The Root Dynamics Group at the IBG-2. Thank you so much for being a bunch of amazing people. You have probably seen me during my best and worst times but have always been understanding. I enjoyed spending time with you, either during coffee breaks or after work: Tanja Ehrlich, Jana Kelm, Helena Bochmann, Lisa Mau, Dr. Allene Macabuhay (from the UoM), Sebastian Erdrich and Elena Sturm. Moreover, my second lab has been the Degradomics Lab of Pitter. First, thank you Pitter for being an amazing collaborator and supervisor during my M.Sc. and PhD. Your Team, consisting of Melissa Mantz, Maithreyan Kuppusamy, Henrique Baeta, Michelle Hupert, Andrea Stärk, have always been very supportive. Thank you for all the time you have spent on helping me with troubleshooting, measurements and sharing all the data! Lastly, I want to mention the Roessner Lab at the University of Melbourne, which I call my 'second home' since my short stay. From the very first day, I felt welcome and included in the lab and community. Special thanks go to Heber Dias de Oliveira, Alina Ebert, Soumitra Bhide and Rucha Patil. I am so happy to have met you!

Thanks to all the other people, who I have met during my stay: You made this a unique experience.

Thanks to my friends Johannes Curdts and Carsten Henningsen for being incredible patient with me and listening to endless stories about science and the PhD life.

In the end, I want to thank my parents Franz-Hubert and Sylvia-Regina Sanow for being supportive parents during the past years. Thanks to my brother Christian Sanow, for everything in the past and present.

Contents

List of Figures

represent the condition compared to limited N controls. Means were compared using two-way ANOVA followed by Tukey's honestly significant difference (HSD) test and can be found in Supplementary Table S3.1 and S3.2.

Figure 4.1. Principal component analyses of root and shoot whole-proteome (WP) datasets. A) PCA of the root whole-proteome; B) PCA of the shoot whole-proteome.

Figure 4.2. Proteomics data overview. A) Root volcano plot of the comparison: Sufficient N Ctrl vs. Limited N Ctrl; B) Root volcano plot of the comparison: Limited N + *Pk* vs. Limited N Ctrl; C) Root volcano plot of the comparison: Sufficient N + *Pk* vs. Sufficient N Ctrl; D) Shoot volcano plot of the comparison: Sufficient N Ctrl vs. Limited N Ctrl; E) Shoot volcano plot of the comparison: Limited N + *Pk* vs. Limited N Ctrl; F) Shoot volcano plot of the comparison: Sufficient N + *Pk* vs. Sufficient N Ctrl; Data shown are 100% valid values of the respective data set. Volcano plots represent the -log10 transformed adjusted p values from Tukey's HSD with a p-value threshold set for $\alpha < 0.05$ and no threshold set for log2FC (= 0). Values in the plot represent the number of proteins in each group (red = less abundant, grey = not significant, blue = higher abundant; matching the colours of data points).

Figure 4.3. GO-term analyses (Biological processes). A) Root GO term analysis; B) Shoot GO term analysis. Only statistical significant proteins were imported into PantherDB statistical enrichment test (Mi et al., 2019), followed by REVIGO (Supek et al., 2011). Log10 (p-values) were used to calculate the %-distribution (x-axis) of GO-terms (y-axis).

Figure 4.4. Central N metabolism in roots and shoots (whole proteome). Data represented are 100% valid values. Mapped proteins, log2FC and significances (indicated with asterisks in log2FC column) are shown in Supplementary Table S4.1. MapMan version 3.5.1R2 (Thimm et al., 2004) was used. The following pathways were used and modified from Feng et al., 2020: X4.1 N-uptake R1.0. Modified pathways will be submitted to the MapMan store (https://mapman.gabipd.org/mapmanstore). Mapping file was created using Mercator4 V2.0 (Schwacke et al., 2019). Comparisons are mentioned on top or below of each box: HNC / LNC = Sufficient N Control vs. Limited N Control; LNP / LNC = Limited N + *Pk* vs. Limited N Control; HNP / HNC = Sufficient N + *Pk* vs. Sufficient N Control. Abbreviations: AA, Amino acid; AMT, ammonium transporter family; AS, Asparagine synthase; GDH, Glutamate dehydrogenase; GOGAT, glutamine oxoglutarate aminotransferase; GS1, (cytosolic) Glutamine synthetase 1 isoforms; GS2, (plastidial) Glutamine synthetase 2 isoforms; NiR, Nitrite reductase; NR, Nitrate reductase; NRT, Nitrate transporter family.

Figure 4.5. Kinases in roots and shoots (whole proteome). Data represented are 100% vv. Mapped proteins, log2FC and significances (indicated with asterisks in log2FC column) are shown in Supplementary Table S4.1. MapMan version 3.5.1R2 (Thimm et al., 2004) was used. The following pathways were used and modified from Shiu and Bleecker, 2001: X4.1_Kinase_Families_R1.0. Mapping file was created using Mercator4 V2.0 (Schwacke et al., 2019). Comparisons are mentioned on top of each box: HNC / LNC = Sufficient N Control vs. Limited N Control; LNP / LNC = Limited N + *Pk* vs. Limited N Control; HNP / HNC = Sufficient N + *Pk* vs. Sufficient N Control.

Figure 4.6. Lipid metabolism overview in roots (whole proteome). Data represented are 100% vv. Mapped proteins, log2FC and significances (indicated with asterisks in log2FC column) are shown in Supplementary Table S4.1. MapMan version 3.5.1R2 (Thimm et al., 2004) was used. The following pathways were used and modified: X4.5 Lipid metabolism R5.0. Mapping file was created using Mercator4 V2.0 (Schwacke et al., 2019). Abbreviations: ptFAS, plastidial fatty acid synthase; mtFAS, mitochondrial fatty acid synthase; FAE, fatty acid elongase. Comparisons are mentioned next to each box: HNC / LNC = Sufficient N Control vs. Limited N Control; LNP / LNC = Limited N + *Pk* vs. Limited N Control; HNP / HNC = Sufficient N + *Pk* vs. Sufficient N Control.

Figure 4.7. PCA and heatmaps of root Lipids 19, 20 and 21 DAS (time-resolved). All manually curated lipids (255 features) were used for PCA and were mapped using hierarchical cluster analysis (HCA), Pearson distance measurement and average distance. Abundances were log10 transformed and scaled using Pareto scaling.

List of Tables

List of Supplementary Figures

following pathways were used and modified from Feng et al., 2020: X4.1 N-uptake R1.0. Modified pathways will be submitted to the MapMan store (https://mapman.gabipd.org/mapmanstore). Mapping file was created using Mercator4 V2.0 (Schwacke et al., 2019). Comparisons are mentioned on top or below of each box: HNC / LNC = Sufficient N Control vs. Limited N Control; LNP / LNC = Limited N + *Pk* vs. Limited N Control; HNP / HNC = Sufficient N + *Pk* vs. Sufficient N Control. Abbreviations: AA, Amino acid; AMT, ammonium transporter family; AS, Asparagine synthase; GDH, Glutamate dehydrogenase; GOGAT, glutamine oxoglutarate aminotransferase; GS1, (cytosolic) Glutamine synthetase 1 isoforms; GS2, (plastidial) Glutamine synthetase 2 isoforms; NiR, Nitrite reductase; NR, Nitrate reductase; NRT, Nitrate transporter family.

Supplementary Figure S4.4. Kinases in roots (microsomal fraction). Data represented are 100% vv. Mapped proteins, log2FC and significances (indicated with asterisks in log2FC column) are shown in Supplementary Table S4.4. MapMan version 3.5.1R2 (Thimm et al., 2004) was used. The following pathways were used and modified from Shiu and Bleecker, 2001: X4.1_Kinase_Families_R1.0. Mapping file was created using Mercator4 V2.0 (Schwacke et al., 2019). Comparisons are mentioned on top of each box: HNC / LNC = Sufficient N Control vs. Limited N Control; LNP / LNC = Limited N + *Pk* vs. Limited N Control; HNP / HNC = Sufficient N + *Pk* vs. Sufficient N Control.

Supplementary Figure S4.5. Lipid metabolism overview in roots (microsomal fraction). Data represented are 100% vv. Mapped proteins, log2FC and significances (indicated with asterisks in log2FC column) are shown in Supplementary Table S4.4. MapMan version 3.5.1R2 (Thimm et al., 2004) was used. The following pathways were used and modified: X4.5 Lipid metabolism R5.0. Mapping file was created using Mercator4 V2.0 (Schwacke et al., 2019). Abbreviations: ptFAS, plastidial fatty acid synthase; mtFAS, mitochondrial fatty acid synthase; FAE, fatty acid elongase. Comparisons are mentioned on next to each box: HNC / LNC = Sufficient N Control vs. Limited N Control; LNP / LNC = Limited N + *Pk* vs. Limited N Control; HNP / HNC = Sufficient N + *Pk* vs. Sufficient N Control.

Supplementary Figure S4.6. GO-term analyses (Molecular Function). A) Root GO term analysis; B) Shoot GO term analysis. Only statistical significant proteins were imported into PantherDB statistical enrichment test (Mi et al., 2019), followed by REVIGO (Supek et al., 2011). Log10 (p-values) were used to calculate the %-distribution (x-axis) of GO-terms (y-axis).

List of Supplementary Tables

Abbreviations

%Ndfa	% of nitrogen derived from air
°C	Degree Celsius
^{15}N	Heavy-labelled isotope of nitrogen
2D / 3D	Two-dimensional / Three-dimensional
ACC	1-aminocyclopropane-1-carboxylic acid
ADGGA	Acyl diacylglycerol glucuronide
AMT	Ammonium transporter family
ANOVA	Analysis of variance
Asn	Asparagine
BCA	Bicinchoninic acid assay
BNF	Biological nitrogen fixation
C	Carbon
Ca^{2+}	Calcium
$CaCl_2$	Calcium chloride
CAMK	Ca^{2+}/calmodulin-dependent protein kinase superfamily
CCD	Charge-coupled device
Cer	Ceramides
CFU	Colony forming units
CL	Cardiolipin
cm	Centimetre
cm^2	Square centimetre
CNR	Coleoptile nodal root
$CoCl_2$	Cobalt chloride
CT	Computed tomography
$CuSO_4$	Copper sulfate
CV	Coefficient of variance
Da	Dalton
DAPG	2,4-Diacetylphloroglucinol
DAS	Days after sowing
DDA	Data dependent acquisition

DG	Diacylglycerol
DGDG	Digalactosyldiacylglycerol
DIA	Data independent acquisition
DTT	Dithiothreitol
DW	Dry weight
EDTA	Ethylenediaminetetraacetic acid
ESI	Electrospray ionisation
FA	Fatty acyls
FAE	Fatty acid elongase
Fd	Ferredoxin
FDR	False Discovery Rate
Fe	Iron
$FeSO_4$	Iron sulfate
FW	Fresh weight
FZJ	Forschungszentrum Jülich
g	Gram (weight) / Gravitational constant (centrifuge)
GL	Glycerolipids
Gln	Glutamine
GP	Glycerophospholipids
GPAT	Glycerol-3-phosphate acyltransferase
GS / GLN	Glutamine synthase
GS/GOGAT	Glutamine-synthetase/Glutamate synthase
H	Hydrogen
h	Hours
H_2O	Water
H_3BO_4	Boric acid
HATS	High-affinity transport system
HCA	Hierarchical cluster analysis
HNC	Sufficient Nitrogen control
HNP	Sufficient Nitrogen + *Pk*
hpi	Hours post inoculation

HSV	Hue, Saturation, Value
IAA	Indole acetic acid
IBG	Institute of Bio- and Geosciences
IPA	Isopropyl alcohol
ISR	Induced systemic resistance
JA	Jasmonic acid
KCl	Potassium chloride
KH_2PO_4	Potassium dihydrogen phosphate
LATS	Low-affinity transport system
LB	Luria-Bertani
LC-MS/MS	Liquid chromatography coupled with tandem mass spectrometry
LNC	Limited Nitrogen control
LNP	Limited Nitrogen + *Pk*
LNR	Leaf nodal root
Log2FC	Log2 fold change
LPC	Lysophosphatidylcholine
LPE	Lysophosphatidylethanolamine
LR	Lateral root length
LRR kinase family	Leucine rich repeat kinase family
m	Metre
m/z	Mass to charge
MES	2-(N-morpholino)ethanesulfonic acid
MF	Microsomal fraction
MFS	Major Facilitator Superfamily
mg	Milligram
MGDG	Monogalactosyldiacylglycerol
$MgSO_4$	Magnesium sulfate
min	Minutes
mm	Millimetre
mM	Millimolar
$MnSO_4$	Manganese sulfate

MP	Mobile phase
MS2 or MS/MS	Tandem mass spectrometry
mtFAS	Mitochondrial Fatty Acid Synthesis
N	Nitrogen
N_2	Dinitrogen
Na_2EDTA	Ethylenediaminetetraacetic acid disodium salt
Na_2HPO_4	Disodium hydrogen phosphate
Na_2MoO_4	Sodium molybdate
NaCl	Sodium chloride
NADH	Nicotinamide Adenine Dinucleotide
NaF	Sodium fluoride
ncRNA	Non-coding RNA
NDM	Nitrogen deficient medium
NH_3	Ammonia
NH_4^+	Ammonium
NH_4NO_3	Ammonium nitrate
Nif	Nitrogen-fixing genes
NiR	Nitrite reductase
NO	Nitric oxide
NO_2	Nitrite
NR	Nitrate reductase
NRT	Nitrate transporter family
NUE	Nutrient use efficiency
OD_{600}	Optical density (600 nm)
P	Phosphorus
P. spp.	*Pseudomonas species*
PA	Phosphatidic acids
PBQC	Pooled biological quality controls
PC	Phosphatidylcholine
PCA	Principal component analysis
PCV	Plant cultivation vessel

PE	Phosphatidylethanolamine
PET	Positron emission tomography
PG	Phosphatidylglycerol
PI	Phosphatidylinositol
Pk	*Pseudomonas koreensis Ps9-14T*
PK	Polyketides
PLA / PLC / PLD	Phospholipase A / C/ D
PMI	Plant microbe interaction
PR	Prenol lipids
PSR	Primary seminal root length
ptFAS	Plastidial fatty acid synthesis
RGB	Red, Green, Blue
rpm	Rounds per minute
RT	Room temperature
S	Sulfur
s	Seconds
SA	Salicylic acid
SL	Saccharolipids
Snrk/SnF	Sucrose non-fermenting related protein kinases
SP	Sphingolipids
SQDG	Sulfoquinovosyldiacylglycerol
SSP	Single Superphosphate
ST	Sterol lipids
SWATH	Sequential Window Acquisition of All Theoretical
TG	Triacylglycerol
TRL	Total root length
Tukey's HSD	Tukey's honestly significant differences
UAV	Unmanned aerial vehicle
UHPLC	Ultra-high pressure liquid chromatography
UV	Ultraviolet
V	Volt

v:v	Volume per volume
VOC	Volatile organic compounds
vv	Valid values
w:v	Weight per volume
w:w	Weight per weight
WP	Whole proteome
ZEA-3	Central Institute for Engineering, Electronics and Analytics
$ZnSO_4$	Zinc sulfate
µg	Microgram
µl	Microlitre
µM	Micromolar
µmol	Micromole

Chapter 1

Preface to Chapter 1

This chapter provides an overarching introduction to the topic of plant-microbe interactions, with particular focus on their ability to improve total plant Nitrogen (N) content under limited N conditions.

It covers the entirety of the included manuscripts/published articles and lays out the general questions and aims of the thesis by illustrating the general importance of discovering biological alternatives to synthetic fertilizer usage, thus reducing environmental impact caused by synthesis and application of those fertilizers.

1.1 General introduction

The world population is growing together with the increased food demand. On the other hand, the available arable land is unchanged or decreasing, with often deteriorating soil quality due to overuse. Thus, alternatives have to be found to maintain and further increase food production. In the past, the synthesis of fertilizer via the Haber-Bosch process has led to increased crop productions all over the world. However, the synthesis and application of this synthetic fertilizer comes with a cost. Besides being energy demanding and expensive, the synthesis increases environmental pollution (Smith & Torrente-Murciano (2020); Wang et al., 2021). The application of these fertilizers is causing various environmental hazards, such as eutrophication of freshwater resources, due to extensive application and the inability of plants to take up nitrogen efficiently (Huang et al., 2017). Excessive nitrogen is washed out by rain into the ground water bodies (nitrate leaching), causing the important ground water to become toxic for all living species (Mahvi et al., 2005).

Cereals are among the most important plants to meet the above-mentioned food demand and include different species, such as *Hordeum vulgare*, *Triticum aestivum*, *Oryza sativa* and *Zea mays*. In this thesis, the model plant *Brachypodium distachyon* was cultivated with a focus on vegetative growth. *B. distachyon* is a close relative of the cereals

and can therefore be used to study molecular mechanisms (Draper et al., 2001; Watt et al., 2009; Girin et al., 2014). With a small phenotype, a short generation time and a fully sequenced genome, it is a suitable model organism for studying monocot plant-microbe interactions in a closed growth system, in which biotic and abiotic conditions can be highly controlled (Watt et al., 2009; Girin et al., 2014).

Bacteria of the genus *Pseudomonas* are found all over the world (Trivedi et al., 2020). The strain *Pseudomonas koreensis* Ps9-14T used in this PhD project was first isolated from soils in Korea and characterized by Kwon et al. (2003). It is a 2 µm sized bacterium which is motile with multiple, polar flagella (Kwon et al., 2003). The closest relative *Pseudomonas koreensis* IB-4 shows the potential to fix atmospheric N (Rafikova et al., 2016), while the here used strain Ps9-14T has not been tested as a PGPB yet.

Biological Nitrogen Fixation (BNF) is a process in which organisms fix atmospheric dinitrogen (N_2) via *nif* genes in a complex protein apparatus (Dixon & Kahn 2004). N_2 is converted into NH_3 via the enzyme nitrogenase and protonated to NH_4^+ depending on the pH (Dixon & Kahn 2004; Ishikita & Knapp 2007). Once it is available in the form of NH_4^+, it is suitable for plant uptake and assimilation through dedicated transporters of the Ammonium transporter (AMT) family. The process of N-fixation can be conveyed through nodulating and non-nodulating pathways. N-fixation in nodules is exclusive to legumes and necessitates a specific interaction with bacteria of the genus Rhizobium (Oldroyd et al., 2013; Thiebaut et al., 2022). Rhizobia reside within specialized organs derived from lateral roots known as nodules, which provide an environment ensuring Nitrogenase activity in these bacteria (Drapek et al., 2023). Conversely, diazotrophic non-nodulating bacteria can fix N by colonizing the root interior (endophytic), associating with the root surface, or existing as free-living organisms in the rhizosphere (Carvalho et al., 2016; Thiebaut et al., 2022).

For plants, two main forms of mineral N are available for uptake via ammonium transporters (AMT) and nitrate transporters (NRT). While transporters of the NRT family can be distinguished into low- and high affinity transport systems (LATS and HATS, respectively), transporters of the AMT family are predominantly HATS due to low external

NH_4^+ concentrations in soils (Crawford & Glass (1998); Bajgain et al., 2018). Nitrate first needs to undergo a two-step conversion to nitrite (NO_2^-) via the enzyme Nitrate reductase (NR), followed by conversion to ammonium (NH_4^+) via the enzyme Nitrite reductase (NiR). At this point, NH_4^+ can be assimilated via plastidial isoforms of the enzyme glutamine synthase (GS or GLN), which can subsequently be further processed by the Glutamate synthethase (GOGAT) (Balotf & Kholdebarin 2016). NH_4^+ deriving from AMT uptake can directly be assimilated via cytosolic isoforms of GS or GLN, followed by further assimilation via the GOGAT enzymes (Balotf & Kholdebarin 2016).

1.2 Aim of this thesis (Objectives)

During my previous study (M.Sc.), I tested the influence of *Pseudomonas koreensis* Ps9-14T (hereafter, referred to as *Pk*) on *Brachypodium distachyon* (Bd21-3) under two N levels (limited / low and sufficient / high N) in an open growth system (hydroponics). Since plants showed an improved overall phenotype and promising growth promotion, it was decided that it would be interesting to further investigate the underlying molecular mechanisms during this plant-microbe interaction. In a supplementary study (Kuang et al., 2022), we found that precise control of the abiotic environment allowed us to identify two potential modes of interaction, dependent on nitrogen availability. Therefore, my project aimed to establish the plant-microbe interaction in a controlled environment, using a plant culture vessel (PCV) system as published earlier (Hassi et al., 2023) with some modifications (Fig. 3.3).

The aim of this thesis was to determine the changes on protein and lipid level in *Brachypodium distachyon* inoculated with *Pseudomonas koreensis* under two N levels (limited and sufficient N). With the descriptive data generated within this study, putative candidates responding in this plant-microbe interaction can be identified for further investigation to determine their function in a targeted manner. In future studies, the allelic diversity of the candidate genes could be explored in diverse crop panels to assess their impact on plant performance in the presence or absence of Pseudomonas. Furthermore, using clustered regularly interspaced palindromic repeats (CRISPR)-Cas9 knockout mutants of the candidate genes could provide additional insights into the

underlying processes, potentially identifying key transcription factors involved in this plant-microbe interaction. Although this thesis primarily examines N-related metabolic pathways, it's important to recognize that other pathways, such as hormonal pathways, may also play a significant role in this interaction, potentially enhancing overall plant sustainability. Once these complex processes are understood in *Brachypodium distachyon*, the knowledge could then be transferred to important cereals, such as barley, maize, rice, sorghum, and wheat. If plant growth promotion can be observed in those plants, it could further be tested whether the plant-microbe interaction is also suitable for agricultural application to reduce fertilizer input and thus decrease environmental impact.

To achieve these aims, the thesis is structured to answer the following objectives:

1. Test the N-fixing ability of *Pseudomonas koreensis.*
2. Investigate morphological, nutritional, and physiological effects of the inoculation in Brachypodium.
3. Investigate the molecular mechanisms of Brachypodium acclimation to beneficial microbes using proteomics (whole proteome).
4. Investigate the changes in membrane-bound proteins, including transporters (microsomal enrichment) in Brachypodium.
5. Investigate the changes in the lipid profile in Brachypodium using lipidomics.

1.3 Chapter synopsis (with COVID-19 impacts)

Chapter 2 of the thesis contains the literature review and more detailed introduction into the topic of plant-Pseudomonas interactions. This chapter was published in the journal Molecular Plant Microbe Interactions (MPMI) (Sanow, S., Kuang, W., Schaaf, G., Huesgen, P., Schurr, U., Roessner, U., Watt, M. & Arsova, B. (2023). Molecular mechanisms of Pseudomonas assisted plant nitrogen uptake-opportunities for modern agriculture. Molecular Plant-Microbe Interactions, (https://doi.org/10.1094/MPMI-10-22-0223-CR)). The aim of this chapter is to summarize the current knowledge on Pseudomonas-driven plant beneficial interactions, with particular focus on the interaction of plant-microbes.

Chapter 3 describes the main experiments conducted during this thesis and addresses the main objectives of the thesis. The N-fixing capability of *Pseudomonas koreensis* was tested using the ^{15}N natural abundance method. To test the response of *B. distachyon* roots on biotic (bacteria) and abiotic (N) factors, plants were grown in self-modified sterile systems using sand, with the aim to quantify the plant's physiological response and generate sufficient plant material for morphological and biochemical analyses in Chapter 4. Chapter 3 includes non-invasive shoot and invasive whole-plant phenotyping, including (projected) leaf area, root length, fresh weight, dry weight, and C & N content. In this chapter, three independent experiments were conducted: (i) ^{15}N natural abundance, (ii) time-series experiment and (iii) plant growth for proteomics. The time-series experiment was used for time-resolved phenotyping with three consecutive harvests at 19, 20 and 21 DAS, and was also the basis for the time-resolved lipidomics data in Chapter 4.

Chapter 4 describes the biochemical analyses to elucidate the molecular mechanism in this plant microbe interaction. The time-series experiment did not yield enough material for phenotyping, proteomics and lipidomics in one batch, thus an independent experiment was conducted for proteomics, with a 21 DAS end-point harvest only. This was required to meet the high initial biomass demands for microsomal enrichment and whole-proteome analyses. This chapter integrates the biochemical data with the obtained phenotyping data in Chapter 3.

Chapter 3 and 4 were strongly affected by the COVID-19 pandemic. During the early stages (optimisation of protocols), lockdowns and limited access to the Forschungszentrum Jülich campus slowed down the progress. Additionally, reduced staff resources led to more delays, including the ordering of consumables (supply chain issues), working at other institutes (ZEA-3) and communication (written only). A LC-MS/MS break down during the pandemic caused further delays in optimisation of the proteomics platform, as service and repair required more time, causing further delays as samples for measurements were queueing up. The pandemic caused a drastically shortened stay at the partner institution (University of Melbourne), which was shortened from 12 months (expected during my 2nd year) to 2 months at the end of my 3rd year (Dec. 2022 – early

Feb 2023). As a consequence, my proteomics samples were only completed at the end of my contract, and the lipidomics only focused on the roots.

Chapter 5 summarizes and integrates all the outcomes of the previous chapters. This chapter provides reasoning for the proposed beneficial effects of microbial application on nitrogen deficiency, connecting morphological with biochemical phenotypes. Future directions for further studies are suggested.

1.4 References

Bajgain, P., Russell, B., & Mohammadi, M. (2018). Phylogenetic analyses and in-seedling expression of ammonium and nitrate transporters in wheat. Scientific reports, 8(1), 7082.

Balotf, S., Kavoosi, G., & Kholdebarin, B. (2016). Nitrate reductase, nitrite reductase, glutamine synthetase, and glutamate synthase expression and activity in response to different nitrogen sources in nitrogen-starved wheat seedlings. Biotechnology and applied biochemistry, 63(2), 220-229.

Carvalho, T. L. G., Ballesteros, H. G. F., Thiebaut, F., Ferreira, P. C. G., & Hemerly, A. S. (2016). Nice to meet you: genetic, epigenetic and metabolic controls of plant perception of beneficial associative and endophytic diazotrophic bacteria in non-leguminous plants. Plant molecular biology, 90, 561-574.

Crawford, N. M., & Glass, A. D. (1998). Molecular and physiological aspects of nitrate uptake in plants. Trends in plant science, 3(10), 389-395.

Dixon, R., & Kahn, D. (2004). Genetic regulation of biological nitrogen fixation. Nature Reviews Microbiology, 2(8), 621-631.

Drapek, C., Radzman-Mohd, N. A., Rizza, A., Schiessl, K., Dos Santos Barbosa, F., Wen, J., Oldroyd, G. E.D. & Jones, A. M. (2023). Cellular gibberellin dynamics govern indeterminate nodule development, morphology and function. bioRxiv, 2023-09.

Draper, J., Mur, L. A., Jenkins, G., Ghosh-Biswas, G. C., Bablak, P., Hasterok, R., & Routledge, A. P. (2001). Brachypodium distachyon. A new model system for functional genomics in grasses. Plant physiology, 127(4), 1539-1555.

Girin, T., David, L. C., Chardin, C., Sibout, R., Krapp, A., Ferrario-Méry, S., & Daniel-Vedele, F. (2014). Brachypodium: a promising hub between model species and cereals. Journal of experimental botany, 65(19), 5683-5696.

Hassi, U., Hu, J., Sleutel, S., & De Neve, S. (2023). Recovery of soil microbial community structure and activity following partial sterilization with gamma irradiation. Applied Soil Ecology, 187, 104839.

Huang, J., Xu, C. C., Ridoutt, B. G., Wang, X. C., & Ren, P. A. (2017). Nitrogen and phosphorus losses and eutrophication potential associated with fertilizer application to cropland in China. Journal of Cleaner Production, 159, 171-179.

Ishikita, H., & Knapp, E. W. (2007). Protonation states of ammonia/ammonium in the hydrophobic pore of ammonia transporter protein AmtB. Journal of the American Chemical Society, 129(5), 1210-1215.

Kwon, S. W., Kim, J. S., Park, I. C., Yoon, S. H., Park, D. H., Lim, C. K., & Go, S. J. (2003). Pseudomonas koreensis sp. nov., Pseudomonas umsongensis sp. nov. and Pseudomonas jinjuensis sp. nov., novel species from farm soils in Korea. International journal of systematic and evolutionary microbiology, 53(1), 21-27.

Mahvi, A. H., Nouri, J., Babaei, A. A., & Nabizadeh, R. (2005). Agricultural activities impact on groundwater nitrate pollution. International Journal of Environmental Science & Technology, 2, 41-47.

Oldroyd, G. E. (2013). Speak, friend, and enter: signalling systems that promote beneficial symbiotic associations in plants. Nature Reviews Microbiology, 11(4), 252-263.

Rafikova, G. F., Korshunova, T. Y., Minnebaev, L. F., Chetverikov, S. P., & Loginov, O. N. (2016). A new bacterial strain, Pseudomonas koreensis IB-4, as a promising agent for plant pathogen biological control. Microbiology, 85, 333-341.

Smith, C., Hill, A. K., & Torrente-Murciano, L. (2020). Current and future role of Haber–Bosch ammonia in a carbon-free energy landscape. Energy & Environmental Science, 13(2), 331-344.

Thiebaut, F., Urquiaga, M. C. D. O., Rosman, A. C., da Silva, M. L., & Hemerly, A. S. (2022). The Impact of Non-Nodulating Diazotrophic Bacteria in Agriculture: Understanding the Molecular Mechanisms That Benefit Crops. International Journal of Molecular Sciences, 23(19), 11301.

Wang, M., Khan, M. A., Mohsin, I., Wicks, J., Ip, A. H., Sumon, K. Z., ... & Kibria, M. G. (2021). Can sustainable ammonia synthesis pathways compete with fossil-fuel based Haber–Bosch processes?. Energy & Environmental Science, 14(5), 2535-2548.

Watt, M., Schneebeli, K., Dong, P., & Wilson, I. W. (2009). The shoot and root growth of Brachypodium and its potential as a model for wheat and other cereal crops. Functional Plant Biology, 36(11), 960-969.

Chapter 2

Preface to Chapter 2

This chapter summarizes the current knowledge on plant-*Pseudomonas* interactions.

This work has been published in the journal Molecular Plant Microbe Interactions (MPMI) with the title “Molecular mechanisms of *Pseudomonas* assisted plant nitrogen uptake – opportunities for modern agriculture” (Sanow, S., Kuang, W., Schaaf, G., Huesgen, P., Schurr, U., Roessner, U., Watt, M., & Arsova, B. (2023). Molecular mechanisms of *Pseudomonas* assisted plant nitrogen uptake-opportunities for modern agriculture. *Molecular Plant-Microbe Interactions*, (https://doi.org/10.1094/MPMI-10-22-0223-CR).). It is presented in Chapter 2 in the publication format. I contributed 80% of the work, which includes preparation of the figures, literature review and writing of the manuscript.

As published in MPMI (2023)

Molecular mechanisms of *Pseudomonas* assisted plant nitrogen uptake - opportunities for modern agriculture.

Sanow, S.[1,6], Kuang, W.[2], Schaaf, G.[4], Huesgen, P.[3], Schurr, U.[1], Roessner, U.[5], Watt, M.[6] and Arsova, B.[1] *

[1] Institute for Bio- & Geosciences, Plant Sciences (IBG-2), Forschungszentrum Juelich GmbH, Germany

[2] College of life and Environmental Sciences, Hunan University of Arts and Science, China

[3] Central institute for Engineering, Electronics and Analytics (ZEA-3), Forschungszentrum Juelich GmbH, Germany

[4] Institute of Crop Science and Resource Conservation, University of Bonn, 53115 Bonn, Germany

[5] Research School of Biology, The Australian National University, Acton, 2601 ACT, Australia

[6] School of BioSciences, Faculty of Science, The University of Melbourne, Parkville, 3010 Victoria, Australia

* Corresponding author: B. Arsova; E-Mail: b.arsova@fz-juelich.de

Abstract

Pseudomonas spp. make up 1.6% of the bacteria in the soil and are found throughout the world. More than 140 species of this genus have been identified, some beneficial to the plant. Several species in the family Pseudomonadaceae, including *Azotobacter vinelandii* AvOP, *Pseudomonas stutzeri* A1501, *Pseudomonas stutzeri* DSM4166, *Pseudomonas*

szotifigens 6HT33bT and *Pseudomonas* sp. K1 can fix nitrogen from the air. The genes required for these reactions are organized in a nitrogen fixation island, obtained via horizontal gene transfer from *Klebsiella pneumoniae*, *Pseudomonas stutzeri* and *Azotobacter vinelandii.* Today, this island is conserved in *Pseudomonas spp.* from different geographical locations, which in turn have evolved to deal with different geo-climatic conditions.Here, we summarize the molecular mechanisms behind *Pseudomonas* driven plant growth promotion, with particular focus on improving plant performance at limiting nitrogen (N) and improving plant N content. We describe *Pseudomonas*-plant interaction strategies in the soil, noting that the mechanisms of denitrification, ammonification, and secondary metabolite signalling are only marginally explored. Plant growth promotion is dependent on the abiotic conditions, and differs at sufficient and deficient N. The molecular controls behind different plant response are not fully elucidated. We suggest that superposition of transcriptome, proteome, and metabolome data and their integration with plant phenotype development through time will help fill these gaps. The aim of this review is to summarize the knowledge behind *Pseudomonas* driven nitrogen fixation and to point to possible agricultural solutions.

Keywords: *Pseudomonas*, Plant Growth Promoting Bacteria, N-fixation, Biological Nitrogen Fixation, molecular mechanism.

Introduction: the paradox of nitrogen fertilizers

Synthesised fertilizers containing nitrogen (N) have become obligatory in today's agriculture to meet global food demand (Erisman et al., 2008). N-fertilizer production is one of the most important innovations for humanity allowing to feed an increasing world population. A conservative study estimates that a majority of today's population (7.75 billion), relies on mineral fertilizer (Fig. 2.1, Erisman et al., 2008).

However, mineral fertilizer is a double-edged sword creating a number of problems inherent to its production and use. First, N fertilizer production by the Haber-Bosch process is energy intensive and currently still driven by fossil fuels resulting in greenhouse gas emissions (Smith et al., 2020). Second, in addition to the growing price of fertilizer, a looming problem is excessive nitrogen use that can lead to nitrate leaching

into ground water, or depending on soil pH, redox potential and microbial activity to NH_3 or N_2O emissions causing N losses and environmental pollution (Ravishankara 2009, Hirel et al., 2011; Padilla et al., 2018, Klimczyk et al. 2021). Thus, governments have started to restrict application of N fertilisers (Bundesministerium für Ernährung und Landwirtschaft (BMEL), 2020). Recent global events like the pandemic, the Russian invasion of Ukraine and the consequent rising of energy prices by 80% during 2021 not only increased fertilizer prices (Hassen & Bilali 2022), but more importantly affected the fertilizer export chains. This in turn threatens the productivity of agriculture in other parts of the world (Mustafa, 2022; Jagtap et al., 2022). In the future, the invasion of Ukraine is expected to put further pressure on fertilizer availability (Jagtap et al., 2022).

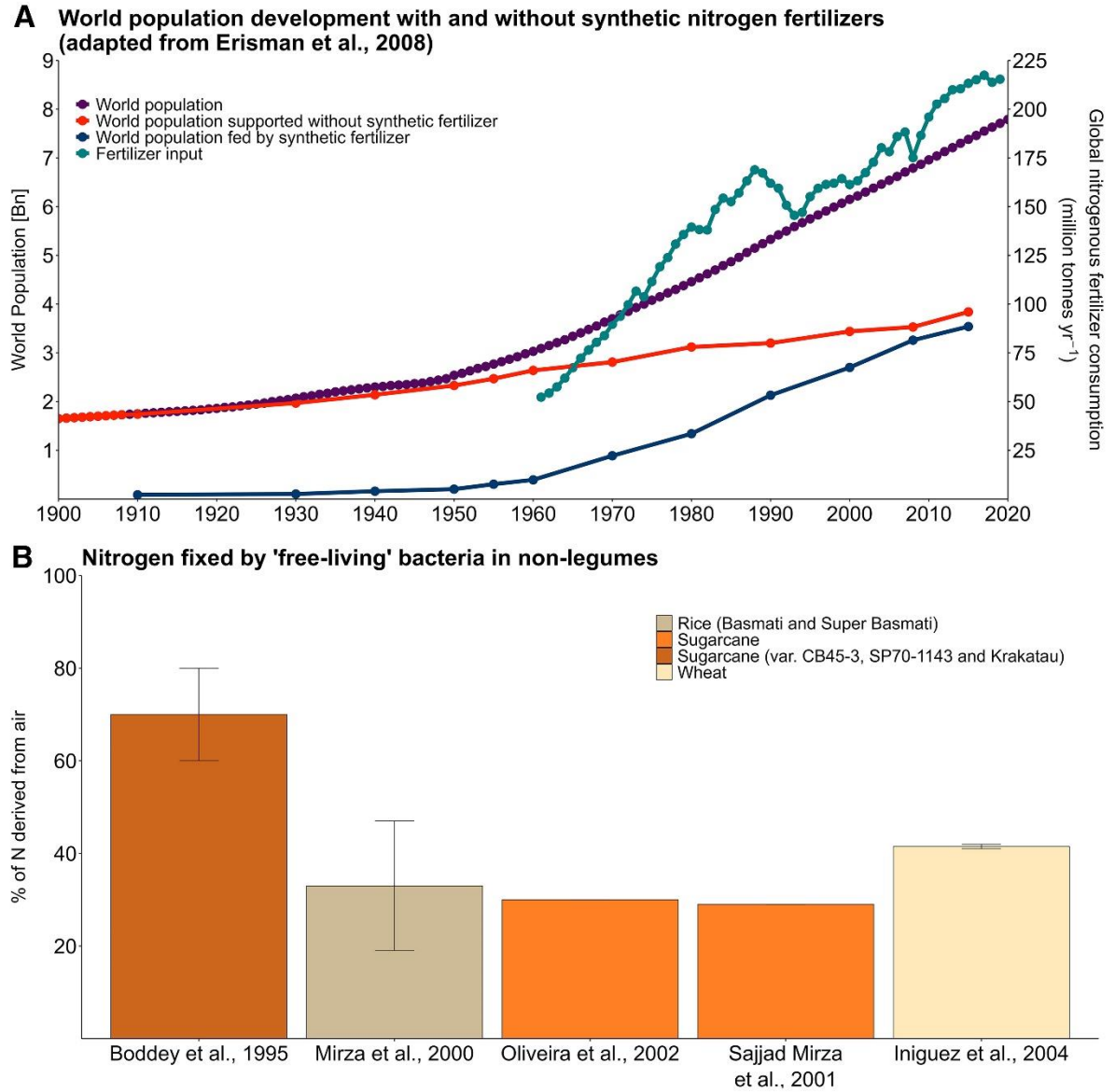

Figure 2.1. A, World population development with and without the support of synthetic fertilizer during the 20th century, as calculated, simulated, and estimated by Erisman et al. 2008 and the United States Department of Agriculture. The purple line represents world population development, while the red line represents the estimated global population that could be fed without the invention of reactive nitrogen from the Haber-Bosch process. The blue line provides the estimated global population that is fed by synthesized nitrogen. The global consumption of nitrogenous fertilizer in million ton per year is represented in teal. **B,** Nitrogen fixed by 'free-living' bacteria in non-legumes, especially in rice, wheat, and sugarcane variants. Free-living bacteria used in the studies involve *Acetobacter* spp., *Azospirillum* spp., *Burkholderia* spp., *Enterobacter* sp., *Herbaspirillum* spp., and *Klebsiella* sp. Data shown are the average percentages of N content in plants derived from the air via biological nitrogen fixation (BNF) of the bacteria. Error bars are the standard error, representing the range of contribution to total N content via BNF data from Boddey et al. 1995, Mirza et al. 2000, Sajjad Mirza et al. 2001, Oliveira et al. 2002, and Iniguez et al. 2004.

Restricted N fertiliser use may eventually result in lower yields in existing farming systems, with today's crop cultivars and soil management practices. An estimate from the EU is that the caps led to a 10 - 15.9% yield reduction in wheat over the past six years (Bundesministerium für Ernährung und Landwirtschaft (BMEL), 2020). This will cause less food production and increased prices unless new reliable solutions are found through more nutrient efficient plant varieties, new farming practices, or new biological N-fixation associations that are reliable across a variety of field conditions.

Nitrogen (N) is a crucial nutrient for plants, incorporated as the main building block of amino acids, proteins, and many secondary metabolites. In most agricultural systems N deficiency plays a major role in plant growth limitation (Bakkou 2011). It is mainly available to the plant in two distinct forms: ammonium (NH_4^+) or nitrate (NO_3^-). Ammonium is be taken up by plants via the AMT/MEP/Rh-type ammonium transport system. Studies in Arabidopsis place most AMTs in the root, contributing to ammonium uptake. One has been found in pollen and one AMT2.1 contributing to xylem loading and root to shoot ammonium transport (Giehl et al., 2017; Bindel et al 2021). In Rice, AMT1.1 and AMT1.3, contribute to ammonium uptake under limited nitrogen conditions and in case of AMT1.3 also under sufficient nitrogen conditions (Ranathunge et al., 2014). While ammonium can be directly assimilated to glutamine in the root, nitrate is first transported to the shoot and reduced to ammonium by nitrate- and nitrite- reductase. Nitrate can be taken up by plants via the nitrate transport system (Bock & Wagner (2001); Daims et al., 2015). Among the multiple nitrate transporters, we mention NRT2.1 as an important component of the inducible high-affinity transport system for NO_3^- in the root (Cerezo et al., 2001; Filleur et al., 2001; Li et al., 2007; Trinh et al., 2018). NRT2.1 is induced by NO_3^-,

but strongly repressed by high N supply to the plant (Lejay et al., 1999; Zhuo et al., 1999; Filleur et al., 2001; Girin et al., 2007), which leads to an altered root system based on nutrition. During N-deficiency, the higher abundance of NRT2.1 leads to lateral root initiation, coordinating the development of lateral roots and therefore increases N uptake (Remans et al., 2006). An interaction with a partner protein, NAR2.1, is required for NRT2.1 to transport NO_3^- (Okamoto et al., 2006; Orsel et al., 2006). Plants are also able to take up certain organic N-compounds such as urea, amino acids, nucleic acids and small peptides that are naturally present in soils or are added as fertilisers as is the case for urea (Sopanen et al., 1977; Owen and Jones, 2001; Liu et al. 2003, Waterworth et al. 2006 Merígout et al., 2008, Girke et al. 2014 Beier et al. 2019). Molecular nitrogen is abundant in the atmosphere (78.1%), and is accessible to certain bacterial strains, which can fix it for their own use. As such it presents an untapped resource that can be used for agriculture. Symbiotic biological nitrogen fixation (BNF) in nodules converts atmospheric nitrogen (N_2) into ammonia (NH_3), which is subsequently protonated to ammonium (NH_4^+) upon export in the peribacteroid space, which is in an acidic pH range (Lam et al., 1996; Day et al., 2001; Raymond et al., 2004; Franche et al., 2009). Free-living bacterial nitrogen fixation results in ammonia (Smercina et al., 2019), which can either be protonated in the soil to ammonium (requires acidic environment) or converted to nitrate via nitrifiers. Subsequently, second reduction of nitrate to ammonium is performed by plant metabolism, as explained above. Ammonia-oxidizing bacteria, Archea and nitrite-oxidizing bacteria, such as *Nitrospira* bacteria, can either convert (i) ammonia to nitrite and in a consecutive step to nitrate or (ii) ammonia directly to nitrate via the enzymes ammonia monooxygenase or nitrite oxidoreductase, respectively (Daims et al., 2015). The ammonia used during nitrification is not necessarily derived from BNF. One of the best studied group of plants, that form symbiotic relationships with rhizobacteria are legumes. Readers interested in nodule-related processes can consult Gautrat et al., (2020) and Etesamy and Adl (2020). Here we will focus on non-legumes and so called “free-living” plant associated microorganisms from the genus *Pseudomonas*. Historically, there are numerous examples of transfer of N from bacteria to plants in non-legume systems (Fig. 2.1 B), however the potential is not fully exploited yet. We propose that a greater understanding of the molecular mechanisms in the interaction between N-fixing

Pseudomonas spp. and the plant is crucial for further development of their application in agriculture.

Plant growth promotion by bacteria of the genus *Pseudomonas*

Pseudomonas spp., make up 1.6% of the bacteria in the soil and are found in all areas in the world (Trivedi et al., 2020). They attract major attention due to their various growth promoting characteristics, good root colonisation, and production of enzymes and metabolites that positively impact plant growth (Kloepper et al., 1989; Glick and Bashan 1997; Ramamoorthy et al, 2001; Podile and Kishore, 2007; Saharan et al., 2011). The means by which beneficial *Pseudomonas spp. (P. spp.)* promote the growth of the host plants can be categorised into three areas (Fig. 2.2). The first is by producing plant growth regulators, such as gibberellin, auxins (IAA) and the cytokinin - zeatin. IAA increases seedling root growth and thus nutrient foraging. Often, the increase in IAA comes with a higher abundance of the enzyme 1-aminocyclopropane-1-carboxylate (ACC) deaminase, which lowers the increased ethylene levels caused by stress, resulting in e.g. an increased salt stress tolerance (IAA, ACC-deaminase) (Egamberdieva et al., 2009; Nadeem et al., 2010; Glick et al., 2014). *P. spp.* can alter salicylic acid (SA) and jasmonic acid (JA) pathways in the plant leading to induced systemic resistance (ISR) (Glick et al., 1995; Glick et al., 1999; Ryu et al., 2003). The second way by which *P. spp.* can influence plants is through volatile organic compounds produced by *P. spp.* These include geosmin, 2,3-butanediol, acetoin and tridecane, which can promote plant growth (Panpatte et al., 2017). Other *P. spp.* can produce compounds for biocontrol, including methanethiol, dimethyl sulfite and dimethyl trisulfite (Panpatte et al., 2017). Finally, the third way is by *P. spp*. increasing the availability of nutrients in the rhizosphere by nitrogen fixation, phosphate solubilisation or siderophore production, making more N, P and Fe, respectively, available to plants (Fig. 2.2; Kloepper et al., 1989; Walter et al., 1994; Glick et al., 1995; Glick et al., 1999; Richardson (2001); Vessey 2003; Nadeem et al., 2010; Liu et al, 2017).

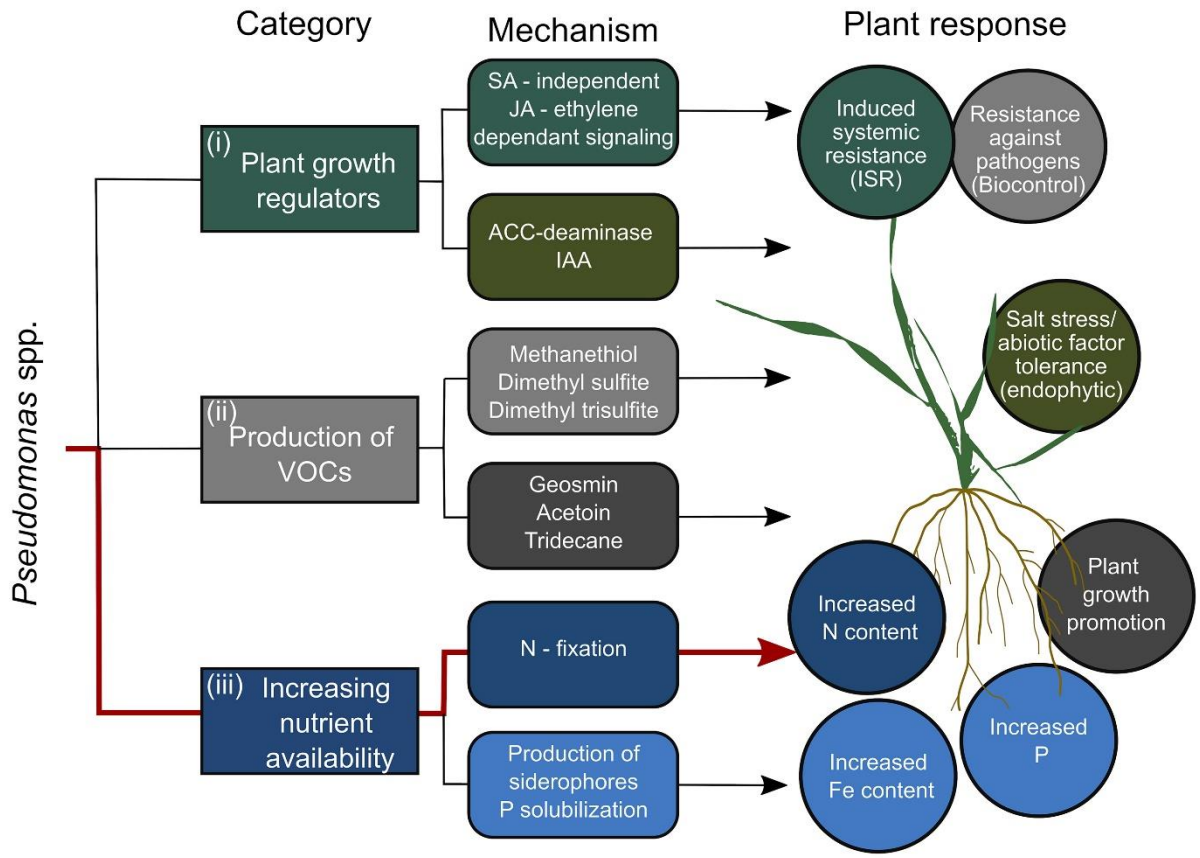

Figure 2.2. Overview of plant growth promoting traits by *Pseudomonas* spp. Beneficial pseudomonads can interact with plants by i) regulating plant growth via the hormonal pathways, ii) producing volatile organic compounds (VOCs), and iii) increasing nutrient availability, resulting in various plant growth promoting traits, increased resistance against diverse pathogens and abiotic factor tolerance. SA = salicylic acid, JA = jasmonic acid, ACC = 1-aminocyclopropane-1-carboxylic acid, IAA = indole acetic acid.

Pseudomonas **driven soil nitrogen biochemistry, relevant for improvement of plant N**

Pseudomonas spp. can improve the availability of inorganic N to roots by three main strategies exemplified in Fig. 2.3. These are: (i) ammonification of organic N (e.g. by *P. psychrotolerans*, Kang et al., 2020), (ii) Stimulation of adjacent bacterial strains to increase N- fixation (e.g. between *P. fluorescens* and *A. brasilense*, Combes-Meynet et al., 2011), and (iii) production and release of NH_4^+ in the rhizosphere (e.g. by *P. stutzeri*, Zhang et al., 2012).

(i) Ammonification and denitrification

The process of ammonification allows the conversion of organic nitrogen (amino acids, amino sugars, urea, nucleotides) into NH_4^+ (Song & Tobias 2011), which contributes to an increase of plant-available N in the soil (Fig. 2.3(i), Fig. 2.4, Kang et al., 2020). On the other hand, denitrification decreases the amount of NO_3^- in the soil by reducing NO_3^- to $N_2O_{(g)}$ and $N_{2(g)}$ (Fig. 2.4). Until 2016, it was widely believed that denitrification and ammonification did not occur within the same bacterium. However, Torres et al. (2016) show that at least three bacteria (*Opitutus terrae* strain PB90-1, *Marivirga tractuosa* strain DSM 4126 and *Gammaproteobacterium Sh. Loihica* strain PV-4) contain the complete set of genes for denitrification and respiratory ammonification based on genome analyses (Sanford et al., 2012; Torres et al., 2016). Interestingly *P. psychrotolerans* CS51 also contains genes for both processes: Kang et al. (2020) found that ammonification would be possible via the three nitrate ABC transporter genes and *NasT (response regulator),* while denitrification via the genes nitrite reductase (*nirB*), nitrate reductase (*napA*) and nitric oxide reductase (*norB*) (Kang et al., 2020). The enzymes nirB, napA and norB convert nitrate to nitrite to nitric oxide and finally to nitrous oxide (N_2O), notably nosZ -for the conversion to gaseous nitrogen, was not found (Smith et al., 2007; Wang et al., 2017; Kang et al., 2020). Additionally, the genes involved in ammonia assimilation *GlxC* (*Glutamate synthase [NADPH] putative GlxC chain* (EC 1.4.1.13)) and *GlxB* (Glutamine amidotransferase protein GlxB (EC 2.4.2.-)) have been found in the genome of *P. psychrotolerans* (Kang et al., 2020). This leads to the hypothesis that *P. psychrotolerans* CS51 could also perform both ammonification and denitrification.

(ii) Production of secondary metabolites that stimulate N-fixation in adjacent bacterial strains

In the case of *Pseudomonas fluorescens* F113 and *Azospirillum brasilense* S245, Combes-Meynet *et al.* (2011) found an example of positive interaction, where one strain stimulates N-fixation in another. *Pseudomonas fluorescens* F113 produces a secondary metabolite, 2,4-diacetylphloroglucinol (DAPG), that acts as a signal for *Azospirillum brasilense* S245.

When *A. brasilense* detects DAPG, it upregulates the *nirK* and *nifX-nifB* genes, which leads to increased nitrogen fixation. This was demonstrated by co-inoculating wheat with both strains (Combes Meynet et al., 2011) (Fig. 2.3 (ii), Fig. 2.4, Table 2.1). Sequence analysis of DAPG-induced promotors, followed by functional prediction of the corresponding downstream ORF identified that their deduced protein sequences is homologous to the nitrogen-fixation genes nifX-nifB (Rubio & Ludden 2008; Combes-Meynet et al., 2011). This highlights the importance of using bacterial combinations (communities) where the members function in an additive manner to unlock their full potential. It needs to be kept in mind however that, using bacterial inoculants in the field will lead to interactions with the native microbiome. While the full extent of the interactions is not clear, we speculate that there might be events where inoculants may become overrun by the native microbial varieties or like in the case of *P. taiwanensis* used for maize inoculation and *P. fluorescens* LBUM677 and oilseed crops, there might be changes in the microbiome around the plant roots (Jiménez *et al*., 2020, Chaudhary *et al.*, 2021). Further understanding of the suitability of inoculants to specific soil environments is needed to ensure reproductive results in the field.

(iii) Production and release of NH_4^+ via Biological Nitrogen Fixation in *Pseudomonas*

Another step of enhancing the N available for plants is achieved by ammonium excretion of bacteria (Fig. 3 (iii)). The step of ammonification, oxidation of organic N to ammonium, releases energy for metabolic processes. The excess ammonium will be excreted by the microorganism to avoid ammonium toxicity and can either be used for nitrification or taken up by the plant via dedicated AMT transporters (if excreted by root-associated bacteria). The *Pseudomonas* genes *amtB1* and *amtB2* have been demonstrated to regulate the internal ammonia pool and excretion of ammonium (Zhang et al., 2012) (Table 2.1). A *P. stutzeri* strain A1501 mutant expressing *nifA* constitutively showed an increased ammonia excretion. Coincidently, no increase in nitrogenase activity was detected, leaving the role of constitutively expressed *nifA* unclear (Zhang et al., 2012).

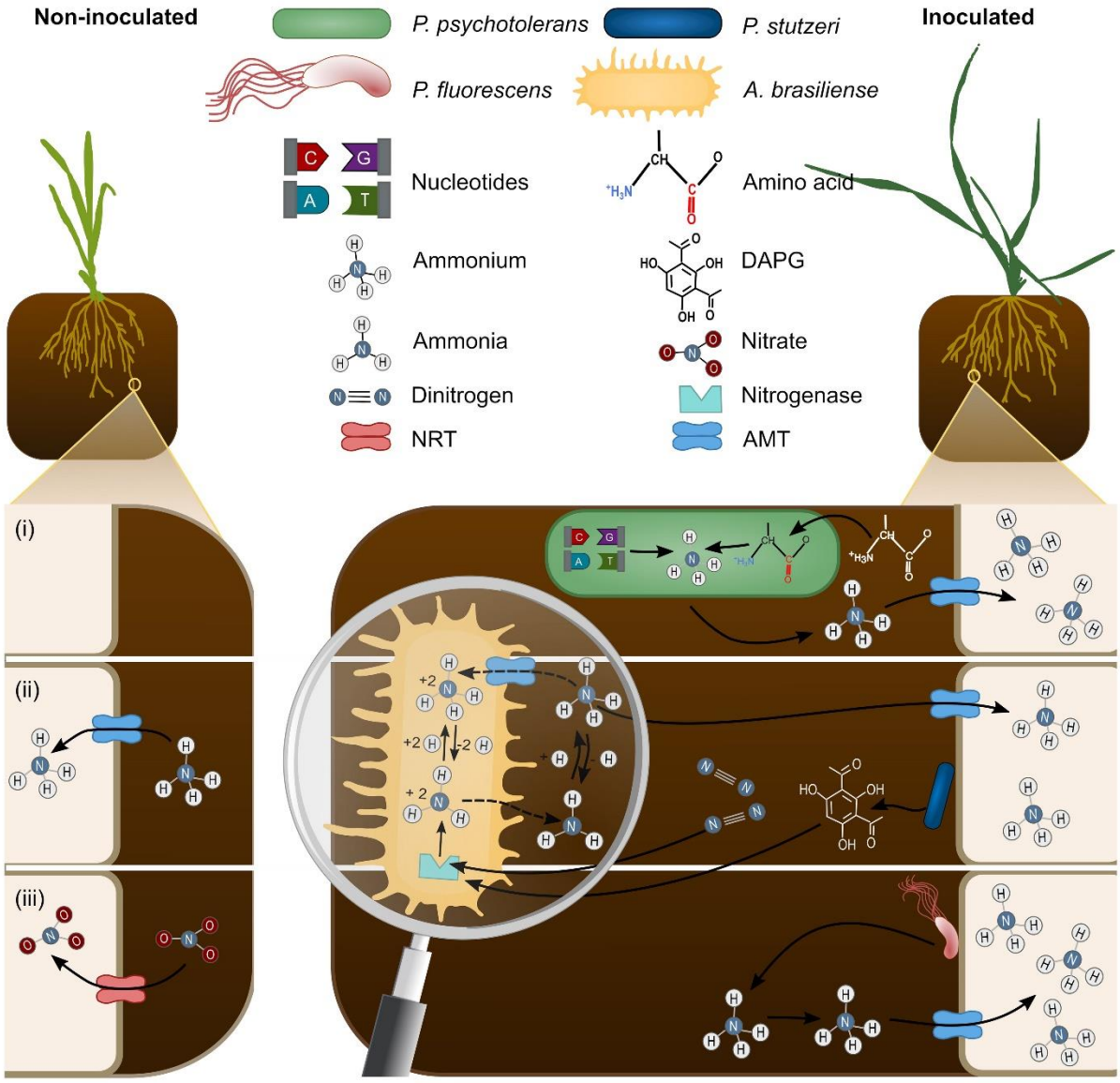

Figure 2.3. Conceptual figure of shared nitrogen biochemistry and transport across root and bacterial cells in the rhizosphere. Bacterial processes that impact plant N content. The left side represents plants growing on limited N resulting in a decreased aerial biomass and increased root growth, whereas the right side represents potential plant growth-promoting mechanisms by *Pseudomonas* species increasing the aerial biomass under the same limited N conditions. Ammonium (NH_4+) and nitrate (NO_3-) are taken up by the plant via dedicated transporters of the AMT and NRT families, respectively (Bock and Wagner 2001; Daims et al. 2015). Plant growth-promoting bacteria increase availability of inorganic N to plants via following mechanisms: i) ammonification of organic N by *Pseudomonas psychrotolerans* (Kang et al. 2020), ii) *Pseudomonas stutzeri* upregulating *nif* genes in *Azospirillum brasilense* via 2,4-diacetylphloroglucinol (DAPG), resulting in the conversion of N_2 into NH_4+ (biological nitrogen fixation) (Day et al. 2001; Combes-Meynet et al. 2011) and iii) production and release of NH_4+ by *P. fluorescens* (Zhang et al. 2012). Dashed lines indicate reactions from or to the bacterium that occur based on the concentration of each reaction product in the respective space and pH of the environment.

Pseudomonas genetic machinery that could provide alternative Nitrogen

Diazotrophic bacteria fix nitrogen via proteins encoded by the nitrogenase gene cluster, and the organisation, abundance and regulation of nitrogen-fixation related genes is different from species to species (Yan et al., 2008). Several species in the family of Pseudomonaceae, including *Azotobacter vinelandii* AvOP, *Pseudomonas stutzeri* A1501, *Pseudomonas stutzeri* DSM4166, *Pseudomonas szotifigens* 6HT33bT and *Pseudomonas* sp. K1 have been demonstrated to be capable of nitrogen fixation (Setten et al., 2013).

Specific to *Pseudomonas*, a nitrogen-fixation island (NFI) was discovered and found to be conserved in *P. stutzeri* strains from geographically close (<300 km within Greece) or distant (China, Germany, Greece) locations (Venieraki et al., 2014). The NFI was presumably acquired by lateral gene transfer of a common ancestor of *Klebsiella pneumoniae*, *Pseudomonas stutzeri* and *Azotobacter vinelandii* and inserted between cobalamin synthase (*cobS*) and glutathione peroxidase (*gspH*) (Yan et al., 2008, Setten et al., 2013).

The size of the NFI in *P. stutzeri* is about 49 kb and contains 52 *nif*-related genes, which are organized into 11 putative NifA-σ54-dependent operons (Table 1, Yan et al., 2010; Yang et al., 2018). The σ54 transcription factor (or RpoN) is a well-known alternative factor for RNA polymerase that enables the transcription of *nif* genes in conjunction with the transcriptional activator NifA or activates other genes involved in nitrogen metabolism and functions with the nitrogen regulatory protein C (NtrC), the *psp* operon transcriptional activator (*pspF*) and C4-dicarboxylate transport transcriptional regulatory protein DctD (Yan et al., 2010). *Pseudomonas protegens* Pf-5 was genetically modified to contain the X940 cosmid, that includes all genes, numbered from PST1302-PST1359), from the nitrogen fixation island of *P. stutzeri* A1501. X940 with nitrogenase activity was transferred to various other *Pseudomonas spp.*, including *P. putida*, *P. veronii*, *P. taetrolens*, *P. balearica* and *P. stutzeri* (Setten et al., 2013).

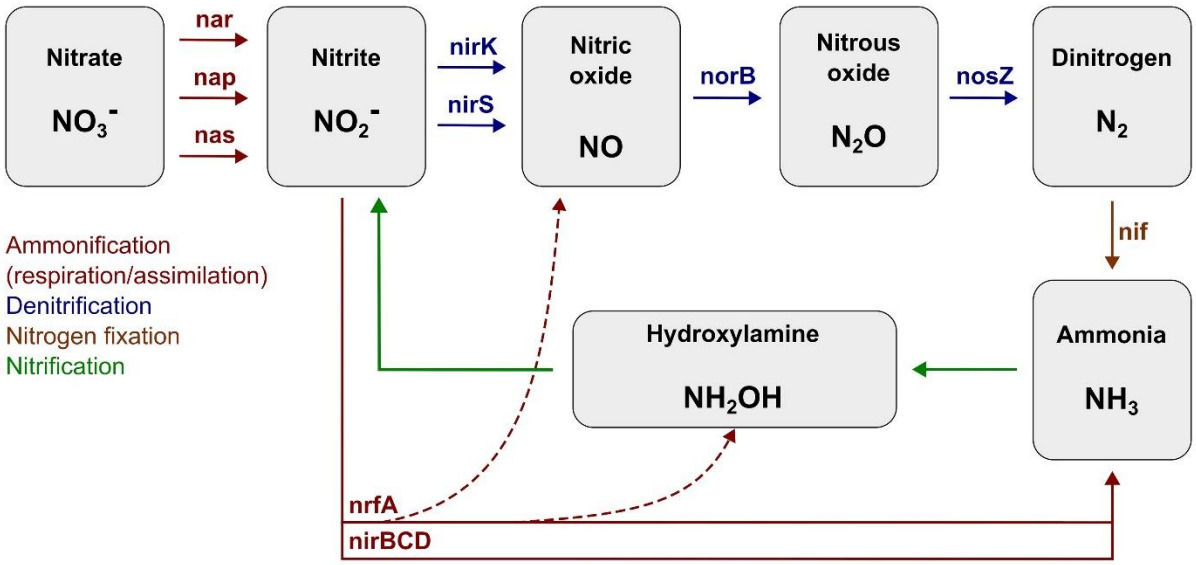

Figure 2.4. Bacterial inorganic nitrogen cycle. Ammonification, denitrification, nitrogen fixation, and nitrification are displayed by colored solid lines, with genes involved in the pathway. Dotted lines show additional formation of nitric oxide and hydroxylamine during nitrite ammonification. Figure adapted from Rodionov et al. 2005.

A constitutive nitrogenase activity and high ammonium production was observed in all mentioned strains except *P. balearica* and *P. stutzeri*, indicating that a genome context is required for the activity of the X940 cosmid (Setten et al., 2013). Nitrogen fixation and assimilation are intrinsically coupled and controlled by complex regulatory circuits, favouring the assimilation of fixed nitrogen into biomass instead of excreting it. The processes are controlled by the PII complex, which includes signal transduction proteins such as GlnB and GlnK; enzymes responding to metabolite control via reversible post-translational modifications of proteins (GlnD and GlnE); and a two-component regulatory system (NtrB or NRII and NtrC or NRI) controlling many nitrogen metabolism genes. PII tightly regulates NifA, a positive regulatory element (Table 2.1) to fix nitrogen by demand. Readers wanting a comprehensive review can refer to Batista and Dixon (2019).

Table 2.1. The *nif* genes and their known or proposed roles during nitrogen fixation in all species[a]

Cluster/gene	Function
nifQ	Involved in FeMo-co synthesis; proposed to function in early MoO_4^{2-} processing
nifB	Required for FeMo-co synthesis; its metabolic product, nifB-co, is a specific Fe and S donor to FeMo-co
nifA	Positive regulatory element
nifL	Negative regulatory element
rnfABCDGEH	Involved in electron transport to nitrogenase, possibly functioning to drive the thermodynamically unfavorable reverse electron transfer from NADH to ferredoxin
nifHDKTY	
nifH	Fe protein; required for FeMo-co biosynthesis and apo-MoFe protein maturation; electron donor to MoFe protein during nitrogenase
nifD	Alpha subunit of MoFe protein; forms an $\alpha_2\beta_2$ tetramer with the β subunit; the site of substrate reduction, FeMo-co, is within the α subunit of MoFe protein
nifK	Beta subunits of MoFe protein P clusters are present at each αβ subunit interface
nifT	Unknown
nifY/nafY	Chaperone for the apo-MoFe protein NafY is also a FeMo-co carrier and is proposed to aid in the insertion of FeMo-co into apo-MoFe protein
nifENX	
nifE	Forms $\alpha_2\beta_2$ tetramer with NifN; required for FeMo-co synthesis; proposed to function as a scaffold on which FeMo-co is synthesized
nifN	Required for FeMo-co synthesis; tetramer with NifE
nifX	Involved in FeMo-co synthesis; accumulates a FeSMo-containing precursor
nifUSV	
nifU	Molecular scaffold for the formation of Fe-S cluster for nitrogenase components
nifS	Involved in mobilization of S for Fe-S cluster synthesis and repair
nifV	Homocitrate synthase, involved in FeMo-co synthesis
nifWZM	
nifW	Involved in stability of MoFe protein
nifZ	Unknown
nifM	Required for the maturation of NifH
nifF	Flavodoxin; physiological electron donor to NifH in *Klebsiella pneumoniae*
modABC	Encodes an ABC-type, high-affinity, molybdate transporter
hesB	Binding to a 2 iron, 2 sulfur (2Fe-2S) cluster; this cluster consists of two iron atoms, with two inorganic sulfur atoms found between the irons and acting as bridging ligands
cysE	Biosynthesis of cysteine

[a] As reported by Rubio and Ludden 2005; Yan et al. 2008.

To unravel the underlying genetic mechanism of the *P. stutzeri* NFI genes, the complete NFI was transferred into the recombinant *E. coli* strain EN-01 and investigated by transcriptomics and proteomics for functional investigation (Yang et al., 2018). In the genetically engineered *E. coli* strain EN-01 harbouring the heterologous NFI island from *P. stutzeri*, primary nitrogen assimilation is achieved by synthesis of glutamate from ammonium and 2-oxoglutarate, catalysed by two alternative pathways (Yang et al., 2018). In an N-rich environment, the pathway involving the enzyme glutamate dehydrogenase (GDH) was active. Alternatively, in an N-limited environment, the enzymes glutamate synthetase (GS gene *glnA*) and glutamine oxoglutarate aminotransferase (GOGAT gene *gltBD*) were predominantly active (Yang et al., 2018). This is in agreement with data showing that bacterial cellular nitrogen is composed of 75% - 88% of glutamate and 12% - 25% glutamine which act as main nitrogen donors (Prusiner & Stadtman (1973); Yang et al. 2018).

In *P. stutzeri* A1501, the expression of the *nif*-specific regulatory protein NifLA is controlled by the nitrogen regulatory cascade AmtB-GlnK-NtrBC (Yang et al., 2018). During N-fixing conditions, genes of the NFI had a >10-fold higher transcript level and were

downregulated after ammonium shock (Yan et al., 2010; Yang et al., 2018). *NtrC* and *glnK* are necessary for the expression of NifA, and in turn NifA is expected to play a major role in the expression of *Ntr* (Nitroreductase) genes. Under constitutively expression of NifA in a *P. stutzeri* A1501 *glnK*$^{-}$ mutant, nitrogenase activity and nitrogen fixation have been restored and observed under presence of ammonia (He et al., 2008). Thus, it was proposed that GlnK acts as a key regulatory element in control of ammonia assimilation, *nifA* expression and in modulation of NifA activity by NifL (He et al., 2008).

The study by Yang et al., 2018 showed that other microbes can be genetically engineered to acquire the ability to fix nitrogen via the NFI. Furthermore, it successfully combines multi-omics approaches in the study of microbes and their metabolic processes. Understanding the microbial process of N-fixation is fundamental to shed light on the molecular mechanism of the plant-microbe interaction. However, this knowledge has to be put into context with plant responses too, to fully understand the interaction between plants and *Pseudomonas spp*. during N-fixation.

Plant molecular components involved in uptake of *Pseudomonas* derived N

(i) Root nitrogen transporters and central N metabolism

It has been shown that in cases of excess or deficient N supply, the plant transporters of the ammonium transport system (AMT) and the nitrate transport system (NRT) will be adjusted accordingly, together with other crucial enzymes of central N metabolism such as nitrate reductase (NR), nitrite reductase (NiR), glutamine synthetase (GS), glutamine-oxoglutarate aminotransferase (GOGAT) (Muratore et al., 2021).

To check if this is true under bacterial inoculation, Trinh *et al*. (2018) investigated the expression of N-related genes during *A. thaliana* and *Lactuca sativa* (lettuce) interaction with *P. nitroreducens strain IHB B 13561 (PnIHB).* They focused on the nitrate transporter genes NRT1.1, NRT1.2, NRT2.1, NRT2.2, NRT2.5, and NRT2.6 (Mantelin et al. 2006); NIR1, NLP6, and NLP7, which are involved in nitrate response; EIN1 and ERF1, which play roles in the ethylene response pathway; ARF19, ARF7, and AXR4, which are involved in the auxin signalling pathways; and the ammonium transporters AMT1.1, AMT1.2, and AMT2 (Trinh

et al, 2018). Out of these genes in *A. thaliana,* higher expression levels were found for NRT2.1, NRT2.2 and NRT2.6. However, a lower N content was measured in the seedlings during inoculation with *PnIHB*, which the authors assumed to be based on a higher rate of cell division requiring a more rapid nitrate metabolism. In return, a lower inner nitrate content induced NRT2 genes, increasing nitrate uptake (Trinh et al., 2018). Thus in Arabidopsis, *PnIHB* influenced root physiology (Fig. 2.5).

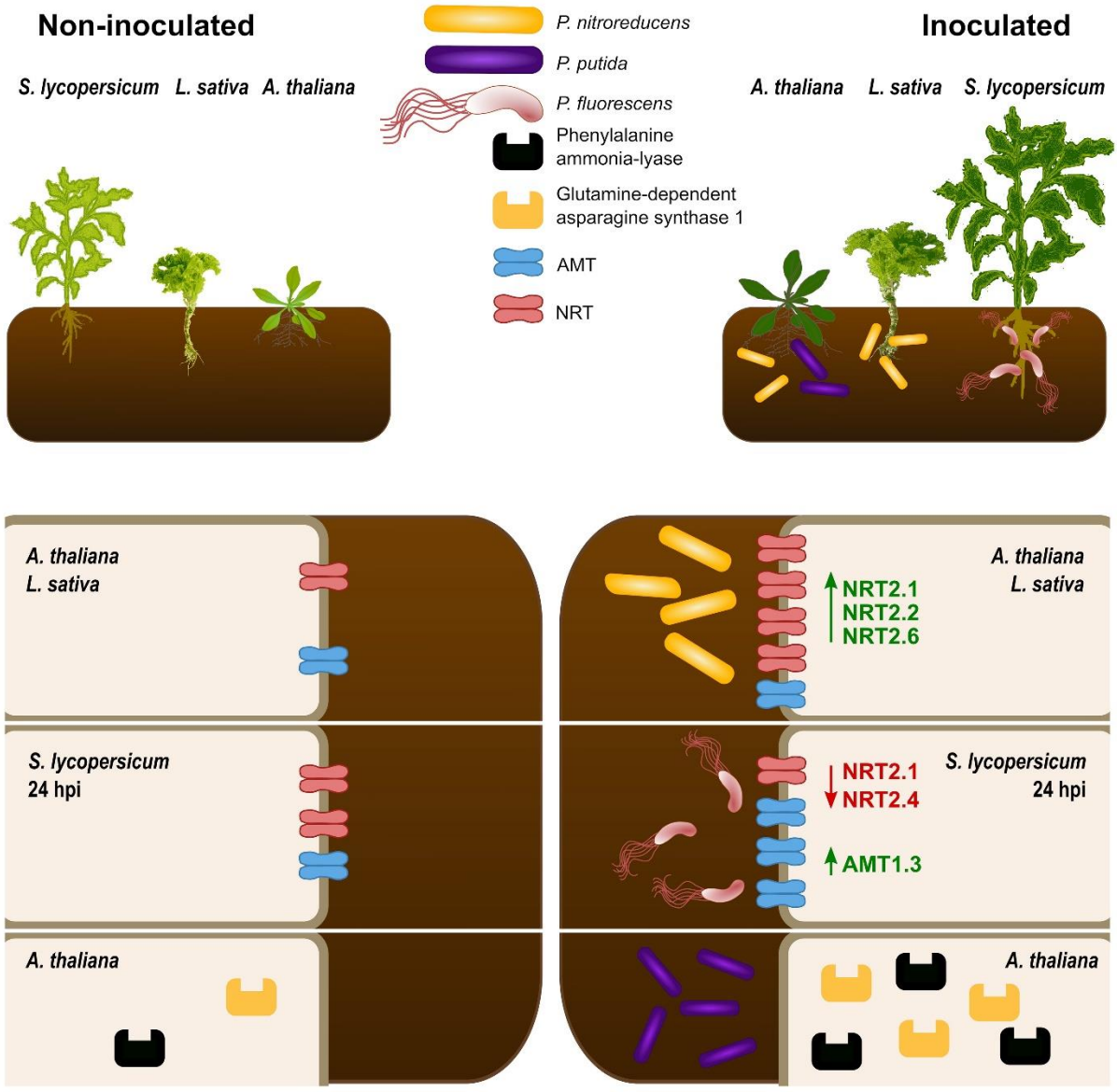

Figure 2.5. Molecular mechanisms of plant-microbe interactions. Colonization with beneficial bacteria alters the expression of genes, transcripts, and proteins. Inoculation with *Pseudomonas nitroreducens* increases the abundance of N-related transporters NRT2.1, NRT2.2, NRT2.6, while inoculation with *Pseudomonas fluorescens* increases abundance of AMT1.3 but decreases NRT2.1 and NRT2.4. Genes encoding glutamine-dependent asparagine synthase 1 and phenylalanine ammonia lyase are upregulated in response to inoculation with *Pseudomonas putida*.

Similarly, in lettuce, three nitrate transporter genes (*LsNRT1*, *LsNRT2*, *LsNRT2.5*) were examined *after* inoculation with *PnIHB*. LsNRT1 and LsNRT2 showed higher levels of expression. LsNRT2 and AtNRT2.1 are highly similar in their sequence alignments, suggesting similar responses in these 2 different species. Consequently, *PnIHB* inoculation increased the nitrate uptake and promoted growth by increasing the levels of transcripts of NRT2.1 in both *A. thaliana* and *L.* sativa (Poitout et al., 2014, Trinh et al., 2018, Fig. 2.5). In addition, metabolic stimulation and induction of cell development is proposed to be a driving force for the growth promotion in both *A. thaliana* and *L. sativa* by *PnIHB* (Trinh et al., 2018). It is speculated that ammonium is primarily used for the elevated cell division to synthesize essential proteins and other compounds (Howitt and Udvardi, 2000; Pratelli and Pilot, 2014). Interestingly, increased transcripts of transporters of the NRT2 family were observed in both *L. sativa* and *A. thaliana* during this study, while the nitrate levels in the plant declined (Trinh et al., 2018), indicating that the assimilation of nitrate is preferred over storage in the vacuole. *PnIHB* seems to be a promising candidate for improved plant performance by increasing plant growth in *A. thaliana* and *L. sativa* and improving soil nitrate utilization (Fig. 2.5 top, Trinh et al., 2018). *Solanum lycopersicum* (Tomato) inoculated with *P. fluorescens* Pf-16 (Pf-16) showed a molecular reprogramming during the early stages of inoculation (Fig. 2.5 middle; Scotti et al., 2019). The stages can be distinguished into <48h and >48h. During the earlier stage Pf-16

inoculation led to increased gene expression of AMT1.3 (Solyc03g045070.1.1) while decreasing gene expression of NRT2.1 (Solyc00g090860.1.1) and NRT2.4 (Solyc11g069760.1.1) (Fig. 2.6). In the later stage, almost no changes in the expression of AMT1.3, NRT2.1 and NRT2.4 were detectable, while cell wall modifications and upregulations of plant growth promotion genes were observed (Scotti et al., 2019 Supplementary dataset). The main finding of the study by Scotti et al. (2019) was that Pf-16 inoculation can both increase the tolerance against biotic and abiotic stresses and promotes plant growth simultaneously. However, the authors have also shown that nitrogen related transcript dynamics during the early stage of plant-microbe interaction, measuring the plant response over a longer period, might give further insight in the molecular mechanism. Those dynamics could be used to identify the time point of growth

promotion during plant-microbe interactions and would clarify whether the plant responds only for a short period after inoculation, requiring more frequent inoculations to improve plant growth, or if a single inoculation is sufficient.

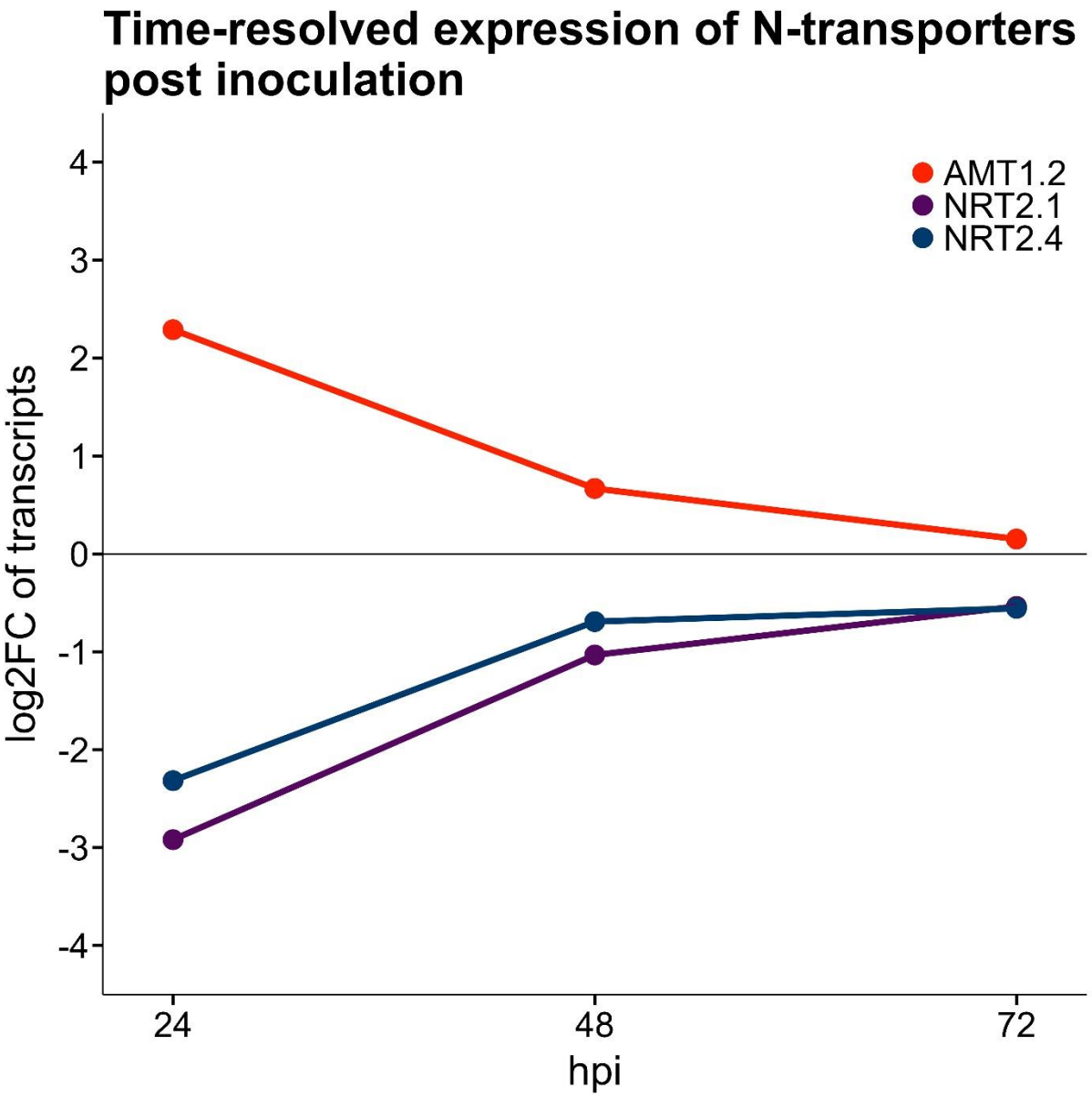

Figure 2.6. Time-resolved changes on transcript level of N-related transporters postinoculation with *Pseudomonas fluorescens*. Log_2 fold changes (log2FC) of AMT1.3, NRT2.1, NRT2.4 in *Solanum lycopersicum* roots inoculated with *P. fluorescens* 24, 48, and 72 h post inoculation (hpi). A strong early response can be observed soon after inoculation (24 hpi), which declines over time (72 hpi). During the early stage of inoculation (24 hpi), NRT2.1 and NRT2.4 are downregulated, whereas AMT1.3 is upregulated. Data from Scotti et al. (2019).

(ii) Amino acid metabolism

Besides changes on N-related transporters or enzymes, other pathways are involved in promoting plant growth during PMI. Transcription analyses discovered the upregulation of 2 genes in Arabidopsis inoculated with *P. putida* MTCC5279: At3g47340, a glutamine-dependent asparagine synthase 1, and At3g10340, an ammonia ligase (Fig. 2.5 bottom, Srivastava et al., 2012). Asparagine (Asn), due to its high N:C ratio and stability, is the preferred form for long distance transport and storage of N in most higher plants and can account for 86% of transported N (Lea and Miflin, 1980; Urquhart and Joy, 1981; Sieciechowicz et al., 1988). The higher abundance of transcripts of the glutamine-dependent asparagine synthase 1 (At3g47340) indicate that assimilated nitrogen might be converted into glutamine (Gln) and further into Asn for potential transport within the plant during plant-microbe interaction. Thus, it might be interesting to analyze the amino acid profile of plants during plant-microbe interactions to investigate this hypothesis. At3g10340 encodes the Phenylalanine ammonia lyase 4 (PAL4), which is involved in the phenylpropanoid pathway, catalysing the first step of non-oxidative deamination of L-phenylalanine (L-Phe) to 7,8-unsaturated *trans*-cinnamic acid and an ammonium ion. Ammonium is directly recycled via GS/GOGAT to regenerate arogenate, which is required for further metabolism of cinnamic acid to various phenylpropanoids and their derivatives. The phenylpropanoid pathway is responsible for the synthesis of a large range of natural products in plants, including flavonoids (pigments and UV protectants), the structural polymer lignin, and antimicrobial furanocoumarin and isoflavonoid phytoalexins (Hahlbrock and Scheel, 1989; Dixon and Paiva, 1995). Salicylic acid, which is involved in the establishment of both local and systemic plant defense responses, is also a product of this pathway (Klessig and Malamy, 1994).

(iii) Open questions

Despite several approaches to study molecular mechanisms, a big challenge is missing characterisations of proteins involved in PMI, showing the importance of functional characterisation approaches to update databases and allow further research in this area.

One example is a study about the interaction of *P. fluorescens* strain PICF7 with wheat and barley on a molecular basis by performing a proteomics approach (Fröhlich et al. 2012). The root proteome of inoculated seedlings of wheat and barley revealed 14 and 24 proteins exclusively abundant during PICF7 inoculation, respectively. However, only 3 out of the 14 proteins in wheat have shown similarities to databases, namely a putative Nodal modulator 3, a phosphoenolpyruvate carboxylase (PEPC) and an S-formylglutathione hydrolase-like (SFGH) protein, whereas the proteins of barley are predicted or uncharacterized proteins (0/6 known proteins in barley).

Biological Nitrogen Fixation in *Pseudomonas spp.* and the influence of the abiotic environment to plant growth promotion

To test the contribution of biological nitrogen fixation (BNF) to total plant N content, maize and wheat were grown in ^{15}N-supplemented soil, with *P. protegens* Pf-5 with and without the X940 cosmid in the greenhouse (Table 2.2, Fox et al, 2016). ^{15}N was used to increase the ^{15}N/^{14}N ratio in the soil. Thus, nitrogen originating from the air would have a comparatively higher ^{14}N fraction than that from soil and would be indicative of N-fixation. BNF was proposed to be active from the early stages of plant growth since measurements of the δ^{15}N value one month after inoculation showed significantly lower ^{15}N in root, leaf and stem tissues of Pf-5 X940 treated maize and wheat plants than in those of Pf-5-treated plants (Fox et al., 2016). Two months after inoculation, the nitrogen content derived from gaseous nitrogen (%Ndfa) in Pf-5 X940-treated maize and wheat plant organs was 74% and 85% for roots, 63% and 78% for leaves and 70% and 82% for stems, respectively, indicating the assimilation of nitrogen derived from air. Plant growth promotion was also shown in various flowering plant species inoculated with Pf-5 X940 under sterile hydroponic growth-chamber conditions (Table 2.2). The beneficial effect might be the result of an increased ammonium excretion (Fox et al, 2016). Confocal microscopy with GFP-tagged Pf-5 and Pf-5 X940 demonstrated that both strains appear to colonise solely the rhizosphere and neither the endosphere nor the phyllosphere (Fox et al., 2016). Due to the functionality of the X940 cosmid in different *Pseudomonas spp.*, transformation of established *Pseudomonas* strains with the X940 cosmid and application in agriculture might lead to increased plant performance and yield.

Table 2.2. Summary of plant phenotype responses upon inoculation with various *Pseudomonas* spp.[a]

Plant species	Inoculant	Sterile	Plant response (inoculated vs. control)			Citation
			Nutrient content	Biomass[a]	Root phenotype	
Zea mays (Pannar BIOGENE BG6607YR)	PF-X940	X	Shoot: +170% (N) Seed: +556% (N)		Bacteria contribution to N: increased	Fox et al. 2016
Triticum aestivum (Bobwhite 26)	PF-X940	X	Shoot: +85% (N) Seed: +379% (N)		Bacteria contribution to N: increased	Fox et al. 2016
Maize	*P. stutzeri* A1501	X	Shoot: +14.1–23.6% (N)	SDW: +20.2% RDW: +31.2%		Ke et al. 2019
	P. stutzeri A1501 (natural growth conditions)	√	Shoot: +17.5–27.8% (N)	SDW: +59% RDW: +93%		Ke et al. 2019
Rice (Super Basmati)	*Pseudomonas* sp. strain K1	X		SDW: +100% Seed: +55%		Mirza et al. 2006
Rice (Super Basmati 385)	*Pseudomonas* sp. strain K1	X		SDW: +59% Seed: +93%		Mirza et al. 2006
Brassica juncea (brown mustard)	*P. aeruginosa* (seed-coated)	X	Whole-plant: +40.61% (N); +100% (P)		Root length: +25%	Roychowdhury et al. 2019
	P. aeruginosa (rhizosphere-inoculation)	X	Whole plant: +19.9% (N)		Root length: +6.25%	Roychowdhury et al. 2019
Phaseolus vulgaris L. (common bean)	*Rhizobium* sp. + *Pseudomonas* sp. strain Luc2	X	Shoot: −8% (N) Bacteria contribution to N: −31.4% (N)	SDW: −1.25% RDW: +5.76%	Root length: +21%	Stajkovic et al. 2011
Phaseolus vulgaris L. (common bean)	*Rhizobium* sp. + *Pseudomonas* sp. strain LG	X	Shoot: +29.1% (N) Bacteria contribution to N: +113.8% (N)	SDW: +27.9% Root: −2.2%	Root length: +13.4%	Stajkovic et al. 2011
Glycine max (soybean)	*Pseudomonas* sp. strain 54RB	X	Seed: +17.4% (N); +11.9% (P)	Seed: +75.6% Shoot: +29.5% Root: +21.7%		Afzal et al. 2010

[a] SDW = shoot dry weight; RDW = root dry weight.

Ke et al. (2018) tested the contribution of *P. stutzeri* A1501 to BNF in well-watered and water deficient conditions using maize. Using sterilized soil, an increase of 27.8% %Ndfa was measured in well-watered conditions, while under water deficiency only 17.5% %Ndfa was observed. In absolute values, a total of 0.90 g plant^{-1} N was fixed in well-watered conditions and 0.30 g plant^{-1} in water deficient conditions. When grown in natural soil, the nitrogen derived from N_2 was 0.72 g/plant (23.6%) and 0.18 g/plant (14.1%) for well-watered and water deficient conditions, respectively. Ke et al. (2018) was able to show the actual amounts of nitrogen fixed by *P. stutzeri* A1501, both in sterile and natural conditions. This shows the potential use of *P. stutzeri* A1501 to increase total N content in plants and therefore increase the biomass production (Ke et al., 2018) and underlines the importance of water supply for successful PMI.

P. psychrotolerans CS51, having genes for both denitrification and ammonification, could not only be used for plant growth promotion, but also for denitrification of soils. This could mean that in anoxic environments, such as soils containing a lot of water (like rice fields), NO_3^- could be used for denitrification, while in dry soils, respiratory ammonification occurs (Torres et al., 2016). As denitrification is not linked to plant growth

promotion, the application of this strain seems to be limited to plants growing in dry soils. This strain might become more relevant with the future challenges we are facing, such as climate change and drought. Additionally, it indicates that soil properties impact the direction of the chemical reaction. Importantly, increased metabolism involving NO_3^- could remove highly abundant nitrate from the soil, resulting in a decreased nitrate leaching to ground water.

Afzal et al. (2010) shows that not only the water and nitrogen availability or N_2-fixation play a major role in increasing the plant N content, but that other nutrients are important too. The authors tested the co-inoculation of *Glycine max* (Soybean) with *Bradyrhizobium japonicum* strain TAL 377 and *Pseudomonas* strain 54RB under varying phosphorus availability. For the pot experiments, a dose of 0.3 g/pot of nitrogen was applied in form of urea and different phosphorus levels were introduced by adding either no additional P or 1.35 g of P_2O_5 (50 kg/ha) in form of Single Superphosphate (SSP) to treated conditions. However, one has to keep in mind that SSP also contains Ca and S, indicating that the following plant phenotypic changes are not only based on an increased P, but also Ca and S level. Co-inoculation with both strains had positive effects in P_2O_5 treated conditions in terms of number of pods, grain yield, seed N and P, and total available P and N in soil. The available N content in soil was increased by 72% over P_2O_5 only treated plants, indicating that the availability of other nutrients (nutrient-crosstalk) is also decisive for better N content in plants (Afzal et al., 2010). Observing *Pseudomonas strain* 54RB promoting plant growth on its own and increasing available N in cooperation with another strain hints to its compatibility in microbial communities, and future combinations could include P-solubilizing microbes to avoid limitations as per Liebig's law of the minimum. The exchange of nutrients and carbon between plants and microbes can occur at the plant root surface or within the plant root tissue (symplastic, apoplastic). The cumulative activity of the bacterial transmembrane transporters, the so-called transportome, plays a crucial role in plant-microbe interactions and determines which ecological niche is occupied in the rhizosphere (Silby et al., 2009; Larsen et al., 2015, Wilton et al., 2018). The activity of the bacterial transportome of several *Pseudomonas spp*. can lead to protection against nutrient stresses (Shinde et al., 2017; Wilton et al., 2018).

Moreover, the ability of many *Pseudomonas spp.* to grow on lower temperatures ensures propagation and survivability in fields, despite changing temperatures of the soils (Kwon et al., 2003). An outstanding example is *Pseudomonas migulae*. *P. migulae* was isolated from the Chhiplakot region, in the Western Indian Himalaya (Suyal et al., 2014). This N_2-fixing strain has adapted to different abiotic stresses, including cold temperature, height and oxidative stress, which made it possible to fix N at temperatures of 5-10 °C (Suyal et al., 2014). This shows once more that testing different strains from various geographical locations is valuable as it gives into the mechanistic acclimation to varying environmental factors (c.f. *P. stutzeri* tested from different geographical locations; Venieraki et al., 2014). Consequently, beneficial *Pseudomonas* species could be collected, applicable for fields in various geo-climatic regions.

Conclusions and open questions

A number of plant species were tested with *Pseudomonas spp.* and have shown beneficial response, which can be linked to improved N content in the plant. This encourages the further study for use of *Pseudomonas spp.* for future agricultural applications to ultimately reduce the application of N fertiliser, while maintaining the required amount of biomass. Due to the genus' ubiquitous distribution in the world soils and inherently to the adaptation to most global conditions, strains can be found that will work in fields across the globe. Despite the potential depicted, here we note that many of the mentioned studies tested the plant growth promoting effects in natural soil, but not directly in the field. Field trials come with more challenges like ever-changing conditions and microbial communities, compared to controlled environments. Nevertheless, *P. stutzeri* A1501 stands out as a good candidate for plant growth promotion in conditions with limited water supply (Ke et al., 2018). One additional gap is clear understanding of how these strains would perform in field microbial communities and under a variety of abiotic stresses. In terms of yield, no clear evidence is displayed in this review, leaving the question open. Furthermore, we must keep in mind that although we focus on N-fixation, *Pseudomonas* (as other strains) has the potential to promote plant growth by promoting a greater root system, which in turn will reflect in better nutrients scavenging. An important example for this was recently published for a different clade of bacteria, certain

Oxalobacteraceae particular of the genus *Massilia* that affect lateral root development of maize and thereby increase N acquisition under N-limitation without bacterial N_2 fixation (Yu et al. 2021). Interestingly, only certain maize genotypes were able to attract and stimulate the propagation of these bacteria by secreting distinct flavones under N-limitation suggesting that crops can influence the abundance of root-associated microbiota via exudation of specific compounds (Yu et al. 2021). This in consequence suggests that root-rhizobacteria interactions cannot only be established by inoculation of plants with beneficial microbes but potentially more robustly by targeted plant breeding which we propose should be investigated for crops other than maize. We note a gap in understanding the plant responses on protein level and through plant development (e.g. from moment on inoculation) as this was only addressed in few studies. In further approaches, key regulatory genes, peptides, proteins, enzymes, signalling molecules and metabolites/lipids could be investigated and used for testing potential conserved plant growth promoting domains throughout the *Pseudomonas* genus. In the ideal case, this knowledge could be transferred to other genera of bacteria.

Funding

Stefan Sanow is grateful for the financial support from the Forschungszentrum Jülich, which was provided through the Jülich-University of Melbourne Post-graduate Academy (JUMPA) program. Michelle Watt holds the Adrienne Clarke Chair of Botany which is supported through the University of Melbourne Botany Foundation. Gabriel Schaaf acknowledges funding by the Deutsche Forschungsgemeinschaft under Germany's Excellence Strategy—EXC 2070—390732324 (PhenoRob). Borjana Arsova and Ulrich Schurr acknowledge the Helmholtz association funding provided by IBG-2 in the Program „Changing Earth" Topic 7, and the CEPLAS excellence cluster (Deutsche Forschungsgemeinschaft under Germany's Excellence Strategy, EXC 2048). The open access of this publication is funded by the Deutsche Forschungsgemeinschaft (DFG, German Research Foundation)—grant 491111487.

References

Afzal, A., Bano, A., Fatima, M., 2010. Higher soybean yield by inoculation with N-fixing and P-solubilizing bacteria. Agron. Sustain. Dev. 30, 487–495.

Akiyama, K., & Hayashi, H. (2006). Strigolactones: chemical signals for fungal symbionts and parasitic weeds in plant roots. Annals of botany, 97(6), 925-931.

Aubry, S., Brown, N.J., Hibberd, J.M., 2011. The role of proteins in C3 plants prior to their recruitment into the C4 pathway. Journal of Experimental Botany 62, 3049–3059.

Bakkou, N. (2011). Characterization of the endosymbiotic forms of Sinorhizobium sp. strain NGR234 (Doctoral dissertation, University of Geneva).

Beier MP, Fujita T, Sasaki K, Kanno K, Ohashi M, Tamura W, Konishi N, Saito M, Imagawa F, Ishiyama K, Miyao A, Yamaya T, Kojima S. The urea transporter DUR3 contributes to rice production under nitrogen-deficient and field conditions. Physiol Plant. 2019 Sep;167(1):75-89. doi: 10.1111/ppl.12872. Epub 2019 Jan 9. PMID: 30426495.

Ben Hassen, T., & El Bilali, H. (2022). Impacts of the Russia-Ukraine war on global food security: toward more sustainable and resilient food systems? Foods, 11(15), 2301.

Berenguer, P., Santiveri, F., Boixadera, J., Lloveras, J., 2009. Nitrogen fertilisation of irrigated maize under Mediterranean conditions. European Journal of Agronomy 30, 163–171

Berkhout, P., Bergevoet, R., & van Berkum, S. (2022). A brief analysis of the impact of the war in Ukraine on food security (No. 2022-033). Wageningen Economic Research.

Bindel, N., & Neuhäuser, B. (2021). High-affinity ammonium transport by Arabidopsis thaliana AMT1; 4. *Acta Physiologiae Plantarum*, *43*, 1-5.

Bock, E. & Wagner, M. in The Prokaryotes: A Handbook on the Biology of Bacteria (eds Dworkin, M. et al.) 457–495 (Springer, 2001)

Bueno Batista, M., Dixon, R., 2019. Manipulating nitrogen regulation in diazotrophic bacteria for agronomic benefit. Biochemical Society Transactions 47, 603–614.

Cerezo, M., Tillard, P., Filleur, S., Muños, S., Daniel-Vedele, F., Gojon, A., 2001. Major Alterations of the Regulation of Root NO 3 − Uptake Are Associated with the Mutation of Nrt2.1 and Nrt2.2 Genes in Arabidopsis. Plant Physiol. 127, 262–271.

Chaudhary, P., Khati, P., Chaudhary, A., Maithani, D., Kumar, G., & Sharma, A. (2021). Cultivable and metagenomic approach to study the combined impact of nanogypsum and Pseudomonas taiwanensis on maize plant health and its rhizospheric microbiome. *PLoS One*, *16*(4), e0250574.

Combes-Meynet, E., Pothier, J.F., Moënne-Loccoz, Y., Prigent-Combaret, C., 2011. The *Pseudomonas* Secondary Metabolite 2,4-Diacetylphloroglucinol Is a Signal Inducing Rhizoplane Expression of Azospirillum Genes Involved in Plant-Growth Promotion. MPMI 24, 271–284.

Daims, H., Lebedeva, E.V., Pjevac, P., Han, P., Herbold, C., Albertsen, M., Jehmlich, N., Palatinszky, M., Vierheilig, J., Bulaev, A., Kirkegaard, R.H., von Bergen, M., Rattei, T., Bendinger, B., Nielsen, P.H., Wagner, M., 2015. Complete nitrification by Nitrospira bacteria. Nature 528, 504–509.

Day, D. A., Kaiser, B. N., Thomson, R., Udvardi, M. K., Moreau, S., & Puppo, A. (2001). Nutrient transport across symbiotic membranes from legume nodules. Functional Plant Biology, 28(7), 669-676.

Dixon, R. & Paiva, N. Stress-Induced Phenylpropanoid Metabolism. Plant Cell 7, 1085–1097 (1995). Egamberdieva, D. (2009). Alleviation of salt stress by plant growth regulators and IAA producing bacteria in wheat. Acta Physiologiae Plantarum, 31(4), 861-864.

Erisman, J. W., Sutton, M. A., Galloway, J., Klimont, Z., & Winiwarter, W. (2008). How a century of ammonia synthesis changed the world. Nature geoscience, 1(10), 636-639.

Etesami, H., & Adl, S. M. (2020). Can interaction between silicon and non–rhizobial bacteria benefit in improving nodulation and nitrogen fixation in salinity–stressed legumes? A review. Rhizosphere, 100229.

Filleur, S., Dorbe, M.-F., Cerezo, M., Orsel, M., Granier, F., Gojon, A., Daniel-Vedele, F., 2001. An Arabidopsis T-DNA mutant affected in Nrt2 genes is impaired in nitrate uptake. FEBS Letters 489, 220–224.

Fox, A.R., Soto, G., Valverde, C., Russo, D., Lagares, A., Zorreguieta, Á., Alleva, K., Pascuan, C., Frare, R., Mercado-Blanco, J., Dixon, R., Ayub, N.D., 2016. Major cereal crops benefit from biological nitrogen fixation when inoculated with the nitrogen-fixing bacterium *Pseudomonas* protegens Pf-5 X940: Robust biological nitrogen fixation in major cereal crops. Environ Microbiol 18, 3522–3534.

Franche, C., Lindström, K., Elmerich, C., 2009. Nitrogen-fixing bacteria associated with leguminous and non-leguminous plants. Plant Soil 321, 35–59.

Fukayama, H., Hatch, M.D., Tamai, T., Tsuchida, H., Sudoh, S., Furbank, R.T., Miyao, M., n.d. Activity regulation and physiological impacts of maize C4-specific phosphoenolpyruvate carboxylase overproduced in transgenic rice plants 13.

Gautrat, P., Laffont, C., Frugier, F., & Ruffel, S. (2020). Nitrogen Systemic Signaling: From Symbiotic Nodulation to Root Acquisition. Trends in Plant Science.

Giehl, R. F., Laginha, A. M., Duan, F., Rentsch, D., Yuan, L., & von Wirén, N. (2017). A critical role of AMT2; 1 in root-to-shoot translocation of ammonium in Arabidopsis. *Molecular plant*, *10*(11), 1449-1460.

Girin, T., Lejay, L., Wirth, J., Widiez, T., Palenchar, P.M., Nazoa, P., Touraine, B., Gojon, A., Lepetit, M., 2007. Identification of a 150 bp cis -acting element of the AtNRT2.1 promoter involved in the regulation of gene expression by the N and C status of the plant: Identification of cis -elements involved in the regulation of NO 3 - uptake. Plant, Cell & Environment 30, 1366–1380.

Girke, C., Daumann, M., Niopek-Witz,S., Möhlmann,T. et al. (2014). "Nucleobase and nucleoside transport and integration into plant metabolism." Frontiers in plant science 5.

Glick, B.R., 1995. The enhancement of plant growth by free-living bacteria. Can. J. Microbiol. 41, 109–117.

Glick, B.R., Bashan, Y., 1997. Genetic manipulation of plant growth-promoting bacteria to enhance biocontrol of phytopathogens. Biotechnology Advances 15, 353–378.

Glick, B. R., Holguin, G., Patten, C. L., & Penrose, D. M. (1999). Biochemical and genetic mechanisms used by plant growth promoting bacteria. World Scientific.

Glick, B.R., Todorovic, B., Czarny, J., Cheng, Z., Duan, J., McConkey, B., 2007. Promotion of Plant Growth by Bacterial ACC Deaminase. Critical Reviews in Plant Sciences 26, 227–242.

Glick, B. R. (2014). Bacteria with ACC deaminase can promote plant growth and help to feed the world. Microbiological research, 169(1), 30-39.

Hahlbrock, K., n.d. Physiology and Molecular Biology of Phenylpropanoid Metabolism 23.

Haskett, T. L., Tkacz, A., & Poole, P. S. (2020). Engineering rhizobacteria for sustainable agriculture. The ISME Journal, 1-16.

Häusler, R.E., Rademacher, T., Li, J., Lipka, V., Fischer, K.L., Schubert, S., Kreuzaler, F., Hirsch, H., 2001. Single and double overexpression of C4-cycle genes had differential effects on the pattern of endogenous enzymes, attenuation of photorespiration and on contents of UV protectants in transgenic potato and tobacco plants. Journal of Experimental Botany 52, 1785–1803.

He, S., Chen, M., Xie, Z., Yan, Y., Li, H., Fan, Y., ... & Elmerich, C. (2008). Involvement of GlnK, a PII protein, in control of nitrogen fixation and ammonia assimilation in Pseudomonas stutzeri A1501. *Archives of microbiology*, *190*(1), 1-10.

Hernández-León, R., Rojas-Solís, D., Contreras-Pérez, M., Orozco-Mosqueda, Ma. del C., Macías Rodríguez, L.I., Reyes-de la Cruz, H., Valencia-Cantero, E., Santoyo, G., 2015. Characterization of the antifungal and plant growth-promoting effects of diffusible and volatile organic compounds produced by Pseudomonas fluorescens strains. Biological Control 81, 83–92.

Hirel B, Tétu T, Lea PJ, Dubois F. 2011. Improving Nitrogen Use Efficiency in Crops for Sustainable Agriculture. *Sustainability* 3: 1452–1485.

Howitt, S.M., Udvardi, M.K., 2000. Structure, function and regulation of ammonium transporters in plants. Biochimica et Biophysica Acta (BBA) - Biomembranes 1465, 152–170.

Iglewski BH. Pseudomonas. In: Baron S, editor. Medical Microbiology. 4th edition. Galveston (TX): University of Texas Medical Branch at Galveston; 1996. Chapter 27. Available from: https://www.ncbi.nlm.nih.gov/books/NBK8326/

Jaffe D. Nitrogen Cycle, Atmospheric. In: Encyclopedia of Physical Science and Technology [Internet]. Elsevier; 2003 [cited 2021 May 4]. p. 431–40. Available from: https://linkinghub.elsevier.com/retrieve/pii/B0122274105009224

Jagtap, S., Trollman, H., Trollman, F., Garcia-Garcia, G., Parra-López, C., Duong, L., ... & Afy-Shararah, M. (2022). The Russia-Ukraine conflict: Its implications for the global food supply 589 chains. Foods, 11(14), 2098.

Jiménez JA, Novinscak A and Filion M (2020) Inoculation With the Plant-Growth-Promoting Rhizobacterium Pseudomonas fluorescens LBUM677 Impacts the Rhizosphere Microbiome of Three Oilseed Crops. Front. Microbiol. 11:569366. doi: 10.3389/fmicb.2020.569366

Kang, S.-M., Asaf, S., Khan, A.L., Lubna, Khan, A., Mun, B.-G., Khan, M.A., Gul, H., Lee, I.-J., 2020. Complete Genome Sequence of Pseudomonas psychrotolerans CS51, a Plant Growth-Promoting Bacterium, Under Heavy Metal Stress Conditions. Microorganisms 8, 382.

Ke, X., Feng, S., Wang, J., Lu, W., Zhang, W., Chen, M., Lin, M., 2019. Effect of inoculation with nitrogen fixing bacterium Pseudomonas stutzeri A1501 on maize plant growth and the microbiome indigenous to the rhizosphere. Systematic and Applied Microbiology 42, 248–260.

Klessig, D. F., & Malamy, J. (1994). The salicylic acid signal in plants. Plant molecular biology, 26(5), 1439-1458.

Klimczyk M, Siczek A, Schimmelpfennig L. Improving the efficiency of urea-based fertilization leading to reduction in ammonia emission. Sci Total Environ. 2021 Jun 1;771:145483. doi: 10.1016/j.scitotenv.2021.145483. Epub 2021 Jan 30. PMID: 33736136.

Kloepper, J.W., Lifshitz, R., Zablotowicz, R.M., 1989. Free-living bacterial inocula for enhancing crop productivity. Trends in Biotechnology 7, 39–44.

Kwon, S. W., Kim, J. S., Park, I. C., Yoon, S. H., Park, D. H., Lim, C. K., & Go, S. J. (2003). Pseudomonas koreensis sp. nov., Pseudomonas umsongensis sp. nov. and Pseudomonas jinjuensis sp. nov., novel species from farm soils in Korea. *International journal of systematic and evolutionary microbiology*, *53*(1), 21-27.

Lam, H.-M., Coschigano, K.T., Oliveira, I.C., Melo-Oliveira, R., Coruzzi, G.M., 1996. THE MOLECULAR-GENETICS OF NITROGEN ASSIMILATION INTO AMINO ACIDS IN HIGHER PLANTS. Annu. Rev. Plant. Physiol. Plant. Mol. Biol. 47, 569–593.

Larsen, P. E., Collart, F. R., & Dai, Y. (2015). Predicting ecological roles in the rhizosphere using metabolome and transportome modeling. PloS one, 10(9), e0132837.

Lejay, L., Tillard, P., Lepetit, M., Olive, F.D., Filleur, S., Daniel-Vedele, F., Gojon, A., 1999. Molecular and functional regulation of two NO3- uptake systems by N- and C-status of Arabidopsis plants. Plant J 18, 509–519.

Li, W., Wang, Y., Okamoto, M., Crawford, N.M., Siddiqi, M.Y., Glass, A.D.M., 2007. Dissection of the AtNRT2.1 : AtNRT2.2 Inducible High-Affinity Nitrate Transporter Gene Cluster. Plant Physiol. 143, 425–433.

Li, Q., Li, H., Yang, Z., Cheng, X., Zhao, Y., Qin, L., ... & Willemsen, V. (2022). Plant Growth-Promoting rhizobacterium Pseudomonas sp. CM11 Specifically Induces Lateral Roots. *New Phytologist*.

Liu LH, Ludewig U, Frommer WB, von Wirén N. AtDUR3 encodes a new type of high-affinity urea/H+ symporter in Arabidopsis. Plant Cell. 2003 Mar;15(3):790-800. doi: 10.1105/tpc.007120. PMID: 12615950; PMCID: PMC150031.

Liu, R., Zhang, Y., Chen, P., Lin, H., Ye, G., Wang, Z., Ge, C., Zhu, B., Ren, D., 2017. Genomic and phenotypic analyses of Pseudomonas psychrotolerans PRS08-11306 reveal a turnerbactin biosynthesis gene cluster that contributes to nitrogen fixation. Journal of Biotechnology 253, 10–13.

Mantelin, S., Desbrosses, G., Larcher, M., Tranbarger, T.J., Cleyet-Marel, J.-C., Touraine, B., 2006. Nitrate dependent control of root architecture and N nutrition are altered by a plant growth-promoting Phyllobacterium sp. Planta 223, 591–603.

Mercado-Blanco, J., Alós, E., Rey, M.D., Prieto, P., 2016. Pseudomonas fluorescens PICF7 displays an endophytic lifestyle in cultivated cereals and enhances yield in barley. FEMS Microbiology Ecology 92, fiw092.

Mergaert, P., Van Montagu, M., & Holsters, M. (1997). Molecular mechanisms of Nod factor diversity. Molecular microbiology, 25(5), 811-817.

Mérigout, P., Gaudon, V., Quilleré, I., Briand, X., Daniel-Vedele, F., 2008. Urea Use Efficiency of Hydroponically Grown Maize and Wheat. Journal of Plant Nutrition 31, 427–443.

Mirza, M.S., Mehnaz, S., Normand, P., Prigent-Combaret, C., Moënne-Loccoz, Y., Bally, R., Malik, K.A., 2006. Molecular characterization and PCR detection of a nitrogen-fixing Pseudomonas strain promoting rice growth. Biol Fertil Soils 43, 163–170.

Miyao, M., Fukayama, H., 2003. Metabolic consequences of overproduction of phosphoenolpyruvate carboxylase in C3 plants. Archives of Biochemistry and Biophysics 414, 197–203.

Muratore, C., Espen, L., & Prinsi, B. (2021). Nitrogen uptake in plants: the plasma membrane root transport systems from a physiological and proteomic perspective. *Plants*, *10*(4), 681.

Mustafa, S. E. (2022). The importance of Ukraine and the Russian Federation for global agricultural markets and the risks associated with the current conflict.

Nadeem, S.M., Zahir, Z.A., Naveed, M., Ashraf, M., 2010. Microbial ACC-Deaminase: Prospects and Applications for Inducing Salt Tolerance in Plants. Critical Reviews in Plant Sciences 29, 360–393. Nimmo, H.G., 2000. The regulation of phosphoenolpyruvate carboxylase in CAM plants. Trends in Plant Science 5, 75–80.

Okamoto, M., Kumar, A., Li, W., Wang, Y., Siddiqi, M.Y., Crawford, N.M., Glass, A.D.M., 2006. High Affinity Nitrate Transport in Roots of Arabidopsis Depends on Expression of the NAR2 -Like Gene AtNRT3.1. Plant Physiol. 140, 1036–1046.

Orozco-Mosqueda, Ma. del C., Duan, J., DiBernardo, M., Zetter, E., Campos-García, J., Glick, B.R., Santoyo, G., 2019. The Production of ACC Deaminase and Trehalose by the Plant Growth

Promoting Bacterium Pseudomonas sp. UW4 Synergistically Protect Tomato Plants Against Salt Stress. Front. Microbiol. 10, 1392.

Orsel, M., Chopin, F., Leleu, O., Smith, S.J., Krapp, A., Daniel-Vedele, F., Miller, A.J., 2006. Characterization of a Two-Component High-Affinity Nitrate Uptake System in Arabidopsis. Physiology and Protein-Protein Interaction. Plant Physiol. 142, 1304–1317.

Oteino, N., Lally, R.D., Kiwanuka, S., Lloyd, A., Ryan, D., Germaine, K.J., Dowling, D.N., 2015. Plant growth promotion induced by phosphate solubilizing endophytic Pseudomonas isolates. Front. Microbiol. 6.

Owen, A.G., Jones, D.L., 2001. Competition for amino acids between wheat roots and rhizosphere microorganisms and the role of amino acids in plant N acquisition. Soil Biology and Biochemistry 33, 651–657.

Padilla, F. M., Gallardo, M., & Manzano-Agugliaro, F. (2018). Global trends in nitrate leaching research in the 1960–2017 period. *Science of the Total Environment*, *643*, 400-413.

Panpatte, D. G., Shukla, Y. M., Shelat, H. N., Vyas, R. V., & Jhala, Y. K. (2017). Bacterial volatile organic compounds: a new insight for sustainable agriculture. In Microorganisms for Green Revolution (pp. 672 151-166). Springer, Singapore.

Pant, G., Garlapati, D., Agrawal, U., Prasuna, R. G., Mathimani, T., & Pugazhendhi, A. (2020). Biological approaches practised using genetically engineered microbes for a sustainable environment: A review. Journal of Hazardous Materials, 124631.

Podile, A. R. & Kishore, G. K. Plant growth-promoting rhizobacteria. in Plant-Associated Bacteria (ed. Gnanamanickam, S. S.) 195–230 (Springer Netherlands, 2006). doi:10.1007/978-1-4020-4538-76.

Poitout, A., Martinière, A., Kucharczyk, B., Queruel, N., Silva-Andia, J., Mashkoor, S., Gamet, L., Varoquaux, F., Paris, N., Sentenac, H., Touraine, B., Desbrosses, G., 2017. Local signalling pathways regulate the Arabidopsis root developmental response to Mesorhizobium loti inoculation. Journal of Experimental Botany 68, 1199–1211.

Pratelli, R., Pilot, G., 2014. Regulation of amino acid metabolic enzymes and transporters in plants. Journal of Experimental Botany 65, 5535–5556.

Prusiner, S., & Stadtman, E. R. (1973). The enzymes of glutamine metabolism. Academic Press.

Ramamoorthy, V., Viswanathan, R., Raguchander, T., Prakasam, V., Samiyappan, R., 2001. Induction of systemic resistance by plant growth promoting rhizobacteria in crop plants against pests and diseases. Crop Protection 20, 1–11.

Ranathunge, K., El-Kereamy, A., Gidda, S., Bi, Y. M., & Rothstein, S. J. (2014). AMT1; 1 transgenic rice plants with enhanced NH4+ permeability show superior growth and higher yield under optimal and suboptimal NH4+ conditions. Journal of experimental botany, 65(4), 965-979.

Ravishankara, A. R., Daniel, J. S., Portmann, R. W., (2009). "Nitrous Oxide (N_2O): The Dominant Ozone Depleting Substance Emitted in the 21st Century." Science 326(5949): 123-125.

Raymond, J., Siefert, J.L., Staples, C.R., Blankenship, R.E., 2004. The Natural History of Nitrogen Fixation. Molecular Biology and Evolution 21, 541–554.

Remans, T., Nacry, P., Pervent, M., Girin, T., Tillard, P., Lepetit, M., & Gojon, A. (2006). A central role for the nitrate transporter NRT2. 1 in the integrated morphological and physiological responses of the root system to nitrogen limitation in Arabidopsis. *Plant physiology*, *140*(3), 909-921.

Richardson, A. E. (2001). Prospects for using soil microorganisms to improve the acquisition of phosphorus by plants. Functional Plant Biology, 28(9), 897-906.

Rodionov, D. A., Dubchak, I. L., Arkin, A. P., Alm, E. J., & Gelfand, M. S. (2005). Dissimilatory metabolism of nitrogen oxides in bacteria: comparative reconstruction of transcriptional networks. PLoS computational biology, 1(5), e55.

Roychowdhury, R., Qaiser, T.F., Mukherjee, P., Roy, M., 2019. Isolation and Characterization of a Pseudomonas aeruginosa Strain PGP for Plant Growth Promotion. Proc. Natl. Acad. Sci., India, Sect. B Biol. Sci. 89, 353–360.

Rubio, L. M., & Ludden, P. W. (2005). Maturation of nitrogenase: a biochemical puzzle. *Journal of Bacteriology*, *187*(2), 405-414.

Rubio, L.M., Ludden, P.W., 2008. Biosynthesis of the Iron-Molybdenum Cofactor of Nitrogenase. Annu. Rev. Microbiol. 62, 93–111.

Ryu, C., Hu, C., Reddy, M.S., Kloepper, J.W., 2003. Different signaling pathways of induced resistance by rhizobacteria in Arabidopsis thaliana against two pathovars of Pseudomonas syringae. New Phytologist 160, 413–420.

Saharan, B., Nehra, V., n.d. Plant Growth Promoting Rhizobacteria: A Critical Review 30.

Saiz-Fernández, I., De Diego, N., Sampedro, M. C., Mena-Petite, A., Ortiz-Barredo, A., & Lacuesta, M. (2015). High nitrate supply reduces growth in maize, from cell to whole plant. Journal of Plant Physiology, 173, 120-129.

Sanford, R. A., Wagner, D. D., Wu, Q., Chee-Sanford, J. C., Thomas, S. H., Cruz-García, C., ... & Löffler, F. E. (2012). Unexpected nondenitrifier nitrous oxide reductase gene diversity and abundance in soils. Proceedings of the National Academy of Sciences, 109(48), 19709-19714.

Sasse, J., Martinoia, E., Northen, T., 2018. Feed Your Friends: Do Plant Exudates Shape the Root Microbiome? Trends in Plant Science 23, 25–41.

Scotti, R., D'Agostino, N., Zaccardelli, M., 2019. Gene expression profiling of tomato roots interacting with Pseudomonas fluorescens unravels the molecular reprogramming that occurs during the early phases of colonization. Symbiosis 78, 177–192.

Setten, L., Soto, G., Mozzicafreddo, M., Fox, A.R., Lisi, C., Cuccioloni, M., Angeletti, M., Pagano, E., Díaz Paleo, A., Ayub, N.D., 2013. Engineering Pseudomonas protegens Pf-5 for Nitrogen Fixation and its Application to Improve Plant Growth under Nitrogen-Deficient Conditions. PLoS ONE 8, e63666

Sieciechowicz, K.A., Joy, K.W., Ireland, R.J., 1988. The metabolism of asparagine in plants. Phytochemistry 27, 663–671.

Singh, J.S., Pandey, V.C., Singh, D.P., 2011. Efficient soil microorganisms: A new dimension for sustainable agriculture and environmental development. Agriculture, Ecosystems & Environment 140, 339–353.

Silby, M. W., Cerdeño-Tárraga, A. M., Vernikos, G. S., Giddens, S. R., Jackson, R. W., Preston, G. M., ... & Thomson, N. R. (2009). Genomic and genetic analyses of diversity and plant interactions of Pseudomonas fluorescens. Genome biology, 10(5), 1-16.

Smercina, D. N., Evans, S. E., Friesen, M. L., & Tiemann, L. K. (2019). To fix or not to fix: controls on free-living nitrogen fixation in the rhizosphere. Applied and Environmental Microbiology, 85(6), e02546-18.

Smith, C.J., Nedwell, D.B., Dong, L.F., Osborn, A.M., 2007. Diversity and Abundance of Nitrate Reductase Genes (narG and napA), Nitrite Reductase Genes (nirS and nrfA), and Their Transcripts in Estuarine Sediments. AEM 73, 3612–3622.

Smith, C., Hill, A. K., & Torrente-Murciano, L. (2020). Current and future role of Haber–Bosch ammonia in a carbon-free energy landscape. *Energy & Environmental Science*, *13*(2), 331-344.

Sopanen, T., Burston, D., Matthews, D.M., 1977. Uptake of small peptides by the scutellum of germinating barley. FEBS Letters 79, 4–7.

Srivastava, S., Chaudhry, V., Mishra, A., Chauhan, P.S., Rehman, A., Yadav, A., Tuteja, N., Nautiyal, C.S., 2012. Gene expression profiling through microarray analysis in Arabidopsis thaliana colonized by Pseudomonas putida MTCC5279, a plant growth promoting rhizobacterium. Plant Signaling & Behavior 7, 235–245.

Stajkovic, O., Delic, D., Josic, D., Kuzmanovic, D., Rasulic, N., & Knezevic-Vukcevic, J. (2011). Improvement of common bean growth by co-inoculation with Rhizobium and plant growth-promoting bacteria. Romanian Biotechnological Letters, 16(1), 5919-5926.

Torres, M.J., Simon, J., Rowley, G., Bedmar, E.J., Richardson, D.J., Gates, A.J., Delgado, M.J., 2016. Nitrous Oxide Metabolism in Nitrate-Reducing Bacteria, in: Advances in Microbial Physiology. Elsevier, pp. 353–432.

Trinh, C.S., Lee, Hyeri, Lee, W.J., Lee, S.J., Chung, N., Han, J., Kim, J., Hong, S.-W., Lee, Hojoung, 2018. Evaluation of the plant growth-promoting activity of Pseudomonas nitroreducens in Arabidopsis thaliana and Lactuca sativa. Plant Cell Rep 37, 873–885.

Trivedi, P., Leach, J. E., Tringe, S. G., Sa, T., & Singh, B. K. (2020). Plant–microbiome interactions: from community assembly to plant health. Nature reviews microbiology, 18(11), 607-621.

Urquhart, A.A., Joy, K.W., 1981. Use of Phloem Exudate Technique in the Study of Amino Acid Transport in Pea Plants. Plant Physiol. 68, 750–754.

United States Department for Agriculture (USDA) Economic Research Service. International Agricultural Productivity.

Venieraki, A., Dimou, M., Vezyri, E., Vamvakas, A., Katinaki, P.-A., Chatzipavlidis, I., Tampakaki, A., Katinakis, P., 2014. The Nitrogen-Fixation Island Insertion Site Is Conserved in Diazotrophic Pseudomonas stutzeri and Pseudomonas sp. Isolated from Distal and Close Geographical Regions. PLoS ONE 9, e105837.

Vessey, J. K. (2003). Plant growth promoting rhizobacteria as biofertilizers. Plant and soil, 255(2), 571-586.

Walter, A., Römheld, V., Marschner, H., & Crowley, D. E. (1994). Iron nutrition of cucumber and maize: effect of Pseudomonas putida YC 3 and its siderophore. Soil Biology and Biochemistry, 26(8), 1023-1031.

Wang, H., Deng, N., Wu, D., Hu, S., 2017. Quantitative response relationships between net nitrogen transformation rates and nitrogen functional genes during artificial vegetation restoration following agricultural abandonment. Sci Rep 7, 7752.

Waterworth WM, Bray CM. Enigma variations for peptides and their transporters in higher plants. Ann Bot. 2006 Jul;98(1):1-8. doi: 10.1093/aob/mcl099. Epub 2006 May 30. PMID: 16735405; PMCID: PMC2803549.

Wilton, R., Ahrendt, A. J., Shinde, S., Sholto-Douglas, D. J., Johnson, J. L., Brennan, M. B., & Kemner, K. M. (2018). A new suite of plasmid vectors for fluorescence-based imaging of root colonizing pseudomonads. Frontiers in plant science, 8, 2242.

Yan, Y., Yang, J., Dou, Y., Chen, M., Ping, S., Peng, J., Lu, W., Zhang, W., Yao, Z., Li, H., Liu, W., He, S., Geng, L., Zhang, X., Yang, F., Yu, H., Zhan, Y., Li, D., Lin, Z., Wang, Y., Elmerich, C., Lin, M., Jin, Q., 2008. Nitrogen fixation island and rhizosphere competence traits in the genome of root associated Pseudomonas stutzeri A1501. Proceedings of the National Academy of Sciences 105, 7564–7569.

Yang, Z., Han, Y., Ma, Y., Chen, Q., Zhan, Y., Lu, W., Cai, L., Hou, M., Chen, S., Yan, Y., Lin, M., 2018. Global investigation of an engineered nitrogen-fixing Escherichia coli strain reveals regulatory coupling between host and heterologous nitrogen-fixation genes. Sci Rep 8, 10928.

Yu, P., He, X., Baer, M. et al. Plant flavones enrich rhizosphere Oxalobacteraceae to improve maize performance under nitrogen deprivation. Nat. Plants 7, 481–499 (2021). https://doi.org/10.1038/s41477-021-00897-y

Zahir, Z. A., Arshad, M., & Frankenberger, W. T. (2004). Plant growth promoting. *Advances in agronomy*, *81*, 97.

Zhang, T., Yan, Y., He, S., Ping, S., Alam, K.M., Han, Y., Liu, X., Lu, W., Zhang, W., Chen, M., Xiang, W., Wang, X., Lin, M., 2012. Involvement of the ammonium transporter AmtB in nitrogenase regulation and ammonium excretion in Pseudomonas stutzeri A1501. Research in Microbiology 163, 332–339.

Zhuo, D., Okamoto, M., Vidmar, J. J., & Glass, A. D. (1999). Regulation of a putative high-affinity nitrate transporter (Nrt2; 1At) in roots of Arabidopsis thaliana. *The Plant Journal*, *17*(5), 563-568.

Chapter 3

Preface to Chapter 3

This chapter of the thesis introduces the morphological responses of *Brachypodium distachyon* to inoculation with the beneficial microbe *Pseudomonas koreensis*, with focus on the roots of *B. distachyon* under two different nitrogen levels that represent limited and sufficient N. The plant-microbe interaction was investigated using ^{15}N natural abundance, temporal phenotyping and elemental analyses.

This study showed that the plant growth-promoting bacterium *Pseudomonas koreensis Ps9-14* can double the overall biomass of *B. distachyon* under limited N in both root and shoot tissues. An overall increase of the total root length was observed, which is based on an increase in lateral root length after inoculation of Brachypodium under limited N. Non-invasive and invasive leaf area measurements showed an increase in Brachypodium leaf area under limited N inoculation with *P. koreensis*. To test the hypothesis of biological N fixation (BNF), a ^{15}N natural abundance experiment was conducted, showing trends of reduced $\delta^{15}N$ signature after inoculation with *P. koreensis* under zero and limited N (11.1 – 29.1%). Simultaneously, in limited nitrogen conditions post-inoculation with *Pk*, nitrogen content in Brachypodium increased by up to 0.140 mg. This study has demonstrated that nitrogen deprivation can be overcome with the use of the beneficial *P. koreensis* and thus might be able to support the reduction of synthetic fertilizer synthesis and application.

3.1 Introduction

Traditional phenotyping to quantify plant traits is performed with manual, destructive (invasive) harvests. Invasive phenotyping requires to damage or destroy the plants at fixed timepoints or phenological stages to quantify the measured parameter(s). However, invasive phenotyping is labor-intensive and time-consuming, and the throughput is limited by the individual carrying out the phenotyping. Person-derived errors are also more common due to the necessity to involve multiple people.

High-throughput phenotyping can scale up the number of plants used for phenotyping, by automation of imaging and data processing. The review by Poorter et al., 2023

summarises the advantages and disadvantages of high-throughput phenotyping, including studies reporting the use of fully automated systems (Furbank and Tester, 2011; Fiorani and Schurr, 2013; Tardieu et al., 2017; Lorence and Jimenez, 2022, Poorter et al., 2023). The use of automated processes is both achieved in a controlled environment (Nagel et al., 2012) and field trials, by the use of ground vehicles (White and Conley, 2013; Deery et al., 2014), drones or unmanned aerial vehicles (UAV) (Vargas et al., 2020; Roth et al., 2022; Poorter et al., 2023).

The use of non-invasive phenotyping has made significant advances in recent years, allowing higher resolution of different plant phenotypic traits over time, by using a wide range of non-destructive sensors. These sensors include digital RGB (red, green and blue), hyperspectral, fluorescence and thermal cameras or laser scanners (Li et al., 2014; Poorter et al., 2023). Digital RGB cameras are using silicon sensors for visible light imaging, charge-coupled device (CCD) cameras for imaging fluorescent signals, thermal cameras for imaging of surface temperatures, or multispectral/hyperspectral cameras imaging a wide range of wavelengths (Li et al., 2014; Poorter et al., 2023).

However, plant phenotyping comes with challenges, such as the environmental conditions or variance in the phenotype within the same genotype of plants (Poorter et al., 2023). A wide range of phenotypic traits can already be measured non-invasively, such as root morphology (Walter et al., 2009; Clark et al., 2011; Flavel et al., 2012; Kumar et al., 2014), biomass (Menzel et al., 2009; Golzarian et al., 2011), leaf characteristics (Jansen et al., 2009; Arvidsson et al., 2011), photosynthetic efficiency (Bauriegel et al., 2011), yield related traits (Duan et al., 2011) and biotic or abiotic stress responses (Balachandran et al., 1997; Rao et al., 2013; Li et al., 2014). Algorithms predicting these invasively measured traits need proper calibration, often limited to a controlled environment. With the recent advances in these techniques, it is realistic that more and more non-invasive and invasive traits will become available in high-throughput phenotyping in the near future. These advances will both increase the experimental throughput, such as genotype and plant yield screening.

A combination of different cameras/sensors will lead to improved plant phenotyping on various levels, such as physiological, molecular or biochemical level. The review by Li et al., 2014 summarizes the different sensors and their applications in detail (Li et al., 2014). A more recent review about high-throughput plant phenotyping platforms was written by Yang et al., 2020, summarizing various high-throughput plant phenotyping platforms and their limitations and advantages (Yang et al., 2020). As visible light images produced by digital RGB cameras are limited to physiological phenotyping, it is a very affordable and an easy-to-use option, as digital RGB cameras with sufficient solution can be found for instance in smartphones. The images reflect human perception and are represented digitally by pixels, which use the three spectral bands of visible light: Red (~600 nm), green (~550 nm) and blue (~450 nm) forming the RGB colour space (Li et al., 2014). Digital cameras are commonly used in a laboratory or field environment to monitor various parameters of shoots and roots non-invasively through time. For shoots, visible light images can be used to measure shoot biomass (Golzarian et al., 2011; Arvidsson et al., 2011), leaf morphology (Hoyos-Villegas et al., 2014) and root architecture (Iyer-Pascuzzi et al., 2010; Clark et al., 2011; Li et al., 2014).

Fluorescence imaging is associated with invasive harvests, as most fluorescence imaging techniques involve a microscope and are therefore limited to, for instance, single leaf or single cell studies (e.g. protoplasts). For fluorescent signals, samples have to be excited with specific wavelengths using lasers, limiting its application on the field. However, using fluorescence imaging, phenotyping at physiological and biochemical level can be performed. While many plant components are autofluorescent at different wavelengths, the autofluorescence already yields much information about processes happening in the plant. Wavelengths between 680 – 700 nm and 720 – 735 nm are associated with the photosystem II and I, respectively, and thus can give indications about the chlorophyll content (Barbagallo et al., 2003; Li et al., 2014; Donaldson 2020). An overview about the use of fluorescent imaging using the autofluorescence in plants was published by Lloyd Donaldson (2020). Fluorescent imaging is currently used in disease detection (Swarbrick et al., 2006; Bürling et al., 2010; Rolfe and Scholes 2010), estimation of photosynthesis (Jansen et al., 2009), colocalization studies (Pedrosa et al., 2023), detection of secondary

metabolites (Fluorescence Lifetime Spectroscopy, FLIM) and protein-protein interactions (Förster Resonance Emission Transfer, FRET) (Li et al., 2014).

Tomographic imaging includes Magnet Resonance Imaging (MRI), X-ray computed tomography (CT) and Positron Electron Transmission (PET). In MRI, nuclear resonance signals from ^{1}H, ^{13}C, ^{14}N and ^{15}N are detected to generate images (Moradi et al., 2010; Melkus et al., 2011, van As and van Duynhoven 2013). This way it is possible to generate non-invasively three-dimensional (3D) images representing the water content in plants (Windt et al., 2006) or labelled molecules (Melkus et al., 2011). The nuclear imaging technique PET is able to detect non-invasively labelled compounds, like ^{11}C, ^{13}N or ^{52}Fe (Kiyomiya et al., 2001; Jahnke et al., 2009; Tsukamoto et al., 2009). CT uses X-rays to generate a 2D radiographic image, which can be transformed to a 3D image by taking multiple images around a single axis of rotation (Li et al., 2014). This method allows to monitor the root non-invasively and gives information about volumes, densities, and root system architecture (Lontoc-Roy et al., 2006; Perret et al., 2007; Hargreaves et al., 2009; Tracy et al., 2010; Lucas et al., 2011). However, the tomographic imaging is time-intensive and therefore low-throughput but offers high resolution.

Non-invasive phenotyping of roots is especially challenging on a lab-scale, as systems such as Rhizoslides (Le Marie et al., 2014), Rhizoponics (Mathieu et al., 2015) or RhizoTubes (Jeudy et al., 2016) require roots to grow in a liquid medium or agar, not reflecting the normal growing conditions (Yang et al., 2020). This was overcome by the GROWSCREEN-Rhizo platform (Nagel et al., 2012), which was further equipped with sensors to monitor root water content and lignin changes non-invasively (Bodner et al., 2018).

When the data acquisition is upscaled, the data processing also needs to be upscaled. Therefore, algorithms using, for instance, machine- and deep learning approaches have already been developed (Anubha Pearline et al., 2019; Khan et al., 2021) and need further improvement. Additionally, the use of artificial intelligence (AI) is rising and can support image analyses or data processing (Yigit et al., 2019; Singh & Bedi 2021).

The combination of automated phenotyping and data analyses will result in promising high-throughput phenotyping, thus important developments have to be made in multiple directions. Combining these automated processes with the different imaging techniques will ultimately lead to high-throughput phenotyping experiments, useful for breeding or genetic screening approaches. With the combination of the different cameras and their measured parameters, monitoring plant morphological, physiological, and biochemical processes will be achieved non-invasively.

3.2 Material & Methods

3.2.1 Plant cultivation system preparation

Plants were grown in self-modified Plant Cultivation Vessel (hereafter, referred to as PCV) GA-3 containers (#330151, Kisker Biotech). Three individual PCV were stacked on top of each other to obtain a single, closed system (Supplementary Figure 3.1). The middle PCV had its bottom wall sawed off and was stacked on top of the third PCV, using micropore tape (3M) to fix the two containers. The inverted PCV used as a lid was linked to a middle (upright) container using the commercially available connector (#330153, Kisker Biotech). For better gas exchange, a total of 3 holes were drilled in the lid, allowing horizontal and vertical gas exchange. The drilled holes were covered with Micropore Tape to avoid contamination.

The PCV were filled with 900 g of 0.7 - 1.4 mm quartz sand (Quarzwerke Witterschlick), and the whole system (except connector) was autoclaved. The sterilized and filled autoclaved PCV were dried in an oven. From this step on, all further steps take place only in a sterile environment, provided that the closed systems have to be opened for this purpose. Precisely 54.0 g of modified Hoagland solution (composition in a liter of Milli-Q water: 1.76 ml 0.5 M KH_2PO_4, 2.64 ml 1M MES (pH 5.7), 4.39 ml 10 mM $FeSO_4$ + 10 mM Na_2EDTA, 1.76 ml 1 M $CaCl_2$, 1.76 ml 0.375 M $MgSO_4$, 1.76 / 17.6 ml 1 M NH_4NO_3 (limited and sufficient N, respectively) and 0.44 ml micronutrients (50 mM H_3BO_3, 10 mM $MnSO_4$, 2 mM $ZnSO_4$, 5 mM KI, 0.2 mM Na_2MoO_4, 0.1 mM $CoCl_2$, 1 mM $CuSO_4$)) was added to each. To obtain a homogeneous distribution, the sand-medium mixture was shaken manually, and the PCV was tapped on the surface of the bench 7 times to remove sand particles

from the top PCV and compact the sand. A sowing template was used to evenly distribute 3 holes in the PCV. The plan for the sowing template, produced by a 3D laser cutter (Trotec, Speedy 100) is available in Supplementary Figure S3.9. The sowing template (3 mm thickness) is pressed into the PCV until it is flush with the rim. Then, three holes were poked in the sand using a glass stirring rod, with a stopper at depth of 1.3 cm. This ensures that 3 seeds can be placed in each PCV at the exact same positions and depths.

3.2.2 Seed sterilization, sowing and stratification

Brachypodium distachyon Bd21-3 (Vogel & Hill, 2007) (hereafter, referred to as Brachypodium) seeds were removed from long-term storage at 4°C, dehusked and surface sterilized using 70% (v:v) ethanol and 6% (v:v) sodium hypochlorite with 0.01% (v:v) Triton-X 100 as described in Sasse et al. (2019). The following steps were performed in a biosafety cabinet: Sufficient seeds were placed in a 15 ml Falcon tube (Sarstedt) to be washed in 70% ethanol for 30 sec. The ethanol was replaced with 6% sodium hypochlorite and 0.1% Triton X-100 for 5 min and finally washed with sufficient sterile Milli-Q water (5 times). Seeds were stored overnight in water at 4 °C (stratification) before sowing the following day. A single seed was placed in each of the three pre-made holes with sterile tweezers and covered with some sand. Five days after sowing (DAS) excess seedlings were removed and only 1 plant was left in each PCV. Here, seedlings were selected for a homogeneous shoot (emergence) height to conduct the experiment.

3.2.3 Bacterial cultivation and inoculation

Pseudomonas koreensis Ps9-14T (DSM16610, Germany) was cultivated using Luria-Bertani (LB) medium (optional 1% agar w:v for plates). Four DAS, a single colony was picked from an agar plate and cultivated overnight in LB liquid medium at 220 rpm, 29 °C. Using a portable photometer, the optical density (OD_{600}) of 1 ml bacteria suspension was measured. A bacterial growth curve was recorded and established that OD_{600} of 0.5 corresponds to $1x10^8$ CFU ml^{-1}. If the bacterial OD was in the exponential phase of growth, bacteria from the overnight culture were centrifuged at 3000 rpm for 15 minutes and the supernatant (LB medium) was removed. The bacteria were dissolved in 1 ml of the appropriate modified Hoagland solution (limited or sufficient N) and further diluted to

$5x10^6$ CFU ml^{-1} in a dilution series. From this bacterial solution, 100 µl per system were added directly to the seed of each seedling ($5x10^5$ CFU). For control plant (non-inoculated), 100 µl of the respective Hoagland solution was used, and added to keep equal amounts of nutrients in each system. Magenta jars were imaged for non-invasive shoot phenotyping (c.f. Non-invasive shoot phenotyping) before being closed and transferred to growth chambers.

3.2.4 Plant growth conditions and experimental setup

Plants were grown in growth chambers (CLF PlantClimatics GmBH, Model AR-22L) under a long day period of 16/8 h with 23/18 °C day/night, 100-140 µmol/$m^{-2}s^{-1}$ of light and 35% relative humidity.

The experimental design for the three independent experiments is displayed in Fig. 3.1. The plants were cultivated for 21 DAS and were removed from the growth chamber at 5 DAS for inoculation and non-invasive shoot phenotyping (every 2 days) and watering at 7 and 14 DAS. The sterile, closed growth system was only opened and operated inside a biosafety cabinet.

The closed plant growth systems were placed inside of multiple growth chambers with the same settings due to space requirements and randomized across the different growth chambers (Plants changed position at each imaging time-point).

3.2.5 Non-invasive shoot phenotyping

Magenta Jars were moved to the biosafety cabinet and, with the lid removed, imaged from 3 different angles (90° rotation clockwise), while maintaining the same distance and angle of the camera. As biosafety cabinets are limited in space, a small photobox with beige background (Proxistar Studiogeräte) was used. The non-invasive shoot phenotyping interval was as following: 5, 7, 9, 11, 13, 15, 17, 19, 20, 21 DAS. Invasive harvests were conducted at 19, 20, 21 DAS.

The shoot images were captured using a smartphone (Samsung Galaxy Note8, 2017). A mobile smartphone clamp-on holder was attached to the window at the biosafety cabinet and supported by a lab stand (Supplementary Figure S3.8). Using a color space-based segmentation tool (Müller-Linow et al., 2022), the projected leaf area was calculated based on the masked plant pixel count in the HSV color space. The following thresholds were applied: Hue (44.4 - 127.5), Saturation (66.6 - 255), Value (6.75 - 255). Conversion to cm^2 from the number of pixels was calculated as Pixel count x 0.0001728 for limited N and Pixel count x 0.000205 for sufficient N plants.

3.2.6 Invasive root and shoot phenotyping

While all available plants were imaged at each time-point, at 19, 20, 21 DAS, a subset of plants for each treatment (total n = 44) was harvested. Five plants at each time point and treatment were used for invasive phenotyping, while 6 plants were used for molecular analyses (Chapter 4).

After removing the roots from the Magenta Jars, they were carefully washed in a small beaker filled with sterile Milli-Q water to remove all sand particles stuck to the roots. Roots and shoots were separated using a sterilized scissor and fresh weight was determined. Depending on their purpose, tissues were either directly frozen in liquid N for molecular analyses or used for phenotyping. Roots and shoots for phenotyping were both scanned individually using the WinRhizo platform, followed by drying in a drying oven at 65 °C for 3 days. Dry weight was determined, and the tissues were homogenised using a ball mill (Retsch, MM 400) with a single bead (3 mm) for 1 min with a frequency of 30 hz. Ground tissues were used for elemental analyses of the N and C content.

The WinRhizo (Regent Instruments Inc., Ottawa, ON, Canada) generated root images were then loaded into PaintRhizo (Nagel et al., 2012), the total root length was dissected in primary seminal root (PSR) length and lateral root length (LR).

Total N and C content was analysed using dried roots and shoots, using a CHNS analyser (Vario EL Cube, Elementar) with thermal conductivity detection.

3.2.7 ^{15}N natural abundance

An independent experiment was conducted for ^{15}N measurements. Sixty plants were grown under ^{15}N natural abundance (non-enriched) and ^{15}N-enriched conditions. For each enrichment, 30 plants were grown in 6 conditions (n = 5 per condition): Zero N Control, Zero N + *Pk*, Limited N Control, Limited N + *Pk* sufficient N Control, Sufficient N + *Pk*. The experiment was conducted just as described above, except for the enriched systems containing an enrichment of 300 per mill double-labelled $^{15}NH_4$-$^{15}NO_3$ (Campro scientific, CAS #43086-60-8). Plants were harvested at 21 DAS and freeze-dried using a lyophilisator.

Dried plant samples were cut with scissors into small pieces to enable weighing and packing. About 0.5 – 1.5 mg dry plant material was packed in tin capsules for stable nitrogen isotope (δ^{15}N) analyses. Samples were combusted at 1060 °C with excess oxygen in an elemental analyser (Flash2000, Thermo Fisher, USA) and measured with a coupled isotope ratio mass spectrometer (DeltaV plus, Thermo Fisher; USA). International and laboratory standards (HZM (Holzmaar sediment), Acetanilide, Alanine, Histidine and Serin) were measured together with the samples. Calibration of laboratory standards and scale-normalisation of δ^{15}N raw values is based upon the international reference standards IAEA-N-2 (δ^{15}N = 20.3‰), IAEA-N-1 (δ^{15}N = 0.4‰) and USGS25 (δ^{15}N = -30.4‰).

Isotope results are reported as δ-values in ‰ according to the equation:

$$\delta = R_S / R_{St} - 1.$$

R_S is the isotope ratio (^{15}N/^{14}N) of the sample and R_{St} of the respective standard. δ-values for nitrogen are normalized to AIR (atmospheric nitrogen) scale (Coplen 2011). The average standard deviation of replicate measurements of standards was <0.20‰ for δ^{15}N.

3.2.8 Data Analysis and Statistics

Statistics performed on each data set were two-way ANOVA ($p < 0.05$) followed by post-hoc Tukey's honestly significant differences (Tukey's HSD) ($p < 0.05$). Statistical tests and visualisation were conducted with R (https://www.r-project.org/).

3.3 Results

Since molecular measurements (proteomics, lipidomics; Chapter 4) required high amounts of initial tissues, three independent experiments were conducted with four conditions: Limited N, Limited N + *Pk*, Sufficient N and Sufficient N + *Pk*. As displayed in Fig. 3.1, the experiments were conducted identically, with different harvests: Harvests (I) were time-resolved, end-point harvests at 19, 20 and 21 DAS, each contributing with n = 5 plants to phenotyping and n = 6 to lipidomics, and Harvest (II) was an end-point harvest at 21 DAS with n = 12 plants for proteomics (Fig. 3.1). Plants of harvest (II) were pooled into 6 replicates with n = 2 plants per pool to meet the required amounts for proteomics (microsomal enrichment + whole proteome). The correlation coefficient for the three independent experiments was calculated (c.f. 3.3.4, Fig. 3.7). Based on the correlation coefficient, it can be concluded that all experiments were behaving very similarly (r = 0.98, 0.98, 0.99) and thus measurements are comparable.

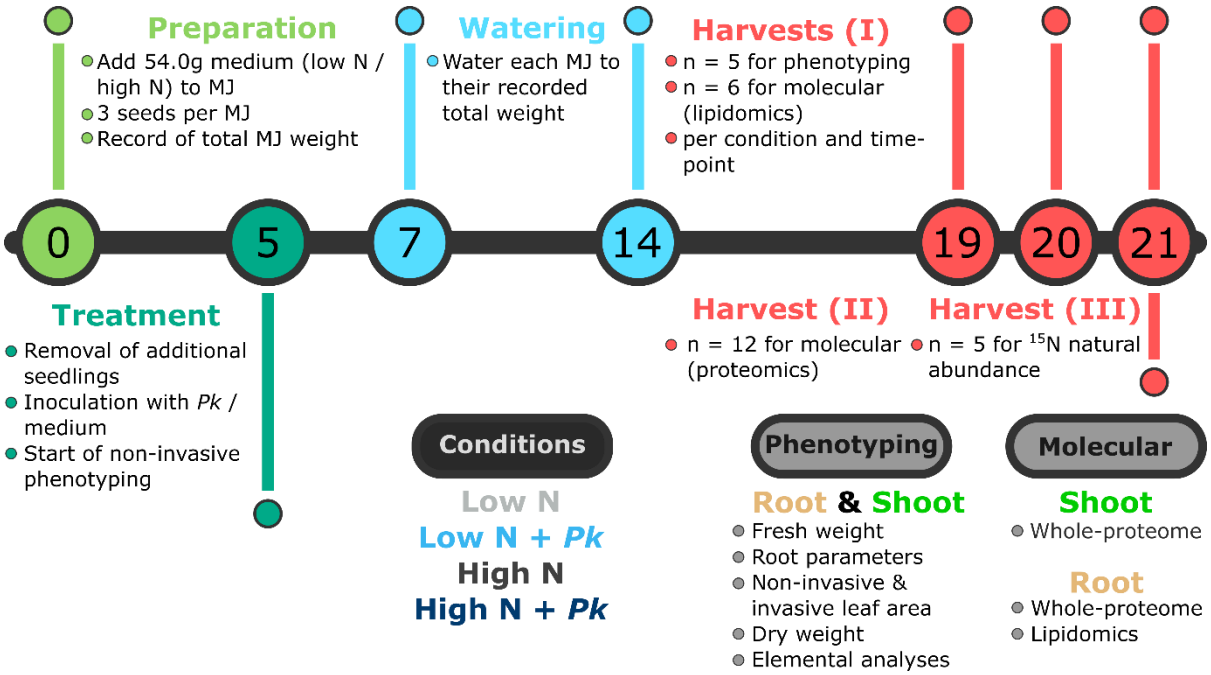

Figure 3.1. Schematic overview of the experimental setup. Numbers in the circles represent days after sowing (DAS). Non-invasive phenotyping was carried out every 2 days after 5 DAS, and on each harvest day. Plants were grown under four different conditions: Limited N, Limited N + *Pk*, Sufficient N, Sufficient N + *Pk*. Three independent experiments were harvested: Harvest (I) Time-series with consecutive harvests on 19, 20, 21 DAS, n = 5 plants for phenotyping and n = 6 plants for lipidomics measurements per condition and per timepoint; Harvest (II) Endpoint 21 DAS harvest with n = 12 plants for proteomic measurements, and Harvest (III) Endpoint 21 DAS harvest with n = 5 plants for ^{15}N natural abundance. Abbreviations: PCV = Plant cultivation vessel, *Pk* = *Pseudomonas koreensis.*

3.3.1 Optimisation of Plant Cultivation Vessels (PCV)

An initial setup was attempted with a single plant cultivation vessel (PCV). With very limited space for plant development especially the root (Fig. 3.2 left), an extension of the system was required. Commercially available PCV and polypropylene frames, connecting two PCV to each other, were ordered from Kisker Biotech, enabling more space for unrestricted plant development (Fig. 3.2 middle). However, a spatial distribution of 50% for root and 50% for shoot development was insufficient for unrestricted root development, thus optimizing the space for root development was required. An additional PCV in between the 'bottom' and 'top' PCV was then added, resulting in 2/3 of the system being filled with sand for root development and 1/3 for shoot development (Fig. 3.2 right).

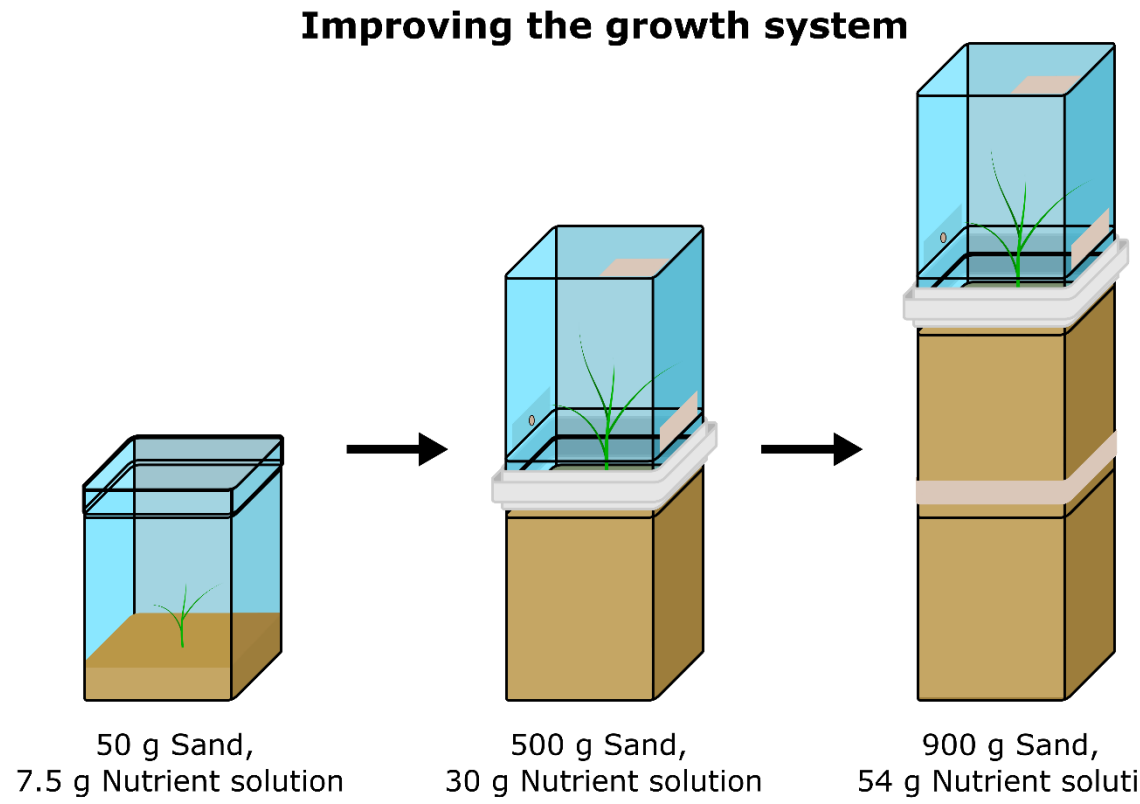

Figure 3.2. Optimization of the PCV system. A single PCV (left) was used for initial trials and the commercially available extension of the system (middle) was used for optimization of the growth conditions. An additional extension (right) was required for the final experiments.

To achieve this, the 'middle' PCV had to be modified and its bottom was removed, and it then was inserted into the 'bottom' PCV. The connecting seam was covered with micropore tape to ensure sterility of the system. These two connected PCVs were then connected to the 'top', inverted PCV via the Polypropylene frame. To enable gas exchange, the 'top' PCV was modified by drilling three holes (2 horizontal, 1 vertical). These holes were again covered with micropore tape, allowing gas exchange while remaining sterility of the system. The final setup and its components and assembly of the PCV are depicted in Figure 3.3.

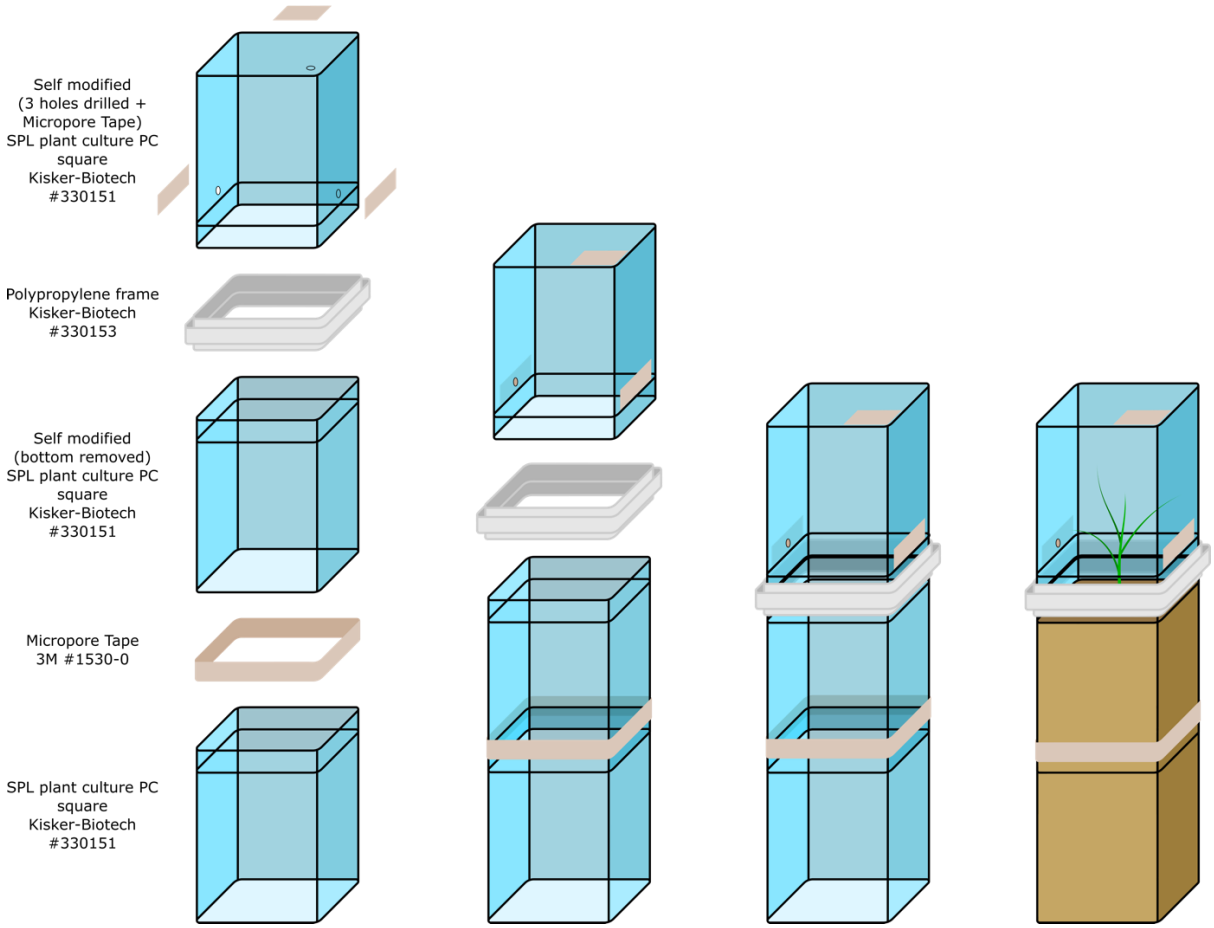

Figure 3.3. Schematic overview of the self-modified plant culture vessels (PCV). The single pieces (left) are assembled after sterilization into the closed growth system, filled with sand and medium. Three seeds are added at 0 days after sowing (DAS) to start the experiment, and at 5 DAS plants are selected for a homogenous shoot emergence height, followed by inoculation of the plants with *P. koreensis*.

3.3.2 Optimisation of plant growth conditions

First, the system was tested for sterility. Therefore, LB-Agar was poured in the PCV and kept under various conditions (growth chamber, office, lab) (Fig. 3.4). The closed system remained sterile without a single colony growing on the LB-Agar for 28 days, then opened once in a non-sterile environment to confirm that contaminants are growing on the medium.

Figure 3.4. Sterility test of the PCV system. Agar was cast in the setup and left in different environments and temperatures. All systems remained sterile for over 28 days.

During the trial experiments, substantial condensation within the closed growth systems was observed. Initially, reducing the condensation was aiming towards the non-invasive shoot phenotyping, so the lid did not have to be removed for imaging. This was not achievable, due to reflections and condensation impacting the shoot detection by the used software. Nevertheless, Brachypodium is a mediterranean grass and therefore not used to high humidity. Thus, I tested different water to weight (w:w) concentrations, testing for optimal growth and the least condensation. The humidity in the growth chamber was also adjusted to allow proper gas exchange, including water vapor. A range between 8.5% (w:w) and 13.5% (w:w) was tested, with 8.5% (w:w) being the best suiting condition (Fig. 3.5) (6% (w:w) nutrient solution + 2.5% (w:w) sterile water). In the course of the time, the final concentration was further reduced to 6% (w:w), by removal of the additional water added to the PCV in addition to the nutrient solution (Tab. 3.1).

The final optimisation of the nutrient solution was the most challenging and time-consuming optimisation, as it required a fine tuning of the limited N conditions. The aim was to increase the N content in limited N conditions to generate more plant material for morphological and biochemical analyses (Chapter 3, Chapter 4, respectively).

Table 3.1. Optimisation process table. Values printed in bold represent the selected condition within the tested range.

PCV	Nutrient solution [ml]	N concentrations [mM]	Holes in lid	Growth conditions	Growth chamber humidity [%]
1	7.5	Low: 0.1 High: 1	no	Light (PAR): 100-140 µmol m^{-2} s^{-1}	60
2	**42.5**, 50.0, 57.5, 65	Low: 0.1, 0.2, 0.3, 0.4, 0.5, **1.0** High: 1, 2, 3, 4, 5, **10**	yes	Day / Night: 16 h / 8 h	**30**, **40**, 50, 60, 70
3	54	Low: 1.5, **1.6**, 1.7 High: 15, **16**, 17	yes	Temperature: 24 / 18 °C	30 - 40

Based on the previous established conditions in a hydroponic system, I started with 0.1 mM and 1 mM for low and sufficient N, respectively. Further nutrient solutions in the range of 0.1 - 0.5 mM (0.1 mM increments) and 1 – 5 mM (1 mM increments) were tested for low and sufficient N, respectively. Using these nutrient concentrations, even the supposedly sufficient N plants showed phenotypic signs of N deficiency, such as chlorotic tissues. Thus, the N content in the nutrient solution was further concentrated and a final concentration of 1 mM and 10 mM for low and sufficient N, respectively, was used in the 2 PCV setup (Fig. 3.6). After further extension of the system, the nutrient content had to be readjusted in a further experiment. Based on previous assumptions and calculations of the available N content, the range in the final setup was narrowed down to 1.5 mM / 15 mM, 1.6 mM / 16 mM and 1.7 mM / 17 mM for low and sufficient N, respectively. As a final concentration, 1.6 mM and 16 mM for low and sufficient N, respectively, was chosen to conduct the time-series experiments (Tab. 3.1).

3.3.3 Optimisation of inoculation method and inoculation quantity

Optimisation of the inoculation method and quantity was a two-step process with two aims: (i) Identify the best inoculation method (seed immersion or seedling inoculation)

and (ii) Identify the best CFU quantity for plant growth promotion. First, a bacteria growth curve matching the measured OD_{600} to the CFU amount was established. Therefore, the liquid bacteria suspension was monitored over 7 hours. LB medium was inoculated with 100 µl of the overnight culture and immediately measured for OD_{600}. Aliquots were prepared for plating using a serial dilution, describing the starting timepoint (0 h). These steps were performed every hour to generate plates with a bacterial density of 30 – 300 CFU. According to their dilution factor, an estimated amount of CFU was determined for each measured OD_{600} and the following bacteria growth curve was generated (Fig. 3.5 (1)).

Initially, a wide range of inoculums containing $1x10^4$ – $1x10^8$ CFU were tested, to narrow down the range into the most promising spectrum. Two inoculation methods, seed immersion and seedling inoculation, have been tested with the mentioned inoculum concentrations. For seed immersion, the seeds were stored for 30 min in 1 ml of liquid culture (LB) containing the desired amount of CFU. Afterwards, the seeds were transferred to the PCV. In terms of seedling inoculation, plants were isolated at 5 DAS and 100 µl of the inoculum with the desired CFU amount was added directly to the seed of the selected seedling. In the method comparison, seedling inoculation showed more beneficial effects on plant development, while the seed immersion showed no effects. Testing $1x10^4$, $1x10^6$ and $1x10^8$ CFU revealed that $1x10^6$ CFU had the biggest impact on plant phenotype. Thus, further optimisation was conducted with the seedling inoculation. The range of the inoculum concentration was narrowed down to $1x10^5$, $1x10^6$ and $1x10^7$ CFU and a follow-up experiment showed that both $1x10^5$ and $1x10^6$ CFU were promising conditions, leading to the conclusion that $5x10^5$ CFU was the optimal CFU amount for seedling inoculation. An additional optimisation was to remove the potential influence of the LB-medium added to the plants. Therefore, the LB bacteria suspension was spun down at max. 3000 g for 15 min, the LB medium was removed, and the remaining pellet was resuspended in the according nutrient solution (limited or sufficient N), before being diluted (Fig. 3.5 (2)). The plants were isolated at 5 DAS (Fig. 3.5 (3)) and afterwards the inoculum was added to the remaining seedling (Fig. 3.5 (4); c.f. Chapter 3.2.2 and 3.2.3). Controls were inoculated with their respective medium only (Fig. 3.5 (4)). The full procedure of plant inoculation is depicted in Fig. 3.5

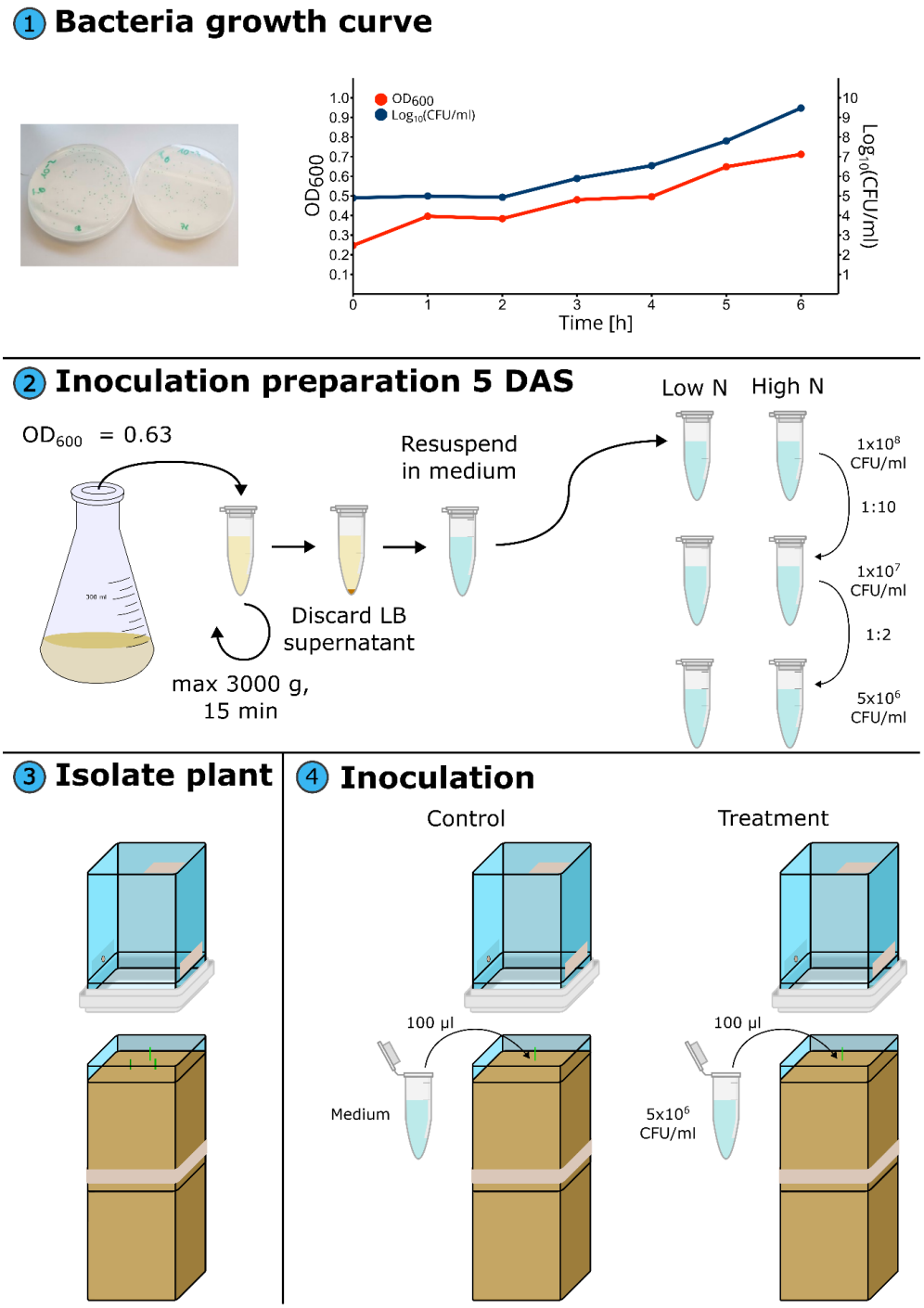

Figure 3.5. Plant inoculation procedure. (1) Example LB agar plates used for colony counting (30 – 300 CFU per plate) to generate the bacteria growth curve; (2) Preparation of inoculum according to the bacteria growth curve, removal of LB medium, dilution to $5x10^6$ CFU/ml; (3) Isolation of the 3 germinated plants by shoot emergence height; (4) Inoculation of the seedling with either medium (controls) or 100 µl of $5x10^6$ CFU/ml ($5x10^5$ CFU).

3.3.4 Establishment and optimisation of non-invasive shoot phenotyping

The non-invasive shoot phenotyping was established early on and further improved by generating more phenotyping data sets to calibrate the factor of conversion between pixels and cm^2. One of the major challenges were non-detected tissues, as the colour-based segmentation software is only recognising green tissues. Limited N plants have developed chlorosis due to N deficiency, while sufficient N plants had partially brown leaves possibly due to an endophytic contamination, most likely in the seeds. Therefore, it was required to calibrate the factors individually for low and sufficient N plants. Every time plants were harvested for phenotyping and leaf area was measured invasively, the data were used to further calibrate the factor of conversion in both conditions. This way, also a high range of leaf area of low and sufficient N plants was used to convert the pixels from the images to the actual leaf area and ultimately monitor the leaf area non-invasively through time.

In the example images (Fig. 3.6), images were chosen, which highlight the problem of non-detected tissues in limited N controls and sufficient N controls, while also showing a perfect fit of the mask on the limited N + *Pk* plant. In case of low and sufficient N controls, both have half a leaf not being detected by the software due to chlorotic tissues (limited N control, Fig. 3.6 top) or a brownish leaf (sufficient N control, Fig. 3.6 bottom). With the adjusted parameters, green tissues are recognized perfectly (limited N + *Pk*, Fig. 3.6 middle) without background being detected. However, non-detectable tissues were found in all conditions, thus the conversion factors were not additionally calibrated to each individual condition. The two used conversion factors were the following:

$$0.000173 \times \text{pixel count} = \text{projected leaf area } [cm^2] \text{ for limited N}$$

$$0.000205 \times \text{pixel count} = \text{projected leaf area } [cm^2] \text{ for sufficient N}$$

I applied the two conversion parameters to the images obtained during the three final, independent experiments (^{15}N, time-series and proteomics) to compare the growth dynamics of the different experiments.

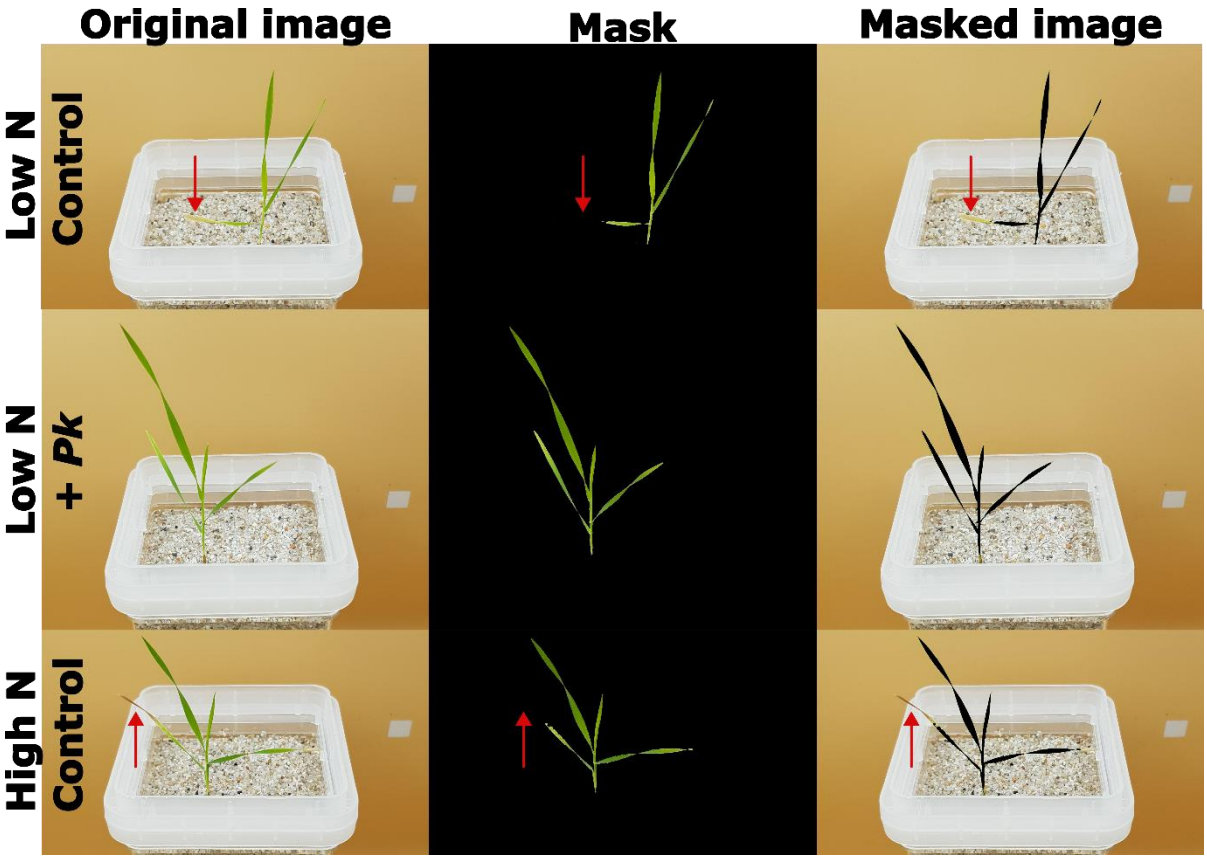

Figure 3.6. Non-invasive shoot phenotyping on example images of time-series harvest (21 DAS). Displayed are original image, mask and the mask applied to the image (from left to right).

Using the non-invasive shoot phenotyping, the repeatability and robustness of the experiments was evaluated using the Pearson correlation coefficient r (Fig. 3.7). This has shown that all experiments correlated very well with each other (r = 0.98 – 0.99) and thus are evidence for comparable experiments and results (Fig. 3.7).

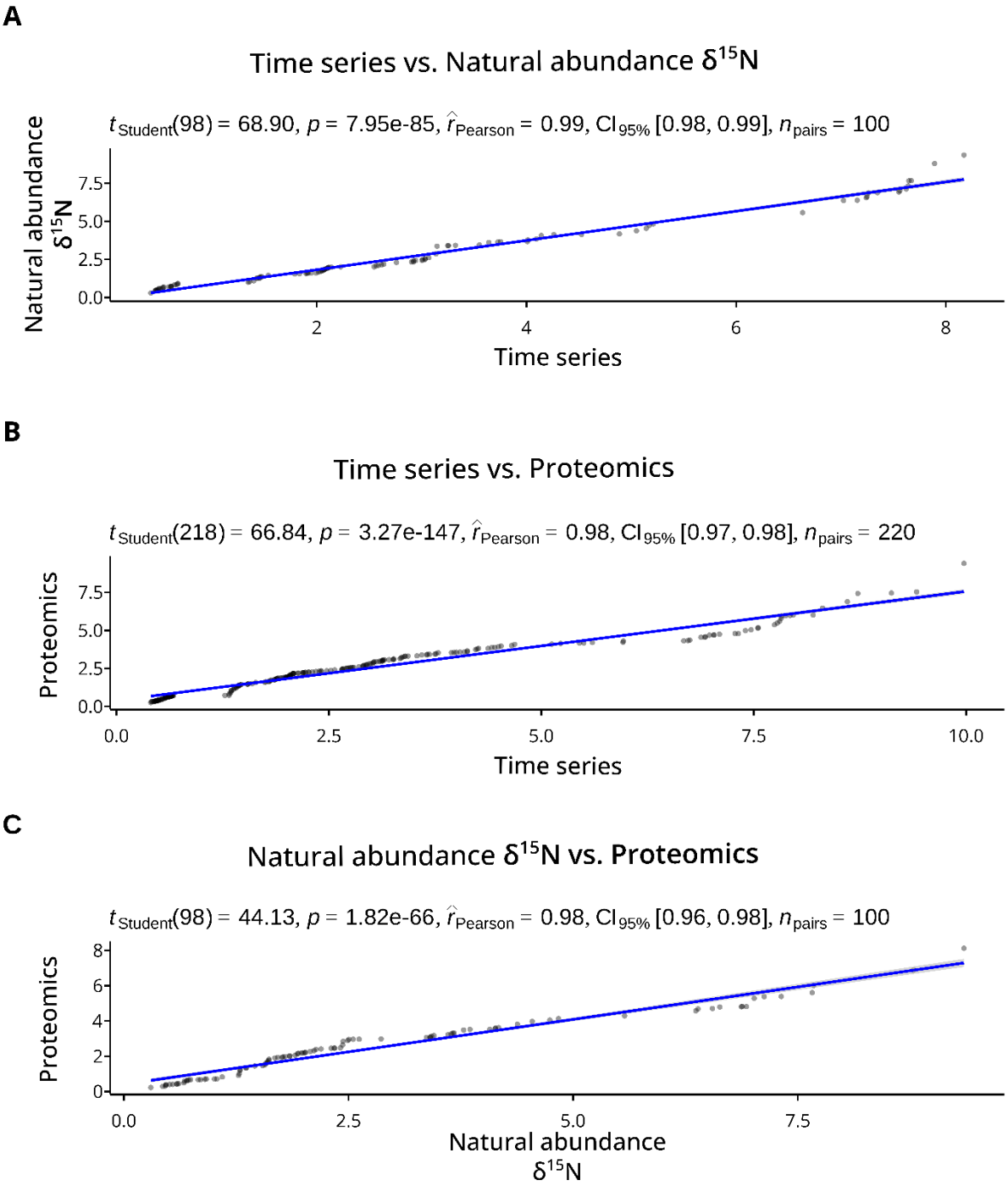

Figure 3.7. Correlation matrices of projected leaf area between all 3 performed experiments. A) Correlation matrix between time series and natural abundance $\delta^{15}N$ (r = 0.99); B) Correlation matrix between time series and proteomics (r = 0.98); C) Correlation matrix between natural abundance $\delta^{15}N$ and proteomics (r = 0.98). Correlations have been calculated using the Pearson correlation coefficient r.

3.3.5 ^{15}N Natural abundance shows trends of nitrogen fixation

When organisms contribute fixed N to a closed system, we expect a reduction in the plant δ^{15}N signature, due to the fixed N having a δ^{15}N signature of ±0, representing value of atmospheric nitrogen, which is not the case for N deriving from fertilizer. Thus, plants grown together with N-fixing organisms should show a decreased δ^{15}N signature versus air compared to control plants grown without N-fixing organism.

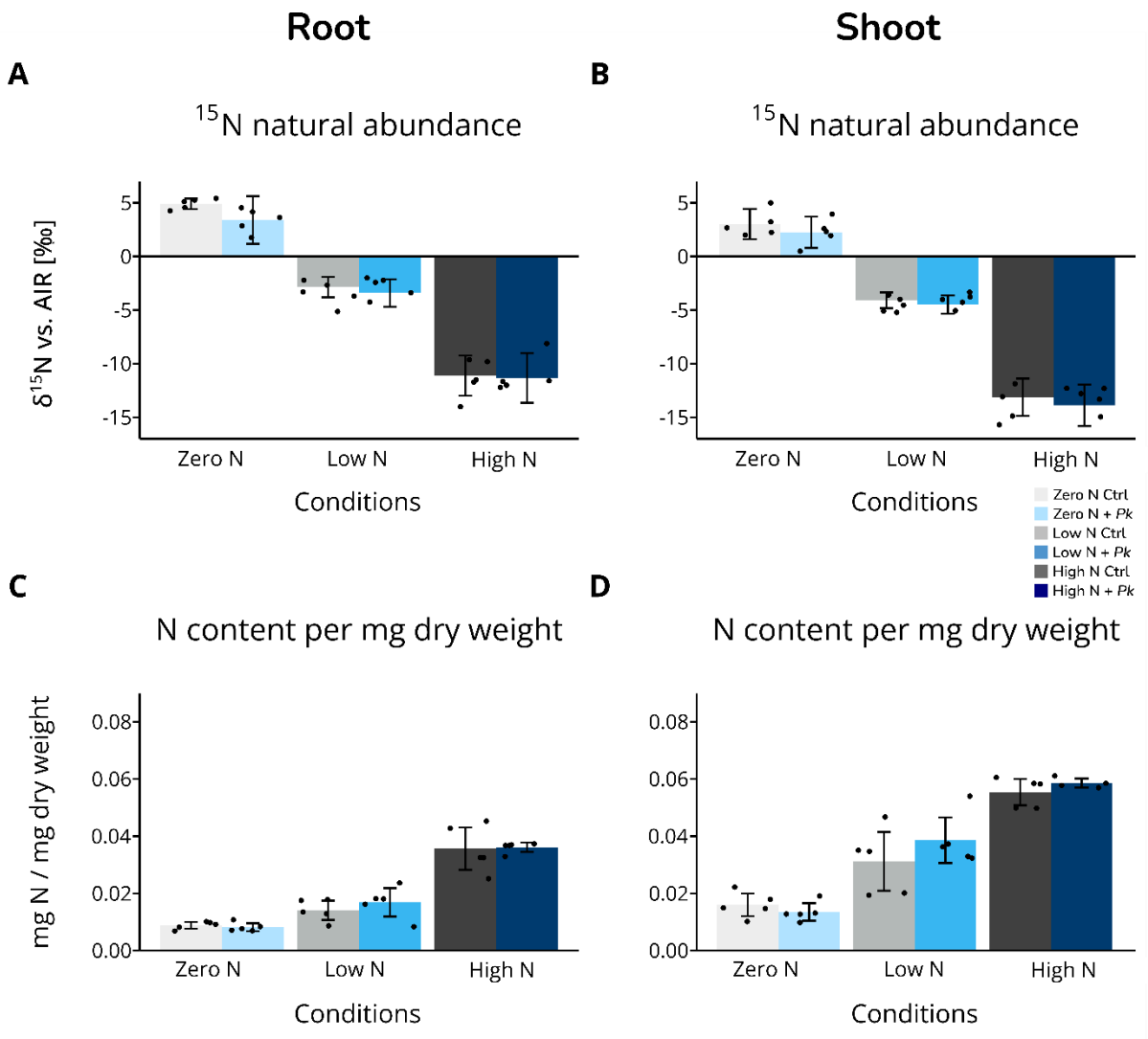

Figure 3.8. Measurement of ^{15}N natural abundance in plant tissue at various N availabilities. A, B) Mean δ^{15}N signatures vs. AIR (n = 5) given as deviation from the medium (δ^{15}N vs. AIR of medium is subtracted) ± standard deviation in root and shoot, respectively; C, D) Absolute N contents in root and shoot per mg dry weight, respectively. Individual replicates are shown as dots on top of their respective bars. Means were compared using two-way ANOVA followed by Tukey's honestly significant difference (HSD) test.

Indeed, measuring the $\delta^{15}N$ signature of Brachypodium, after inoculation with *Pk,* revealed a trend to decreased $\delta^{15}N$ under zero N in roots (29.1%) and shoots (12.8%) and limited N conditions in both root (27.3%) and shoot tissues (11.1%). Under sufficient N, only shoots show a trend of decreased $\delta^{15}N$ signature, (Fig. 3.8 A, B).

In addition, the work of a M.Sc. student under my supervision (Elena Sturm, University of Heidelberg, Germany) showed that *Pk* grown on N deficient medium could continue growing, as could several other *Pseudomonas* strains (*P. syringae PV lapsa*, *P. taiwanensis VLB120*), whereas *E. coli*, which does not have *nif* genes, could not. (Fig. 3.9). This shows *Pk* can fix N at least for its own growth.

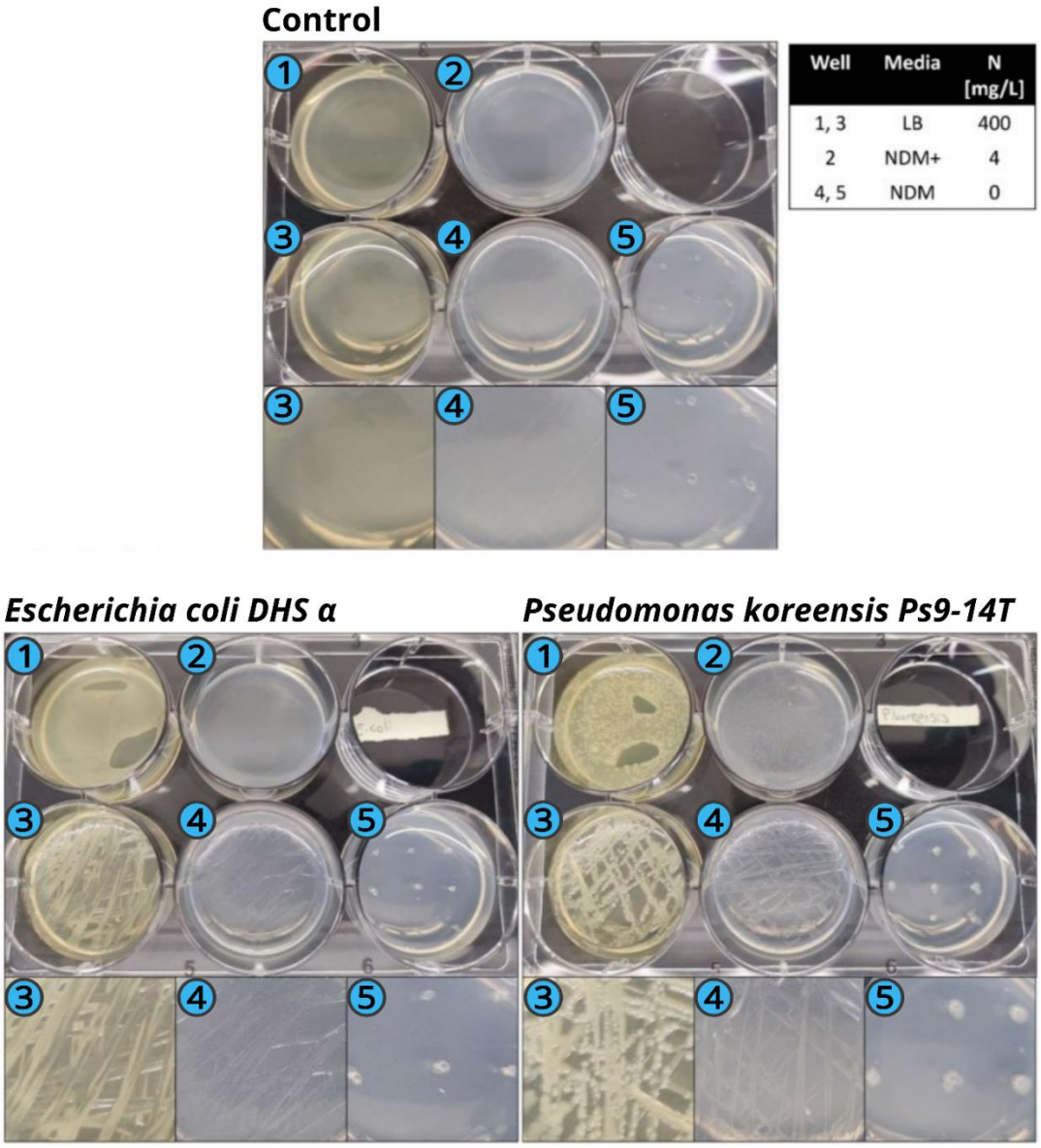

Figure 3.9. Nitrogen fixation plate assay. Represented are three individual plates, containing no bacteria (control, top), *E. coli DHS α* (negative control, bottom left) and *P. koreensis Ps 9-14T* (bottom right). The six-well plates contained LB-medium in wells one and three, nitrogen deficient medium + 4 mg/L N (NDM+) in well two, and nitrogen deficient medium (NDM) in wells four and five.

3.3.6 Brachypodium under limited N shows faster growth and higher biomass when inoculated with *Pk*

Non-invasive measurement of the leaf area revealed that up to 15 DAS, plants mainly responded to the different N availability. However, at 17 DAS, the inoculated plants at limited N started showing an increase in the leaf area. Especially at 20 and 21 DAS, a significant increase in projected leaf area (26.7% and 39.9%, respectively) was observed in *Pk* inoculated plants at limited N, compared to their non-inoculated controls (Fig. 3.10 A). *Pk* inoculation did not impact the leaf area at sufficient N (Fig. 3.10 A).

Analysis of the root architecture revealed a significant increase in total root length (TRL) under limited N and after inoculation with *Pk* at 21 DAS. Dissecting the root system in primary seminal roots (PSR) and lateral roots (LR) showed that the increase in TRL is completely based on an increase LR length (Fig. 3.10 B).

In terms of fresh weight (FW), sufficient N control plants tend to slightly decrease root FW, but significantly increase shoot FW (Fig. 3.10 C) compared to limited N control plants. Inoculation with *Pk* under limited N significantly increased root and shoot FW compared to limited N control plants, with shoot FW being comparable to sufficient N plants (Fig. 3.10 C). Inoculation under sufficient N did not affect root or shoot FW (Fig. 3.10 C).

Comparing the root and shoot biomass of sufficient N control to limited N control plants, we observed a similar distribution to the FW, whereas the root and shoot dry weight (DW) is not significantly different (Fig. 3.10 D). However, inoculation with *Pk* under limited N led to significantly increased root and shoot biomass by 100% compared to their control (Fig. 3.10 D). *Pk* inoculation under sufficient N led to slightly increased root and shoot DW (Fig. 3.10 D).

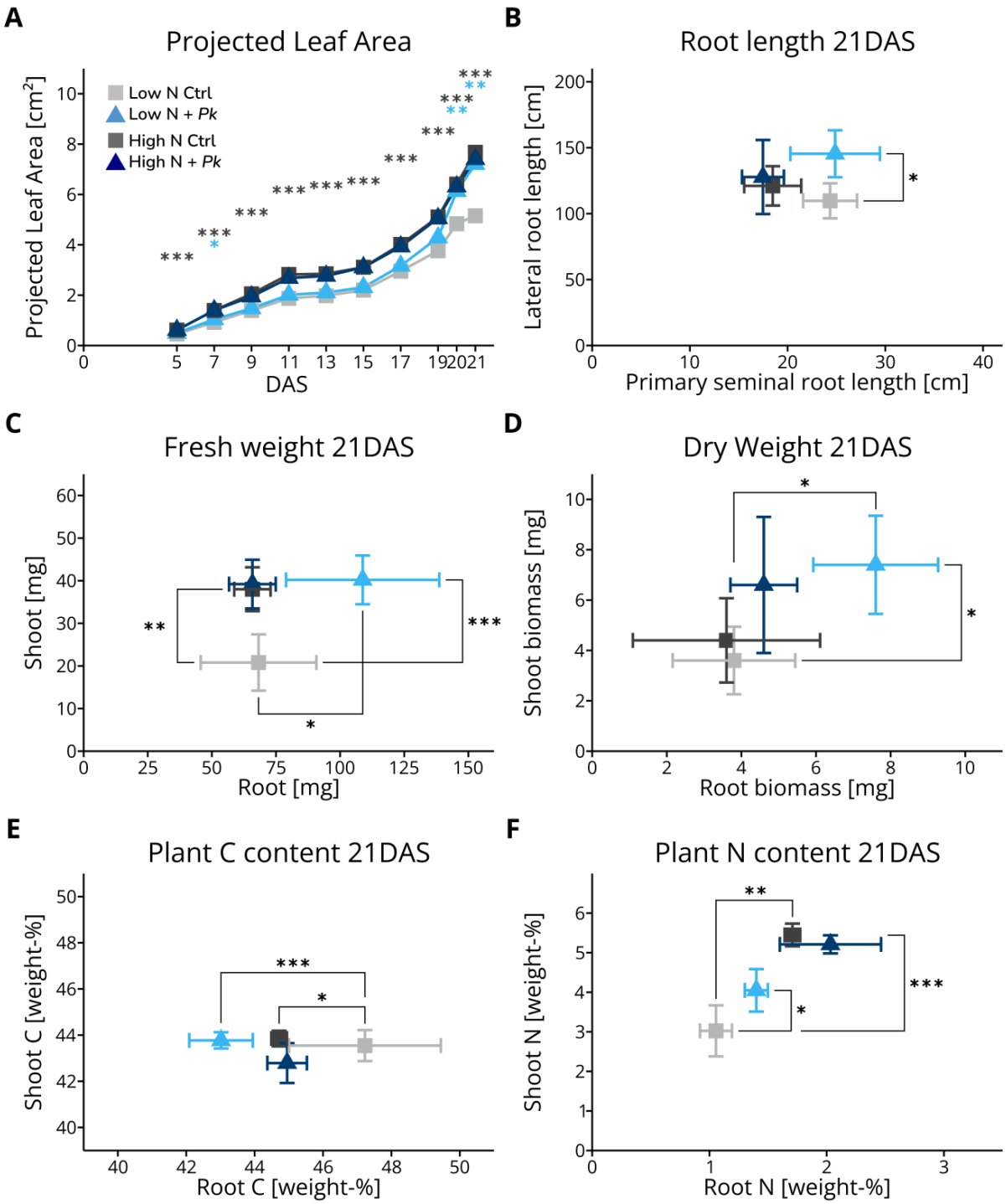

Figure 3.10. Phenotype overview 21 DAS for harvest II (a comparison of plant growth in all 3 independent experiments is shown in Fig 3.1). A) Non-invasive shoot phenotyping of the time-series. B) Root length distribution with Primary seminal root length (x axis) lateral root length (y axis); C) Fresh weight plot with shoot DW (x axis) shoot FW (y axis); D) Dry weight plot with root biomass (x axis), shoot biomass (y axis); E) Plant C content with root C content (x axis), shoot C content (y axis); F) Plant N content with Root N content (y axis) and root N content (y axis). Colored asterisks in plot A represent the condition compared to limited N controls. Means were compared using two-way ANOVA followed by Tukey's honestly significant difference (HSD) test and can be found in Supplementary Table S3.1 and S3.2.

3.3.7 Increased N content in Brachypodium after inoculation with *Pk* in an N-limited environment

Using elemental analyses, the C and N content of the plants were measured. The shoot C content was similar among all conditions (Fig. 3.10 E). Sufficient N control roots have a significantly decreased root C content compared to limited N controls (Fig. 3.10 E). Inoculation of Brachypodium under limited N decreased root C content significantly in comparison to their respective controls. Under sufficient N, inoculation did not affect plant C content significantly (Fig. 3.10 E).

Looking at plant N content, sufficient N control plants have significantly increased root and shoot N content compared to limited N controls (Fig. 3.10 F). Under limited N, inoculation with *Pk* significantly increased shoot N content, while root only showed a trend to increased N content compared to their controls (Fig. 3.10 F). Under sufficient N, inoculation with *Pk* did not affect plant N content significantly (Fig. 3.10 F).

Comparing the total N content (Fig. 3.10 F) to the biomass (Fig. 3.10 D), the biomass did not always correspond to the N content. Although sufficient N control plants had a higher N content than limited N control plants, only minor biomass increases were observed. In contrast, limited N inoculated plants showed increased total plant N content, which can also be observed in the total plant biomass. Under sufficient N, inoculation led to a slightly increased N content in roots compared to their control, while the overall plant biomass is slightly increased. Although limited N + *Pk* plants have less relative plant N content (weight-%) than sufficient N control plants, inoculation increased the absolute amount of N and biomass.

3.4 Discussion

3.4.1 The whole-plant phenotype of Brachypodium is altered by *P. koreensis* under limited N

The influence of *Pk* on the phenotype of Brachypodium was observed in this study under limited N conditions, whereas no beneficial effects were observed under sufficient N. In terms of projected leaf area, limited N plants inoculated with *Pk* had comparable leaf area to plants grown under sufficient N (Fig. 3.10 A). The root system architecture was changed, with an overall increased root length in limited N inoculated plants compared to limited N and sufficient N controls. While the primary seminal root length is comparable to limited N controls, the lateral root length has significantly increased (Fig. 3.10 B). It was not investigated whether the increase in lateral root length is based on (i) increased lateral root number, (ii) increased branching or (iii) longer, already existing, lateral roots. One hypothesis is that the bacterium increases the N uptake in the rhizosphere by increasing lateral root development to scavenge for N (Jia et al., 2021). As the limited N plants are growing in a 10x lower N concentration than sufficient N plants, the depletion of N is achieved faster under limited N, thus there is a need to develop a much bigger root system for sufficient N uptake, based on the abiotic (nutrient) condition (Jia et al., 2020; Gaudinier et al., 2023). In this case, *Pk* supports the acquisition of rare nutrients and can help in plant development by a better nutrient uptake efficiency or via N-fixation. This would be in line with observed significant increased shoot N contents and increased root N contents in Brachypodium grown under limited N after inoculation with *Pk* (Fig. 3.8; Fig. 3.9; Fig. 3.10 F). However, hormones play an essential role in N acquisition and lateral root development as well. Auxin serves multiple functions in the formation and development of lateral roots. It is involved in various processes such as lateral root positioning, initiation, outgrowth, and emergence (Du & Scheres, 2018), and contributes to the stimulation of root foraging for nitrogen (Jia et al., 2021). Jia et al. (2021) demonstrated that auxin is locally synthesized in the roots through the auxin biosynthesis protein YUCCA8 (YUC8) and accumulates in lateral root tips under nitrogen deficiency. Furthermore, a reliance on brassinosteroid (BR) function for local auxin biosynthesis in lateral roots was uncovered, indicating that local auxin biosynthesis occurs downstream of BR signaling (Jia et al., 2021).

The lateral root development will be discussed in more detail in Chapter 4, considering the molecular changes (4.4.2).

Under limited N, the FW of Brachypodium shoots and roots after inoculation with *Pk* was significantly increased compared to limited N controls, with shoot FW being comparable to sufficient N control plants (Fig. 3.10 C). In terms of DW, the inoculation of *Pk* led to 100% increased biomass in both roots and shoots compared to limited N controls (Fig. 3.10 D), which is also in line with the increased whole-plant N content (Fig. 3.10 F). Interestingly, the limited N inoculated plants had an overall increased N content in absolute values compared to low and sufficient N plants, despite the 10x difference in N concentration. With the minor changes in $d^{15}N$ signature, it is very unlikely that *Pk* can fix these amounts of N. However, *Pk* can increase the local N concentration via N-fixation in the rhizosphere, thus N-sensing mechanisms could lead to a change in root system architecture. This will be discussed in more detail in Chapter 4 (4.4.2).

3.4.2 N-fixation

The hypothesis of N-fixation needs further investigation, as the ^{15}N natural abundance approach (Fig. 3.8) only shows trends of N-fixation under zero and limited N conditions. A follow-up experiment has further elaborated this question by growing various bacteria on nitrogen free medium. The basis for this is that only N-fixing bacteria can grow on N-free medium, thus testing *Pk* together with various *Pseudomonas spp.* and *E. coli* as a negative control gave us information about the N-fixing ability of *Pk*. The experiment has shown that *Pk* was able to grow on N-free medium, while *E. coli* was not able to grow on this medium (Fig. 3.9). This confirms that *Pk* is N-fixing at least for itself and could contribute to the total N content in the plant. Based on the ^{15}N natural abundance experiment, the actual amount of fixed N seems not to be significant, but sufficient to induce these growth improvements. I hypothesize that the N derived from N-fixation is not the only driving force in the improved plant performance during this plant-microbe interaction (Chapter 4, 4.4.2).

To control for any potential impact of the inoculum, the nitrogen input introduced by the inoculum was assessed. Given that the average bacterial cell mass ranges from 248 fg (*S. epidermidis*) to 763 fg (*E. coli K-12*) (Sanz-Jimenez et al., 2022), and assuming that *Pk* has a similar size and mass to *E. coli K-12*, and that soil bacteria typically contain 10–30% nitrogen (Hoorman, 2016), the inoculum containing $5x10^5$ CFU would contain 0.0763 µg of nitrogen (0.763 pg x 0.2 x 500,000 CFU). Relating this to the total nitrogen introduced from the medium (2.66 mg N under limited nitrogen conditions / 26.6 mg N under sufficient nitrogen conditions), the bacteria contribute an estimated 0.287 and 0.0287 parts per million to the total nitrogen content in the closed system under limited and sufficient nitrogen conditions, respectively. This analysis suggests that the inoculum's contribution to the total nitrogen content in the system is neglectable.

3.4.3 Growth optimisation / technical improvements

The technical and growth condition optimisations have been conducted prior to the final experiments. The major challenge was to modify the growth system while remaining it sterile for the conducted experiments. The first modification included drilling three holes in the top container for horizontal and vertical gas exchange, required for transpiratory processes. Covering the holes with micropore tape was an easy solution to keep the system sterile.

Initially, the water content was tested to reduce the condensation in the growth systems. Once I figured out that the condensation and reflections of the PCV obscure the masking of the shoot via the segmentation tool, I further reduced the water content, as Brachypodium is a mediterranean grass and thus naturally growing in an arid, oligotrophic environment (Stritt et al., 2018). In general, the condensation would have been an uncontrollable variable and might have introduced more variability in the projected leaf area data. Since the systems had to be opened for imaging every two days, a mobile phenotyping station in a space limited environment was required (Supplementary Figure S3.8). This setup was sterilized via UV light for 15 min prior to imaging of the plants. The mobile non-invasive shoot phenotyping setup allowed

repeatable and proper imaging with the same lighting conditions for every single image with no background noise detection in the segmentation tool.

Transferring the nutrient concentration from the previous experimental setup using liquid medium (hydroponics) resulted in a very poor phenotype. There are two possible explanations: (i) Hydroponics had an increased absolute N content compared to the PCV setup due to its container size and (ii) a difference in the mass flow and diffusion of the nutrients within the different media (liquid medium compared to sand) (Marschner & Rengel (2023)). Thus, higher concentrations were required, increasing the overall plant phenotype. During the optimisation process, I recognized that the container size using 2 PCV was limiting the root development, thus a further extension to the 3 PCV setup was required (Poorter et al., 2012). This extension led to further optimisation, because the nutrient conditions needed proper adjustment again, while a 1:1 upscaling based on the mass of the sand was not sufficient.

Pk was initially incubated in YMB medium, which led to distortion in OD_{600} measurements, as insoluble particles were randomly absorbing light in the photometer. Per correspondence with the manufacturer, the company was not aware of the problem. The incubation medium was afterwards changed to LB medium, after correspondence with another PhD student at the IBG-1, FZJ. Using LB medium, the bacteria growth curve was generated (Fig. 3.7).

3.4.4 Future perspective

Nitrogen and Carbon metabolism are tightly linked. In the previous chapters, I only focussed on the N content in plants, whereas the C content is also of major interest. At 21 DAS, a significantly decreased C content in limited N Brachypodium roots inoculated with *Pk* was observed. This could be an indicator for root exudation during this plant-microbe interaction. In plant-microbe interactions, plant roots exudate C-containing compounds in exchange for N from the bacteria. While this study did not focus on plant root exudates, it might be an interesting approach in future experiments to further elucidate the interaction between Brachypodium and *Pseudomonas*. Additionally,

measuring the plant hormones might lead to additional insight in the understanding of this plant-microbe interaction.

With the descriptive molecular data presented in Chapter 4, a more in-depth phenotyping of Brachypodium in the same experimental setup can be performed. Non-invasive root phenotyping would give a lot of insight into the root development through time. This knowledge might be useful to address the before mentioned unclarities about the root development. The experimental setup could therefore be transferred to Rhizotrons (Nagel et al., 2012) and tested for viability in the greenhouse under non-sterile conditions.

3.5 Supplementaty Material

3.5.1 Statistics to Figures 3.8 and 3.10

Supplementary Table S3.1. Statistics to Fig. 3.8. Represented are the (adjusted) p-values of the two-way ANOVA and post-hoc Tukey's HSD. Values in bold represent significant values ($p < 0.05$).

^{15}N		**p (adjusted)**	
		Root	**Shoot**
		21	**21**
Two-way ANOVA	Nitrogen	**<2e-16**	**<2e-16**
	Bacteria	0.1120	0.1440
	Nitrogen:Bacteria	0.4980	0.9220
Tukey's HSD	Low_N:Ctrl-High_N:Ctrl	**0.0000**	**0.0000**
	Zero_N:Ctrl-High_N:Ctrl	**0.0000**	**0.0000**
	High_N:*Pk*-High_N:Ctrl	0.9998	0.9164
	Zero_N:Ctrl-Low_N:Ctrl	**0.0000**	**0.0000**
	Low_N:*Pk*-Low_N:Ctrl	0.9819	0.9926
	Zero_N:*Pk*-Zero_N:Ctrl	0.4253	0.8872

Supplementary Table S3.2. Statistics to Fig. 3.10. Represented are the (adjusted) p-values of the two-way ANOVA and post-hoc Tukey's HSD. Values in bold represent significant values ($p < 0.05$).

Leaf Area (A)		**p (adjusted)**									
		5	**7**	**9**	**11**	**13**	**15**	**17**	**19**	**20**	**21**
Two-way ANOVA	Nitrogen	**1.2E-09**	**<2e-16**	**<2e-16**	**<2e-16**	**<2e-16**	**<2e-16**	**4.0E-12**	**1.1E-09**	**0.0004**	**0.0009**
	Bacteria	0.3260	**0.0371**	0.7712	0.9940	0.7670	0.4560	0.5930	0.1436	**0.0163**	**0.0341**
	Nitrogen: Bacteria	0.3300	0.0562	**0.0256**	**0.0436**	0.1100	0.4120	0.2170	0.0773	**0.0049**	**0.0044**
Tukey's HSD	Low_N:Ctrl-High_N:Ctrl	**0.0000**	**0.0000**	**0.0000**	**0.0000**	**0.0000**	**0.0000**	**0.0000**	**0.0000**	**0.0001**	**0.0002**
	High_N:*Pk*-High_N:Ctrl	1.0000	0.9996	0.2767	0.4729	0.7893	0.9999	0.9593	0.9963	0.9916	0.9565
	Low_N:*Pk*-Low_N:Ctrl	0.5092	**0.0257**	0.5074	0.4794	0.5337	0.6834	0.5924	0.1034	**0.0016**	**0.0034**
	Low_N:*Pk*-High_N:*Pk*	**0.0007**	**0.0000**	**0.0000**	**0.0000**	**0.0000**	**0.0000**	**0.0001**	**0.0050**	0.9499	0.9847

Supplementary Table S3.3. Statistics to Fig. 3.10. Represented are the (adjusted) p-values of the two-way ANOVA and post-hoc Tukey's HSD. Values in bold represent significant values ($p < 0.05$).

		p (adjusted)									
		(B)		**(C)**		**(D)**		**(E)**		**(F)**	
		X	**Y**	**X**	**Y**	**X**	**Y**	**X**	**Y**	**X**	**Y**
Two-way ANOVA	Nitrogen	**0.0003**	0.7203	**0.0197**	**0.0067**	0.0609	1.0000	0.6100	0.2235	**0.0000**	**0.0000**
	Bacteria	0.8688	**0.0264**	**0.0340**	**0.0011**	**0.0081**	**0.0038**	**0.0025**	0.1371	**0.0057**	0.0730
	Nitrogen: Bacteria	0.6065	0.1141	**0.0340**	**0.0030**	0.0968	0.3800	**0.0010**	**0.0284**	0.9251	**0.0072**
Tukey's HSD	Low_N:Ctrl-High_N:Ctrl	0.0488	0.7926	0.9973	**0.0013**	0.9979	0.9180	**0.0261**	0.8496	**0.0022**	**0.0000**
	High_N:*Pk*-High_N:Ctrl	0.9602	0.9457	1.0000	0.9876	0.8096	0.3292	0.9905	0.0550	0.1684	0.8433
	Low_N:*Pk*-Low_N:Ctrl	0.9941	0.0454	**0.0221**	**0.0004**	**0.0178**	0.0359	**0.0003**	0.9315	0.1338	**0.0131**
	Low_N:*Pk*-High_N:*Pk*	0.0112	0.4945	**0.0150**	0.9927	0.0714	0.9180	0.1055	0.0818	**0.0030**	**0.0050**

3.5.2 Time-resolved invasive leaf area measurements

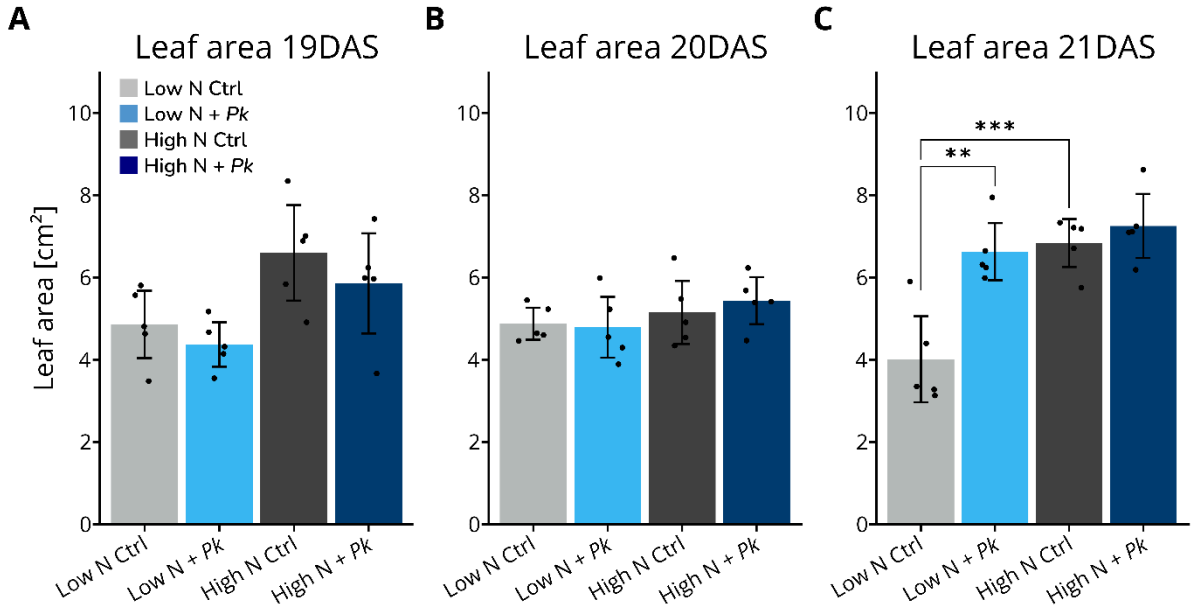

Supplementary Figure S3.1. Time-resolved invasive leaf area measurements. A) Invasive leaf area (y) at 19 DAS; B) Invasive leaf area (y) at 20 DAS; C) Invasive leaf area (y) at 21 DAS. Means were compared using two-way ANOVA followed by Tukey's honestly significant difference (HSD) test and can be found in Supplementary Table S3.4.

Supplementary Table S3.4. Statistics to Fig. S3.1. Represented are the (adjusted) p-values of the two-way ANOVA and post-hoc Tukey's HSD. Values in bold represent significant values ($p < 0.05$).

Leaf Area (invasive)		**p (adjusted)**		
		Y		
		19	**20**	**21**
ANOVA	Nitrogen	**0.0044**	0.167	**0.0005**
	Bacteria	0.2246	0.755	**0.0015**
	Nitrogen:Bacteria	0.7986	0.565	**0.0136**
Tukey's HSD	Low_N:Ctrl-High_N:Ctrl	0.0936	0.9278	**0.0006**
	High_N:*Pk*-High_N:Ctrl	0.7081	0.9174	0.881
	Low_N:*Pk*-Low_N:Ctrl	0.8917	0.9974	**0.0014**
	Low_N:*Pk*-High_N:*Pk*	0.1771	0.4942	0.6886

3.5.3 Time-resolved root length

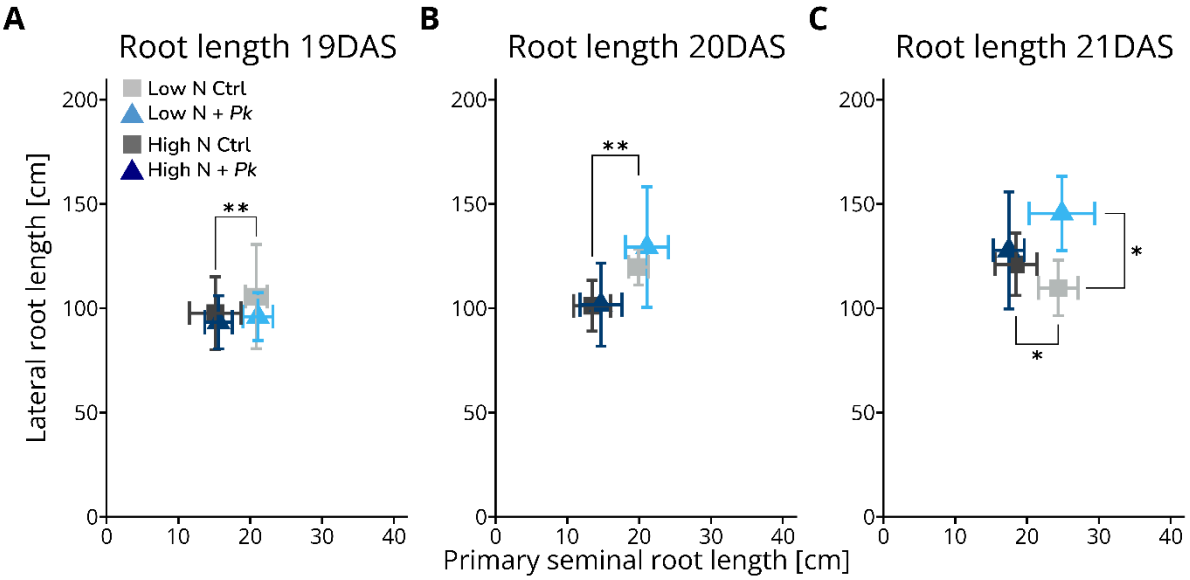

Supplementary Figure S3.2. Time-resolved root length. A) Primary seminal root length (x) and lateral root length (y) at 19 DAS; B) Primary seminal root length (x) and lateral root length (y) at 20 DAS; C) Primary seminal root length (x) and lateral root length (y) at 21 DAS. Means were compared using two-way ANOVA followed by Tukey's honestly significant difference (HSD) test and can be found in Supplementary Table S3.5.

Supplementary Table S3.5. Statistics to Fig. S3.2. Represented are the (adjusted) p-values of the two-way ANOVA and post-hoc Tukey's HSD. Values in bold represent significant values ($p < 0.05$).

Root length		**p (adjusted)**					
		X			**Y**		
		19	**20**	**21**	**19**	**20**	**21**
Two-way ANOVA	Nitrogen	**0.0001**	**0.0000**	**0.0003**	0.5090	**0.0155**	0.7203
	Bacteria	0.7620	0.3060	0.8688	0.3870	0.5644	**0.0264**
	Nitrogen:Bacteria	0.9220	0.9780	0.6065	0.7410	0.6073	0.1141
Tukey's HSD	Low_N:Ctrl-High_N:Ctrl	**0.0087**	**0.0050**	**0.0488**	0.8895	0.4359	0.7926
	High_N:*Pk*-High_N:Ctrl	0.9913	0.8677	0.9602	0.9789	1.0000	0.9457
	Low_N:*Pk*-Low_N:Ctrl	0.9988	0.8847	0.9941	0.8217	0.8594	**0.0454**
	Low_N:*Pk*-High_N:*Pk*	**0.0116**	**0.0054**	**0.0112**	0.9949	0.1431	0.4945

3.5.4 Time-resolved fresh weight

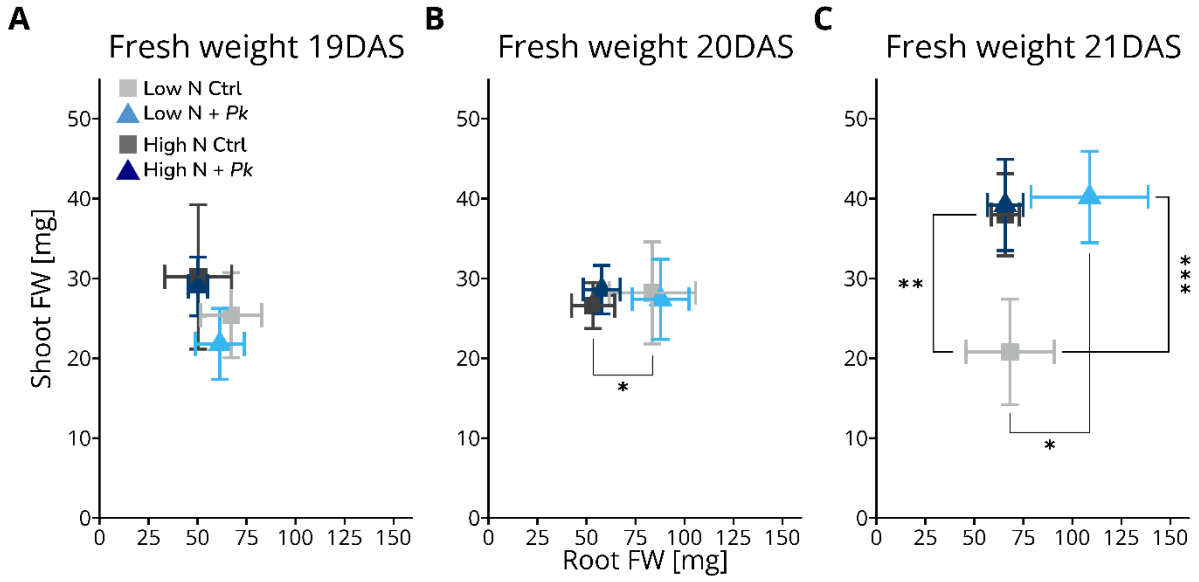

Supplementary Figure S3.3. Time-resolved fresh weight. A) Root fresh weight (FW) (x) and shoot FW (y) at 19 DAS; B) Root FW (x) and shoot FW (y) at 20 DAS; C) Root FW (x) and shoot FW (y) at 21 DAS. Means were compared using two-way ANOVA followed by Tukey's honestly significant difference (HSD) test and can be found in Supplementary Table S3.6.

Supplementary Table S3.6. Statistics to Fig. S3.3. Represented are the (adjusted) p-values of the two-way ANOVA and post-hoc Tukey's HSD. Values in bold represent significant values ($p < 0.05$).

Fresh Weight		**p (adjusted)**					
		X			**Y**		
		19	**20**	**21**	**19**	**20**	**21**
Two-way ANOVA	Nitrogen	**0.0323**	**0.0004**	**0.0197**	**0.0395**	0.9230	**0.0067**
	Bacteria	0.6222	0.5310	**0.0340**	0.3831	0.7730	**0.0011**
	Nitrogen:Bacteria	0.6454	0.9883	**0.0340**	0.6598	0.5030	**0.0030**
Tukey's HSD	Low_N:Ctrl-High_N:Ctrl	0.2326	0.0268	0.9973	0.5948	0.9443	**0.0013**
	High_N:*Pk*-High_N:Ctrl	1.0000	0.9660	1.0000	0.9885	0.8988	0.9876
	Low_N:*Pk*-Low_N:Ctrl	0.9006	0.9702	**0.0221**	0.7781	0.9923	**0.0004**
	Low_N:*Pk*-High_N:*Pk*	0.5603	0.0280	**0.0150**	0.2658	0.9751	0.9927

3.5.5 Time-resolved dry weight

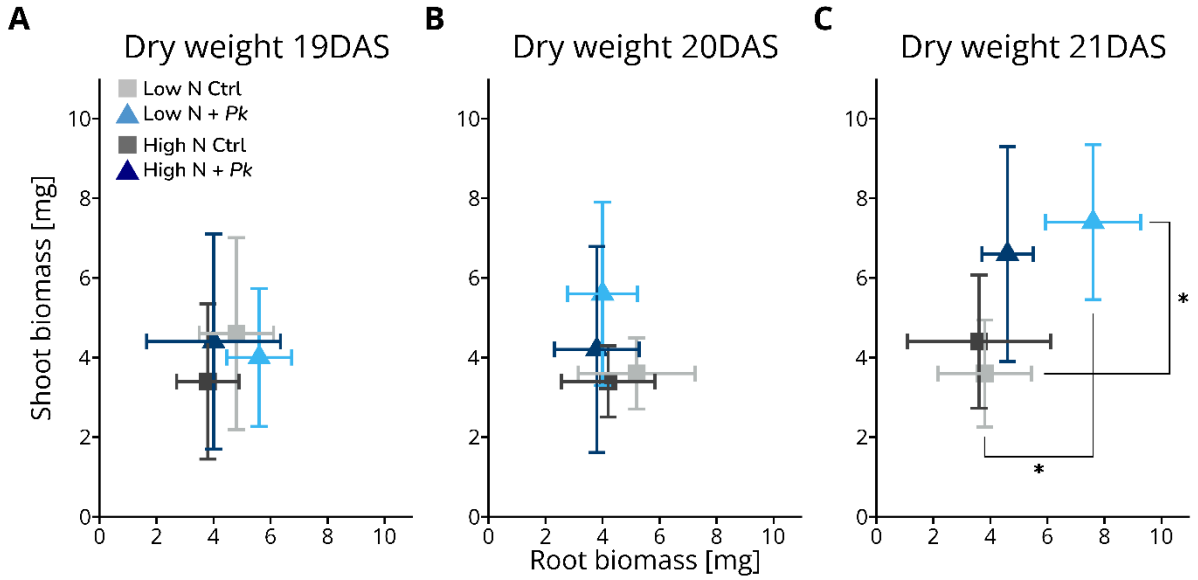

Supplementary Figure S3.4. Time-resolved dry weight. A) Root dry weight (DW) (x) and shoot DW (y) at 19 DAS; B) Root DW (x) and shoot DW (y) at 20 DAS; C) Root DW (x) and shoot DW (y) at 21 DAS. Means were compared using two-way ANOVA followed by Tukey's honestly significant difference (HSD) test and can be found in Supplementary Table S3.7.

Supplementary Table S3.7. Statistics to Fig. S3.4. Represented are the (adjusted) p-values of the two-way ANOVA and post-hoc Tukey's HSD. Values in bold represent significant values ($p < 0.05$).

Dry Weight		**p (adjusted)**					
		X			**Y**		
		19	**20**	**21**	**19**	**20**	**21**
Two-way ANOVA	Nitrogen	0.0804	0.4220	0.0609	0.6940	0.3460	1.0000
	Bacteria	0.4831	0.2880	**0.0081**	0.8440	0.1090	**0.0038**
	Nitrogen:Bacteria	0.6724	0.5900	0.0968	0.4340	0.4770	0.3800
Tukey's HSD	Low_N:Ctrl-High_N:Ctrl	0.7430	0.7673	0.9979	0.8296	0.9981	0.9180
	High_N:*Pk*-High_N:Ctrl	0.9969	0.9794	0.8096	0.8921	0.9009	0.3292
	Low_N:*Pk*-Low_N:Ctrl	0.8478	0.6561	**0.0178**	0.9733	0.3484	0.0359
	Low_N:*Pk*-High_N:*Pk*	0.3935	0.9973	0.0714	0.9917	0.6353	0.9180

3.5.6 Time-resolved plant C-content

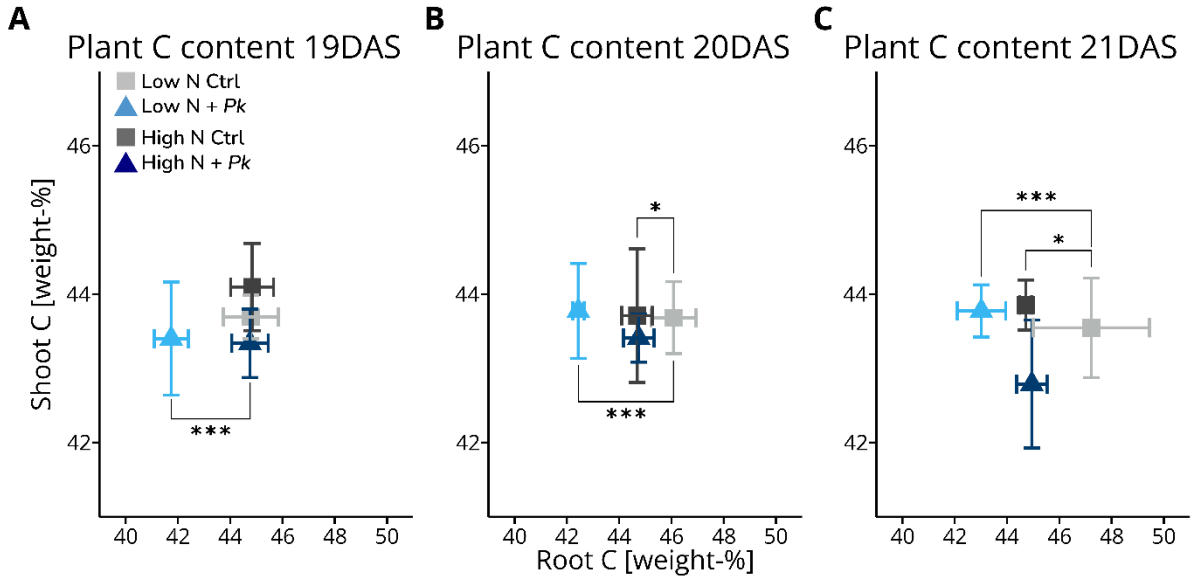

Supplementary Figure S3.5. Time-resolved plant C content. A) Relative root C content (x) and shoot C content (y) at 19 DAS; B) Relative root C content (x) and shoot C content (y) at 20 DAS; C) Relative root C content (x) and shoot C content (y) at 21 DAS. Means were compared using two-way ANOVA followed by Tukey's honestly significant difference (HSD) test and can be found in Supplementary Table S3.8.

Supplementary Table S3.8. Statistics to Fig. S3.5. Represented are the (adjusted) p-values of the two-way ANOVA and post-hoc Tukey's HSD. Values in bold represent significant values ($p < 0.05$).

Carbon content		**p (adjusted)**					
		X			**Y**		
		19	**20**	**21**	**19**	**20**	**21**
Two-way ANOVA	Nitrogen	**0.0007**	0.1120	0.6100	0.5019	0.5540	0.2235
	Bacteria	**0.0006**	**0.0000**	**0.0025**	**0.0494**	0.7120	0.1371
	Nitrogen:Bacteria	**0.0009**	**0.0000**	**0.0010**	0.3624	0.4910	**0.0284**
Tukey's HSD	Low_N:Ctrl-High_N:Ctrl	0.9997	**0.0110**	**0.0261**	0.6659	0.9999	0.8496
	High_N:*Pk*-High_N:Ctrl	0.9985	0.9986	0.9905	0.1750	0.8691	0.0550
	Low_N:*Pk*-Low_N:Ctrl	**0.0001**	**0.0000**	**0.0003**	0.8346	0.9954	0.9315
	Low_N:*Pk*-High_N:*Pk*	**0.0001**	**0.0001**	0.1055	0.9979	0.7912	0.0818

3.5.7 Time-resolved plant N-content

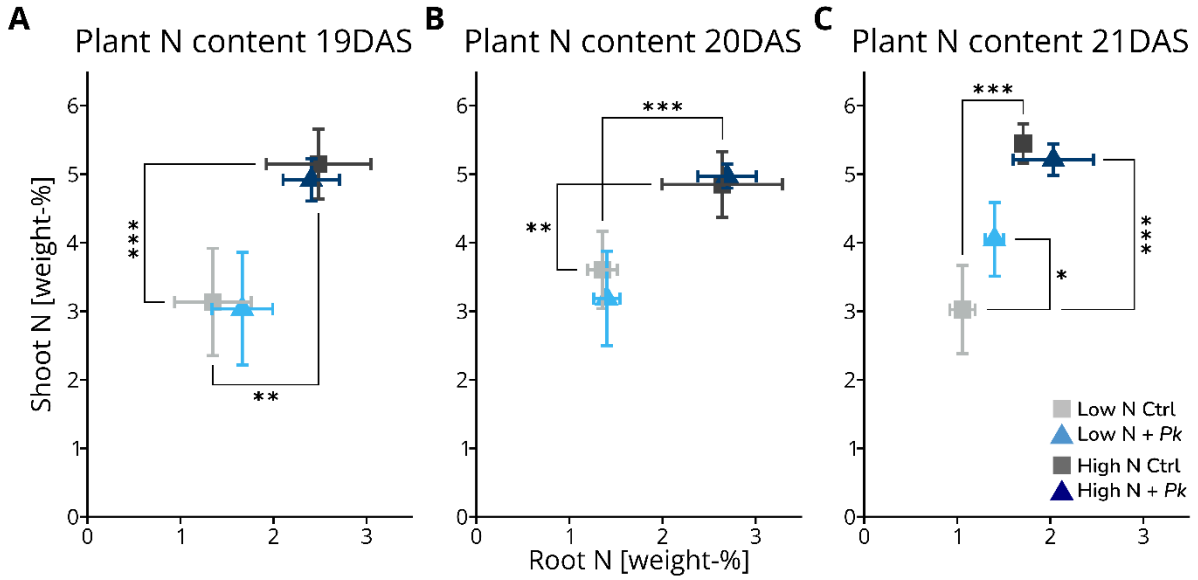

Supplementary Figure S3.6. Time-resolved plant N content. A) Relative root N content (x) and shoot N content (y) at 19 DAS; B) Relative root N content (x) and shoot N content (y) at 20 DAS; C) Relative root N content (x) and shoot C content (y) at 21 DAS. Means were compared using two-way ANOVA followed by Tukey's honestly significant difference (HSD) test and can be found in Supplementary Table S3.9.

Supplementary Table S3.9. Statistics to Fig. S3.6. Represented are the (adjusted) p-values of the two-way ANOVA and post-hoc Tukey's HSD. Values in bold represent significant values ($p < 0.05$).

Nitrogen content		**p (adjusted)**					
		X			**Y**		
		19	**20**	**21**	**19**	**20**	**21**
Two-way ANOVA	Nitrogen	**0.0001**	**0.0000**	**0.0000**	**0.0000**	**0.0000**	**0.0000**
	Bacteria	0.5284	0.7780	**0.0057**	0.5750	0.5310	0.0730
	Nitrogen:Bacteria	0.3018	0.9810	0.9251	0.8210	0.2590	**0.0072**
Tukey's HSD	Low_N:Ctrl-High_N:Ctrl	**0.0025**	**0.0003**	**0.0022**	**0.0007**	**0.0072**	**0.0000**
	High_N:*Pk*-High_N:Ctrl	0.9904	0.9961	0.1684	0.9403	0.9813	0.8433
	Low_N:*Pk*-Low_N:Ctrl	0.6295	0.9976	0.1338	0.9948	0.5874	**0.0131**
	Low_N:*Pk*-High_N:*Pk*	0.0519	**0.0003**	**0.0030**	**0.0014**	**0.0003**	**0.0050**

3.5.8 Automated sand washing setup

Supplementary Figure S3.7. Automated sand washing setup. Bottle is filled with sand to max ¾ of volume and connected via a hose to the sink.

3.5.9 Non-invasive shoot phenotyping setup

Supplementary Figure S3.8. Mobile non-invasive shoot phenotyping setup inside a clean bench.

3.5.10 Sowing template blueprint for 3D laser cutter

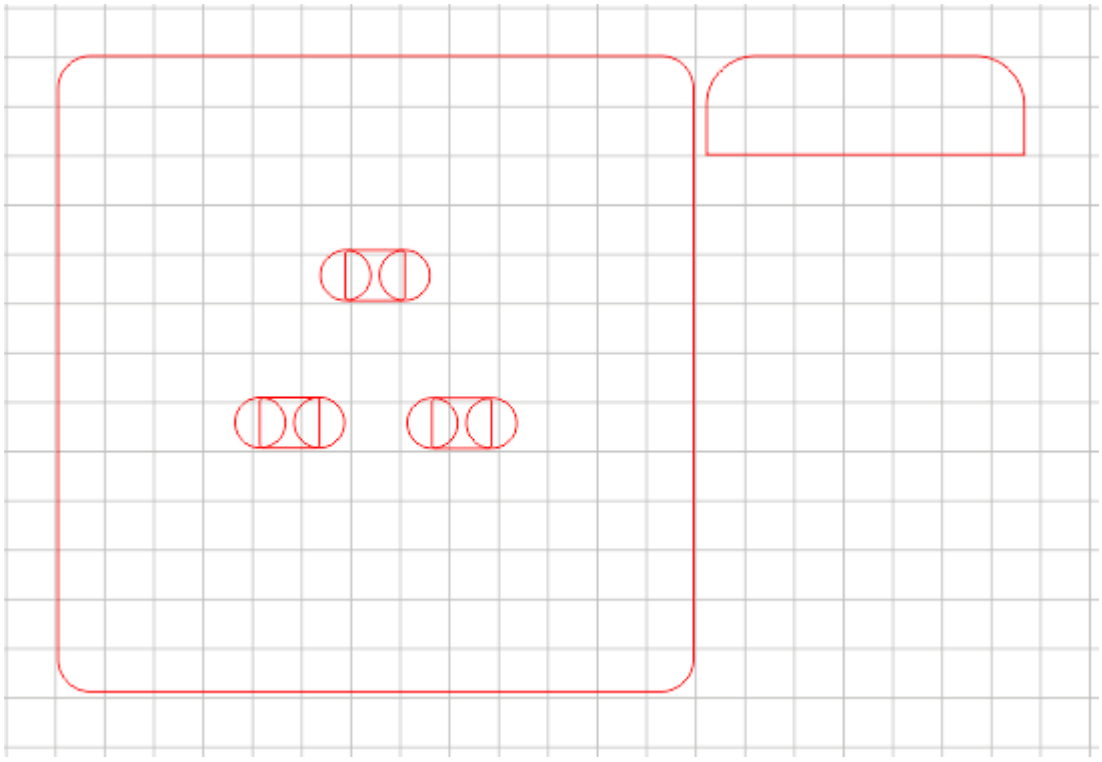

Supplementary Figure S3.9. Sowing template blueprint for 3D laser cutter. The single segment on the top right is glued to the base as a handle.

3.6 References

Anubha Pearline, S., Sathiesh Kumar, V., & Harini, S. (2019). A study on plant recognition using conventional image processing and deep learning approaches. Journal of Intelligent & Fuzzy Systems, 36(3), 1997-2004.

Arvidsson, S., Pérez-Rodríguez, P., & Mueller-Roeber, B. (2011). A growth phenotyping pipeline for Arabidopsis thaliana integrating image analysis and rosette area modeling for robust quantification of genotype effects. New Phytologist, 191(3), 895-907.

Balachandran, S., Hurry, V. M., Kelley, S. E., Osmond, C. B., Robinson, S. A., Rohozinski, J., ... & Sims, D. A. (1997). Concepts of plant biotic stress. Some insights into the stress physiology of virus-infected plants, from the perspective of photosynthesis. Physiologia Plantarum, 100(2), 203-213.

Barbagallo, R. P., Oxborough, K., Pallett, K. E., & Baker, N. R. (2003). Rapid, noninvasive screening for perturbations of metabolism and plant growth using chlorophyll fluorescence imaging. Plant physiology, 132(2), 485-493.

Bauriegel, E., Giebel, A., & Herppich, W. B. (2011). Hyperspectral and chlorophyll fluorescence imaging to analyse the impact of Fusarium culmorum on the photosynthetic integrity of infected wheat ears. Sensors, 11(4), 3765-3779.

Bodner, G., Nakhforoosh, A., Arnold, T., and Leitner, D. (2018). Hyperspectral imaging: a novel approach for plant root phenotyping. Plant Methods 14:84

Bürling, K., Hunsche, M., & Noga, G. (2010). Quantum yield of non-regulated energy dissipation in PSII (Y (NO)) for early detection of leaf rust (Puccinia triticina) infection in susceptible and resistant wheat (Triticum aestivum L.) cultivars. Precision agriculture, 11, 703-716.

Clark, R. T., MacCurdy, R. B., Jung, J. K., Shaff, J. E., McCouch, S. R., Aneshansley, D. J., & Kochian, L. V. (2011). Three-dimensional root phenotyping with a novel imaging and software platform. Plant physiology, 156(2), 455-465.

Deery, D., Jimenez-Berni, J., Jones, H., Sirault, X., & Furbank, R. (2014). Proximal remote sensing buggies and potential applications for field-based phenotyping. Agronomy, 4(3), 349-379.

Donaldson, L. (2020). Autofluorescence in plants. Molecules, 25(10), 2393.

Duan, L., Yang, W., Huang, C., & Liu, Q. (2011). A novel machine-vision-based facility for the automatic evaluation of yield-related traits in rice. Plant methods, 7(1), 1-13.

Fiorani, F., & Schurr, U. (2013). Future scenarios for plant phenotyping. Annual review of plant biology, 64, 267-291.

Flavel, R. J., Guppy, C. N., Tighe, M., Watt, M., McNeill, A., & Young, I. M. (2012). Non-destructive quantification of cereal roots in soil using high-resolution X-ray tomography. Journal of Experimental Botany, 63(7), 2503-2511.

Furbank, R. T., & Tester, M. (2011). Phenomics–technologies to relieve the phenotyping bottleneck. Trends in plant science, 16(12), 635-644.

Golzarian, M. R., Frick, R. A., Rajendran, K., Berger, B., Roy, S., Tester, M., & Lun, D. S. (2011). Accurate inference of shoot biomass from high-throughput images of cereal plants. Plant methods, 7, 1-11.

Hargreaves, C. E., Gregory, P. J., & Bengough, A. G. (2009). Measuring root traits in barley (Hordeum vulgare ssp. vulgare and ssp. spontaneum) seedlings using gel chambers, soil sacs and X-ray microtomography. Plant and Soil, 316, 285-297.

Hoorman, J. J. (2016). Role of Soil Bacteria: Update and Revision.

Jansen, M., Gilmer, F., Biskup, B., Nagel, K. A., Rascher, U., Fischbach, A., ... & Walter, A. (2009). Simultaneous phenotyping of leaf growth and chlorophyll fluorescence via GROWSCREEN FLUORO allows detection of stress tolerance in Arabidopsis thaliana and other rosette plants. Functional Plant Biology, 36(11), 902-914.

Jeudy, C., Adrian, M., Baussard, C., Bernard, C., Bernaud, E., Bourion, V., Busset, H., Cabrera-Bosquet, L., Cointault, F., Han, S., et al. (2016). RhizoTubes as a new tool for high throughput imaging of plant root development and architecture: test, comparison with pot grown plants and validation. Plant Methods 12:31.

Jia, Z., Giehl, R. F., & von Wirén, N. (2020). The root foraging response under low Nitrogen depends on DWARF1-mediated brassinosteroid biosynthesis. Plant Physiology, 183(3), 998-1010.

Khan, R. U., Khan, K., Albattah, W., & Qamar, A. M. (2021). Image-based detection of plant diseases: from classical machine learning to deep learning journey. Wireless Communications and Mobile Computing, 2021, 1-13.

Kiyomiya, S., Nakanishi, H., Uchida, H., Tsuji, A., Nishiyama, S., Futatsubashi, M., ... & Mori, S. (2001). Real time visualization of 13N-translocation in rice under different environmental conditions using positron emitting tracer imaging system. Plant Physiology, 125(4), 1743-1753.

Kumar, P., Huang, C., Cai, J., & Miklavcic, S. J. (2014). Root phenotyping by root tip detection and classification through statistical learning. Plant and soil, 380, 193-209.

Le Marie, C., Kirchgessner, N., Marschall, D., Walter, A., and Hund, A. (2014). Rhizoslides: paper-based growth system for non-destructive, high throughput phenotyping of root development by means of image analysis. Plant Methods 10:13.

Li, L., Zhang, Q., & Huang, D. (2014). A review of imaging techniques for plant phenotyping. Sensors, 14(11), 20078-20111.

Lontoc-Roy, M., Dutilleul, P., Prasher, S. O., Han, L., Brouillet, T., & Smith, D. L. (2006). Advances in the acquisition and analysis of CT scan data to isolate a crop root system from the soil medium and quantify root system complexity in 3-D space. Geoderma, 137(1-2), 231-241.

Lorence, A., & Jimenez, K. M. (Eds.). (2022). High-Throughput Plant Phenotyping: Methods and Protocols (Vol. 2539). Springer Nature.

Lucas, M., Swarup, R., Paponov, I. A., Swarup, K., Casimiro, I., Lake, D., ... & Bennett, M. J. (2011). Short-Root regulates primary, lateral, and adventitious root development in Arabidopsis. Plant Physiology, 155(1), 384-398.

Marschner, P., & Rengel, Z. (2023). Nutrient availability in soils. In Marschner's Mineral Nutrition of Plants (pp. 499-522). Academic press.

Mathieu, L., Lobet, G., Tocquin, P., and Perilleux, C. (2015). "Rhizoponics": a novel hydroponic rhizotron for root system analyses on mature Arabidopsis thaliana plants. Plant Methods 11:3.

Melkus, G., Rolletschek, H., Fuchs, J., Radchuk, V., Grafahrend-Belau, E., Sreenivasulu, N., ... & Borisjuk, L. (2011). Dynamic 13C/1H NMR imaging uncovers sugar allocation in the living seed. Plant biotechnology journal, 9(9), 1022-1037.

Menzel, M. I., Tittmann, S., Buehler, J., Preis, S., Wolters, N., Jahnke, S., ... & KRAUSE, H. J. (2009). Non-invasive determination of plant biomass with microwave resonators. Plant, cell & environment, 32(4), 368-379.

Moradi, A. B., Oswald, S. E., Nordmeyer-Massner, J. A., Prüssmann, K. P., Robinson, B. H., & Schulin, R. (2010). Analysis of nickel concentration profiles around the roots of the hyperaccumulator plant Berkheya coddii using MRI and numerical simulations. Plant and soil, 328, 291-302.

Müller-Linow, M. (2022). A versatile tool for semantic plant segmentation via color space thresholding. Zenodo.

Nagel, K. A., Putz, A., Gilmer, F., Heinz, K., Fischbach, A., Pfeifer, J., ... & Schurr, U. (2012). GROWSCREEN-Rhizo is a novel phenotyping robot enabling simultaneous measurements of root and shoot growth for plants grown in soil-filled rhizotrons. Functional Plant Biology, 39(11), 891-904.

Perret, J. S., Al-Belushi, M. E., & Deadman, M. (2007). Non-destructive visualization and quantification of roots using computed tomography. Soil Biology and Biochemistry, 39(2), 391-399.

Pedrosa, A. G., Reglinski, K., Lismont, C., Kors, S., Costello, J., Rodrigues, T. A., ... & Ribeiro, D. (2023). Peroxisomes: novel findings and future directions.

Poorter, H., Bühler, J., van Dusschoten, D., Climent, J., & Postma, J. A. (2012). Pot size matters: a meta-analysis of the effects of rooting volume on plant growth. Functional Plant Biology, 39(11), 839-850.

Poorter, H., Hummel, G. M., Nagel, K. A., Fiorani, F., Von Gillhaussen, P., Virnich, O., ... & Wiese-Klinkenberg, A. (2023). Pitfalls and potential of high-throughput plant phenotyping platforms. Frontiers in Plant Science, 14.

Rao, N. K. S., & Laxman, R. H. (2013). Phenotyping horticultural crops for abiotic stress tolerance. In Climate-Resilient Horticulture: Adaptation and Mitigation Strategies (pp. 147-157). India: Springer India.

Rolfe, S. A., & Scholes, J. D. (2010). Chlorophyll fluorescence imaging of plant–pathogen interactions. Protoplasma, 247, 163-175.

Roth, L., Barendregt, C., Bétrix, C. A., Hund, A., & Walter, A. (2022). High-throughput field phenotyping of soybean: Spotting an ideotype. Remote Sensing of Environment, 269, 112797.

Sanow, S., Kuang, W., Schaaf, G., Huesgen, P., Schurr, U., Roessner, U., ... & Arsova, B. (2023). Molecular mechanisms of Pseudomonas assisted plant nitrogen uptake-opportunities for modern agriculture. Molecular Plant-Microbe Interactions, (ja).

Sanz-Jiménez, A., Malvar, O., Ruz, J. J., García-López, S., Kosaka, P. M., Gil-Santos, E., ... & Tamayo, J. (2022). High-throughput determination of dry mass of single bacterial cells by ultrathin membrane resonators. Communications Biology, 5(1), 1227.

Sasse, J., Kant, J., Cole, B. J., Klein, A. P., Arsova, B., Schlaepfer, P., ... & Northen, T. R. (2019). Multilab EcoFAB study shows highly reproducible physiology and depletion of soil metabolites by a model grass. New Phytologist, 222(2), 1149-1160.

Schwacke, R., Ponce-Soto, G. Y., Krause, K., Bolger, A. M., Arsova, B., Hallab, A., ... & Usadel, B. (2019). MapMan4: a refined protein classification and annotation framework applicable to multi-omics data analysis. Molecular plant, 12(6), 879-892.

Singh, T., Kumar, K., & Bedi, S. S. (2021). A review on artificial intelligence techniques for disease recognition in plants. In IOP Conference Series: Materials Science and Engineering (Vol. 1022, No. 1, p. 012032). IOP Publishing.

Swarbrick, P. J., SCHULZE-LEFERT, P. A. U. L., & Scholes, J. D. (2006). Metabolic consequences of susceptibility and resistance (race-specific and broad-spectrum) in barley leaves challenged with powdery mildew. Plant, Cell & Environment, 29(6), 1061-1076.

Stritt, C., Gordon, S. P., Wicker, T., Vogel, J. P., & Roulin, A. C. (2018). Recent activity in expanding populations and purifying selection have shaped transposable element landscapes across natural accessions of the Mediterranean grass Brachypodium distachyon. Genome biology and evolution, 10(1), 304-318.

Tardieu, F., Cabrera-Bosquet, L., Pridmore, T., & Bennett, M. (2017). Plant phenomics, from sensors to knowledge. Current Biology, 27(15), R770-R783.

Thimm, O., Bläsing, O., Gibon, Y., Nagel, A., Meyer, S., Krüger, P., ... & Stitt, M. (2004). MAPMAN: a user-driven tool to display genomics data sets onto diagrams of metabolic pathways and other biological processes. The Plant Journal, 37(6), 914-939.

Tracy, S. R., Roberts, J. A., Black, C. R., McNeill, A., Davidson, R., & Mooney, S. J. (2010). The X-factor: visualizing undisturbed root architecture in soils using X-ray computed tomography. Journal of experimental botany, 61(2), 311-313.

Tsukamoto, T., Nakanishi, H., Uchida, H., Watanabe, S., Matsuhashi, S., Mori, S., & Nishizawa, N. K. (2009). 52Fe translocation in barley as monitored by a positron-emitting tracer imaging system (PETIS): evidence for the direct translocation of Fe from roots to young leaves via phloem. Plant and Cell Physiology, 50(1), 48-57.

Van As, H., & Van Duynhoven, J. (2013). MRI of plants and foods. Journal of Magnetic Resonance, 229, 25-34.

Vargas, J. Q., Bendig, J., Mac Arthur, A., Burkart, A., Julitta, T., Maseyk, K., ... & Rascher, U. (2020). Unmanned aerial systems (UAS)-based methods for solar induced chlorophyll fluorescence (SIF) retrieval with non-imaging spectrometers: state of the art. Remote sensing, 12(10), 1624.

Vogel, J., & Hill, T. (2008). High-efficiency Agrobacterium-mediated transformation of Brachypodium distachyon inbred line Bd21-3. Plant cell reports, 27, 471-478.

Walter, A., Silk, W. K., & Schurr, U. (2009). Environmental effects on spatial and temporal patterns of leaf and root growth. Annual review of plant biology, 60, 279-304.

White, J. W., & Conley, M. M. (2013). A flexible, low-cost cart for proximal sensing. Crop Science, 53(4), 1646-1649.

Windt, C. W., Vergeldt, F. J., De Jager, P. A., & Van As, H. (2006). MRI of long-distance water transport: a comparison of the phloem and xylem flow characteristics and dynamics in poplar, castor bean, tomato and tobacco. Plant, Cell & Environment, 29(9), 1715-1729.

Yang, W., Feng, H., Zhang, X., Zhang, J., Doonan, J. H., Batchelor, W. D., ... & Yan, J. (2020). Crop phenomics and high-throughput phenotyping: past decades, current challenges, and future perspectives. Molecular Plant, 13(2), 187-214.

Yigit, E., Sabanci, K., Toktas, A., & Kayabasi, A. (2019). A study on visual features of leaves in plant identification using artificial intelligence techniques. Computers and electronics in agriculture, 156, 369-377.

Chapter 4

Preface to Chapter 4

This chapter of the thesis introduces the biochemical responses of *Brachypodium distachyon* to inoculation with the beneficial microbe *Pseudomonas koreensis*, with focus on the roots of *B. distachyon* under two different nitrogen levels. The plant-microbe interaction was investigated using time-resolved lipidomics, coupled with an end-point proteomics (whole-proteome and microsomal enrichment) approach. Untargeted proteomics and lipidomics techniques were employed to produce descriptive datasets aimed at identifying potential novel target proteins and lipids, facilitating further investigation into the underlying mechanism.

This study showed that Brachypodium grown under limited N and inoculated with the plant growth-promoting bacterium *Pseudomonas koreensis Ps9-14* has a more similar protein profile to control plants grown under sufficient N. The root lipid profile shows minor changes in some lipid classes during the earlier stage (19 DAS) of the interaction, indicating that the changes on lipid level are prior to changes on the protein level. While proteins are responding to *Pk* inoculation, the lipids are primarily responding to the different N levels. This study has demonstrated that nitrogen deprivation can be overcome with the use of the beneficial *P. koreensis* and thus might be able to support the reduction of synthetic fertilizer synthesis and application.

4.1 Introduction

Plants can take up N in different forms with ammonium (NH_4^+) and nitrate (NO_3^-) being the predominantly available sources. The former (NH_4^+) is taken up via dedicated transporters belonging to the ammonium transporter family (AMT), the latter (NO_3^-) via the nitrate transporter family (NRT). In addition, N uptake also occurs in form of urea or amino acids (Mérigout et al., 2008; Tegeder & Rentsch 2010). The uptake system is classified as low affinity- or high affinity transport system (LATS and HATS,), being active in environments with high or low external N concentrations, respectively. NH_4^+ and NO_3^- assimilation follows different pathways. NO_3^- assimilation requires a two-step reduction of NO_3^- to NO_2^- via the enzyme nitrate reductase (NR) and consecutively to NH_4^+ via the

enzyme nitrite reductase (NiR). The NH_4^+ derived from nitrate assimilation is then converted to glutamine via the plastidial glutamine synthase (GS / GLN) isoforms entering the GS/GOGAT cycle, while NH_4^+ derived from ammonium assimilation enters the GS/GOGAT cycle via cytosolic GS isoforms (Fig 4.4).

To study the protein and lipid profiles of Brachypodium, liquid chromatography (LC) coupled with tandem mass spectrometry (MS/MS) was utilized. LC-MS/MS is the preferred method for analysing complex biological samples and combines physico-chemical separation (LC) and mass analysis (MS) (Ju-Seop Kang, 2012). Using tandem MS, two different data acquisition modes are available: Data-dependent acquisition (DDA) and data-independent acquisition (DIA). In DDA approaches, only the highest abundant precursor ions are selected and measured in MS2 (Hu et al., 2016). This can lead to gaps in the different samples within a dataset, while the drawback is that low abundant peptides / ions are underrepresented or entirely omitted (Veneable et al., 2004; Hu et al., 2016). In general, DDA approaches have a lower precision and reproducibility than DIA approaches (Hu et al., 2016). In DIA, all peptides / ions of a selected mass range are fragmented and analysed in the MS2. This is advantageous in samples with unknown protein compositions and allows quantification of all peptides (Bilbao et al., 2015; Hu et al., 2016). DIA requires spectral libraries containing empirically determined precise fragmentation patterns for each peptide / ion in the library (Hu et al., 2016).

In the shotgun proteomics approach, proteins are digested to peptides with a specific protease, such as Trypsin. The mixture of peptides is then measured via LC-MS/MS and submitted to an automated database search, resulting in a quantitative data output of predicted protein abundances based on the detected peptides (Matallana-Surget et al., 2010). DIA was used in this chapter on both whole-proteome and microsomal enrichment samples. The microsomal enrichment was used to increase the resolution of quantification of membrane-bound proteins, such as transporters, which might not be quantified in the whole-proteome extract. Microsomes are membrane-derived vesicles formed during cell lysis (LaMontagne et al., 2016).

Beside important proteins being located on the plant cell membranes, the constituents of the cell membrane itself are of particular interest: lipids. Lipids fulfil different important biological functions, including structure and function of membranes (Okazaki & Saito 2014), energy and carbon storage (Okazaki & Saito 2014), cell signalling (Wang, 2004; Wang et al., 2006; Munnik and Testerink, 2009, Okazaki & Saito 2014) and regulation of stress responses (Gaude et al., 2008; Nakamura et al., 2009; Moellering et al., 2010; Gasulla et al., 2013; Okazaki et al., 2013; Okazaki & Saito 2014). Additionally, lipids are important molecules in the communication between plants and microbes (Macabuhay et al., 2022) and therefore interesting targets to study in plant microbe interactions.

Lipids can be categorized in different categories according to Macabuhay et al. (2022), namely fatty acyls (FA), Glycerolipids (GL), Glycerophospholipids (GP), Sphingolipids (SP), Sterol lipids (ST), Prenol lipids (PR), Saccharolipids (SL) and polyketides (PK) (Macabuhay et al., 2022). Monogalactosyldiacylglycerol (MGDG), digalactosyldiacylglycerol (DGDG), sulfoquinovosyldiacylglycerol (SQDG), phosphatidylcholine (PC), phosphatidylethanolamine (PE), phosphatidylglycerol (PG) and phosphatidylinositol (PI) are signaling lipids derived from membrane lipids (Okazaki & Saito 2014). The review by Macabuhay et al., (2022) focusses on the role of lipids in plant-microbe interactions, especially the signalling processes with the environment (Macabuhay et al., 2022).

4.2 Material and Methods

4.2.1 Sampling for molecular analyses

Plants for molecular analyses (Chapter 3) were transferred from liquid N to storage at -80 °C. Fresh weight was recorded and tissues were homogenised using a ball mill (Retsch, MM 400) and a single bead for 5x 1 min intervals at maximum frequency. Samples were kept from thawing by cooling the samples in between the runs and using a pre-cooled ball-mill block.

Plants from Harvest (I) were used for lipid extractions, plants from Harvest (II) were used for protein extractions (Fig. 3.1).

4.2.2 Sample preparation for 'omics'

Due to sensitivity limitations in the microsomal enrichment process (proteomics), it was required to pool roots or shoots from two individual plants as one biological replicate. Plants were pooled according to their fresh weight, with each biological replicate having at least 100 mg root and ~55 mg shoot tissue. From each root pool, 30 mg were aliquoted for whole-proteome shotgun extraction (4.2.3), while the remaining plant material was used for microsomal enrichment (4.2.4). For shoots, only the whole proteome was extracted.

For time-resolved lipidomics, individual plant roots were sufficient, as only 20 ±1 mg of root tissue was required. The aliquoted frozen root tissues from the 'Time series' (Harvest (I), Fig. 3.1) experiment was used for lipid extraction (4.2.6).

4.2.3 Whole-proteome protein extraction and purification

Proteins were extracted by adding 100 µl denaturing buffer (PBS + 2% SDS) per 10 mg of FW. Protein content was estimated using the bicinchoninic acid (BCA) assay and 25 µg proteins were aliquoted. Proteins were denatured by adding DTT to a final concentration of 10 mM, and incubation at 90 °C for 15 min. After cooling to room temperature (RT), a final concentration of 50 mM chloroacetamide was added to the samples and incubated for 30 min in the dark. The carbamidomethylation was quenched by adding DTT to a final concentration of 50 mM and incubation for 20 min at RT.

To remove SDS from the samples, the SP3 bead cleanup system was used. 1 µl SP3 beads were added for 20 µg of protein and mixed well. 100% pure ethanol was added to the samples to a final concentration of 80% ethanol and incubated for 20 min at RT. Eppendorf tubes were placed in a magnetic stand to bind the beads to the magnet. Supernatant was discarded and the beads were rinsed twice with 400 µl of 90% acetonitrile. Beads were spun down and placed inside a fume hood for maximum 3 minutes to evaporate all remaining liquids. The beads were resuspended in 30 µl of digestion buffer (100 mM HEPES, pH 7.4 + 2.5 mM $CaCl_2$) and trypsin added in a 1:100 protease:protein ratio. The solution was shortly sonicated in a water bath, spun down

and incubated overnight at 37 °C. After digestion, peptides were cleaned up with SDB-RP Stage Tips (3M, #2341). Then, buffer A (0.1 % formic acid in H_2O), buffer B (0.1 formic acid in 80% acetonitrile) and the elution buffer (5% ammoniumhydroxide in 60% acetonitrile) were prepared. Two layers of the membrane were packed in 200 µl pipette tips. Tips were equilibrated with 20 µl 100% Methanol. Stage tips were placed inside of a 2 ml Eppendorf tube containing a stage tip adapter and centrifuged at 500 g for 1 min. Afterwards, 20 µl buffer B, and twice 20 µl Buffer A were added individually to the membrane with a centrifugation step at 500 g for 1 min after each time buffer was added. Samples were acidified to a final concentration of 2% formic acid and the pH value of <= 2 was checked using pH indicator strips. Acidified samples were loaded onto the stage tips and centrifuged at 500 g for 5 min. The peptides bound to the membrane were washed once using 30 µl of buffer A and twice using 30 µl of buffer B, again with centrifugation steps at 500 g for 3 min in between the washing steps. Samples were finally transferred to fresh 1.5 ml Eppendorf tubes prior to elution. For elution, 30 µl elution buffer was added to the stage tip and centrifuged at 500 g for 3 min each time. Eluted peptides were fully dried using a SpeedVac and finally resuspended in 15 µl 0.1 % formic acid in H_2O. 2 µl of the sample were used to determine peptide concentration at the Nanodrop, before injection of 1 µg peptides into LC-MS/MS.

4.2.4 Microsomal enrichment

The ground root tissues were lysed using the Glass/PFE Potter Elvehjem Tissue Grinder (DWK Life Sciences, #885510-0020). Then, 2 ml of homogenization buffer (solved in 100 ml water: 11.42 g Sucrose, 500 µl EDTA (300 mM), 0.74 g KCl, 5 ml TRIS/MES (1M, pH = 7.5), 0.21 g NaF, 1 ml HALT protease inhibitor) were added to the samples and transferred to the Potter, which was continuously cooled on ice. Root tissues were rigorously pottered for 5 min. If root fragments were still visible, an additional 5 min were added to ensure proper cell lysis. After pottering, the solution was filtered using a double layer of Miracloth (Merck, #475855) and directly transferred to a 2 ml Eppendorf tube. Samples were centrifuged at 7500 g at 4 °C for 15 min. Supernatant was transferred to an ultracentrifuge tube (Beckman Coulter, #358119) and placed inside the holder of a MLS 50 Rotor (Beckman Coulter). Sample weight was adjusted to the maximum weight

determined by adding homogenization buffer (1 mg balance tolerance). The ultracentrifuge (Beckman Coulter, Optima Max-XP) was operated with the following settings: 48.000 g, 4 °C, 1.5 h. Samples were carefully removed, and the supernatant (soluble fraction) stored separately. Cloth wipes were inserted into the tubes carefully, to remove every trace of the soluble fraction, especially close to the pellet (microsomal fraction). Afterwards, the microsomal fraction was resuspended in 50 µl PBS-Buffer (solve in 1 liter of water: 8 g NaCl (137 mM), 0.2 g KCl (2.7 mM), 1.44 g Na_2HPO_4 (10 mM), 0.24 g KH_2PO_4 (1.8 mM)) + 2% SDS and transferred to fresh 1.5 ml Eppendorf tubes. The suspension was clarified by an additional centrifugation step at 5000 g at 4 °C for 5 min. Supernatant was again transferred to fresh 1.5 ml Eppendorf tubes. The protein concentration was determined using the BCA assay. From this point the same protocol as for the whole-proteome protein extraction was used.

4.2.5 Proteomics data acquisition

Desalted peptides samples were separated with an UltiMate 3000 RSCL nano-HPLC-system (Thermo) equipped with an µPAC pillar array trap column (1 cm length, PharmaFluidics) and an µPAC pillar array analytical column (50 cm flowpath, PharmaFluidics). The 2h elution protocol included an 80 min separation gradient from 5% to 32.5% ACN with 0.1% FA at a flow rate of 600 nl per min with the column temperature maintained at 40°C. The separated peptides were analysed using a HPLC-coupled Q-TOF mass spectrometer (Impact II, Bruker) equipped with a CaptiveSpray ion source (Bruker) and operated with an ACN-saturated nitrogen gas stream (Beck et al 2015). Data was acquired using a Data Independent Acquisition (DIA) mode with 400-1200 precursor mass windows for MS1, and acquisition of 32 windows of 25 m/z size with 0.5 m/z overlap at 15 Hz in a range from m/z 200-1750 for MS2.

4.2.6 LC-MS untargeted analysis for lipids

The protocol from Kehelpannala et al. (2019) was used with minor modifications. 20 +-1 mg of frozen root tissue (Harvest (I), Fig. 3.1) was transferred to new Eppendorf tubes. 400 µl cold isopropanol + 0.01% butylated hydroxytoluene and a steel ball was added to each tube. Samples were ground as explained above until no visible root fragments were

left (5x 1 min). Samples were afterwards incubated using a thermomixer at 75 °C, 1400 rpm for 15 min, and cooled to room temperature (RT). 1200 µl of solvent mixture containing chloroform:methanol:water (30:41.5:3.5, v:v:v) was added to a final solvent mixture of chloroform:isopropanol:methanol:water (30:25:41.5:3.5, v:v:v:v). Samples were incubated at 25 °C, 300 rpm for 24 h, followed by centrifugation at 15,860 g for 15 min. The supernatant was transferred to a new tube and dried *in vacuo* (freeze-dried) using a lyophilisator (Christ, Alpha 2-4 LSCplus).

The dried lipid extracts were reconstituted in 100 µl of butanol:methanol (1:1, v:v) with 10mM ammonium acetate. The samples were vortexed and shaken at 20 °C for 10 min at 1400 rpm. Afterwards, the samples were centrifuged at RT for 5 min at 13,000 rpm. 70 µl of the supernatant from each sample was transferred to autosampler glass vials for further MS analysis. Also, 7 µl from each sample vial was aliquoted into a separate vial and pooled together to prepare the pooled biological quality control (PBQC) sample for MS analyses.

Samples were acquired on a Sciex Triple TOF 6600 MS interfaced with Sciex ExionLC ultra-high pressure liquid chromatography (UHPLC). The LC-MS/MS platform employed was a high-resolution Q-TOF UHPLC system, using Sequential Window Acquisition of all Theoretical Mass Spectra (SWATH-MS) for data collection. The total runtime for each sample acquisition was 30 min with a flow rate of 0.26 ml/min. The mobile phase (MP) composition was MPA: acetonitrile:water (60:40 v:v + 10 mM ammonium acetate) and MPB: isopropyl alcohol (IPA) :acetonitrile (90:10 v:v + 10 mM ammonium acetate). The gradient condition applied for chromatographic separation the same as in Kehelpannala et al. (2019): Initial concentration 32% of MPB was maintained till 1.5 mins following which the concentration of MPB was subsequently increased step wise as follows: 1.5 – 4 mins, 32-45%; 4 – 5 mins, 45-52%; 5 – 8 mins, 52-58%; 8 – 11 mins, 58-66%; 11 – 14 mins, 66-70%; 14 – 18 mins, 70-75%; 18 – 21 mins, 75-97%; the concentration of MPB was maintained at 97% till 25 mins and was brought down to the initial 32% at 25.1 mins. The column was equilibrated with mobile phase for the remaining 30 mins. A sample volume of 10 µl was injected for each sample onto the analytical column ID 2.1 x 100 mm with 2.7-micron particle size (Agilent Poroshell 120 EC-C18). The column oven temperature

was maintained at 55 °C and the eluent from the column was introduced into the MS with the help of electrospray ionisation (ESI) source. The source parameter conditions maintained during acquisition were 25 for gas 1 & 2, 35 curtain gas, source temperature at 250 °C & ionspray voltage floating at 4500V. Samples were acquired in positive polarity and auto calibration of the MS performed every 6 samples (approx. 3 hours) with the aid of calibrant delivery system delivering ESI positive calibration mix. The TOF MS scan range was set from 100 – 1700 *m/z* & the SWATH TOF-MS/MS were 100 – 1700 *m/z* with 16.2 Da window size. The acquired data file was processed using MS-Dial version 5.1.230719 (RIKEN Center for Sustainable Resource Science, Japan).

The MS data presented corresponds to six individual biological replicates for each treatment group per day.

4.2.7 Proteomics data analyses and visualization

Creation of a theoretical, tryptic library and alignment with the measured spectra was performed using the software DIA-NN (Demichev et al. 2020), version 1.8, based on the Brachypodium database from UniProt (UP000008810_15368, release 2022_04) and the *Pseudomonas koreensis* database (UP001139955, release 2023_04). The Annotation was done via Mercator4 V2.0 (Schwacke et al., 2019) (the annotation file can be found in the repository: Link). Parameters were set to two maximum missed cleavages, and two maximum number of variable peptide modification, a 1% Precursor FDR and fixed carbamidomethylation on. A peptide length of seven to 30 amino acids and a precursor charge range of two to four were considered valid. The query was done in double-pass mode with match between runs (MBR) enabled and heuristic protein interference disabled.

Statistical analyses were performed using ANOVA with a confidence level of 95% followed by a post-hoc Tukey's Honestly Significant Difference (HSD) test. Correlations were calculated using the Pearson coefficient.

Proteins were filtered for 100% valid values (vv) in all conditions (no imputation) using Perseus (Version 1.6.15.0, Tyanova et al., 2016), followed by two-way ANOVA with a confidence level of 95% and post-hoc Tukey's HSD in R (https://www.r-project.org/).

Significantly changed protein intensities are visualized via MapMan version 3.5.1R2, on custom made nitrogen pathway images modified after Feng et al., 2020: X4.1 N-uptake R1.0. The images for kinase families and lipid biosynthesis were used directly from the MapMan store (https://mapman.gabipd.org/mapmanstore).

4.2.8 Lipidomics data analyses and visualization

For lipid analyses, the features were filtered for a retention time window of 1.5 - 25 min a signal/noise (S/N) ratio of >5 and an average score of ≥ 1.5. The coefficient of variance (CV) of the pooled biological quality controls (PBQC) were calculated and every feature with a CV < 25 was kept for manual curation. All filtering steps described previously were conducted using a python script. Feature abundance was log10 transformed and pareto scaled. Heatmaps were created using the normalized data and clustered using hierarchical cluster analysis (HCA) with Pearson correlation as distance measurement and average distance as clustering method.

Lipidomics data were visualized using R for Principal Component Analysis (PCA) and time-resolved plots. The heatmaps were created using MetaboAnalyst.com with the above-mentioned parameters.

4.2.9 Data availability

Proteomics data are available via PRIDE (http://www.ebi.ac.uk/pride) using the following credentials to log in into the reviewer account (Perez-Riverol et al., 2022):

Username: reviewer_pxd050676@ebi.ac.uk

Password: UV5NwdIR

4.3 Results

4.3.1 Brachypodium proteome is influenced after *Pk* inoculation under limited N

In general, 5660 and 6656 unique proteins were identified for the root and shoot whole proteome, respectively (Tab. 4.1). Out of these, 3137 and 3780 proteins were quantified in all root and shoot samples, respectively (Tab. 4.1). In the proteome, 2291 of the 3137 quantified proteins showed significant changes in abundance between any two conditions (ANOVA-test with p-value <0.05), while for shoots 1515 of 3780 were ANOVA significant (Tab. 4.1). Comparing Brachypodium plants grown under sufficient N and limited N, 1324 proteins had significant differences in abundance in roots and 457 in shoots (two-way ANOVA p-value <0.05 with Tukey's HSD test FDR <0.05) (Tab. 4.1). Limited N plants inoculated with *Pk* compared to their respective limited N control have 436 and 360 proteins that had significantly different abundance in roots and shoots, respectively (Tab. 4.1). Sufficient N inoculated compared to sufficient N controls show 16 and 163 proteins with significantly different abundance in roots and shoots, respectively (Tab. 4.1).

Table 4.1. Number of identified proteins in each data set. 100% vv each group column represents proteins detected in 100% of the samples (vv = valid values). ANOVA significant column represents the number of significant proteins according to ANOVA (Perseus Multi-sample test, Permutation-based FDR = 0.05). Limited N + *Pk* vs. Limited N Ctrl (significant) column shows the number of significant proteins in this specific comparison (statistics performed using R. ANOVA followed by post-hoc Tukey's HSD). WP = Whole Proteome; MF = Microsomal Fraction.

	Identified proteins	100% vv each group	ANOVA significant (p-value <0.05)	Sufficient N Ctrl vs. Limited N Ctrl (Tukey's HSD FDR <0.05)	Limited N + *Pk* vs. Limited N Ctrl (Tukey's HSD FDR <0.05)	Sufficient N + *Pk* vs. Sufficient N Ctrl (Tukey's HSD FDR <0.05)
Root_WP	5660	3137	2291	1324	436	16
Root_MF	5617	2700	396	253	158	38
Shoot_WP	6656	3780	1515	457	360	163

The 100% valid values (vv) proteins column from Tab. 4.1 are visualized in the principal component analysis in Fig. 4.1 A, B.

The molecular changes on root level are different from those in shoots. The first two principal components explain 94.5% of the variance in roots (Fig. 4.1 A). Sufficient N control and limited N control root clusters are separated via component 1 (Fig. 4.1 A). However, there is no obvious separation between sufficient N + *Pk* and sufficient N

controls, in addition limited N + *Pk* roots group closer to sufficient N plants than limited N controls, mainly separated via component 1 (Fig. 4.1 A). For shoots, 91.1% of the variance can be explained using the first two principal components, while a clear distinction of the different conditions can be observed (Fig. 4.1 B). Sufficient N control and limited N control shoots are mainly separated via component 2, with one exception for sufficient N controls (Fig. 4.1 B). Limited N + *Pk* shoots are grouped with sufficient N controls, sufficient N + *Pk* shoots are well separated from the sufficient N control and limited N + *Pk* shoots via component 1 (again with one exception 'swapped positions') (Fig. 4.1 B).

Comparing the PCA to the phenotyping data, the clustering of sufficient N Ctrl and sufficient N + *Pk* roots on molecular level (Fig. 4.1 A) can also be observed on phenotype level in root length (Fig. 3.10 B), plant fresh weight (Fig. 3.10 C), plant C and N content (Fig. 3.10 E, F). With this in mind, we will mainly focus on the limited N comparison of inoculated vs non inoculated plants in the following figures.

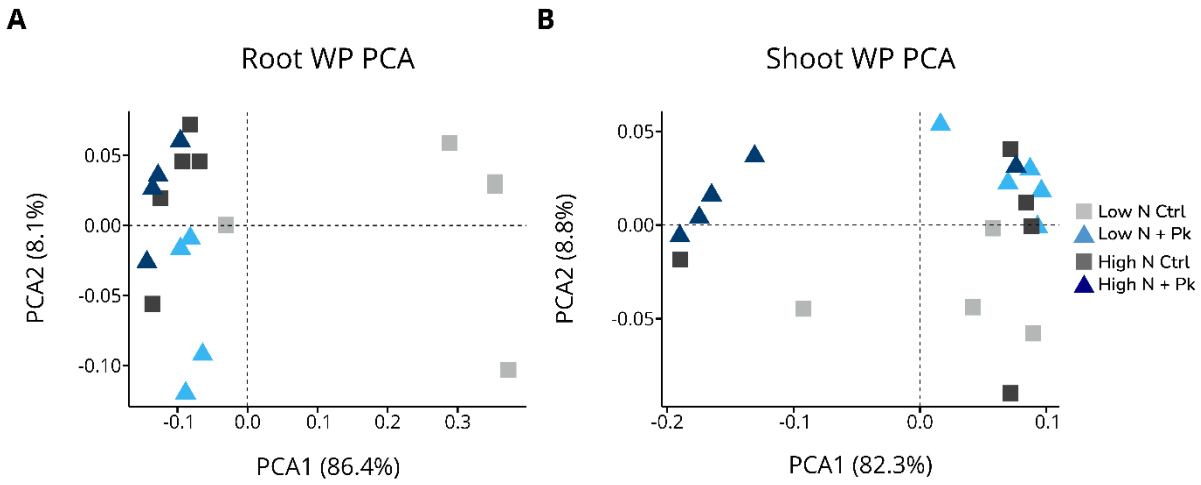

Figure 4.1. Principal component analyses of root and shoot whole-proteome (WP) datasets. A) PCA of the root whole-proteome; B) PCA of the shoot whole-proteome.

The Volcano plots show more proteins, that pass the significance threshold, in the root whole proteome than in shoots. Comparing the roots of sufficient N controls with limited N controls, 683 proteins were significantly more abundant, 641 lower abundant and 1813 not significantly different (Fig. 4.2 A). Looking at the GO terms, the significantly different proteins contribute mainly to the biological processes of cytoplasmic translation, nitrogen

compound transport and ribonucleoprotein complex biogenesis (Fig. 4.3 A). A similar distribution can be observed when comparing limited N + *Pk* roots with limited N control roots of Brachypodium, with 597 proteins significantly more abundant, 691 significantly lower abundant and 1849 not significantly different (Fig. 4.2 B). However, the major biological processes here are categorized in monoatomic transmembrane transport, and similar to the previous comparison, cytoplasmic translation and ribonucleoprotein complex biogenesis (Fig. 4.3 A). The comparison of Sufficient N + *Pk* with sufficient N controls have shown only slight changes in the protein abundance, with 5 proteins being significantly more abundant, 11 significantly less abundant and 3121 unchanged protein abundances (Fig. 4.2 C). In shoots, the number of significantly different abundant proteins is ~2.5 times less than in roots. In shoots, sufficient N controls compared with limited N controls have 260 significantly more abundant, 197 significantly less abundant and 3518 proteins without significant change in abundance (Fig. 4.2 D). Here, the significant different proteins belong to 90% to the biological process of organic substance biosynthetic process, while the remaining 10% contribute to small molecule metabolic processes (Fig. 4.3 B). The comparison of limited N + *Pk* and limited N control shoots revealed 248 significantly more abundant, 112 significantly lower abundant and 3615 not significantly different abundant proteins (Fig. 4.2 E). These proteins are categorized in completely different biological processes, with non-coding RNA (ncRNA) processing being most abundant (Fig. 4.3 B). In shoots, *Pk* inoculation under sufficient N led to 60 proteins significantly more abundant, 103 significantly less abundant and 3812 proteins showing no significant difference in abundance (Fig. 4.2 F). The GO term analysis of the molecular functions is represented in the Supplementary Figure S4.6.

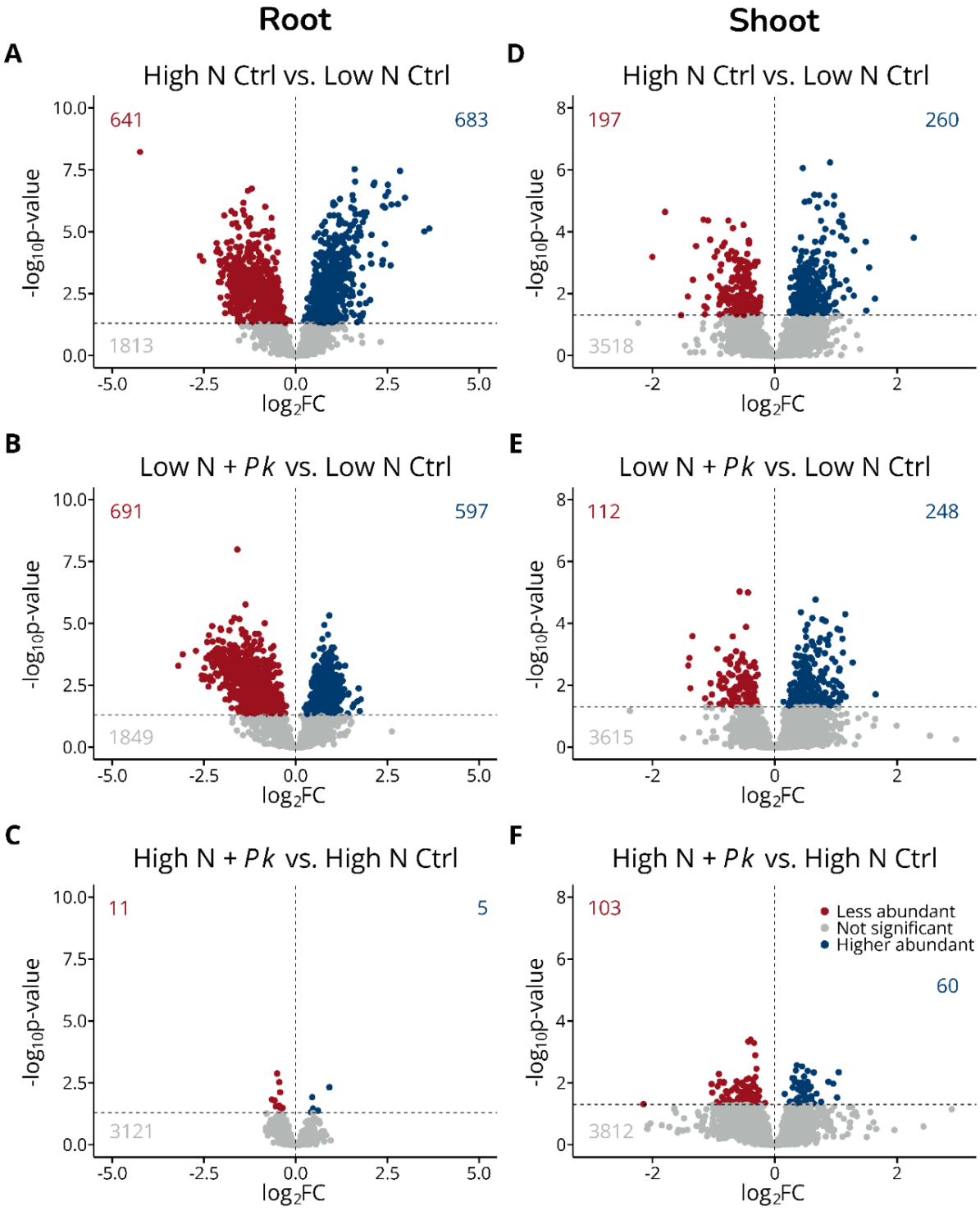

Figure 4.2. Proteomics data overview. A) Root volcano plot of the comparison: Sufficient N Ctrl vs. Limited N Ctrl; B) Root volcano plot of the comparison: Limited N + *Pk* vs. Limited N Ctrl; C) Root volcano plot of the comparison: Sufficient N + *Pk* vs. Sufficient N Ctrl; D) Shoot volcano plot of the comparison: Sufficient N Ctrl vs. Limited N Ctrl; E) Shoot volcano plot of the comparison: Limited N + *Pk* vs. Limited N Ctrl; F) Shoot volcano plot of the comparison: Sufficient N + *Pk* vs. Sufficient N Ctrl; Data shown are 100% valid values of the respective data set. Volcano plots represent the -log10 transformed adjusted p values from Tukey's HSD with a p-value threshold set for α <0.05 and no threshold set for log2FC (= 0). Values in the plot represent the number of proteins in each group (red = less abundant, grey = not significant, blue = higher abundant; matching the colours of data points).

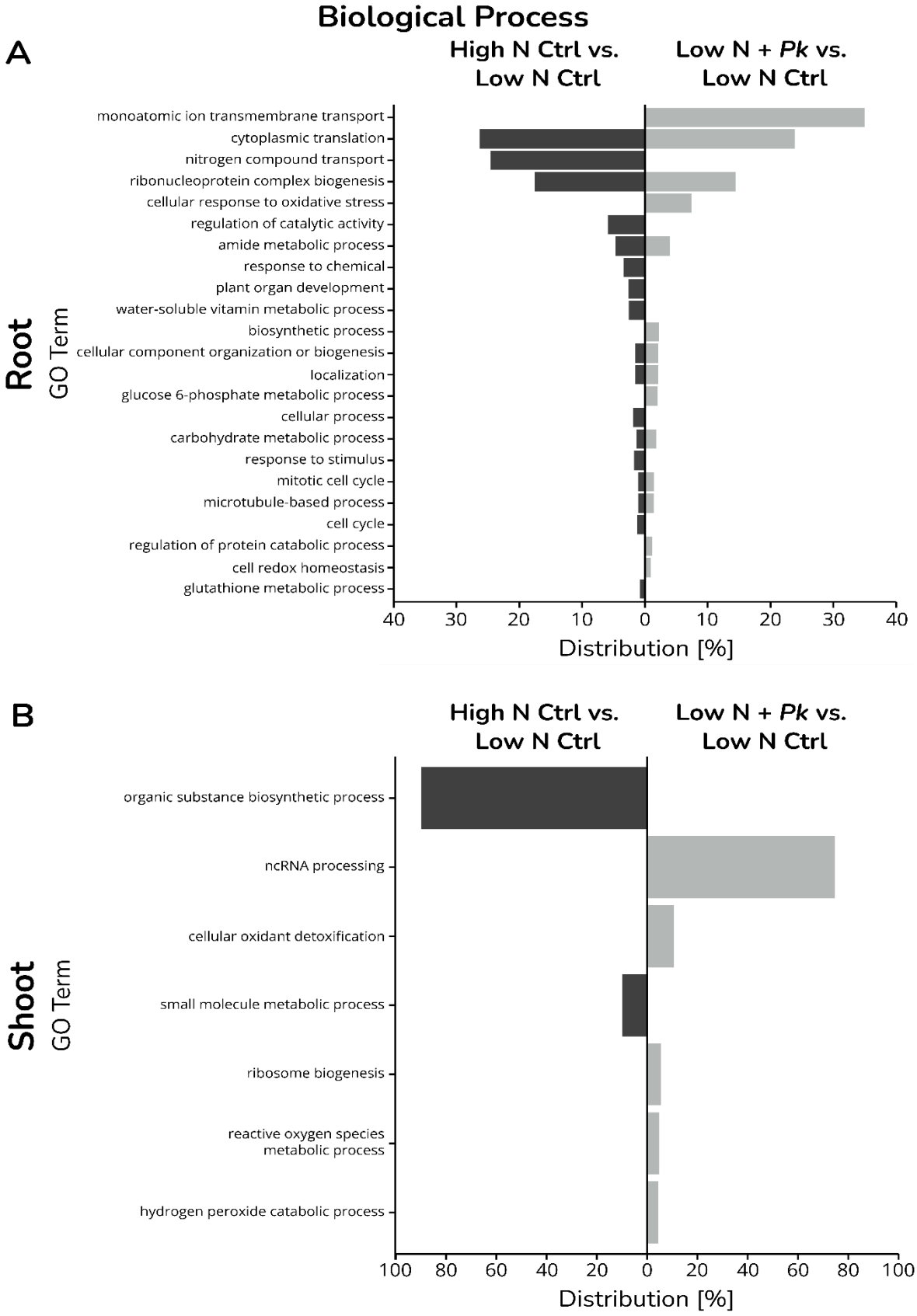

Figure 4.3. GO-term analyses (Biological processes). A) Root GO term analysis; B) Shoot GO term analysis. Only statistically significant proteins were imported into PantherDB statistical enrichment test (Mi et al., 2019), followed by REVIGO (Supek et al., 2011). Log10 (p-values) were used to calculate the %-distribution (x-axis) of GO-terms (y-axis).

4.3.2 *Pk* decreases N-deficiency symptoms in low-N inoculated roots and increases N assimilation enzymes in the shoot

Transporters and enzymes of the central N metabolism of plants are of particular interest, as they are the main actors in assimilating inorganic nitrogen into organic molecules in plants. The 'whole proteome' dataset was used for this analysis aiming to confirm that (i) the limited N plants do indeed show the well-known N deficiency symptoms, as well as (ii) to find out how N metabolism proteins change upon inoculation in the two N conditions. For visualization purposes Limited N control root and shoots were used as the baseline for comparison.

We first established that the limited N plants showed N-deficiency symptoms on the molecular level. Figure 4.4 (sufficient N control (HNC) vs limited N control (LNC)) shows the expected lower abundance of NRT and AMT transporters in sufficient N roots vs. limited N roots (Fig 7, roots). Only one NRT transporter shows higher abundance in sufficient N control roots, and this is a Major Facilitator superfamily (MFS) protein (I1H1D1_BRADI).

It was surprising to identify both Fd- and NADH-GOGAT isoforms in the roots, as these were grown is sand and the roots were protected from light. However, Fd-GOGAT shows mildly higher and NADH-GOGAT shows slightly less abundance in the sufficient N control roots. The Nitrogen regulatory protein P-II is higher abundant in the sufficient N roots, compared to the limited N.

Shoots similarly show the expected behaviour of N deficiency especially in the NO_3^- assimilation pathway (this is visible for the NRT, NR NiR, GS2 and both GOGAT isoforms). Different regulation of the cytosolic Glutamine synthases was observed where the Low affinity GLN1;2 (I1H7X9_BRADI) is less abundant and the high affinity GLN1;1 (I1IFI7_BRADI) is higher abundant in sufficient N control shoots compared to limited N control shoots (Supplementary Table S3.1). An increased abundance of GLN1;2 was also observed in limited N inoculated plants compared to their respective controls.

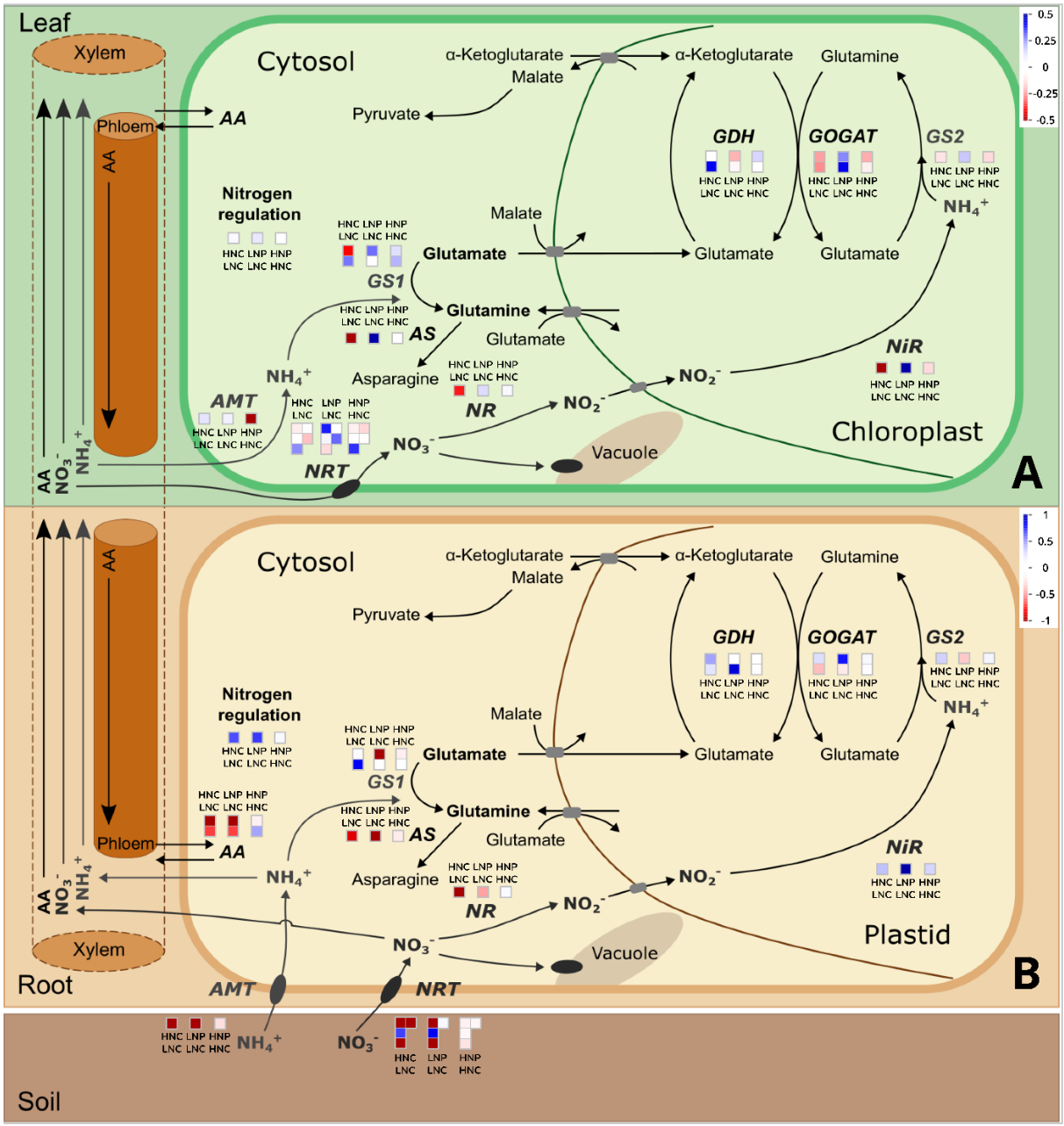

Figure 4.4. Central N metabolism in roots and shoots (whole proteome). Data represented are 100% valid values. Mapped proteins, log2FC and significances (indicated with asterisks in log2FC column) are shown in Supplementary Table S4.1. MapMan version 3.5.1R2 (Thimm et al., 2004) was used. The following pathways were used and modified from Feng et al., 2020: X4.1 N-uptake R1.0. Modified pathways will be submitted to the MapMan store (https://mapman.gabipd.org/mapmanstore). Mapping file was created using Mercator4 V2.0 (Schwacke et al., 2019). Comparisons are mentioned on top or below of each box: HNC / LNC = Sufficient N Control vs. Limited N Control; LNP / LNC = Limited N + *Pk* vs. Limited N Control; HNP / HNC = Sufficient N + *Pk* vs. Sufficient N Control. Abbreviations: AA, Amino acid; AMT, ammonium transporter family; AS, Asparagine synthase; GDH, Glutamate dehydrogenase; GOGAT, glutamine oxoglutarate aminotransferase; GS1, (cytosolic) Glutamine synthetase 1 isoform; GS2, (plastidial) Glutamine synthetase 2 isoform; NiR, Nitrite reductase; NR, Nitrate reductase; NRT, Nitrate transporter family.

In the comparison of Limited N + *Pk* vs Limited N control plants (Fig. 4.4) less abundance of two NRT transporters in the inoculated roots compared to the limited N roots were found (Uncharacterized protein (I1I6K3_BRADI); MFS domain-containing protein

(I1I5R4_BRADI)), with one NAR2.1 (I1IB70_BRADI) showing no change and one was higher abundant: MFS domain-containing protein (I1H1D1_BRADI same as in the comparison of sufficient N roots to limited N roots). There is moderately less abundance (-0.486 Log2FC) of the NR and a very strong increased abundance (1.039 Log2FC) of the NiR. Interestingly, the plastidial GS2 is less abundant, but there is higher abundance of the Fd-GOGAT isoform (I1GRK9_BRADI) and lower abundance of the NADH-GOGAT isoform (I1HQF1_BRADI) and related enzymes (Fig. 4.4, root). The detected AMT and several enzymes involved in assimilation of NH_4^+ in amino acids are less abundant in the limited N inoculated roots, however there is strongly increased abundance in the Nitrogen regulatory protein P-II (Fig. 4.4, root).

In the limited N + *Pk* Shoots compared to the limited N control shoots a consistently increased abundance of the NO_3^- assimilation pathway was observed, as well as increased abundance of enzymes of the ammonium assimilation pathway. Enzymes like AS and GS involved in the synthesis of amino acids are also higher abundant (Fig. 4.4, shoot).

In contrast, in the comparison of sufficient N roots + *Pk* vs sufficient N control roots show very mild differences in abundance in the central N metabolism in the roots (Fig. 4.4, root). Particularly interesting, the nitrogen regulation box is unchanged too. In the shoot there is a higher abundance of a single NRT transporter (MFS; I1H1D1_BRADI) and mild increased abundance of the two detected cytosolic GS isoforms.

4.3.3 The kinase families in Brachypodium respond both to N availability and *Pk* inoculation

The regulation of Nitrogen regulatory protein P-II led to the question if other regulatory proteins are differentially expressed in the inoculated plants. Using the MapMan bin 18 and 27 we investigated the protein intensities of known plant kinase families (Figure 4.5). This is particularly interesting because many of these proteins have a membrane domain and could span the cell or various organellar membranes.

In the root most significantly changed candidates belonged to the Leucine rich repeat (LRR) kinase family and the Ca^{2+}/calmodulin-dependent protein kinase (CAMK)

superfamily. However, representatives from other kinase groups were also found (Fig 4.8.).

Largest changes were found in MAP kinases, CAMK kinase superfamily and LRR kinase family. The mitogen-activated protein kinase (I1I5N8_BRADI) was found to be moderately less abundant in the sufficient N control roots compared to limited N control roots (-0.51 log2FC), much less abundant in roots after inoculation of limited N plants (-1.329 log2FC) and unchanged after inoculation of sufficient N plants (-0.07 log2FC).

The CAMK kinase superfamily contains SnRK2 SNF1-related protein kinases, with various behaviours. The SnRK2 SNF1-related protein kinase SAPK6 (I1IAE4_BRADI) was higher abundant in Sufficient N Controls compared to Limited N Controls (1.046 log2FC), which was also observed after inoculation of limited N plants with *Pk* (0.54 log2FC) and mildly after inoculation of sufficient N plants (0.289 log2FC). The regulatory subunit beta of SNF1-related SnRK1 kinase complex (I1HI64_BRADI) was strongly higher abundant in Sufficient N Controls vs. Limited N controls (0.829 log2FC), which was also observed in limited N inoculated plants (0.595 log2FC), while inoculation under sufficient N only showed slightly increased abundance (0.135 log2FC). SAPK3 (I1I692_BRADI), SAPK7 (I1IXT7_BRADI) and SAPK8 (I1GMZ0_BRADI) were comparably less abundant throughout all conditions, except for SAPK7 and SAPK8 being only slightly less abundant after inoculation of sufficient N plants with *Pk*. The regulatory subunit betagamma of SNF1-related SnRK1 kinase complex (I1GKM6_BRADI) was strongly less abundant in Sufficient N controls compared to Limited N controls (-0.728 log2FC) and after inoculation of limited N plants (-0.912 log2FC), while it was only moderately less abundant in sufficient N inoculated plants (-0.431 log2FC). However, the regulatory subunit gamma of SNF1-related SNRK1 kinase complex (I1HNY1_BRADI), was unchanged in Sufficient N controls compared to limited N controls (0.019 log2FC), but moderately higher abundant in limited N inoculated plants (0.555 log2FC) and moderately less abundant after inoculation of sufficient N plants (-0.427 log2FC). The biggest differences were observed in CPDK protein kinases (I1GMG8_BRADI; I1H269_BRADI), which were less abundant in the comparison of Sufficient N controls vs. Limited N controls (-0.387; -0.182 log2FC, respectively), while being higher abundant after inoculation of limited N plants with *Pk* (0.248; 0.366 log2FC,

respectively). As such they are candidates for further studies of plant specific adaptation to *Pk* under limited N conditions. Inoculation of sufficient N plants did not change their protein abundance (-0.094; -0.055 log2FC, respectively). Another CDPK protein kinase (I1J0Z2_BRADI) was strongly less abundant in sufficient N controls vs. Limited N controls (-1.163 log2FC) and after inoculation of limited N plants (-0.753 log2FC), while being unaffected after inoculation of sufficient N plants (-0.033 log2FC). The same behaviour was observed for the CRK protein kinase (I1GX02_BRADI) (-0.93 log2FC HNC/LNC; -1.107 log2FC LNP/LNC and –0.026 log2FC HPN/HNC).

The LRR-II protein kinase (I1GP23_BRADI) was observed to be strongly higher abundant in sufficient N controls compared to limited N controls (1.023 log2FC) and limited N inoculated plants (0.821 log2FC), but unchanged in sufficient N inoculated plants (-0.056 log2FC). This was also observed for LRR-VIII-1 protein kinases (I1HSU8_BRADI; A0A0Q3KBU7_BRADI) (0.609; 0.908 log2FC in HNC/LNC, 0.99; 0.878 log2FC in LNP/LNC, 0.216; -0.054 log2FC in HNP/HNC, respectively). The LRR-III-protein kinase (I1HBQ9_BRADI) was slightly less abundant in the sufficient N control vs. Limited N control comparison (-0.229 log2FC), while being slightly higher abundant in limited N inoculated plants (0.218 log2FC) and slightly less abundant in sufficient N inoculated plants (-0.229 log2FC). For the LRR-VIII-2 protein kinase (A0A2K2CIK2_BRADI), a slightly lower abundance was observed for sufficient N controls in comparison to limited N controls (-0.115 log2FC), while inoculation with *Pk* under limited N moderately increased the abundance (0.498 log2FC) and no change in sufficient N inoculated plants (-0.009 log2FC). Lastly, the LRR-Xa protein kinase (I1IZ22_BRADI) was slightly higher abundant in sufficient N controls vs. Limited N controls (0.205 log2FC), while being mildly less abundant in limited N inoculated plants (-0.097 log2FC) and sufficient N inoculated plants (-0.047 log2FC).

It was interesting that in the roots, the abundance ratio of kinases in the sufficient N control vs Limited N was very often mimicked by the abundance of the kinases in the Limited N *Pk* vs Limited N ratio, with some exceptions. We find that these kinases are particularly interesting for further study as they might control the plant adaptation to the presence of *Pk*.

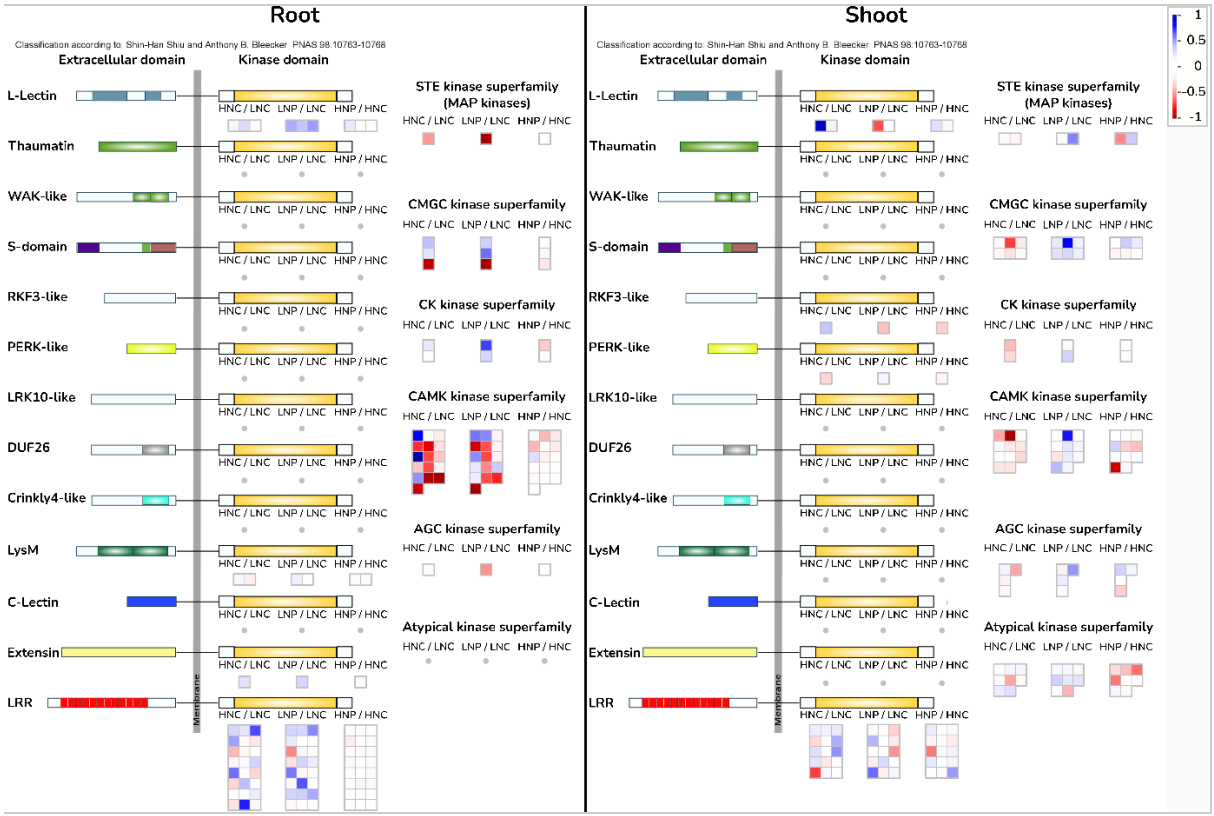

Figure 4.5. Kinases in roots and shoots (whole proteome). Data represented are 100% vv. Mapped proteins, log2FC and significances (indicated with asterisks in log2FC column) are shown in Supplementary Table S4.1. MapMan version 3.5.1R2 (Thimm et al., 2004) was used. The following pathways were used and modified from Shiu and Bleecker, 2001: X4.1_Kinase_Families_R1.0. Mapping file was created using Mercator4 V2.0 (Schwacke et al., 2019). Comparisons are mentioned on top of each box: HNC / LNC = Sufficient N Control vs. Limited N Control; LNP / LNC = Limited N + *Pk* vs. Limited N Control; HNP / HNC = Sufficient N + *Pk* vs. Sufficient N Control.

In the shoot, on the other hand, fewer significantly regulated kinases were found, with more of them having opposite behaviour between the Sufficient N control vs. Limited N control and Limited N inoculated vs. Limited N control.

In the case of L-type lectin receptor kinases, we see higher abundance in Sufficient N than in Limited N, but at limited N + *Pk* decreases the abundance of kinase A0A0Q3KPD2_BRADI in shoots. An opposite behaviour was seen in a representative of the CMGC kinase superfamily (comprising of CDK, MAPK, GSK3 and CLK families), I1I8I8_BRADI, the CAMK kinase superfamily proteins (I1H626_BRADI, I1HPI9_BRADI and I1GKM6_BRADI) and the LRR kinases (I1ID77_BRADI, A0A0Q3EYZ3_BRADI and A0A2K2D9S6_BRADI). These kinases are downregulated under sufficient Nitrogen compared to deficiency, but upregulated at limited N in the presence of *Pk*. I therefore

speculate that these kinases (and other regulated in a similar manner) represent internal plant regulatory adaptations to the presence of the beneficial microbe.

4.3.4 Proteins involved in lipid metabolism respond to the presence of *Pk*

Since many of the kinases contain membrane domains, the question if proteins involved in lipid metabolism (lipid synthesis and degradation) will respond to the presence of *Pk* was asked. Particularly as lipids, among their many functions, are main components of plant membranes.

Distinct similarities between Sufficient N vs Limited N control, and the Limited N + *Pk* vs Limited N in the root were found, in the Acetyl-CoA synthesis and acetyl-CoA carboxylation pathway, as well as the mitochondrial and plastidial fatty acid synthesis pathways (mtFAS, ptFAS; Fig 4.6).

In context of the lipid degradation pathways, *Pk* at limited N reduces the abundance of triacylglycerol lipase (I1HLP4_BRADI), which is the opposite type of regulation than Sufficient N vs Limited N. In terms of phospholipase activities, all quantified proteins have shown similar behaviour between limited N + *Pk* and sufficient N control compared to limited N controls, except for three proteins. Phospholipase C (A0A0Q3GLT1_BRADI) was higher abundant in sufficient N controls, but less abundant in limited N + *Pk* roots. The two remaining proteins, phospholipase C2 and D (I1HVB6_BRADI and I1HCG5_BRADI, respectively), showed higher abundance in sufficient N control roots, and no difference in limited N + *Pk* roots in comparison to limited N control roots.

Proteins involved in glycerolipid synthesis were only quantified for phosphatidic acids (PA), phosphatidyl ethanolamine (PE) and phosphatidyl choline (PC). Cytosolic Glycerol-3-phosphate acyltransferase (I1I6G2_BRADI) showed higher abundance after inoculation of limited N plants with *Pk*, whereas no changes were observable in the comparison between sufficient N and limited N controls. The same behaviour was observed for phosphatidylserine decarboxylase 2 (A0A0Q3N4N1_BRADI) in PE synthesis. All quantified proteins involved in PC synthesis showed similar trends in sufficient N controls and limited N + *Pk* roots compared to limited N controls. Beside these few proteins, the

abundance of lipid metabolism related proteins in limited N + *Pk* roots was comparable to the abundance of sufficient N control plants in comparison to limited N control roots.

The shoot lipid metabolism related proteins were not investigated.

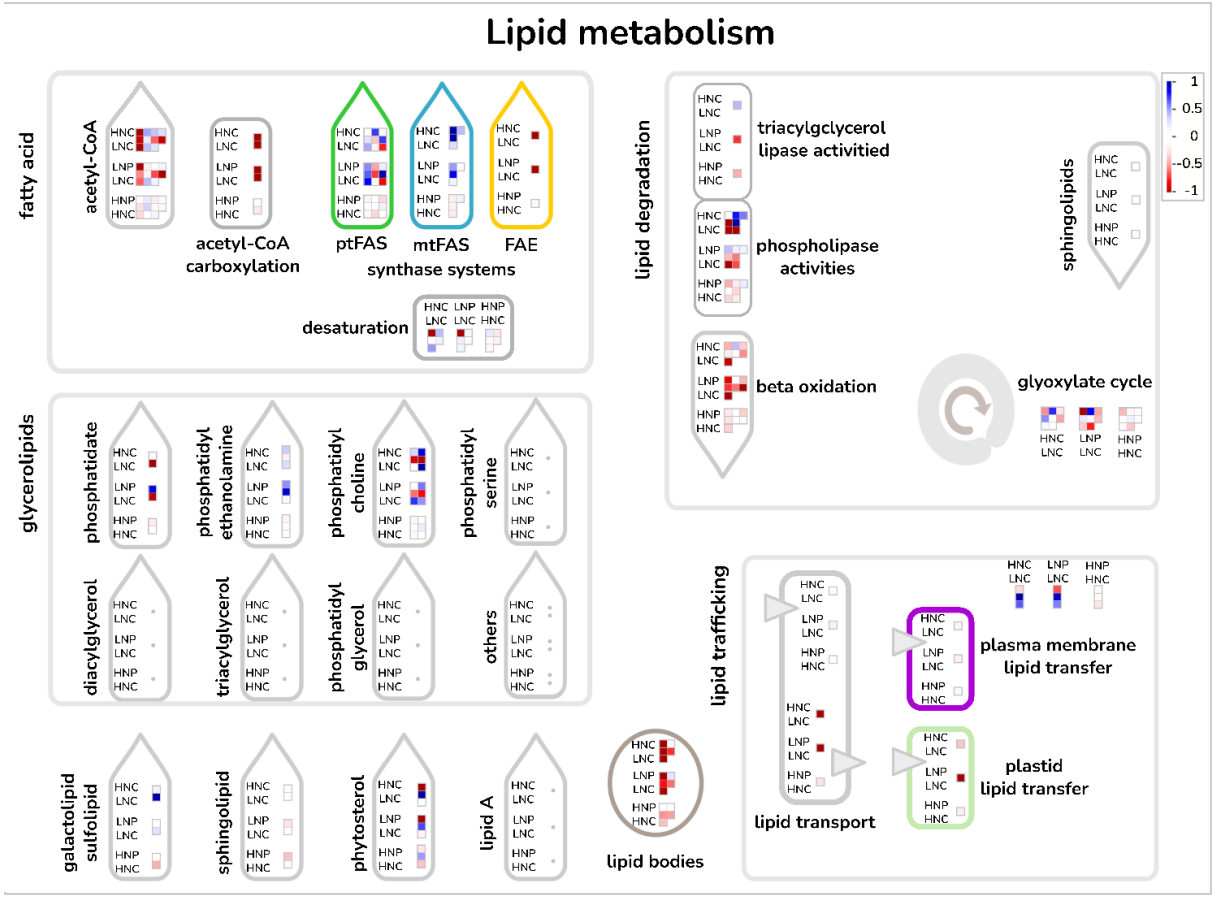

Figure 4.6. Lipid metabolism overview in roots (whole proteome). Data represented are 100% vv. Mapped proteins, log2FC and significances (indicated with asterisks in log2FC column) are shown in Supplementary Table S4.1. MapMan version 3.5.1R2 (Thimm et al., 2004) was used. The following pathways were used and modified: X4.5 Lipid metabolism R5.0. Mapping file was created using Mercator4 V2.0 (Schwacke et al., 2019). Abbreviations: ptFAS, plastidial fatty acid synthase; mtFAS, mitochondrial fatty acid synthase; FAE, fatty acid elongase. Comparisons are mentioned next to each box: HNC / LNC = Sufficient N Control vs. Limited N Control; LNP / LNC = Limited N + *Pk* vs. Limited N Control; HNP / HNC = Sufficient N + *Pk* vs. Sufficient N Control.

4.3.5 The lipidome of Brachypodium mainly responds to different N levels, but only slightly to inoculation with *Pk*

PCA shows differences between sufficient N controls and limited N controls at all timepoints. As a general observation, during the investigated time points, inoculation with *Pk* seems not to affect the lipidome under both low and sufficient N (Fig. 4.7.).

The heatmap (Fig 4.7) displays the differences between high and limited N root lipids. Inoculation with *Pk* seems to change the abundance of various lipids, but these changes are, for the most part, not significant. In general, *Pk* inoculation led to 45 significantly different abundant lipids (comparison: Limited N + *Pk* vs. Limited N Ctrl) among all timepoints. The mainly affected lipid classes are the following: ADGGA (5), Cer (2), CL (2), DG (5), DGDG (4), LPC (1), MGDG (6), PC (3), PE (7), PI (2), PS (2), SQDG (2) and TG (4). At 19 DAS, the biggest response of the lipid profile was observed after *Pk* inoculation under limited N, with 23 significantly different abundant lipids being quantified, whereas 12 and 10 lipids were significantly changed at 20 and 21 DAS, respectively. Thus, it can be hypothesized that changes on the lipid profile might be happening prior to the observed timepoint of 19 DAS which need further investigation though more (earlier) timepoints. Based on this assumption, the remodelling of the lipid profile of Brachypodium could play an essential role within this plant-microbe interaction. The temporal resolved dynamics of the lipids have been visualised in Figure 4.8.

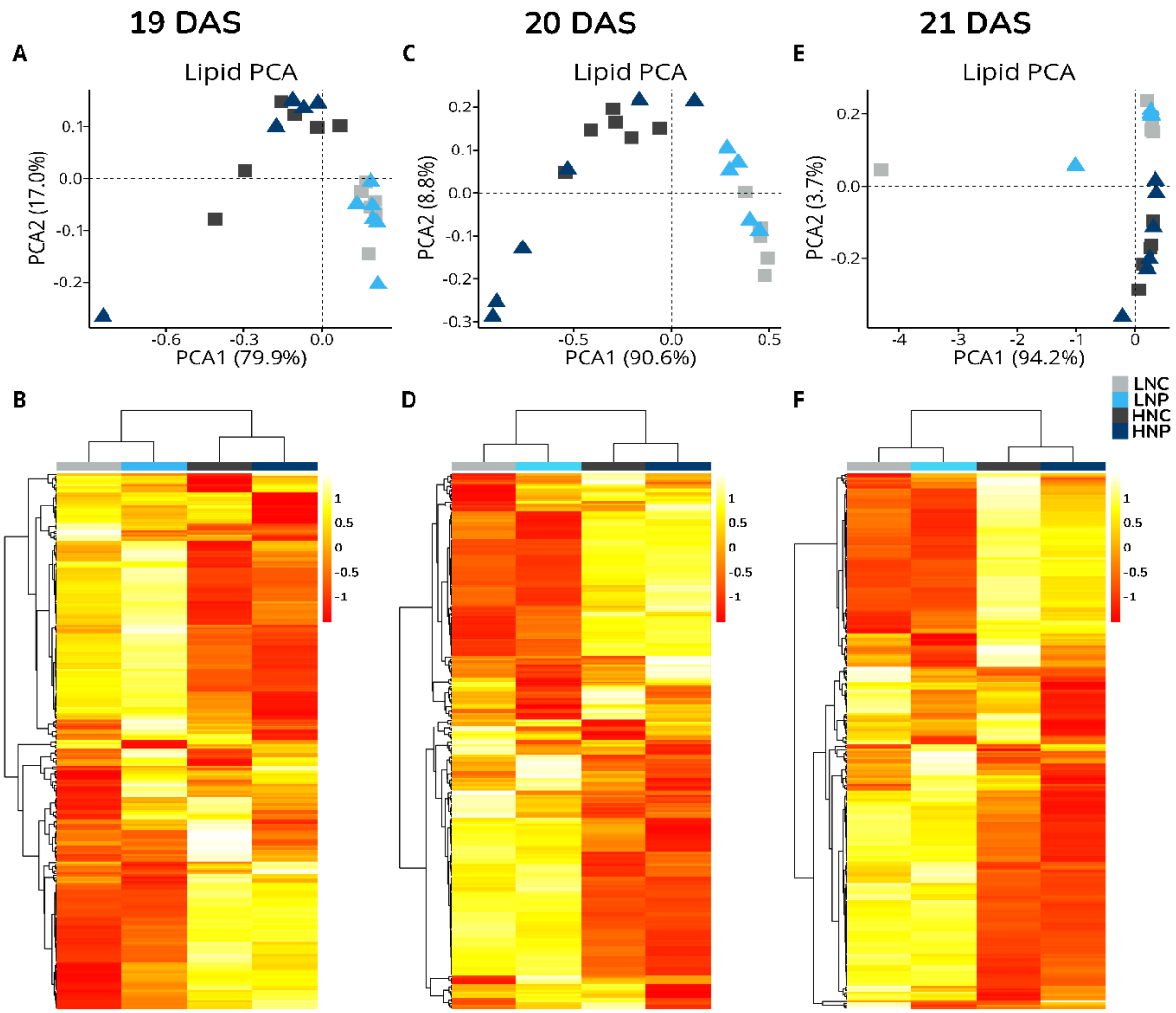

Figure 4.7. PCA and heatmaps of root Lipids 19, 20 and 21 DAS (time-resolved). All manually curated lipids (255 features) were used for PCA and were mapped using hierarchical cluster analysis (HCA), Pearson distance measurement and average distance. Abundances were log10 transformed and scaled using Pareto scaling.

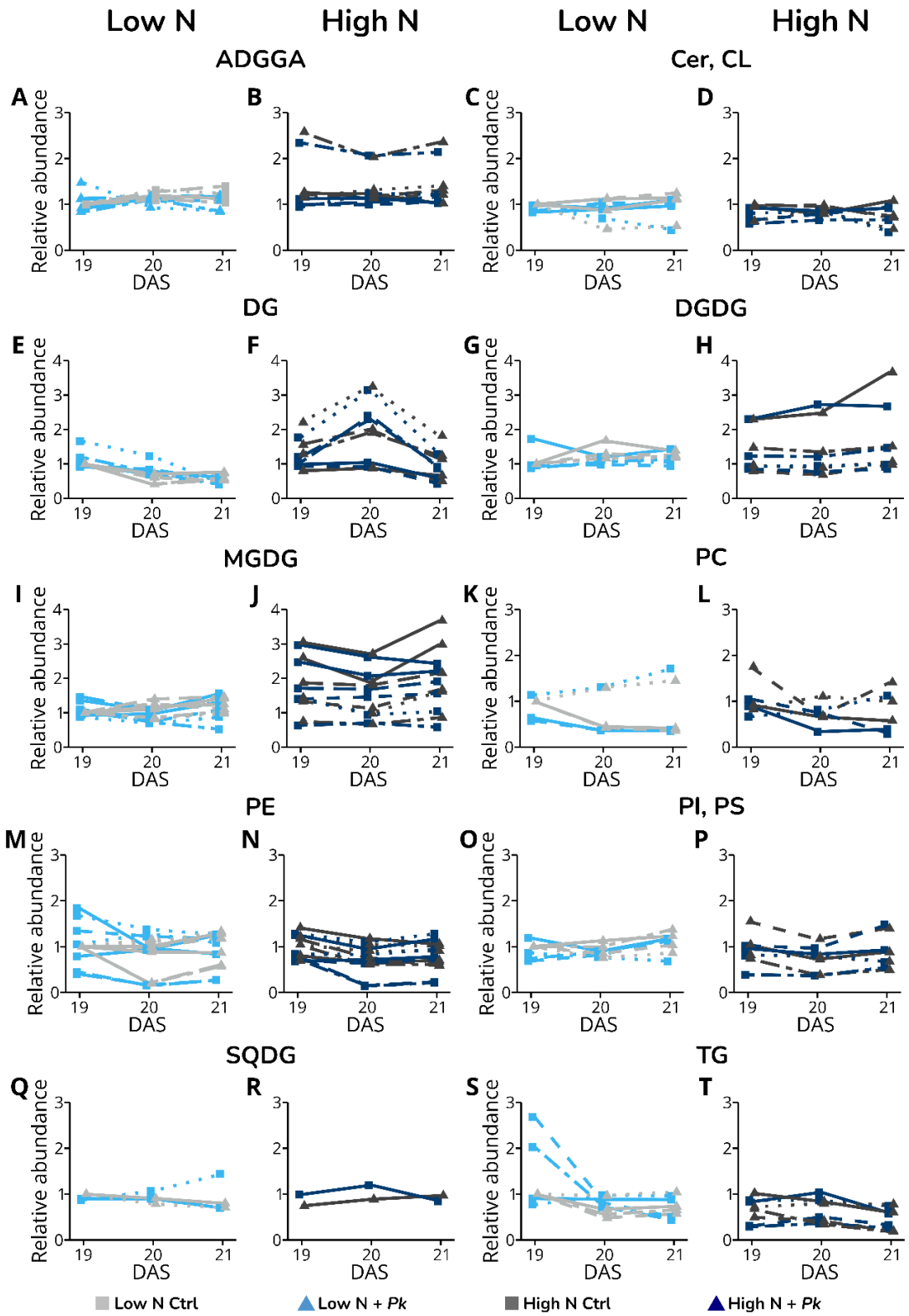

Figure 4.8. Relative abundance of significant lipids in roots. Lipids were split according to their classifications (ADGGA; Cer, CL; DG, DGDG; MGDG; PC; PE; PI, PS; SQDG; TG) and each lipid group is represented in two plots: Limited N (left) and sufficient N (right). Unique features are represented with different linetypes, limited to 5 different linetypes per plot. Relative abundances were calculated based on the abundances of features in limited N controls at 19 DAS (set to 1). Statistics can be found in the Supplementary Table S4.2. Abbreviations: ADGGA, acyl diacylglycerol glucuronide; Cer, ceramides; CL, cardiolipin; DG, diacylglycerol; DGDG, digalactosyldiacylglycerol; MGDG, monogalactosyldiacylglycerol; PC, phosphatidylcholine; PE, phosphatidylethanolamine; PI, phosphatidylinositol; PS, phosphatidylserine; SQDG, sulfoquinovosyldiacylglycerol; TG, triacylglycerol.

4.4 Discussion

4.4.1 Proteomics and lipidomics data integration

The integration of data from different 'omics' is very challenging. On gene, transcript and protein level, data bases have developed over years. Lipidomics in plant-microbe interactions is a far less studied approach, thus no sufficient data bases are available. The proteomics and lipidomics approaches performed in this thesis have generated descriptive data sets, reflecting the abundances of proteins or lipids. Depending on the availability of information, these descriptive data can be set into context with, for instance, metabolic pathways (Fig. 4.4). With the advances in genomic sequencing and more plant species being fully sequenced, the protein data bases are well curated. With approximately 5000 identified unique proteins, there are still big gaps in metabolic pathways, as seen for instance in Figure 4.6. Regardless if this is an identification or detection issue, either fractionation, if applicable, or better resolutions of the LC-MS/MS are required for a more detailed overview about the changes on protein level. With increased resolution and sensitivity, full pathways can be reconstructed, which leads to better predictions of key enzymes involved in the plant-microbe interaction. The molecular mechanisms could then be investigated using knockdown or knockout mutants of the key enzymes, further increasing the understanding of plant-microbe interactions.

Lipids are not as well studied as proteins, especially in plants or plant-microbe interactions. With the current existing data bases, it is possible to integrate lipid with gene, transcript or protein data, but this is limited to the already identified lipids. The lipid database lipidmaps (lipidmaps.org) only contains predicted (*in silico*) lipids and can therefore only be used for identification of lipids. Thus, it is of particular interest to increase the number of identified lipids via untargeted lipidomics approaches. In this study, a descriptive lipid profile was generated based on the identified lipids in *Arabidopsis thaliana* by Kehelpennala et al. (2021). The presence of the identified lipids was confirmed in *B. distachyon* via re-identification in the here conducted experiment. Although temporally resolved data are available (Fig. 4.8), the role of most identified lipids remains unclear, thus only the identified lipid classes are presented. This way, it is

possible to identify potentially relevant lipid classes in plant-microbe interactions and future research could be more targeted to those lipid classes. Unfortunately, it was not possible to fully re-construct the synthesis pathways for specific identified lipids, due to missing protein data of the specific enzymes.

4.4.2 Integration of molecular and phenotypic data

As described in Chapter 3, various significantly different phenotypic parameters were observed. Under limited N, Brachypodium inoculated with *Pk* developed longer lateral roots compared to their controls. On the molecular level, various genes and proteins affect the lateral root development. One of these proteins is the here quantified nitrate transporter-activating protein 2.1 (NAR2.1; I1IB70_BRADI).

Low concentrations of external nitrate led to inhibition of lateral root formation in *Oryza sativa* NAR2.1 knockdown mutants, via reduction of expression levels of PINs in roots (Huang et al., 2015; Sun et al., 2017). The study by Huang et al. (2015) proposed that a combination of nitrate uptake and signalling led to the observed effects on lateral root development, whereas the role of NRT2.1 remains unclear (Sun et al., 2017). Additionally, nitric oxide (NO) was identified as a signal molecule involved in regulation of the plant root system architecture (Chen et al., 2010; Meng et al., 2012; Trevisan et al., 2014 Sun et al., 2017, Siddiqui et al., 2023). Sun et al. (2015) demonstrated that an increased NO content via the NR led to increased N uptake (Sun et al., 2015; Sun et al., 2017). Nitrate signalling pathways can have a stimulatory effect on lateral root development via auxin transport (Sun et al., 2017).

Although an increased N content was observed in plants (Fig. 3.10 F), a decreased abundance of the enzyme NR was observed in limited N inoculated roots and sufficient N control roots compared to limited N control roots. As mentioned before, NO derives from the enzyme NR and could play a role in the lateral root development observed in this thesis. In a future experiment, the root NO content could be measured to test the hypothesis. With NR being the first downstream nitrate assimilation enzyme, a higher abundance was expected as more nitrate would require assimilation. However, in the

comparison of sufficient N control plants with limited N control plants, lower abundance of NR was quantified in the roots, while limited N inoculated roots also showed a mild decreased abundance (Fig. 4.4). In shoots, NR was less abundant in sufficient N control shoots compared to limited N control shoots, while a slightly higher abundance was observed for limited N inoculated with *Pk* shoots compared to limited N control shoots (Fig. 4.4). This leads to the following hypotheses: (i) nitrate is mainly assimilated by the shoots and stored in roots and (ii) ammonium derived from biological nitrogen fixation of *Pk* is primarily assimilated under limited N for plant development. While no vacuolar nitrate importers were quantified in this study, an increased abundance of several downstream central N-metabolism enzymes were quantified. Especially in shoots of inoculated limited N plants all assimilation related enzymes have been quantified in higher abundance than in limited N control plants (NR, NiR, GS, GOGAT, Fig. 4.4). In roots, all GLN isoforms were quantified in lower abundance in limited N inoculated plants compared to their control plants. The assimilation of potentially derived NH_4^+ from BNF of *Pk* would, according to protein data, be conveyed in the shoots. This hints additionally to reallocation of N from roots to shoots after inoculation of Brachypodium under limited N. Brachypodium root to shoot N ratio did not change after inoculation with *Pk*, with the N content increasing proportionally (Fig. 3.10 F).

4.4.3 *Pk* has minor effects on cell membrane lipid composition, but increases storage lipids

25 significantly different abundant lipids out of 250 total identified lipids were quantified on 19 DAS, while only 12 and 10 significant different abundant lipids were quantified at 20 and 21 DAS, respectively (Fig. 4.8). On 19 DAS, no phenotypic differences were observed in the comparison of Brachypodium grown under limited N inoculated with *Pk* and their limited N controls (Chapter 3.5), whereas two days later (21 DAS), almost all measured phenotypic parameters were significantly different. This leads to the hypothesis that the significantly different abundant lipids on 19 DAS play an important role in the plant-growth promotion of Brachypodium by *Pk*. Since the significant differences are declining at 20 DAS, it would be interesting to generate lipid profiles at earlier timepoints, for instance 17, 18 and 19 DAS, to capture the full lipid response

occurring prior to the phenotypic improvements. This way, the identified lipids in this thesis might be confirmed and characterised in future studies, elucidating their role in the plant-microbe interaction.

Nevertheless, 25 significant different lipids at one time point are a good indicator that lipids play a major role in plant-microbe interactions and therefore more research should focus on lipids. In general, a combination of molecular data at all levels – from gene to lipids – without gaps will increase the insight in the molecular reprogramming happening during the interaction. This would increase our understanding of the processes occurring between the plant and microbes, and internal plant regulatory processes for the improved plant development. With these relevant information, other genera of PGPB can be tested for their molecular mechanisms. If multiple bacteria trigger similar regulations within the plant, other plant species could also be tested for plant growth promotion and crucial components missing for a successful plant growth promotion could be identified. Pinpointing these domains could ultimately lead to directed breeding of elite cultivars, enabling plants to benefit from these bacteria, which could also be achieved through genetic engineering.

4.4.4 Whole proteome dataset is more robust than microsomal enrichment

The abundance of many proteins is showing a different behaviour in the whole-proteome extract and the microsomal enrichment extract. Due to robustness, the whole-proteome data were presented in the result chapter (4.3), while the microsomal enrichment data are presented in the Supplementary Material of this chapter (4.5). Microsomal enrichment introduces substantial variability in the data, as only parts of the cytosolic located proteins are stored in the microsomes. Thus, it would have been important to filter the proteins based on their location in the cell, especially for membrane-bound proteins. A membrane-bound protein only dataset would give insight into the protein changes occurring on the plant cell membrane during the plant microbe interaction.

4.4.5 Future directions

Using the generated descriptive datasets, follow-up experiments with mutants of specific N-related transporters or enzymes could be conducted. Interesting targets would be NAR2.1 (I1IB70_BRADI) and the Nitrogen-regulatory protein II (A0A0Q3MUB2_BRADI). Using a NAR2.1 knockdown or knockout mutant, its effect on the lateral root development and/or N content could be answered. This should be expanded to other metabolic pathways to get an overall overview about the metabolic reprogramming happening during this plant microbe interaction. While I would propose to measure the lipid dynamics at an earlier timepoint in this experimental setup, I would also consider investigating the interaction between proteins and lipids. With the former, more relevant lipids can be identified, while the latter could help in changing the lipidome. Using Brachypodium mutants of lipid biosynthetic enzymes of relevant lipids will lead to characterisation of the role of the identified lipids. Furthermore, lipids relevant to the colonization / interaction processes could be identified using Brachypodium mutants. In general, the descriptive dataset is enabling future avenues for research on various metabolic pathways and an overall overview about the different processes occurring at the same time would further increase the understanding of plant-microbe interactions.

4.5 Supplementary Material

4.5.1 Protein abundances in tabular form to Fig. 4.7, 4.8, 4.9

Supplementary Table S4.1. Mapped proteins of the N-metabolism (Fig.4.7), kinase families (Fig. 4.8) and root lipid metabolism (Fig. 4.9). The column 'Mapped under' refers to the caption used in each pathway figure. Log2FC highlighted in bold are significant different in their respective comparison. In case the proteins were not found in a tissue, log2FC were replaced with 'x', and 'o' if not mapped (shoot lipid metabolism). Statistics were performed using ANOVA with a confidence interval of 95% followed by post-hoc Tukey's HSD.

			Root log2FC			Shoot log2FC		
	Mapped under	Uniprot ID	HNC / LNC	LNP / LNC	HNP / HNC	HNC / LNC	LNP / LNC	HNP / HNC
N-metabolism (Fig. 4.7)	AA	I1I0M5_BRADI	**-1.69**	**-1.41**	-0.19	x	x	x
		I1IDC0_BRADI	-0.70	-0.70	0.48	x	x	x
	AMT	I1IBN3_BRADI	**-1.56**	**-1.64**	-0.29	x	x	x
		I1IZJ3_BRADI	x	x	x	-0.13	0.10	**-0.84**
	AS	A0A2K2D9P1_BRADI	x	x	x	**0.87**	**0.83**	-0.01
		I1H6K4_BRADI	-0.88	**-1.78**	-0.22	x	x	x
	GDH	I1GM99_BRADI	0.26	**0.89**	-0.09	**-0.41**	-0.07	0.00
		I1J084_BRADI	**0.49**	-0.05	0.03	0.00	-0.22	0.16
	GOGAT	I1GRK9_BRADI	0.29	**0.78**	0.13	0.25	0.28	-0.23
		I1HQF1_BRADI	-0.41	-0.23	0.07	**0.27**	**0.43**	-0.10
	GS1	I1H7X9_BRADI	0.11	**-1.00**	-0.21	**0.40**	**0.30**	0.14
		I1IFI7_BRADI	**0.83**	-0.07	0.05	-0.30	-0.04	0.22
	GS2	I1J2T4_BRADI	0.34	-0.37	0.16	0.13	0.19	-0.15
	NiR	I1IEV4_BRADI	0.40	**1.04**	0.33	**1.08**	**1.07**	-0.15
	Nitrogen regulation	A0A0Q3MUB2_BRADI	**0.67**	**0.71**	0.13	-0.06	0.12	0.00
	NR	A0A0Q3FHC7_BRADI	**-1.07**	-0.49	0.10	**0.38**	0.15	0.07
	NRT	I1GPH0_BRADI	x	x	x	0.01	0.08	-0.02
		I1H1D1_BRADI	0.70	0.83	-0.14	-0.27	-0.15	0.36
		I1HBQ0_BRADI	x	x	x	0.20	0.31	-0.04
		I1I5R4_BRADI	**-1.34**	**-1.14**	-0.27	-0.04	-0.02	-0.16
		I1I6K3_BRADI	**-1.24**	**-1.47**	-0.19	x	x	x
		I1IAY0_BRADI	x	x	x	0.11	0.38	-0.10
		I1IB70_BRADI	**-4.24**	0.13	-0.15	x	x	x
Kinase families (Fig. 4.8)	AGC kinase superfamily	I1I858_BRADI	0.08	**-0.53**	-0.03	x	x	x
		A0A0Q3HGT3_BRADI	x	x	x	0.47	0.52	0.15
		I1GP76_BRADI	x	x	x	-0.16	-0.18	0.34
		I1HHS0_BRADI	x	x	x	0.19	0.22	-0.03
		I1IWY7_BRADI	x	x	x	0.13	0.09	-0.35
	Atypical kinase families	A0A0Q3IM64_BRADI	x	x	x	-0.12	0.35	-0.59
		I1GL81_BRADI	x	x	x	-0.28	**-0.43**	-0.13
		I1HF02_BRADI	x	x	x	-0.21	-0.08	0.14
		I1HKJ6_BRADI	x	x	x	-0.15	0.14	-0.41
		I1HM71_BRADI	x	x	x	-0.16	-0.14	-0.61

		I1IAV0_BRADI	x	x	x	0.47	0.25	-0.03
		I1IMJ5_BRADI	x	x	x	0.02	0.15	-0.31
		I1J2E3_BRADI	x	x	x	0.10	0.26	-0.02
	CAMK kinase superfamily	I1GKM6_BRADI	**-0.73**	**-0.91**	-0.43	0.24	0.25	-0.35
		I1GLT7_BRADI	-0.38	-0.17	-0.10	x	x	x
		I1GMG8_BRADI	-0.39	0.25	-0.09	x	x	x
		I1GMZ0_BRADI	**-0.86**	-0.66	-0.08	x	x	x
		I1GU02_BRADI	**-0.68**	**-0.55**	-0.09	0.32	0.12	0.00
		I1GX02_BRADI	**-0.93**	**-1.11**	-0.03	x	x	x
		I1H269_BRADI	-0.18	0.37	-0.06	x	x	x
		I1HI64_BRADI	**0.83**	**0.59**	0.13	x	x	x
		I1HNY1_BRADI	0.02	0.56	-0.43	0.02	0.04	-0.11
		I1HPI9_BRADI	**0.53**	0.20	-0.11	0.25	0.42	-0.92
		I1I692_BRADI	-0.29	-0.13	-0.22	-0.08	-0.26	0.08
		I1IAE4_BRADI	**1.05**	0.54	0.29	0.05	0.22	-0.05
		I1IN49_BRADI	**-0.97**	**-0.67**	-0.07	x	x	x
		I1IX12_BRADI	-0.22	-0.15	-0.24	-0.13	0.03	0.34
		I1IXT7_BRADI	**-0.68**	**-0.69**	-0.18	x	x	x
		I1J0Z2_BRADI	**-1.16**	-0.75	-0.03	x	x	x
		I1GQB4_BRADI	x	x	x	0.24	0.16	-0.40
		I1H626_BRADI	x	x	x	**1.64**	0.77	-0.07
		I1H6L6_BRADI	x	x	x	**0.47**	-0.07	-0.02
		I1ITM2_BRADI	x	x	x	0.26	0.16	-0.14
	CK kinase superfamily	I1HFR4_BRADI	0.23	0.70	-0.37	0.42	0.13	0.02
		I1HQU4_BRADI	0.08	0.32	0.11	0.32	0.34	0.06
	CMGC kinase superfamily	I1GNX9_BRADI	0.39	0.35	-0.07	0.23	0.19	0.22
		I1GUL3_BRADI	0.26	0.61	0.12	x	x	x
		I1H4A1_BRADI	**-0.95**	**-1.05**	-0.25	-0.08	0.21	-0.07
		I1HAG7_BRADI	x	x	x	0.09	0.23	0.04
		I1HGU1_BRADI	x	x	x	0.16	0.27	-0.17
		I1HIE2_BRADI	x	x	x	0.27	**0.32**	-0.17
		I1I8I8_BRADI	x	x	x	**0.70**	**0.81**	0.36
	Extensin	A0A0Q3IUM4_BRADI	0.27	0.33	0.09	x	x	x
	L-Lectin	A0A0Q3KPD2_BRADI	0.15	0.46	0.24	**-0.93**	**-0.67**	0.28
		A0A2K2CHP2_BRADI	0.31	0.38	-0.09	-0.18	-0.03	-0.15
		I1I8J5_BRADI	-0.06	0.50	-0.05	x	x	x
	LRR	A0A0Q3EYZ3_BRADI	**0.74**	0.35	-0.32	**0.31**	**0.43**	-0.17
		A0A0Q3GL83_BRADI	**0.50**	**0.32**	0.10	-0.53	-0.53	0.18
		A0A0Q3GU79_BRADI	-0.05	0.01	-0.19	-0.08	0.02	0.15
		A0A0Q3KBU7_BRADI	**0.91**	0.88	-0.05	-0.26	-0.21	0.23
		A0A0Q3KL20_BRADI	**0.48**	**0.49**	-0.09	x	x	x
		A0A0Q3KRE6_BRADI	-0.20	-0.05	-0.03	0.09	-0.01	-0.08
		A0A2K2CIK2_BRADI	-0.12	0.50	-0.01	x	x	x
		A0A2K2CTF7_BRADI	-0.06	**-0.19**	-0.08	x	x	x

		A0A2K2D9S6_BRADI	-0.48	-0.14	0.17	0.24	0.31	0.00
		I1GP23_BRADI	**1.02**	**0.82**	-0.06	-0.20	-0.09	-0.02
		I1GWG0_BRADI	1.13	-0.14	0.11	x	x	x
		I1H403_BRADI	-0.36	-0.10	-0.14	x	x	x
		I1H6F1_BRADI	**-0.65**	**-0.84**	0.06	x	x	x
		I1HA83_BRADI	0.16	0.50	0.03	x	x	x
		I1HBQ9_BRADI	-0.23	0.22	-0.10	x	x	x
		I1HDE7_BRADI	-0.01	0.04	-0.19	x	x	x
		I1HIB3_BRADI	**-0.49**	-0.18	0.05	x	x	x
		I1HP99_BRADI	-0.23	-0.42	-0.20	-0.29	0.01	-0.59
		I1HSU8_BRADI	0.61	**0.99**	-0.22	x	x	x
		I1ID77_BRADI	0.14	**0.52**	0.03	**0.70**	0.61	-0.08
		I1ILV2_BRADI	0.31	**0.70**	0.01	x	x	x
		I1IP60_BRADI	-0.41	-0.18	0.02	x	x	x
		I1IVA7_BRADI	0.39	0.49	-0.04	-0.21	-0.12	0.22
		I1IZ22_BRADI	0.20	-0.10	-0.05	-0.12	-0.21	-0.12
		I1GMT9_BRADI	x	x	x	-0.07	0.15	**0.51**
		I1GR39_BRADI	x	x	x	-0.46	-0.23	-0.22
		I1GZ29_BRADI	x	x	x	-0.24	-0.34	-0.13
		I1IW92_BRADI	x	x	x	0.06	-0.01	0.13
	LysM	A0A0Q3FRN3_BRADI	-0.20	0.05	-0.12	x	x	x
		A0A0Q3I004_BRADI	0.14	0.20	-0.10	x	x	x
	MAP kinases	I1I5N8_BRADI	-0.51	**-1.33**	-0.07	x	x	x
		I1H0Y7_BRADI	x	x	x	0.17	**0.56**	**0.36**
	PERK-like	A0A0Q3MRU1_BRADI	x	x	x	**0.33**	0.16	**-0.16**
	RKF3-like	A0A0Q3G6V2_BRADI	x	x	x	-0.38	-0.40	-0.36
Lipid metabolism (Fig. 4.9)	acetyl-COA	A0A0Q3K0H7_BRADI	0.26	0.16	0.16	o	o	o
		A0A0Q3M1M0_BRADI	0.40	0.41	0.04	o	o	o
		I1GQ11_BRADI	0.22	-0.16	0.33	o	o	o
		I1H338_BRADI	**-0.92**	-0.55	-0.28	o	o	o
		I1HLK9_BRADI	0.29	0.17	0.10	o	o	o
		I1HQ21_BRADI	**-1.75**	**-1.13**	-0.09	o	o	o
		I1I6C4_BRADI	**-1.14**	-0.65	-0.31	o	o	o
		I1IA43_BRADI	**-0.93**	**-1.20**	-0.15	o	o	o
		I1IQ05_BRADI	0.39	-0.03	-0.22	o	o	o
		I1ITV5_BRADI	**-0.63**	**-0.68**	-0.13	o	o	o
		I1IVQ0_BRADI	0.48	-0.20	0.23	o	o	o
	acetyl-CoA carboxylation	A0A0Q3JE04_BRADI	**-1.32**	**-1.01**	0.02	o	o	o
		I1IWF2_BRADI	**-1.67**	**-1.99**	-0.22	o	o	o
	beta oxidation	A0A0Q3JRJ2_BRADI	**-0.94**	**-1.67**	-0.34	o	o	o
		I1HLG5_BRADI	**0.41**	0.06	-0.05	o	o	o
		I1HZH4_BRADI	-0.35	-0.43	-0.35	o	o	o

		I1I3F1_BRADI	-0.44	**-0.87**	-0.23	o	o	o
		I1I4F7_BRADI	-0.10	**-0.60**	-0.08	o	o	o
		I1IDX9_BRADI	**-0.54**	**-1.28**	-0.10	o	o	o
		I1IPG4_BRADI	-0.20	**-0.73**	-0.27	o	o	o
	desaturation	I1HN08_BRADI	-0.04	0.21	-0.12	o	o	o
		I1HSR7_BRADI	**-1.77**	**-1.63**	0.23	o	o	o
		I1HUM5_BRADI	0.18	0.08	-0.19	o	o	o
		I1HVL8_BRADI	0.51	0.17	-0.13	o	o	o
		I1I5F5_BRADI	0.41	0.15	-0.25	o	o	o
	FAE	A0A2K2D3W9_BRADI	-1.10	**-1.87**	-0.11	o	o	o
	galactolipid sulfolipid	I1HIN3_BRADI	0.18	-0.04	-0.02	o	o	o
		I1I6H2_BRADI	**1.93**	0.28	-0.45	o	o	o
	glyoxylate cycle	A0A0Q3F6L1_BRADI	**0.54**	0.24	0.04	o	o	o
		A0A0Q3GPP4_BRADI	-0.10	**-0.76**	-0.37	o	o	o
		I1H6A1_BRADI	-0.48	-0.41	-0.09	o	o	o
		I1HA00_BRADI	0.12	-0.35	-0.07	o	o	o
		I1HZ21_BRADI	-0.54	**-1.09**	-0.43	o	o	o
		I1IG62_BRADI	**-0.26**	**-0.47**	-0.09	o	o	o
		I1IX27_BRADI	**0.74**	**0.83**	0.13	o	o	o
		I1IZE5_BRADI	-0.02	-0.13	0.19	o	o	o
	lipid bodies	A0A0Q3SCX9_BRADI	**-1.95**	**-1.64**	-0.02	o	o	o
		A0A2K2D5E4_BRADI	**-0.99**	**-0.79**	-0.53	o	o	o
		A0A2K2DPB0_BRADI	**-1.16**	**-0.99**	-0.40	o	o	o
		I1HLR0_BRADI	**-0.73**	**-0.61**	**-0.50**	o	o	o
		I1IEG7_BRADI	0.10	0.26	0.03	o	o	o
	lipid trafficking	I1GL63_BRADI	-0.32	**-0.68**	-0.10	o	o	o
		I1H1G1_BRADI	**0.65**	0.57	-0.26	o	o	o
		I1I1B4_BRADI	**1.06**	**0.93**	-0.10	o	o	o
	lipid transport	A0A2K2D1A1_BRADI	**-1.12**	**-1.25**	-0.27	o	o	o
		A0A2K2DFT3_BRADI	0.08	-0.20	0.06	o	o	o
	mtFAS	A0A0Q3R9W8_BRADI	0.29	0.17	-0.23	o	o	o
		I1H2L1_BRADI	**1.78**	0.51	-0.20	o	o	o
		I1H5F3_BRADI	**1.34**	0.83	-0.18	o	o	o
		I1H6F4_BRADI	0.41	-0.09	0.19	o	o	o
	phosphatidate	A0A0Q3FNL6_BRADI	**-1.18**	**-0.94**	-0.02	o	o	o
		I1I6G2_BRADI	0.13	0.88	-0.22	o	o	o
	phosphatidyl choline	A0A0Q3GTN4_BRADI	**0.88**	0.59	-0.08	o	o	o
		A0A2K2D745_BRADI	-0.04	**0.73**	-0.11	o	o	o
		I1GQE0_BRADI	**-0.97**	**-0.81**	0.21	o	o	o
		I1HGU5_BRADI	0.32	0.03	-0.14	o	o	o
		I1HRW0_BRADI	**1.24**	0.53	0.01	o	o	o
		I1HXR8_BRADI	**-0.89**	-0.61	-0.04	o	o	o
	phosphatidyl ethanolamine	A0A0Q3N4N1_BRADI	-0.22	**0.90**	0.07	o	o	o
		A0A2K2CRK8_BRADI	0.36	**0.53**	-0.18	o	o	o

		I1J2C7_BRADI	0.29	0.13	0.08	o	o	o
	phospholipase activities	A0A0Q3FHI6_BRADI	**-1.01**	-0.41	-0.08	o	o	o
		A0A0Q3GLT1_BRADI	**1.16**	-0.58	-0.33	o	o	o
		I1H4V2_BRADI	**-1.12**	**-0.68**	-0.21	o	o	o
		I1HCG5_BRADI	**0.58**	0.18	0.22	o	o	o
		I1HVB6_BRADI	**0.78**	0.21	-0.21	o	o	o
		I1I799_BRADI	0.08	0.40	-0.46	o	o	o
		I1IKD0_BRADI	**-1.26**	**-1.33**	-0.32	o	o	o
	phytosterol	A0A0Q3NTK1_BRADI	**1.20**	0.68	0.50	o	o	o
		I1GV37_BRADI	**-1.55**	**-2.07**	-0.26	o	o	o
		I1IVM8_BRADI	0.04	-0.18	**-0.39**	o	o	o
	plasma membrane lipid transfer	I1H6Z5_BRADI	-0.18	-0.19	-0.11	o	o	o
	plastid lipid transfer	I1IU18_BRADI	-0.38	**-1.14**	-0.19	o	o	o
	ptFAS	A0A0Q3IJU7_BRADI	0.47	**0.83**	-0.12	o	o	o
		A0A2K2CXZ2_BRADI	-0.39	-0.71	-0.06	o	o	o
		I1GKM7_BRADI	0.06	0.55	-0.18	o	o	o
		I1GXN7_BRADI	0.71	**0.98**	0.19	o	o	o
		I1H029_BRADI	0.71	-0.48	-0.03	o	o	o
		I1I9A1_BRADI	0.28	0.64	-0.04	o	o	o
		I1I9U8_BRADI	-0.18	-0.04	-0.32	o	o	o
		I1IRJ8_BRADI	**-0.76**	**-0.81**	0.05	o	o	o
		I1IWW9_BRADI	0.10	0.21	-0.31	o	o	o
	sphingolipid	I1HPK0_BRADI	0.00	-0.04	0.12	o	o	o
		I1IBQ1_BRADI	0.08	-0.26	-0.40	o	o	o
	triacylglycerol lipase activities	I1HLP4_BRADI	0.42	-0.72	-0.46	o	o	o

4.5.2 Lipid abundances in tabular form

Supplementary Table S4.2. Log2-fold changes (log2FC) and p-values of the plotted lipids in Figure S4.8. Only statistically significant lipids are represented in the table at each individual time point (19, 20 and 21 DAS). Statistics were exported from Metaboanalyst.com.

	Lipids	log2FC	p
19 DAS	ADGGA 50:6|ADGGA (O-12:0)18:1_20:5	-0.4968	0.0428
	ADGGA 54:9|ADGGA (O-18:3)18:3_18:3	-0.5249	0.0281
	Cer 42:1;O3|Cer 18:1;O2/24:0;O	-0.2579	0.0124
	CL 72:12|CL 36:6_36:6	-0.4428	0.0312
	CL 72:8|CL 36:3_36:5	-0.4749	0.0149
	DG 32:0|DG 16:0_16:0	-0.3868	0.0487
	DGDG 34:4|DGDG 16:1_18:3	0.5243	0.0023
	DGDG 36:1|DGDG 18:0_18:1	-0.3043	0.0215
	DGDG 42:4|DGDG 24:1_18:3	-0.4105	0.0089
	LPC 16:0/0:0	-1.7173	0.0055

	MGDG 34:1|MGDG 16:0_18:1	-0.3558	0.0154
	MGDG 36:2|MGDG 18:1_18:1	-0.4857	0.0038
	PC 38:2|PC 12:1_26:1	-0.9796	0.0048
	PE 32:0|PE 16:0_16:0	0.6153	0.0410
	PE 36:3|PE 15:0_21:3	-1.4921	0.0001
	PE 36:4|PE 10:1_26:3	-1.6358	0.0002
	PE 36:5|PE 21:1_15:4	-0.5514	0.0373
	PS 36:5|PS 18:2_18:3	-0.7467	0.0015
	PS 42:3|PS 24:0_18:3	-0.6784	0.0201
	SQDG 32:0|SQDG 16:0_16:0	-0.4274	0.0362
	TG 52:0|TG 16:0_18:0_18:0	-0.6846	0.0050
	w/o MS2: PC 32:2|PC 8:1_24:1	-1.1525	0.0048
	w/o MS2: PI 36:5	-0.5352	0.0107
20 DAS	Cer 42:2;O3|Cer 18:2;O2/24:0;O	0.6749	0.0208
	DG 32:3|DG 14:0_18:3	1.0743	0.0318
	DG 32:6|DG 15:3_17:3	0.5681	0.0097
	DG 34:4|DG 16:1_18:3	0.9883	0.0269
	DG 36:4|DG 18:2_18:2	0.8536	0.0465
	DGDG 38:5|DGDG 20:2_18:3	-0.3308	0.0403
	MGDG 38:5|MGDG 20:2_18:3	-0.6570	0.0428
	MGDG 40:2|MGDG 22:0_18:2	-0.3051	0.0233
	PE 34:1|PE 16:0_18:1	0.3164	0.0241
	PE 36:2|PE 18:0_18:2	0.3868	0.0465
	PI 34:1	-0.2267	0.0491
	TG 46:2|TG 14:0_16:0_16:2	0.4701	0.0158
	TG 52:7|TG 16:2_18:2_18:3	0.7897	0.0435
21 DAS	ADGGA 51:5|ADGGA (O-18:2)15:0_18:3	-0.5721	0.0396
	ADGGA 52:3|ADGGA (O-18:2)16:0_18:1	-0.1726	0.0280
	ADGGA 58:4|ADGGA (O-24:0)16:2_18:2	-0.1778	0.0225
	DG 32:0|DG 16:0_16:0	-0.2960	0.0000
	MGDG 40:0|MGDG 16:0_24:0	-0.9633	0.0251
	MGDG 44:2|MGDG 26:0_18:2	0.3680	0.0392
	PC 38:8|PC 18:3_20:5	0.3024	0.0231
	PE 40:6|PE 12:0_28:6	-0.2816	0.0281
	SQDG 34:3|SQDG 16:0_18:3	0.9692	0.0211
	TG 56:8|TG 20:2_18:3_18:3	-0.5048	0.0379

4.5.3 PCA & Volcano plots (microsomal enrichment)

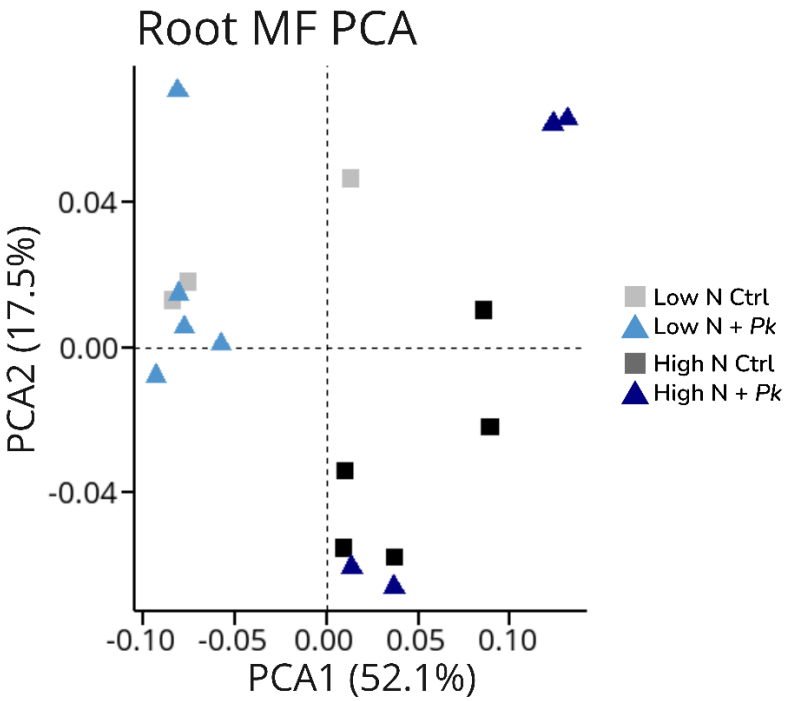

Supplementary Figure S4.1. Principal component analyses of root microsomal fraction (MF) datasets.

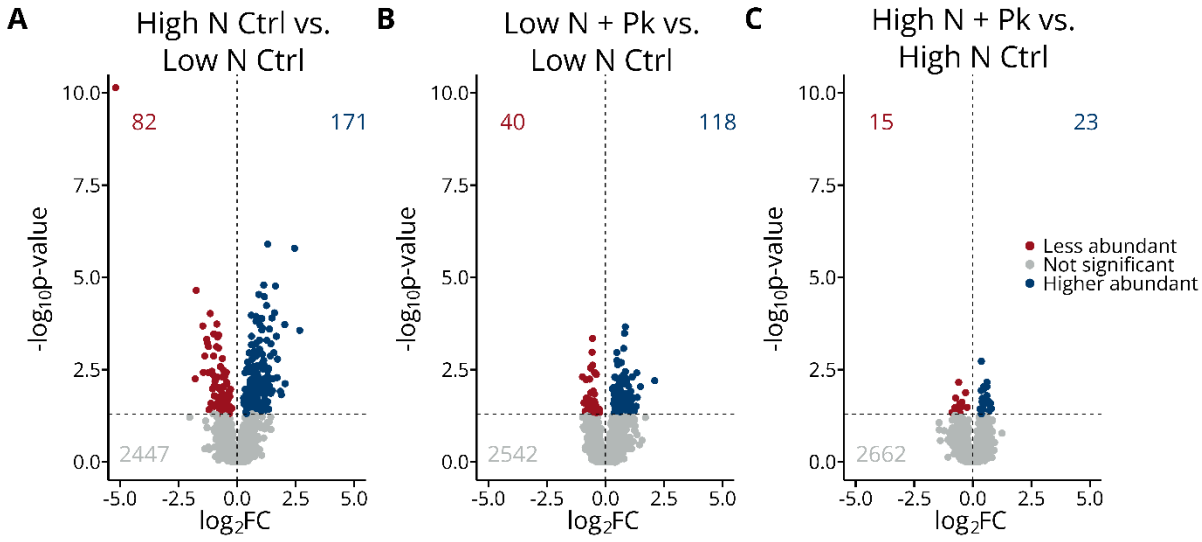

Supplementary Figure S4.2. Proteomics data overview of the root microsomal fraction. A) Root MF volcano plot of the comparison: Sufficient N Ctrl vs. Limited N Ctrl; B) Root MF volcano plot of the comparison: Limited N + *Pk* vs. Limited N Ctrl; C) Root MF volcano plot of the comparison: Sufficient N + *Pk* vs. Sufficient N Ctrl; Data shown are 100% valid values of the respective data set. Volcano plots represent the -log10 transformed adjusted p values from Tukey's HSD with a p-value threshold set for α <0.05 and no threshold set for log2FC (= 0). Values in the plot represent the number of proteins in each group (red = less abundant, grey = not significant, blue = higher abundant; matching the colours of data points).

4.5.4 N-metabolism (microsomal enrichment)

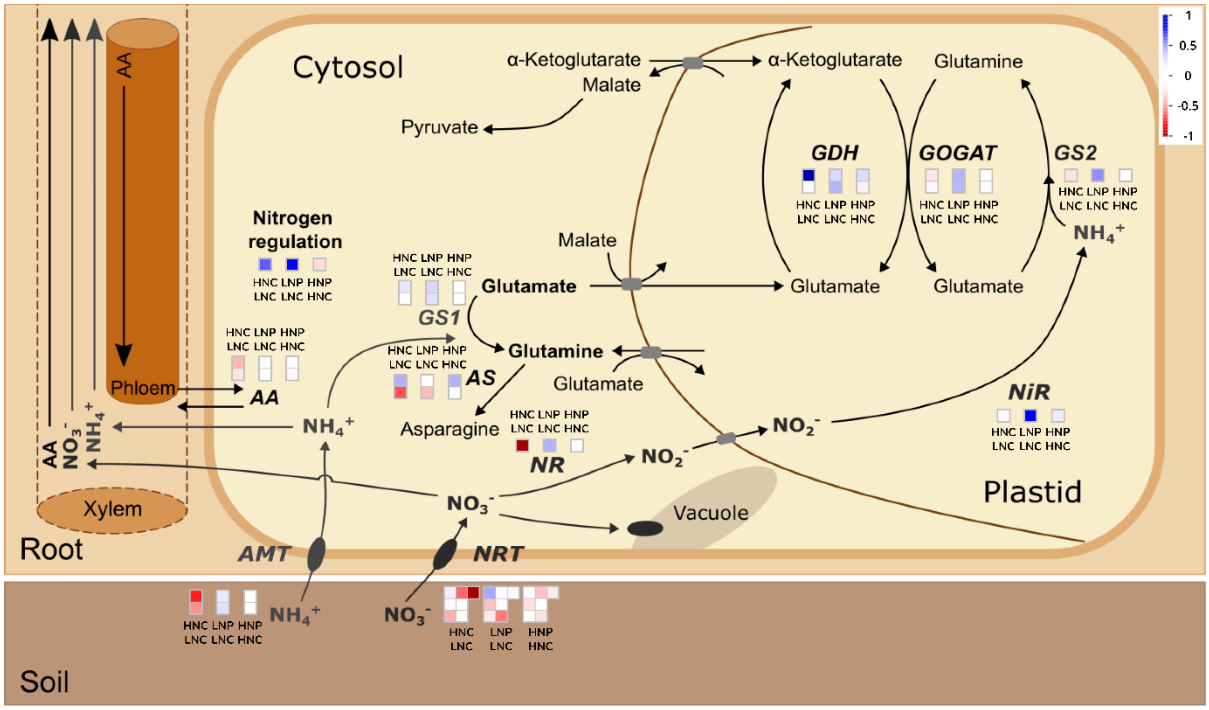

Supplementary Figure S4.3. Central N metabolism in roots (microsomal fraction). Data represented are 100% valid values. Mapped proteins, log2FC and significances (indicated with asterisks in log2FC column) are shown in Supplementary Table S4.3. MapMan version 3.5.1R2 (Thimm et al., 2004) was used. The following pathways were used and modified from Feng et al., 2020: X4.1 N-uptake R1.0. Modified pathways will be submitted to the MapMan store (https://mapman.gabipd.org/mapmanstore). Mapping file was created using Mercator4 V2.0 (Schwacke et al., 2019). Comparisons are mentioned on top or below of each box: HNC / LNC = Sufficient N Control vs. Limited N Control; LNP / LNC = Limited N + *Pk* vs. Limited N Control; HNP / HNC = Sufficient N + *Pk* vs. Sufficient N Control. Abbreviations: AA, Amino acid; AMT, ammonium transporter family; AS, Asparagine synthase; GDH, Glutamate dehydrogenase; GOGAT, glutamine oxoglutarate aminotransferase; GS1, (cytosolic) Glutamine synthetase 1 isoforms; GS2, (plastidial) Glutamine synthetase 2 isoforms; NiR, Nitrite reductase; NR, Nitrate reductase; NRT, Nitrate transporter family.

4.5.5 Kinases (microsomal enrichment)

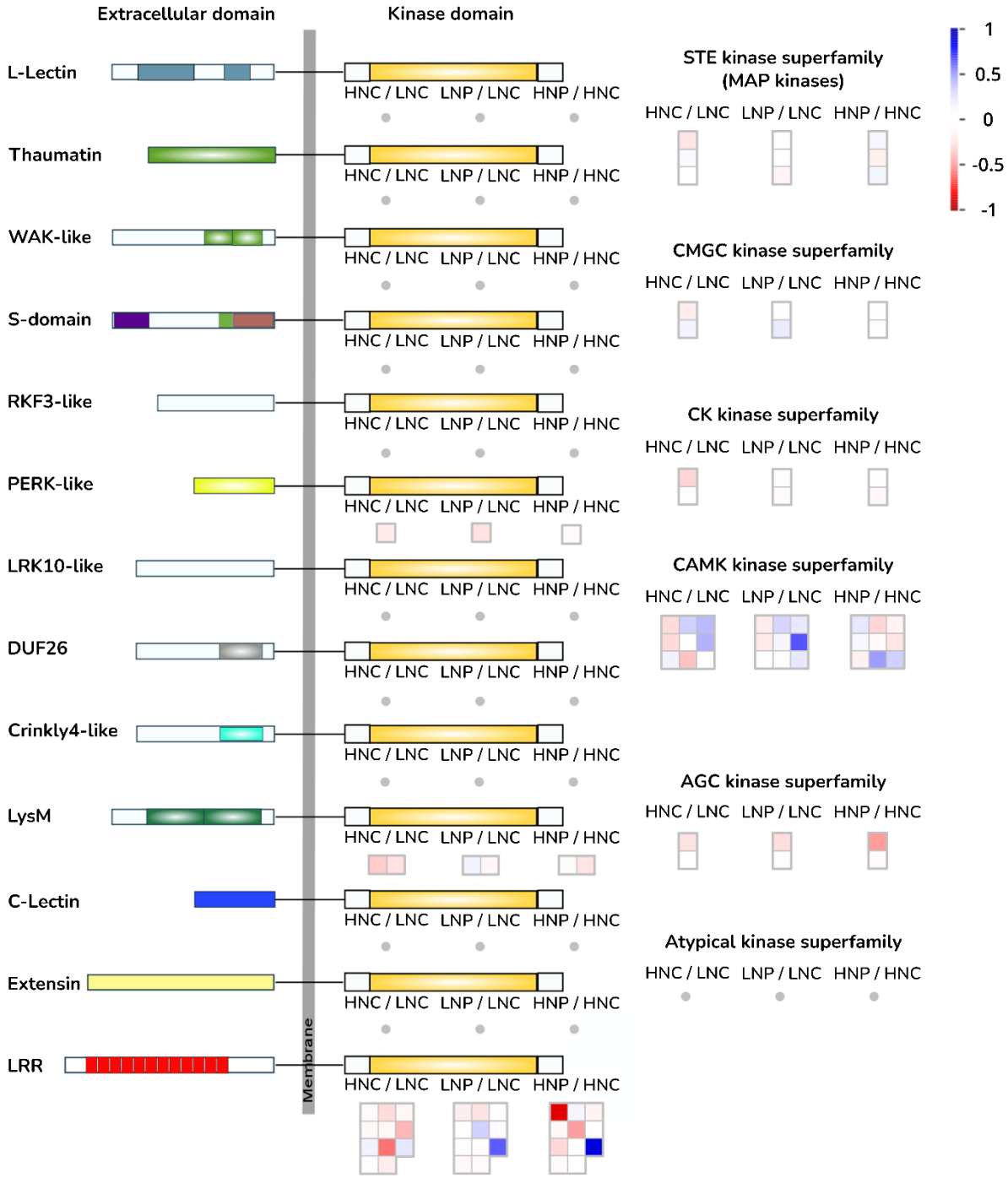

Supplementary Figure S4.4. Kinases in roots (microsomal fraction). Data represented are 100% vv. Mapped proteins, log2FC and significances (indicated with asterisks in log2FC column) are shown in Supplementary Table S4.3. MapMan version 3.5.1R2 (Thimm et al., 2004) was used. The following pathways were used and modified from Shiu and Bleecker, 2001: X4.1_Kinase_Families_R1.0. Mapping file was created using Mercator4 V2.0 (Schwacke et al., 2019). Comparisons are mentioned on top of each box: HNC / LNC = Sufficient N Control vs. Limited N Control; LNP / LNC = Limited N + *Pk* vs. Limited N Control; HNP / HNC = Sufficient N + *Pk* vs. Sufficient N Control.

4.5.6 Lipid metabolism (microsomal enrichment)

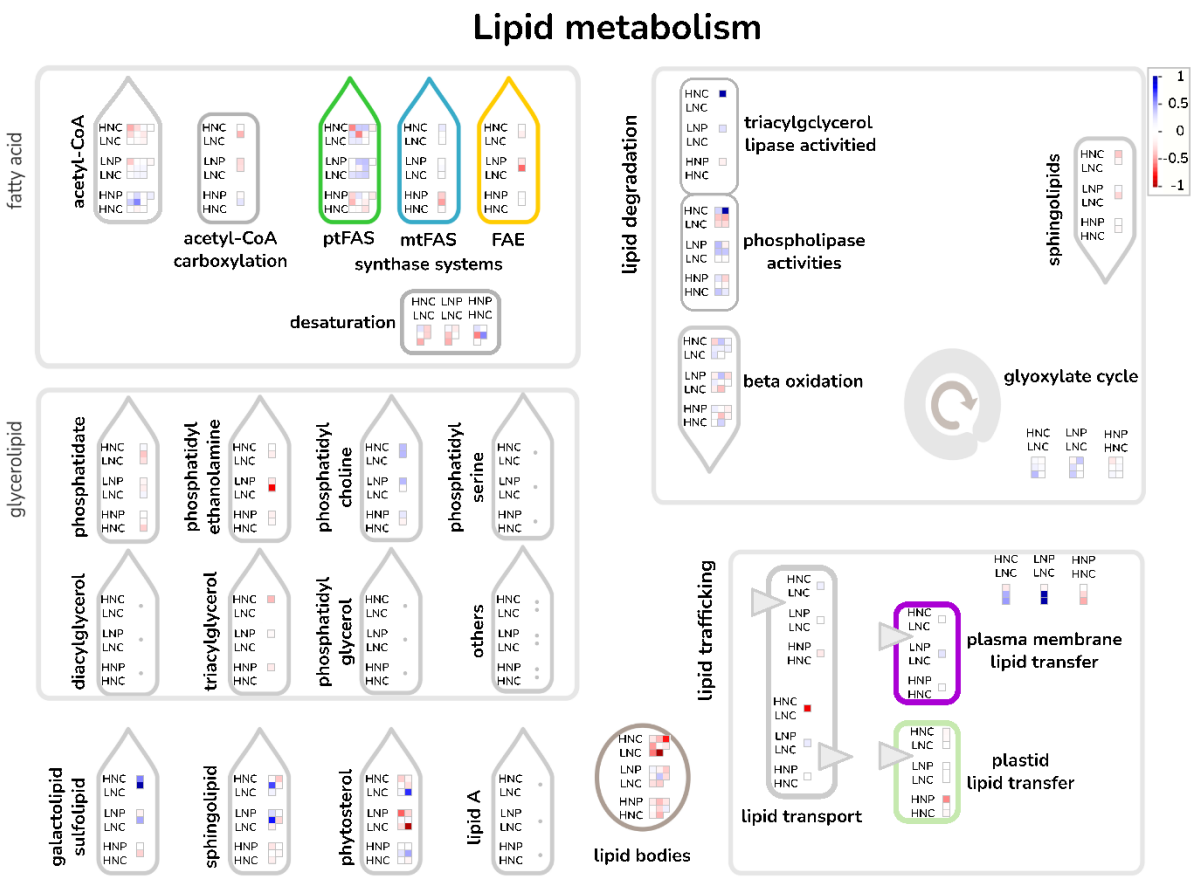

Supplementary Figure S4.5. Lipid metabolism overview in roots (microsomal fraction). Data represented are 100% vv. Mapped proteins, log2FC and significances (indicated with asterisks in log2FC column) are shown in Supplementary Table S4.3. MapMan version 3.5.1R2 (Thimm et al., 2004) was used. The following pathways were used and modified: X4.5 Lipid metabolism R5.0. Mapping file was created using Mercator4 V2.0 (Schwacke et al., 2019). Abbreviations: ptFAS, plastidial fatty acid synthase; mtFAS, mitochondrial fatty acid synthase; FAE, fatty acid elongase. Comparisons are mentioned on next to each box: HNC / LNC = Sufficient N Control vs. Limited N Control; LNP / LNC = Limited N + *Pk* vs. Limited N Control; HNP / HNC = Sufficient N + *Pk* vs. Sufficient N Control.

4.5.7 Protein abundances in tabular form to Fig. S4.3, S4.4, S4.5

Supplementary Table 4.3. Mapped proteins (microsomal enrichment) of the N-metabolism (Supplementary Figure S4.3), kinase families (Fig. S4.4) and root lipid metabolism (Fig. S4.5). The column 'Mapped under' refers to the caption used in each pathway figure. Log2FC highlighted in bold are significant different in their respective comparison. Statistics were performed using ANOVA with a confidence interval of 95% followed by post-hoc Tukey's HSD.

			Root		
	Mapped under	**Uniprot ID**	**HNC / LNC**	**LNP / LNC**	**HNP / HNC**
N-metabolism (Fig. S4.1)	AA	I1I0M5_BRADI	-0.55	0.07	-0.05
		I1I0M7_BRADI	-0.48	0.00	-0.16
	AMT	I1IBN3_BRADI	-0.70	0.25	0.04
		I1IZJ3_BRADI	-0.55	0.34	0.13
	AS	I1H6K4_BRADI	0.44	0.00	0.38
		A0A2K2D9P1_BRADI	-0.66	-0.42	0.18
	GDH	I1J084_BRADI	**1.31**	0.29	0.22
		I1GM99_BRADI	0.01	0.31	-0.18
	GOGAT	I1GRK9_BRADI	-0.26	**0.42**	-0.02
		I1HQF1_BRADI	0.11	0.41	0.11
	GS1	I1H7X9_BRADI	0.36	0.39	0.06
		I1IFI7_BRADI	0.17	0.40	0.16
	GS2	I1J2T4_BRADI	-0.35	0.51	0.00
	NiR	I1IEV4_BRADI	-0.13	**0.99**	0.21
	Nitrogen regulation	A0A0Q3MUB2_BRADI	0.59	**0.76**	-0.31
	NR	A0A0Q3FHC7_BRADI	**-1.38**	0.25	-0.04
	NRT	A0A2K2DG64_BRADI	0.21	0.47	-0.09
		I1GPH0_BRADI	-0.12	-0.40	-0.28
		I1H1D1_BRADI	-0.62	0.09	-0.40
		I1HBQ0_BRADI	-0.05	-0.58	-0.28
		I1I5R4_BRADI	-0.06	0.09	0.01
		I1I6K3_BRADI	-0.45	-0.23	-0.08
		I1IB70_BRADI	**-5.19**	0.10	-0.23
Kinase families (Fig. S4.2)	AGC kinase superfamily	I1GP76_BRADI	-0.26	-0.29	-0.42
		I1HCT2_BRADI	-0.22	-0.05	0.04
	CAMK kinase superfamily	I1H6L6_BRADI	0.16	0.23	-0.05
		I1HNY1_BRADI	-0.43	0.10	0.03
		I1IX12_BRADI	0.42	0.24	-0.18
		I1GKM6_BRADI	-0.30	-0.23	0.14
		I1GMZ0_BRADI	0.04	0.15	-0.10
		I1I692_BRADI	0.44	**0.66**	-0.25
		I1IXT7_BRADI	0.18	0.04	-0.19
		I1GU02_BRADI	-0.39	-0.08	0.50
		I1HPI9_BRADI	-0.30	-0.27	0.16
	CK kinase superfamily	I1HFR4_BRADI	-0.02	0.07	-0.06

		I1HQU4_BRADI	-0.01	0.24	0.34
	CMGC kinase superfamily	I1HAG7_BRADI	-0.25	-0.03	0.14
		I1H4A1_BRADI	0.12	0.02	-0.20
	LRR	A0A0Q3KRE6_BRADI	-0.12	-0.21	-0.87
		I1HP99_BRADI	0.34	0.33	-0.32
		I1IYJ0_BRADI	-0.16	-0.04	-0.18
		A0A0Q3GL83_BRADI	-0.13	0.01	-0.14
		A0A2K2CTF7_BRADI	-0.15	0.34	-0.50
		I1HIB3_BRADI	**-0.43**	0.10	0.03
		I1ID77_BRADI	0.44	0.66	-0.25
		I1IP60_BRADI	-0.60	-0.08	-0.08
		I1GWG0_BRADI	0.18	0.07	-0.31
		I1IZ22_BRADI	0.06	-0.14	-0.11
		A0A2K2CN34_BRADI	-0.22	-0.12	-0.03
	LysM	A0A0Q3I004_BRADI	**-0.36**	0.17	0.02
		I1HY83_BRADI	0.07	-0.10	-0.14
	MAP kinases	I1H6N9_BRADI	-0.30	-0.22	0.25
		I1H0Y7_BRADI	0.25	0.65	0.89
		I1I5N8_BRADI	-0.28	-0.14	-0.31
	PERK-like	A0A0Q3MRU1_BRADI	-0.23	-0.27	-0.09
Lipid metabolism (Fig. S4.3)	acetyl-COA	A0A0Q3K0H7_BRADI	-0.24	0.15	-0.07
		A0A0Q3M1M0_BRADI	-0.09	0.15	-0.13
		I1GQ11_BRADI	-0.09	0.15	**0.59**
		I1H338_BRADI	-0.32	-0.13	0.48
		I1HLK9_BRADI	-0.16	0.16	0.03
		I1HQ21_BRADI	-0.46	-0.37	0.17
		I1I6C4_BRADI	-0.04	0.07	0.07
		I1IA43_BRADI	-0.01	-0.12	0.03
		I1IVQ0_BRADI	-0.30	-0.04	0.24
		I1ITV5_BRADI	0.08	0.04	-0.12
	acetyl-CoA carboxylation	A0A0Q3JE04_BRADI	-0.01	-0.31	-0.15
		I1IWF2_BRADI	-0.32	-0.28	0.30
	beta oxidation	A0A0Q3JRJ2_BRADI	0.04	-0.40	0.33
		I1HLG5_BRADI	0.38	0.40	-0.06
		I1HZH4_BRADI	0.22	0.22	0.07
		I1I3F1_BRADI	-0.33	-0.19	0.20
		I1HP88_BRADI	0.15	-0.31	-0.19
		I1I4F7_BRADI	0.19	0.06	-0.17
		I1IDX9_BRADI	0.27	-0.20	-0.01
		I1IPG4_BRADI	0.19	-0.05	-0.40
	desaturation	I1HN08_BRADI	-0.04	-0.39	-0.57
		I1HSR7_BRADI	0.27	0.12	0.27
		I1HUM5_BRADI	-0.33	-0.02	0.56

		I1HVL8_BRADI	-0.46	-0.45	-0.08
		I1I5F5_BRADI	-0.33	-0.22	-0.02
	FAE	I1HC19_BRADI	-0.23	**-0.62**	-0.01
		A0A2K2D3W9_BRADI	-0.10	**-0.44**	0.12
	galactolipid sulfolipid	I1HIN3_BRADI	0.44	-0.35	-0.03
		I1HJY1_BRADI	**1.64**	0.32	-0.33
	glyoxylate cycle	A0A0Q3F6L1_BRADI	0.19	0.30	0.05
		I1IX27_BRADI	-0.06	0.37	0.06
		I1IZE5_BRADI	0.10	0.03	0.12
		I1HA00_BRADI	0.42	0.36	0.14
		I1HZ21_BRADI	0.11	-0.14	-0.24
		I1IG62_BRADI	0.06	0.04	0.04
	lipid bodies	A0A0Q3SCX9_BRADI	-0.24	0.15	-0.23
		A0A2K2D5E4_BRADI	-0.50	-0.13	-0.04
		A0A2K2DPB0_BRADI	-0.59	-0.28	-0.17
		I1GZ91_BRADI	-0.43	-0.18	-0.42
		I1GR98_BRADI	**-1.29**	-0.35	-0.44
		I1I763_BRADI	-0.25	-0.29	0.20
		I1HLR0_BRADI	-0.77	-0.37	-0.25
		I1IEG7_BRADI	-0.09	0.39	-0.32
	lipid trafficking	I1GL63_BRADI	-0.23	-0.23	0.01
		I1H1G1_BRADI	0.51	**0.99**	-0.46
		I1I1B4_BRADI	0.46	1.56	-0.32
	lipid transport	A0A2K2D1A1_BRADI	-0.91	0.14	0.00
		A0A2K2DFT3_BRADI	-0.08	-0.09	-0.19
	mtFAS	A0A0Q3R9W8_BRADI	0.01	0.12	-0.35
		I1H2L1_BRADI	0.22	0.03	-0.19
		I1H6F4_BRADI	0.02	0.05	-0.09
	phosphatidate	A0A0Q3FNL6_BRADI	-0.27	-0.09	-0.32
		I1HTH7_BRADI	0.12	-0.18	0.03
		I1II20_BRADI	-0.38	-0.49	-0.12
	phosphatidyl choline	I1HGU5_BRADI	0.49	0.42	0.20
		I1HRW0_BRADI	0.42	-0.04	-0.15
	phosphatidyl ethanolamine	I1J2C7_BRADI	-0.03	-0.21	-0.18
		I1GL19_BRADI	-0.08	-0.73	-0.14
	phospholipase activities	A0A0Q3FHI6_BRADI	-0.38	0.39	-0.02
		A0A0Q3GLT1_BRADI	**1.31**	-0.19	-0.33
		I1H4V2_BRADI	**-0.46**	**0.38**	-0.13
		I1HCG5_BRADI	-0.31	-0.06	0.23
		I1IKD0_BRADI	-0.30	-0.04	0.38
		I1I799_BRADI	0.34	0.42	0.25
	phytosterol	A0A0Q3NTK1_BRADI	0.74	-0.98	-0.16
		A0A0Q3M4K0_BRADI	0.12	-0.30	0.06

		I1H2Q5_BRADI	-0.35	**-0.64**	-0.02
		I1HA07_BRADI	-0.05	0.10	0.27
		I1GV37_BRADI	-0.16	-0.33	0.04
		I1HX16_BRADI	-0.29	0.13	**0.48**
	plasma membrane lipid transfer	I1H6Z5_BRADI	-0.01	0.24	0.13
	plastid lipid transfer	I1GVW3_BRADI	-0.15	0.02	-0.45
		I1IIX8_BRADI	-0.12	-0.02	0.00
		I1IU18_BRADI	-0.03	0.01	-0.17
	ptFAS	A0A0Q3IJU7_BRADI	0.22	0.27	-0.05
		A0A2K2CXZ2_BRADI	0.23	0.31	-0.10
		I1GKM7_BRADI	-0.56	-0.01	-0.30
		I1GXN7_BRADI	0.01	0.35	-0.24
		I1H029_BRADI	0.36	0.37	0.13
		I1I9A1_BRADI	0.29	0.07	-0.51
		I1J2H0_BRADI	-0.57	-0.16	0.22
		I1I9U8_BRADI	0.36	0.40	0.00
		I1IRJ8_BRADI	-0.19	0.05	-0.14
		I1IWW9_BRADI	-0.15	0.37	-0.13
	sphingolipid	A0A0Q3GPB5_BRADI	-0.10	0.31	-0.19
		A0A0Q3F989_BRADI	-0.15	-0.32	-0.13
		I1HC77_BRADI	0.18	-0.21	-0.25
		I1HPK0_BRADI	-0.38	0.10	0.06
		I1IBQ1_BRADI	0.69	**0.78**	-0.02
	triacylglyerol lipase activities	I1HLP4_BRADI	**1.44**	0.28	-0.26

4.5.8 GO term Molecular Function (whole proteome)

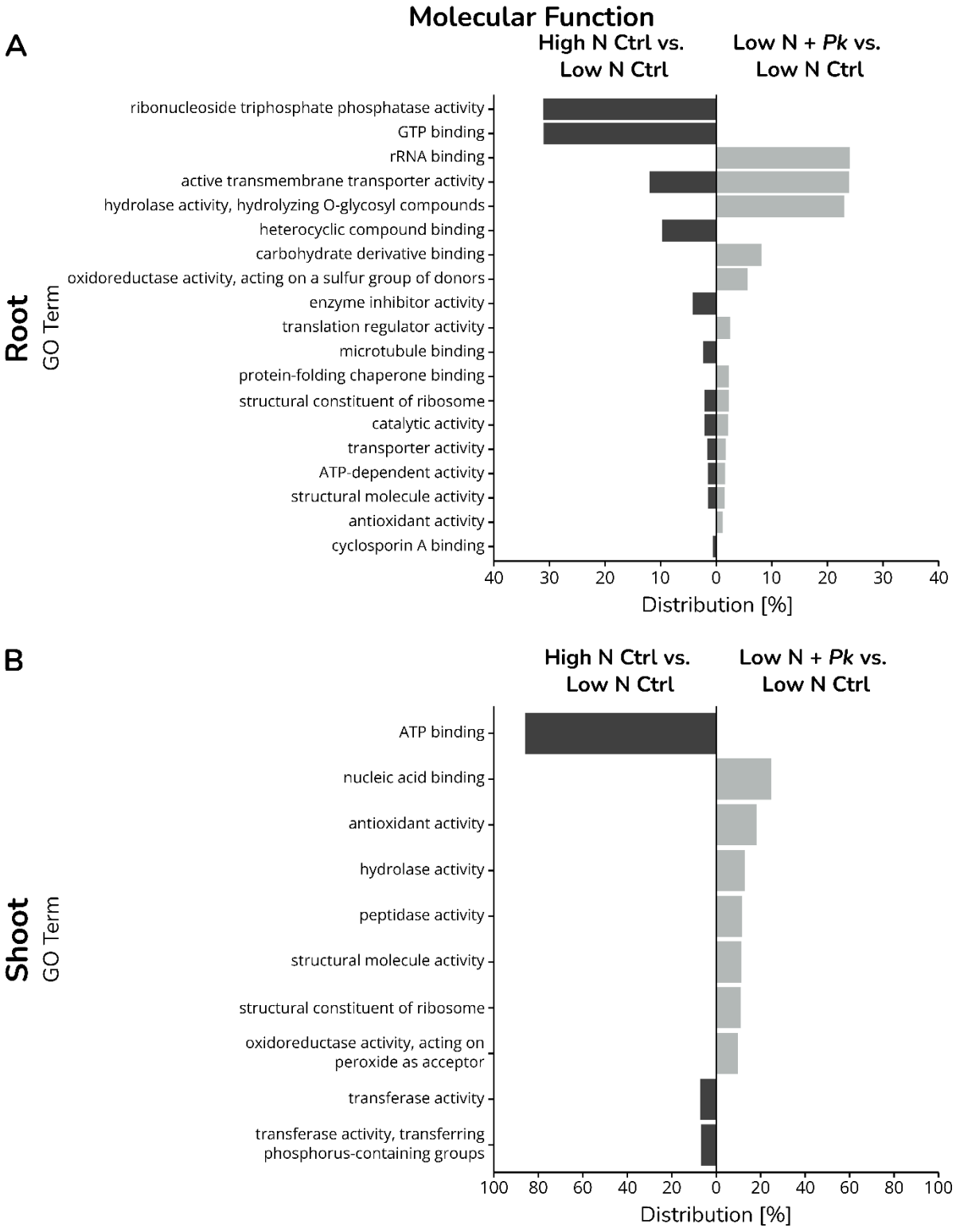

Supplementary Figure S4.6. GO-term analyses (Molecular Function). A) Root GO term analysis; B) Shoot GO term analysis. Only statistical significant proteins were imported into PantherDB statistical enrichment test (Mi et al., 2019), followed by REVIGO (Supek et al., 2011). Log10 (p-values) were used to calculate the %-distribution (x-axis) of GO-terms (y-axis).

4.6 References

Beck, S., Michalski, A., Raether, O., Lubeck, M., Kaspar, S., Goedecke, N., ... & Mann, M. (2015). The impact II, a very high-resolution quadrupole time-of-flight instrument (QTOF) for deep shotgun proteomics. Molecular & Cellular Proteomics, 14(7), 2014-2029.

Bilbao A, Varesio E, Luban J, et al.: Processing strategies and software solutions for data-independent acquisition in mass spectrometry. Proteomics. 2015;15(5–6):964–80. 10.1002/pmic.201400323

Chen, W. W., Yang, J. L., Qin, C., Jin, C. W., Mo, J. H., Ye, T., et al. (2010). Nitric oxide acts downstream of auxin to trigger root ferric-chelate reductase activity in response to iron deficiency in Arabidopsis. Plant Physiol. 154, 810–819. doi: 10.1104/pp.110.161109

Demichev, V., Messner, C. B., Vernardis, S. I., Lilley, K. S., & Ralser, M. (2020). DIA-NN: neural networks and interference correction enable deep proteome coverage in high throughput. Nature methods, 17(1), 41-44.

Gasulla, F., Vom Dorp, K., Dombrink, I., Zähringer, U., Gisch, N., Dörmann, P., & Bartels, D. (2013). The role of lipid metabolism in the acquisition of desiccation tolerance in C raterostigma plantagineum: a comparative approach. The Plant Journal, 75(5), 726-741.

Gaude, N., Nakamura, Y., Scheible, W. R., Ohta, H., & Dörmann, P. (2008). Phospholipase C5 (NPC5) is involved in galactolipid accumulation during phosphate limitation in leaves of Arabidopsis. The Plant Journal, 56(1), 28-39.

Huang, S., Chen, S., Liang, Z., Zhang, C., Yan, M., Chen, J., et al. (2015). Knockdown of the partner protein OsNAR2.1 for high-affinity nitrate transport represses lateral root formation in a nitrate-dependent manner. Sci. Rep. 8:18192. doi: 10.1038/srep18192

Kang, J. S. (2012). Principles and applications of LC-MS/MS for the quantitative bioanalysis of analytes in various biological samples. *Tandem Mass Spectrometry–Applications and Principles*, *29*, 441-92.

Kehelpannala, C., Rupasinghe, T., Pasha, A., Esteban, E., Hennessy, T., Bradley, D., ... & Roessner, U. (2021). An Arabidopsis lipid map reveals differences between tissues and dynamic changes throughout development. The Plant Journal, 107(1), 287-302.

LaMontagne, E. D., Collins, C. A., Peck, S. C., & Heese, A. (2016). Isolation of microsomal membrane proteins from Arabidopsis thaliana. *Current Protocols in Plant Biology*, *1*(1), 217-234.

Macabuhay, A., Arsova, B., Walker, R., Johnson, A., Watt, M., & Roessner, U. (2022). Modulators or facilitators? Roles of lipids in plant root–microbe interactions. Trends in plant science, 27(2), 180-190.

Matallana-Surget, S., Leroy, B., & Wattiez, R. (2010). Shotgun proteomics: concept, key points and data mining. *Expert review of proteomics*, *7*(1), 5-7.

Meng, Z. B., Chen, L. Q., Suo, D., Li, G. X., Tang, C. X., and Zheng, S. J. (2012). Nitric oxide is the shared signaling molecule in phosphorus-and iron-deficiency-induced formation of cluster roots in white lupin (Lupinus albus). Ann. Bot. 109, 1055–1064. doi: 10.1093/aob/mcs024

Mérigout, P., Lelandais, M., Bitton, F., Renou, J. P., Briand, X., Meyer, C., & Daniel-Vedele, F. (2008). Physiological and transcriptomic aspects of urea uptake and assimilation in Arabidopsis plants. Plant Physiology, 147(3), 1225-1238. Chicago

Mi, H., Muruganujan, A., Ebert, D., Huang, X., and Thomas, P. D. (2019). PANTHER version 14: more genomes, a new PANTHER GO-slim and improvements in enrichment analysis tools. Nucleic Acids Res. 47, D419–D426. doi: 10.1093/nar/gky1038

Moellering, E. R., Muthan, B., & Benning, C. (2010). Freezing tolerance in plants requires lipid remodeling at the outer chloroplast membrane. Science, 330(6001), 226-228.

Munnik, T., & Testerink, C. (2009). Plant phospholipid signaling:"in a nutshell". Journal of lipid research, 50, S260-S265.

Nakamura, Y., Koizumi, R., Shui, G., Shimojima, M., Wenk, M. R., Ito, T., & Ohta, H. (2009). Arabidopsis lipins mediate eukaryotic pathway of lipid metabolism and cope critically with phosphate starvation. Proceedings of the national academy of sciences, 106(49), 20978-20983.

Okazaki, Y., Otsuki, H., Narisawa, T., Kobayashi, M., Sawai, S., Kamide, Y., ... & Saito, K. (2013). A new class of plant lipid is essential for protection against phosphorus depletion. Nature communications, 4(1), 1510.

Okazaki, Y., & Saito, K. (2014). Roles of lipids as signaling molecules and mitigators during stress response in plants. *The Plant Journal*, *79*(4), 584-596.

Perez-Riverol Y, Bai J, Bandla C, Hewapathirana S, García-Seisdedos D, Kamatchinathan S, Kundu D, Prakash A, Frericks-Zipper A, Eisenacher M, Walzer M, Wang S, Brazma A, Vizcaíno JA (2022). The PRIDE database resources in 2022: A Hub for mass spectrometry-based proteomics evidences. Nucleic Acids Res 50(D1):D543-D552 (PubMed ID: 34723319).

Schwacke, R., Ponce-Soto, G. Y., Krause, K., Bolger, A. M., Arsova, B., Hallab, A., ... & Usadel, B. (2019). MapMan4: a refined protein classification and annotation framework applicable to multi-omics data analysis. Molecular plant, 12(6), 879-892.

Siddiqui, M. N., Pandey, K., Bhadhury, S. K., Sadeqi, B., Schneider, M., Sanchez-Garcia, M., ... & Ballvora, A. (2023). Convergently selected NPF2. 12 coordinates root growth and nitrogen use efficiency in wheat and barley. New Phytologist.

Sun, H., Li, J., Song, W., Tao, J., Huang, S., Chen, S., et al. (2015). Nitric oxide generated by nitrate reductase increases nitrogen uptake capacity by inducing lateral root formation and inorganic nitrogen uptake under partial nitrate nutrition in rice. J. Exp. Bot. 66, 2449–2459. doi: 10.1093/jxb/erv030

Sun, C. H., Yu, J. Q., & Hu, D. G. (2017). Nitrate: a crucial signal during lateral roots development. *Frontiers in plant science*, *8*, 485.

Supek, F., Bošnjak, M., Škunca, N., and Šmuc, T. (2011). Revigo summarizes and visualizes long lists of gene ontology terms. PLoS One 6:e21800. doi: 10.1371/journal.pone.0021800

Tegeder, M., & Rentsch, D. (2010). Uptake and partitioning of amino acids and peptides. Molecular plant, 3(6), 997-1011.

Trevisan, S., Manoli, A., and Quaggiotti, S. (2014). NO signaling is a key component of the root growth response to nitrate in Zea mays L. Plant Signal. Behav. 9:e28290. doi: 10.4161/psb.28290

Tyanova, S., Temu, T., Sinitcyn, P., Carlson, A., Hein, M. Y., Geiger, T., ... & Cox, J. (2016). The Perseus computational platform for comprehensive analysis of (prote) omics data. Nature methods, 13(9), 731-740.

Venable JD, Dong MQ, Wohlschlegel J, et al.: Automated approach for quantitative analysis of complex peptide mixtures from tandem mass spectra. Nat Methods. 2004;1(1):39–45. 10.1038/nmeth705

Wang, X. (2004). Lipid signaling. Current opinion in plant biology, 7(3), 329-336.

Wang, X., Devaiah, S. P., Zhang, W., & Welti, R. (2006). Signaling functions of phosphatidic acid. Progress in lipid research, 45(3), 250-278.

Chapter 5

5.1 General discussion and outlook

The world population is steadily increasing, while available arable land is decreasing and used for other purposes, such as urban developments (Döös 2002). To meet the global food demand, the use of nitrogenous fertilizers has become obligatory to increase yields in agriculture. However, in the recent years, several new legislation and regulation restricting N fertilizer applications have been introduced in the European agriculture systems (Löw et al., 2021). These restrictions increase the demand for an alternative, biological approach to improve plant performance without environmental damage. Plant growth promoting bacteria have the potential to improve plant performance via various mechanisms. While *Rhizobium spp.* have been studied throughout the past, they form a very specific symbiotic relationship with legumes and require an oxygen-free environment (nodules) to fix N (Dwivedi et al., 2015). Various free-living bacteria have been demonstrated to form associative relationships with plant roots and contribute to the total plant N content via N-fixation (Smercina et al., 2019; Fig. 2.1). The genus *Pseudomonas* is very diverse and multiple *Pseudomonas sp.* have been demonstrated to improve plant performance in various manners (Fig. 2.2), with *P. stutzeri* or *P. aeruginosa* being examples studied for their ability to fix N (Roychowdhury et al., 2019, Chapter 2). Increasing our understanding of the underlying processes occurring during N-fixation and how the plant acclimates to the presence of beneficial microbes is relevant to enable the use of microbes for a sustainable agriculture.

With this thesis, we contribute to the knowledge by elucidating the morphological and biochemical responses of *Brachypodium distachyon* to the N-fixing bacterium *Pseudomonas koreensis* under two N levels. Using a ^{15}N natural abundance approach, we have shown for the first time that *P. koreensis* Ps9-14 has the potential to fix atmospheric N, however this did not provide the ability to quantify absolute amounts of fixed N by the bacteria. Since the ^{15}N natural abundance results showed no significant decreased $\delta^{15}N$ signatures after inoculation, a follow-up experiment was conducted. In this experiment, different bacterial strains (*E. coli, P. taiwanensis, P. koreensis, P. syringae*) were grown on nitrogen-free medium. Bacteria lacking the ability to fix N (*E. coli*) were not able to grow

on the N-free medium, whereas N-fixing bacterial strains were growing. This further confirms the observed trends in the ^{15}N natural abundance approach.

The phenotype of Brachypodium responds to different N concentrations, by increasing root and shoot biomass with an increasing N concentration up to 1200 µM (Poiré et al., 2014). Poiré et al (2014) have demonstrated a linear growth in the root to shoot ratio with increasing N concentrations. Our biomass data (Fig. 3.10 D) reflected this linear increase, whereas sufficient N control plants showed a similar biomass compared to limited N plants. This reduction in the biomass could be the effect of endophytic bacteria in the seeds, which only seem to affect the plant under sufficient N conditions.

The root system architecture of Brachypodium is composed of three main root types: Primary seminal root (PSR), zero to two coleoptile nodal root (CNR) axes and varying leaf nodal root (LNR) axes, emerging after the leaf 4 stage (Watt et al., 2009; Choschois et al., 2012; Poiré et al., 2014). In our experimental setup, we distinguished between the PSR and lateral roots (LR), whereas the formation of a single CNR could be observed in various root scans. We observed no significant difference in the PSR length, which is in line with the observations of Poiré et al. (2014), but an increase in LR length (Ingram et al., 2012) Poiré et al. demonstrated that CNRs do not contribute significantly to the total root length (TRL), whereas they grew better in medium N concentrations (150 – 600 uM) (Poiré et al., 2014). N concentrations have a significant impact on the LNR length and can contribute to 80% of the TRL at the highest applied N concentrations (Poiré et al., 2014). Due to the growth period of 21 days, no formation of LNR were observed in our conducted experiments. Additionally, Poiré et al (2014) have measured the shoot N content, which is saturated at 4% N content at the highest applied N concentration (Poiré et al., 2014). Our limited N inoculated plants have shown a relative shoot N-content of 4% in the time-series experiment, which might explain the comparable biomass at the time point of harvest. Sufficient N plants, with a 10-fold difference in N concentration (16 mM), have shown a relative N content of more than 5%. There are no specific values for Brachypodium root N contents, whereas Salpagarova et al., (2014) propose an average N content of 1.3% for species of the family *Poaceae* (Salpagarova et al., 2014). We observed a comparable relative N content in roots of Brachypodium grown under limited N

inoculated with *Pk* (1.2%), whereas the root N content was increased to 2% under sufficient N inoculated conditions. Considering that the response to increasing N concentrations is saturated at a shoot N-content of 4% (Poiré et al., 2014), our limited N inoculated plants had the optimal amount of N required for physiological and phenotypical development of both roots and shoots, thus developing like sufficient N plants. Higher concentrations of N led to only slightly increased plant N content, which leads to two open questions: (i) For how long can *Pk* inoculation of Brachypodium under limited N maintain these N contents or will N deplete at some stage; and (ii) Is the observed increased N content only based on the additional available N via N-fixation? The first question could be answered by observing a longer growth period of Brachypodium plants coupled with temporal-resolved elemental analyses of the N contents. Depending on the absolute quantities of N fixed by *Pk*, it could also be hypothesized that *Pk* is able to increase the nitrogen uptake efficiency (NUE).

Plant root exudates are used in plant-microbe interactions for communication with microbes (Sasse et al., 2018). We observed a significant decreased C content in limited N inoculated roots on all measured timepoints, indicating that root exudation is an ongoing process which has started at an earlier timepoint during this plant-microbe interaction.

The highly comparable protein profiles between limited N inoculated and sufficient N control plants could be explained with the assumption that *Pk* leads to sufficient whole plant N content. In the central N metabolism, only a few differences were observable in the roots. The first difference was observed in NAR2.1 (I1IB70_BRADI). In the comparison of sufficient N controls to limited N controls, the abundance of this protein was decreased, whereas the abundance in limited N inoculated plants is the same as their control. NAR2.1 is involved in the regulation of the LR architecture (Orsel et al., 2007) and might contribute to the observed LR length increase of Brachypodium roots under limited N after inoculation with *Pk*. N-fixation from beneficial bacteria would result in an increased NH_4^+ content, thus the external nitrate conditions were dependent on the initial NO_3^- amount added, except nitrification occurred. However, one cytosolic isoform of GS (I1H7X9_BRADI; GLN1;2) was observed to be less abundant in roots after inoculation of limited N plants compared to their control, whereas the other isoform (I1IFI7_BRADI;

GLN1;1) was unchanged. Under sufficient N, GLN1;1 was higher abundant compared to limited N controls. NH_4^+ can first be transported to the shoot and assimilated via GLN1 isoforms. In the shoots, we observed again different behaviour in the GLN1 isoforms. While under sufficient N, GLN1;2 was less and GLN1;1 higher abundant compared to limited N control plants, limited N inoculated plants only show an increased abundance of GLN1;2 compared to limited N control plants. The behaviour of the GLN isoforms in shoots is particularly interesting, as the abundance of the low-affinity GLN1;2 is decreased in sufficient N controls but increased in limited N inoculated plants compared to limited N control plants. This could indicate, that a higher NH_4^+ content is available to limited N inoculated shoots compared to sufficient N control shoots, which could be the consequence of N-fixation from *Pk*. In general, the abundance of N assimilation related proteins was increased in limited N shoots of inoculated Brachypodium plants compared to limited N control shoots, which is also different from the sufficient N control shoots. Although there was no evidence for increased N reallocation towards shoots, it can be concluded that *Pk* inoculation increases the abundance of shoot N assimilation proteins.

Kinases are regulators on protein level (Wang et al., 2020) and play an important role in plant development (Becraft 1998; Laurie and Halford 2001). Like in the central N metabolism, the root kinases of limited N inoculated and sufficient N control plants showed a similar behaviour when compared to limited N control roots. Sucrose non-fermenting related protein kinases (Snrk/SnF) are members of the Ca^{2+}/calmodulin-dependent protein kinase (CaMK) family. Snrk1/SnF1 plays an essential role in plant energy homeostasis and sugar sensing, while Snrk2/SnF1 plays important roles in the abscisic acid (ABA) signaling and abiotic stress responses (Halford et al, 1998). Moreover, SnRK1 regulates the carbon metabolism in plants, whereas it is also regulating other important metabolic enzymes, such as NR, via direct phosphorylation (Halford et al., 1998). As the abundance of quantified SnRKs in roots grown under limited N and inoculated with *Pk* were distinct from limited N control roots, different concentrations of Ca^{2+} might be required. Over 35% of the significant proteins in limited N inoculated roots were contributing to the GO term ‘monoatomic ion transmembrane transport’ (biological process, Figure 4.3), Ca^{2+} transport could be affected by *Pk* inoculation. Additional ions,

that are important and might play a crucial role in the plant development include K^+, which is important for water and nutrient transport within the plant (Jarvis et al., 1990; Sardans & Peñuelas 2015) and enzymatic activity and protein synthesis (Armengaud et al., 2004; Armengaud et al., 2009), or Mg^{2+}, as one of the main building blocks for chlorophyll and photosynthetic activity (Farhat et al., 2016). In shoots, the behaviour of limited N inoculated plants and sufficient N control plants in comparison to limited N control plants was in inversed directions, as seen for proteins the central N metabolism. While under sufficient N, most kinases were less abundant in Brachypodium shoots, the abundance of kinases in limited N inoculated shoot was increased compared to limited N control plants. As the protein data were measured at 21 DAS, the abundance of proteins was measured during a later stage of the growth promotion and the increased abundances of shoot proteins might have been the result of the prior observed improved shoot development. In future studies, it would be interesting to determine when these increased abundance of shoot proteins onsets. This could increase the accuracy of predicting vital proteins in this plant-microbe interaction.

The root lipid metabolism related proteins also mimicked the behaviour of sufficient N control roots in comparison to limited N control roots. Some exceptions were observed in the plastidial fatty acid synthesis (ptFAS) and mitochondrial fatty acid synthesis (mtFAS), with changes in abundances of acyl carrier proteins (ACP). ACP are essential cofactors in FAS (Chan & Vogel 2010). In terms of phospholipase activities, limited N inoculated with *Pk* roots showed a decreased abundance of phospholipase A2 (PLA2), C (PLC) and D (PLD) (I1IKD0_BRADI, A0A0Q3GLT1_BRADI, I1H4V2_BRADI, respectively). PLA2 catalyses the hydrolysis of membrane glycerophospholipids at their *sn*-2 position, generating free fatty acids, which are subsequently converted via downstream metabolic enzymes to lysophospholipids, such as lysophosphatidylcholine (LPC) and lysophosphatidylethanolamine (LPE). After inoculation of Brachypodium roots under limited N, we observed one LPC being significantly higher abundant at 19 DAS. The PLC family can be subdivided into phosphatidylinositol-PLC (PI-PLC) and phosphatidylcholine-PLC (PC-PLC), generating signaling molecules, such as DG, IP_3, PA or IP_6 (Singh et al., 2015). PLD is also producing PA (Wang 2002). This could indicate that PC or PI plant lipid

abundances might be reduced after inoculation of Brachypodium with *Pk* under limited N, while PA or DG contents could be increased. Sufficient N control roots were observed with higher abundances of three phospholipases in comparison to limited N control roots. Two additional proteins show a distinct behaviour after inoculation with *Pk* under limited N compared to low and sufficient N control roots: A plastidial glycerol-3-phosphate acyltransferase (GPAT transcript variant X1; I1I6G2_BRADI) and a phosphatidylserine decarboxylase proenzyme 2 (PSD2; A0A0Q3N4N1_BRADI). The former, GPATX1, catalyses a crucial step in the production of membrane phospholipids (PG) and storage lipids (TG) (Chen et al., 2011). PSD2 catalyses the conversion of phosphatidylserine (PS) to phosphatidylethanolamine (PE) and plays a vital role in plant development (Nerlich et al., 2007). This leads to the following hypothesis, that the lipid contents in limited N inoculated roots are changed with a reduction of the PS content, increased PE content and either further increases in phospholipids or storage lipids (Fig. 5.1).

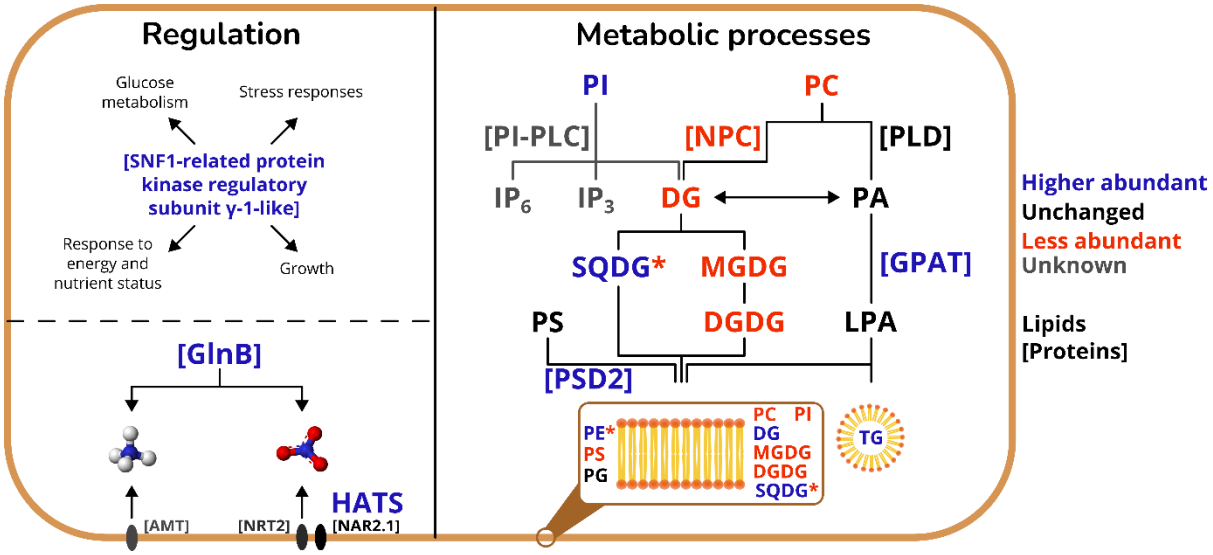

Figure 5.1. Proposed molecular mechanisms occurring during the Brachypodium-*Pseudomonas* interaction. An asterisk at the lipid name indicates opposite behaviour of the individual lipids within one lipid class. Abbreviations: AMT, ammonium transporter family; DG, diacylglycerol; DGDG, digalactosyl diacylglycerol; GlnB, nitrogen regulatory protein P-II; GPAT, plastidial glycerol-3-phosphate acyltransferase; HATS, high-affinity transport system; IP_3, inositol triphosphate; IP_6, inositol hexaphosphate; LPA, lysophosphatidic acid; MGDG, monogalactosyl diacylglycerol; NAR2.1, nitrate transporter-activating protein 2.1; NRT2, nitrate transporter family 2; NPC, non-specific phospholipase C; PA, phosphatidic acid; PC, phosphatidylcholine; PI, phosphatidylinositol; PI-PLC, PI-dependent phospholipase C; PLD, phospholipase D; PS, phosphatidylserine; PSD2, phosphatidylserine decarboxylase proenzyme 2; SQDG, sulfoquinovosyldiacylglycerol; TG, triacylglycerol.

The lipid profiles only show 13 and 10 significant different abundant lipids in the comparison of limited N inoculated roots with limited N control roots at 20 and 21 DAS, respectively. The most prominent changes can be observed at 19 DAS, with 23 significant different abundant lipids. We observed significant differences in the lipid classes DGDG, MGDG, PC, PE, PI and SQDG, which are all membrane-associated lipid classes (Macabuhay et al., 2022). This leads to the hypothesis that the (membrane) lipid profile might be affected by *Pk* inoculation at an earlier timepoint during the plant-microbe interaction, which might be important to establish the associative relationship between plant and microbe. Additionally, some lipids of the class TG were significantly higher abundant after inoculation with *Pk* under limited N in Brachypodium roots compared to their controls. A decrease in abundance of these TG lipids could be observed at 20 and 21 DAS, indicating that the storage lipids might have been utilized during the plant growth promotion for either root or shoot development (Yang & Benning 2018).

The descriptive data generated in this thesis allow multiple follow-up experiments to increase our understanding of the plant-microbe interaction. Whereas a wider range of the molecular dynamics would be useful to identify potential protein and lipid candidates playing an essential role in the plant-microbe interaction, knockdown or knockout mutants of various mentioned proteins can already be tested for their role during this interaction. Earlier proteomics and lipidomics measurements prior to the observed growth promotion should cover 14 – 19 DAS to detect the earliest molecular responses. Characterisation and identification of novel proteins and lipids will help with integration of molecular and phenotypic data. Moreover, root exudates could be measured to identify the crucial compounds involved in this symbiotic relationship. Additionally, the ^{15}N natural abundance measurements could be repeated to quantify the absolute amounts of N contributed by *Pk*. It should also be tested whether *Pk* is able to maintain the plant N contents in a N limited environment or if this is just a short-term effect. *Pk* could also be tested in other cereals and non-sterile environments in greenhouse trials using soil, to test its viability in a competitive environment using microbial communities.

All in all, this work, for the first time, demonstrated that *Pk* is a promising plant-growth promoting bacterium for *Brachypodium distachyon* in limited N environments.

Identification of a novel *Pseudomonas sp.* being a beneficial microbe for plant development further increases the importance of the genus *Pseudomonas*. Increasing our understanding of the underlying molecular mechanisms of *Pseudomonas*-plant interactions might be transferable to other genera of bacteria or help unravelling their molecular mechanisms. Ideally, the use of PGPB will become viable for agricultural application and decrease the synthesis and application of synthetic fertilizers, leading to a more sustainable agriculture while maintaining the required yields.

5.2 References

Armengaud, P., Breitling, R., & Amtmann, A. (2004). The potassium-dependent transcriptome of Arabidopsis reveals a prominent role of jasmonic acid in nutrient signaling. Plant physiology, 136(1), 2556-2576.

Armengaud, P., Sulpice, R., Miller, A. J., Stitt, M., Amtmann, A., & Gibon, Y. (2009). Multilevel analysis of primary metabolism provides new insights into the role of potassium nutrition for glycolysis and nitrogen assimilation in Arabidopsis roots. Plant physiology, 150(2), 772-785.

Becraft, P. W. (1998). Receptor kinases in plant development. Trends in plant science, 3(10), 384-388.

Chan, D. I., & Vogel, H. J. (2010). Current understanding of fatty acid biosynthesis and the acyl carrier protein. Biochemical Journal, 430(1), 1-19.

Chen, X., Snyder, C. L., Truksa, M., Shah, S., & Weselake, R. J. (2011). sn-Glycerol-3-phosphate acyltransferases in plants. Plant signaling & behavior, 6(11), 1695-1699.

Chochois, V., Vogel, J. P., & Watt, M. (2012). Application of Brachypodium to the genetic improvement of wheat roots. Journal of experimental Botany, 63(9), 3467-3474.

Döös, B. R. (2002). Population growth and loss of arable land. Global Environmental Change, 12(4), 303-311.

Dwivedi, S. L., Sahrawat, K. L., Upadhyaya, H. D., Mengoni, A., Galardini, M., Bazzicalupo, M., ... & Ortiz, R. (2015). Advances in host plant and rhizobium genomics to enhance symbiotic nitrogen fixation in grain legumes. Advances in agronomy, 129, 1-116.

Farhat, N., Elkhouni, A., Zorrig, W., Smaoui, A., Abdelly, C., & Rabhi, M. (2016). Effects of magnesium deficiency on photosynthesis and carbohydrate partitioning. Acta physiologiae plantarum, 38(6), 145.

Halford, N. G., & Grahame Hardie, D. (1998). SNF1-related protein kinases: global regulators of carbon metabolism in plants?. Plant molecular biology, 37, 735-748.

Ingram, P. A., Zhu, J., Shariff, A., Davis, I. W., Benfey, P. N., & Elich, T. (2012). High-throughput imaging and analysis of root system architecture in Brachypodium distachyon under differential nutrient availability. Philosophical Transactions of the Royal Society B: Biological Sciences, 367(1595), 1559-1569.

Laurie, S., & Halford, N. G. (2001). The role of protein kinases in the regulation of plant growth and development. Plant growth regulation, 34, 253-265.

Löw, P., Osterburg, B., & Klages, S. (2021). Comparison of regulatory approaches for determining application limits for nitrogen fertilizer use in Germany. Environmental Research Letters, 16(5), 055009.

Macabuhay, A., Arsova, B., Walker, R., Johnson, A., Watt, M., & Roessner, U. (2022). Modulators or facilitators? Roles of lipids in plant root–microbe interactions. Trends in plant science, 27(2), 180-190.

Nerlich, A., von Orlow, M., Rontein, D., Hanson, A. D., & Dörmann, P. (2007). Deficiency in phosphatidylserine decarboxylase activity in the psd1 psd2 psd3 triple mutant of Arabidopsis affects phosphatidylethanolamine accumulation in mitochondria. Plant physiology, 144(2), 904-914.

Orsel, M., Chopin, F., Leleu, O., Smith, S. J., Krapp, A., Daniel-Vedele, F., & Miller, T. (2007). Nitrate signaling and the two component high affinity uptake system in Arabidopsis. Plant signaling & behavior, 2(4), 260-262.

Poiré, R., Chochois, V., Sirault, X. R., Vogel, J. P., Watt, M., & Furbank, R. T. (2014). Digital imaging approaches for phenotyping whole plant nitrogen and phosphorus response in Brachypodium distachyon. Journal of integrative plant biology, 56(8), 781-796.

Roychowdhury, R., Qaiser, T. F., Mukherjee, P., & Roy, M. (2019). Isolation and characterization of a Pseudomonas aeruginosa strain PGP for plant growth promotion. Proceedings of the national academy of sciences, India section b: biological sciences, 89, 353-360.

Salpagarova, F. S., van Logtestijn, R. S., Onipchenko, V. G., Akhmetzhanova, A. A., & Agafonov, V. A. (2014). Nitrogen content in fine roots and the structural and functional adaptations of alpine plants. Biology Bulletin Reviews, 4(3), 243-251.

Sardans, J., & Peñuelas, J. (2015). Potassium: a neglected nutrient in global change. Global Ecology and Biogeography, 24(3), 261-275.

Sasse, J., Martinoia, E., & Northen, T. (2018). Feed your friends: do plant exudates shape the root microbiome?. Trends in plant science, 23(1), 25-41.

Singh, A., Bhatnagar, N., Pandey, A., & Pandey, G. K. (2015). Plant phospholipase C family: regulation and functional role in lipid signaling. Cell Calcium, 58(2), 139-146.

Smercina, D. N., Evans, S. E., Friesen, M. L., & Tiemann, L. K. (2019). To fix or not to fix: controls on free-living nitrogen fixation in the rhizosphere. Applied and Environmental Microbiology, 85(6), e02546-18.

Wang, P., Hsu, C. C., Du, Y., Zhu, P., Zhao, C., Fu, X., ... & Zhu, J. K. (2020). Mapping proteome-wide targets of protein kinases in plant stress responses. Proceedings of the National Academy of Sciences, 117(6), 3270-3280.

Wang, X. (2002). Phospholipase D in hormonal and stress signaling. Current opinion in plant biology, 5(5), 408-414.

Watt, M., Schneebeli, K., Dong, P., & Wilson, I. W. (2009). The shoot and root growth of Brachypodium and its potential as a model for wheat and other cereal crops. Functional Plant Biology, 36(11), 960-969.

Yang, Y., & Benning, C. (2018). Functions of triacylglycerols during plant development and stress. Current Opinion in Biotechnology, 49, 191-198.